FRONTIERS IN THE ORGANOMETALLIC CHEMISTRY OF SILVER: ACCESSING NEW STRUCTURES AND REACTIVITY THROUGH STERICALLY DEMANDING, ELECTRON-RICH N-HETEROCYCLIC CARBENE LIGANDS

A Dissertation
Presented to
The Academic Faculty

by

Brandon K. Tate

In Partial Fulfillment
of the Requirements for the Degree
Doctor of Philosophy in the
School of Chemistry and Biochemistry

Georgia Institute of Technology
December 2015

FRONTIERS IN THE ORGANOMETALLIC CHEMISTRY OF SILVER: ACCESSING NEW STRUCTURES AND REACTIVITY THROUGH STERICALLY DEMANDING, ELECTRON-RICH N-HETEROCYCLIC CARBENE LIGANDS

Approved by:

Dr. Joseph P. Sadighi, Advisor
School of Chemistry and Biochemistry
Georgia Institute of Technology

Dr. Z. John Zhang
School of Chemistry and Biochemistry
Georgia Institute of Technology

Dr. Angus P. Wilkinson
School of Chemistry and Biochemistry
Georgia Institute of Technology

Dr. Jake D. Soper
School of Chemistry and Biochemistry
Georgia Institute of Technology

Dr. Seth R. Marder
School of Chemistry and Biochemistry
Georgia Institute of Technology

Dr. Christopher W. Jones
School of Chemical and Biomolecular Engineering
Georgia Institute of Technology

Date Approved: November 3, 2015

In loving memory of my aunt,

Cheryl Studstill

ACKNOWLEDGEMENTS

I would like to thank my parents, Billy and Betty Tate, for their love and support, and for encouraging me to pursue my dreams. I thank my brother Keith Tate, his wife Amy Tate, and my nephews Colin, Holden, and Brody, for their love, support, and friendship, and for their understanding when I missed birthdays and holidays while attending graduate school.

I thank my girlfriend and soulmate, Emmeline Grommé, for her love and support, for brightening my days with her smile, for her patience when I work long hours, for going with me to get coffee and chocolate chip cookies in the afternoons, for bringing me coffee and chocolate chip cookies when I was busy in the lab, and for the joy she brings to my life.

I thank Joseph Sadighi, for the lessons he has taught me about science and academia and for his guidance in my graduate research.

I thank all the scientists with whom I have had the pleasure of working in the Sadighi Lab: Chelsea Bordley, Joel Starch, Thomas Robilotto, Jens Kück, Valeska Lobo, Hannah Akinosho, John Kevin Busa, Jamie Bitting, Jenna Nguyen, Yu Cao, Kevin Omolo, Nicholas Daugherty, Abraham Jordan, Andrew Royappa, Christopher Sato, and Jonathan Napoline. I am happy to have worked with them all, and I learned valuable lessons from every one of them. I wish them all the best in their future endevours.

I would specifically like to thank Chelsea Wyss Bordley not only for her professional contributions to our several collaborative projects but also for her encouragement, friendship, and personal advice. I also thank Thomas Robilotto for his mentorship and friendship, for encouragement when I needed it the most, for countless

lunches and cups of coffee, and for all the evenings he stayed late in lab waiting for me to finish experiments so that I didn't have to work alone. I thank Jonathan Napoline for insightful discussions of chemistry and academics, and for always being prepared to present results in group meetings when no one else was. I thank Yu Cao and Kevin Omolo for always welcoming me to the lab with a smile and spreading a contagiously positive attitutude. I thank Nicholas Daugherty for sharing his unique perspective in discussions of chemistry and for helping me maintain an inert atmosphere in the glovebox we shared. I thank Abraham Jordan for his advice and for the special insight he offered based on his work with copper hydrides and expanded-ring NHC ligands. I thank Chris Sato for all his creative ideas to improve the efficiency of the lab. I thank John Kevin Busa for sharing his enthusiasm for science. I thank Michael Bayless for his invaluable advice on matters both inside and outside the lab. I thank especially undergraduate researchers Jenna Nguyen and Andrew Royappa for their outstanding contributions to my research. I was honored by the opportunity to work with them and delighted by their enthusiasm and diligence.

I thank Leslie Gelbaum for helping me with NMR experiments, especially those involving the seldom probed silver-109 nucleus. I thank John Bacsa, Kelly Kluge, and Marika Wieliczko, all of the Emory University Crystallography Center, for their crystallographic contributions to my research. I thank Thomas Gray of Case Western Reserve University and Tim Royappa of the University of West Florida for performing computational studies relevant to my research. I thank David Bostwick and Lucas Evans for performing mass spectrometry experiments.

I thank Jake Soper for sharing his insightful perspectives on topics in transition metal coordination chemistry and sustainable energy, and for his unique sense of humor. I thank my teaching supervisers, especially Carrie Shepler and Leigh Bottomley, for helping me develop communication and teaching skills, and for making teaching a rewarding and enjoyable part of my graduate school experience. I also thank my students, unfortunately far too many to name here, for their respect, diligence, hard work, and patience. I thank Cameron Tyson, Kenyetta Johnson, Ashley Edwards, and the rest of the staff of the School of Chemistry and Biochemistry for all the things they do behind the scenes to keep the department running smoothly and to make the lives of graduate students easier.

I thank Anne Gorden for her guidance in my undergraduate research and for encouraging me to pursue a Ph.D. I thank my college professors John Gorden, Christian Goldsmith, Orlando Acevedo, and Traci O'Brien for inspiring me to pursue a career in acadmics and encouraging me to attend graduate school. I thank my high school chemistry teacher Pamela Ray for introducing me to the fascinating world of chemistry. I thank all the teachers and professors who helped me build the academic foundation I needed to succeed in graduate school.

I thank the National Science Foundation, the College of Sciences and the School of Chemistry and Biochemistry of the Georgia Institute of Technology, the William H. Emerson Fellowship in Chemistry, and the Georgia Tech Presidential Fellowship for financial support.

TABLE OF CONTENTS

LIST OF TABLES

LIST OF FIGURES

LIST OF SCHEMES

LIST OF SYMBOLS AND ABBREVIATIONS

°	degree(s)
°C	degree(s) Celsius
”	inch(es)
5Dipp	See L^5
6Dipp	See L^6
7Dipp	See L^7
Å	Angstrom(s)
α	alpha
ATR	attenuated total reflection
app	apparent
B	Lewis base
β	beta
br	broad
Bu	butyl
Bz	benzoyl
Pent	pentyl
C	Celsius
ca.	circa
CCDC	Cambridge Crystallographic Data Centre
CCPh	phenylethynyl
cm	centimeter(s)
d	day(s) (unit of time), doublet (NMR multiplicity)
D	deuterium

DBU	1,8-diazabicyclo[5.4.0]undec-7-ene
dd	doublet of doublets
ddq	doublet of doublets of quartets
δ	delta, chemical shift (relative to tetramethylsilane)
DMSO	dimethylsulfoxide
dqd	doublet of quartets of doublets
dt	doublet of triplets
dtd	doublet of triplets of doublets
ed(s).	editor(s)
e.g.	*exemplī grātiā* (for example)
equiv	molar equivalent(s)
Et	ethyl
etc.	*et cetera* (and so forth)
η	eta
g	gram(s)
h	hour(s)
Hz	hertz
IDipp	1,3-bis(2,6-diisopropylphenyl)imidazol-2-ylidene or IPr
i.e.	*id est* (that is)
IPr	See IDipp
I_{iPr}	1,3-bis(2,6-diisopropyl)imidazol-2-ylidene
IR	infrared
K	Kelvin
k	rate constant
K_{eq}	equilibrium constant

k_H/k_D	See KIE
KIE	kinetic isotope effect
k_n	rate constant of step *n*
L	ligand (see figure caption for definition)
L^5	1,3-bis(2,6-diisopropylphenyl)imidazolin-2-ylidene or SIPr or SIDipp or 5Dipp
L^6	1,3-bis(2,6-diisopropylphenyl)-3,4,5,6-tetrahydropyrimidin-2-ylidene or 6Dipp
L^7	1,3-bis(2,6-diisopropylphenyl)-4,5,6,7-tetrahydro-1,3-diazepin-2-ylidene or 7Dipp
M	molar, or moles per liter
MAS	magic-angle spinning
min	minute(s)
mg	milligram(s)
MHz	megahertz
mL	milliliter(s)
mm	millimeter(s)
mM	millimolar, or millimoles per liter
mmol	millimole(s)
mol	mole(s)
mult	multiplet
Me	methyl
μ	mu
NHC	N-heterocyclic carbene
NMR	nuclear magnetic resonance
ν	wavenumber
ν_{TEP}	Tolman electronic parameter

OTf	triflate or trifluoromethanesulfonate
OTs	tosylate or *p*-toluenesulfonate
p	pressure
Ph	phenyl
π	pi
ppm	parts per million
q	quartet
qdd	quartet of doublets of doublets
quin	quintet
ref(s).	reference(s)
rt	room temperature
s	singlet (NMR multiplicity), strong (spectroscopic absorption)
sept	septet
sext	sextet
SIDipp	See L^5
σ	sigma
SIPr	See L^5
t	triplet
θ	theta, diffraction angle
tt	triplet of triplets
Tf	triflyl or trifluoromethanesulfonyl
THF	tetrahydrofuran
^{t}Bu	*tert*-butyl
^{t}Pent	*tert*-pentyl or 1,1-dimethylpropyl
Ts	*p*-tosyl or *p*-toluenesulfonyl

w	weak
1a	$[(L^5Ag)_2(\mu\text{-}H)]^+$
1a-*d*	$[(L^5Ag)_2(\mu\text{-}D)]^+$
1b	$[(L^6Ag)_2(\mu\text{-}H)]^+$
1b-*d*	$[(L^6Ag)_2(\mu\text{-}D)]^+$
1c	$[(L^7Ag)_2(\mu\text{-}H)]^+$
1c-*d*	$[(L^7Ag)_2(\mu\text{-}D)]^+$
2	L^5AgCl
3a	$L^5Ag(O^tBu)$
3b	$L^6Ag(O^tPent)$
3c	$L^7Ag(O^tPent)$
4	L^5AgOTf
5a	$[(L^5Ag)_2(\mu\text{-}O^tBu)]^+$
5b	$[(L^6Ag)_2(\mu\text{-}O^tPent)]^+$
6	L^5CuF
7	L^5AgF
7b	L^6AgF
7c	L^7AgF
8	L^5AuF
9	$L^5Cu(O^tBu)$
10	$L^5Au(O^tBu)$
11	$[(L^5Cu)_2(\mu\text{-}F)]^+$
12	$[(L^5Ag)_2(\mu\text{-}F)]^+$
13	$[(L^5Au)_2(\mu\text{-}F)]^+$
14a	L^6AgBr

14b L^7AgBr

15a L^6AgOTs

15b L^7AgOTs

16 L^5AgEt

17 L^5AgMe

18 $L^5Ag(CCPh)$

19 $L^5Ag(CF_3)$

20 $[(L^5Ag)_2(\mu\text{-}Et)]^+$

21 $[(L^5Ag)_2(\mu\text{-}Ph)]^+$

22 $[(L^5Ag)_2(\mu\text{-}Me)]^+$

23 $[(L^5Ag)_2(\mu\text{-}CCPh)]^+$

24 $L^5Ag(O_2CEt)$

SUMMARY

Chapter 1: Introduction

NHC ligands generally form labile bonds to silver and tend to form homoleptic complexes, limiting the utility of NHC(silver) complexes beyond their use as NHC-transfer agents. Particularly bulky, electron-rich NHCs form relatively inert bonds to silver, allowing the preparation of a wide variety of interesting heteroleptic NHC-supported complexes.

Chapter 2: An NHC-Supported Disilver Hydride

A triangular $[Ag_2H]^+$ core is stabilized by the NHC ligand 5Dipp. The X-ray crystal structure of this complex reveals a short silver-silver distance, and ^{109}Ag NMR spectroscopy shows substantial coupling between the silver nuclei. The complex persists for hours in solution after exposure to air and moisture. When carbon dioxide is added in the form of a Lewis-basic NHC adduct, a rapid reaction results in hydride transfer to form a bis(NHC) silver(I) formate.

Chapter 3: Fluoride-Bridged Complexes of the Group 11 Metals

Terminal fluoride complexes of the monovalent group 11 metals, supported by NHC ligands, react with one-half equivalent of triphenylmethyl cation to form fluoride-bridged dinuclear cations. An improved preparation of the starting terminal fluorides is introduced. The crystal structures of the cations display bent M–F–M arrangements with large intermetallic separations. The bridging fluorides are highly labile, undergoing facile hydrolysis. The fluoride-bridged digold complex adds across an allene C=C bond to form a diaurated allylic fluoride.

Chapter 4: Hydrogen Activation By Hard-Soft Mismatched Silver Complexes

Alkoxide-bridged disilver cations react with dihydrogen to form hydride-bridged cations, releasing free alcohol. Hydrogenolysis of neutral silver fluorides affords hydride-bridged disilver cations as their bifluoride salts. These reactions proceed most efficiently when the supporting ligands are expanded-ring NHCs derived from six- and seven-membered cyclic amidinium salts. Kinetics studies show that silver fluoride hydrogenolysis is first-order in both silver and dihydrogen.

Chapter 5: Closing a Cycle: Silver-Catalyzed Hydrogenation of Carbon Dioxide

Expanded-ring NHCs increase the rate of CO_2 reduction by dinuclear silver. Despite unsuccessful attempts to isolate or directly observe terminal silver hydrides, the hydrogenolysis of terminal silver alkoxides or fluorides in the presence of CO_2 results in stoichiometric formate production. The addition of excess alkoxide precipitates sodium formate and regenerates silver alkoxide, completing a formal catalytic cycle for CO_2 hydrogenation.

Chapter 6: Thermally Stable Organosilver Compounds

A series of mononuclear and dinuclear complexes of silver(I), supported by an NHC and bound to sp^3-, sp^2-, and sp-hybridized carbanions, has been synthesized. Synthetic routes include transmetalation from organozinc, organomagnesium, and organosilicon reagents, as well as the deprotonation of a terminal alkyne. These complexes exhibit greater thermal stability than typical organosilver reagents, allowing thorough spectroscopic and structural characterization. The carbanion-bridged disilver cations feature three-center, two-electron bonding with short Ag–Ag distances. The intermetallic interactions are probed by X-ray diffraction crystallography and ^{109}Ag NMR

spectroscopy. A mononuclear vinylsilver complex releases organic homocoupling products upon thermal decomposition, while mononuclear alkylsilver complexes exhibit nucleophilic behavior, inserting CO_2 to form silver carboxylates.

CHAPTER 1

INTRODUCTION

1.1 NHC Ligands Employed in This Work

A common theme throughout this thesis is the utilization of sterically protective, strongly σ-basic N-heterocyclic carbene (NHC) ancillary ligands to stabilize unprecedented coordination chemistry about monovalent silver, and to some extent its group 11 congeners copper and gold.[1]

Many NHC complexes of silver can be easily prepared by the deprotonation of air-stable cyclic amidinium halide salts with silver oxide.[2] Because NHC ligands generally form labile bonds to silver, and because the preparation of NHC-silver complexes is so convenient, the primary application of NHC complexes of silver is as NHC transfer agents. NHC ligands readily transfer from silver to many other transition metals.[1f–g,2,3]

The lability of NHC complexes of silver often leads to undesired ligand redistribution,[2,4] significantly limiting the degree to which the structure and reactivity of these complexes can be studied beyond NHC-transfer applications. We[5] and others[4,6] have found, however, that bulky, strongly σ-donating NHC ligands are less likely to exhibit undesired ligand transfers. This affords isolable heteroletpic silver complexes and opens the door for applications of NHC-silver complexes in small-molecule activation and catalysis.

The class of NHC ligands which we have found most useful is a series of carbenes of varying ring size derived from the deprotonation of fully saturated cyclic

amidines bearing symmetrical *N*-diisopropylphenyl substituents. Silver complexes of these ligands exhibit sharp ^{13}C NMR resonances with well-resolved ^{13}C–^{107}Ag and ^{13}C–^{109}Ag coupling, indicative of relatively inert Ag–C bonds.[3,4,7] The five-membered NHC of this class, first isolated as a free carbene by Arduengo and coworkers,[8] is commonly referred to as SIPr or SIDipp (Figure 1.1). In this document, SIPr is given the name 5Dipp in order to keep the abbreviation pattern consistent between NHCs of varying ring size. Generally regarded as a stronger σ-donor than its 4,5-unsaturated analogue known as IPr or IDipp (Figure 1.1),[8,9] 5Dipp forms more inert bonds to silver, allowing the preparation of a more diverse library of heteroleptic complexes. Expanded NHCs, derived from six- and seven-membered cyclic amidines, are less commonly employed than conventional five-membered NHCs but are becoming increasingly popular due to their remarkable σ-basicity, greater steric demand, and facile syntheses.[10] Complexes of the expanded-ring analogues of 5Dipp, commonly known as 6Dipp and 7Dipp (Figure 1.1), with silver(I) have been reported.[11] Interestingly, the expanded ring size renders (NHC)silver halide complexes ineffective for NHC transfer to other metals, presumably as a result of stronger Ag–C bonds.[11,12] Furthermore, Aldridge and coworkers[13] have utilized expanded-ring NHC ligands to stabilize highly electrophilic complexes of gold(I) and demonstrated that they impart a substantial increase in hydridcity to gold(I) hydride complexes. In this document, the ligands 5Dipp, 6Dipp, and 7Dipp are represented in schemes as L^5, L^6, and L^7, respectively.

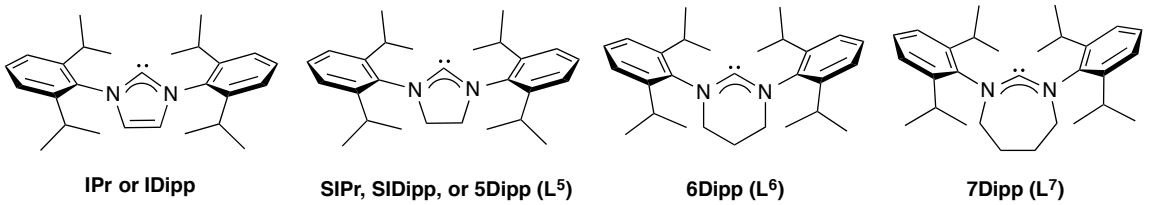

Figure 1.1. Chemical structures of NHC ligands used in this work and, for comparison, IDipp.

Our attempts to prepare highly activated silver complexes using less sterically demanding expanded-ring NHC ancillary ligands such as *N*-xylyl- and *N*-mesityl-substituted varieties resulted in undesired ligand redistribution. In our experience, only NHCs featuring *N*-diisopropylphenyl substituents were suitable for the isolation of heteroleptic NHC-supported silver alkoxides or fluorides.[14] For this reason, we suspect the stabilizing effect of expanded-ring NHCs has not only electronic but also steric origins.

Sterically demanding, strongly basic NHCs open the door for unprecedented applications of silver in homogeneous catalysis and small-molecule activation. Much of my thesis involves the synthesis and characterization of novel compounds relevant to these applications and the demonstration of some fundamental reactivity of these compounds. I hope my contributions to this field lay the foundation for further development of applications of silver in synthesis and catalysis.

1.2 Steric and Electronic Properties of NHC Ligands

Quantification of steric and electronic properties of NHC ligands is challenging and sometimes controversial. Traditionally, the steric and electronic properties of phosphine ligands are quantified by parameters introduced by Tolman: the Tolman cone angle as a measure of steric bulk and the Tolman electronic parameter (ν_{TEP}) as a measure

of electron donating strength.[15] These parameters served as a means to compare and even predict the steric and electronic effects of phosphine ligands on the chemical properties of metal complexes, greatly aiding in the selection and rational design of ligands for new applications or for the improvement of known applications.

Tolman's notion of a cone angle simply represents the angle of the apex of a cone originating at the metal center and encompassing the ligand. However, incredible diversification in ligand design lead to the widespread use of ligands such as NHCs and biaryl phosphines, whose steric occupancy about a metal center is not modeled very accurately as a cone. For instance, NHC ligands such as 5Dipp, 6Dipp, and 7Dipp are more sterically demanding in the plane of their N-heterocycle than in other dimensions. A popular alternative to Tolman cone angle is a parameter known as percent buried volume ($\%V_{bur}$), which approximates the percentage of a metal's coordination sphere that a ligand occupies.[16,17]

For a class of NHC ligands with identical N-substituents, such as the series depicted in Figure 1.1, a more straightforward measure of steric demand is perhaps the N–C–N angle. As this bond angle increases, the flanking aryl substituents are projected further toward the metal center, thereby limiting access of other potential ligands or substrates to the metal center.

The N–C–N angles and percent buried volume for the ligands IDipp, 5Dipp, 6Dipp, and 7Dipp, determined from crystallographic studies of LAuCl complexes, are given in Table 1.1.[18] Either of these steric parameters indicates 5Dipp is somewhat more demanding than IDipp, while the expanded-ring NHCs require substantially more space around a metal than the NHCs derived from five-membered heterocycles. The percent

buried volume for 6Dipp and 7Dipp is actually greater than 50%.[18c] This implies that at the M–C bond lengths found in the model structures (LAuCl), it would be impossible to coordinate two 6Dipp or 7Dipp ligands to the same metal center without deviating from the ligand's ideal stereochemical conformation. Although the rotation of N–C and C–C single bonds, which could alleviate steric repulsions between NHCs sharing a metal center, are often associated with very shallow potential energy wells such that a percent buried volume greater than 50% does not necessarily prohibit the 2:1 coordination of a ligand to a metal, attempts to coordinate multiple 6Dipp and 7Dipp ligands to a gold(I) center have been unsuccessful.[19] Since silver(I) ions are virtually the same size as gold(I) ions,[20] it is likely that the formation of $[L–Ag–L]^+$ complexes is much less favorable for 6Dipp and 7Dipp than for 5Dipp, if not completely inaccessible.

Table 1.1. Electronic and steric parameters of NHC ligands used in this work and, for comparison, IDipp.

	pK_a (in DMSO)[22]	ν_{TEP} (cm^{-1})[23b]	N–C–N angle	$\%V_{bur}$
IDipp	21	2050.7	102°[18c]	44.5[18c]
5Dipp	22	2052.2	106°[18b]	47.0[18b]
6Dipp	27	–	120°[18a]	50.8[18a]
7Dipp	28	–	126°[18a]	52.6[18a]

DMSO = dimethylsulfoxide

The capacity of a ligand, L, to donate electrons, i.e. its Lewis basicity, is often quantified using the Tolman electronic parameter, which is defined as the C–O stretching frequency of the complex $LNi(CO)_3$ as determined by infrared (IR) spectrscopy.[15] The stronger the basicity of L, the stronger the π-back-donation from the metal to the carbonyl ligands, which decreases the strength of the C–O bond and the C–O stretching frequency. Other, more convenient carbonyl complexes, such as $LRh(CO)_2Cl$ or $LIr(CO)_2Cl$ are

often used as alternatives, allowing for the determination of electronic parameters for a wide range of ligands.[17,19] For phosphines, values of the Tolman parameter span a range of over 60 cm^{-1},[15] but for synthetically practical NHC ligands it spans only a narrow range (about 10 cm^{-1}), limiting its utility.[19,21] While the Tolman parameter does provide a measure of basicity which is virtually independent of steric effects, its value largely reflects the overall electron density on a metal and does not distinguish between σ and π interactions with the L ligand.[17,19]

An alternative measure of the basicity of a ligand may be described as its affinity for a proton. Since the only significant acceptor orbital of a proton is its spherically symmetric 1s orbital, the proton may be considered a purely σ acceptor. Thus, either the ligand's proton affinity or the pK_a of the ligand's conjugate acid may be regarded as an approximate measure of its σ-basicity.[22]

Available measures of electron-donating strength for IDipp, 5Dipp, 6Dipp, and 7Dipp are given in Table 1.1. Tolman electronic parameters are unavailable for 6Dipp and 7Dipp, but in general expanded-ring NHCs give rise to lower C–O stretching frequencies than five-membered NHCs.[1c,23] Although the Tolman parameter for IDipp is very slightly lower than that of 5Dipp (by 0.7 cm^{-1}), 5Dipp has a slightly higher proton affinity than IDipp. In practice, 5Dipp and other imidazoline-derived NHCs tend to behave as if they are stronger electron donors than their imidazole-derived analogues, exhibiting a stronger *trans* effect and more inert bonds to metals, for instance.[8] The expanded-ring amidinium ions are substantially less acidic than their five-membered relatives, by about 6 to 7 pK_a units.

Interestingly, the basicity of the NHCs in this series correlates well with their steric demand. The bulkier ligands are more electron-rich. This trend can be rationalized by considering that differences in both steric and electronic properties can be largely attributed to the coordination geometry about the carbene carbon.[17,19] As the N–C–N bond angle increases, not only do the aryl groups shift toward the metal coordination site, but also the hybridization of the carbene carbon is affected, increasing the p character of the carbene donor orbital and thus the orbital's energy and directionality. This allows better spatial overlap with metal acceptor orbitals and results in a stronger σ-bond between the NHC and the metal.

1.3 Interactions of NHC Ligands with Group 11 Metals

While the coordination chemistry of most transition metals is dominated by the interaction of ligand donor orbitals with empty metal d orbitals, the monovalent group 11 metals have a completely occupied valence d subshell, and their lowest acceptor orbital is an s orbital. Similarities between bimetallic gold complexes and metal hydrides first prompted the comparison of the gold cation to a proton[24] using the isolobality principle popularized by Hoffmann, Stone, and Mingos.[25] The isolobal analogy between the gold cation and the proton has since been used extensively to approximate the electronic structures of a wide variety of gold compounds. Of course, like any other application of the isolobality principle, the analogy is imperfect. The gold(I) cation is not completely lacking of π-interactions with ligands, and obviously the size discrepancy between gold and hydrogen is not trivial in discussions of orbital overlap. The resulting perturbations of the electronic properties of gold compounds have been addressed in theoretical studies by Pyykkö and coworkers[26] and an insightful review by Schmidbaur and Raubenheimer.[27]

Despite its imperfections, the analogy between the gold cation and the proton typically serves as a good foundation for a qualitative understanding of the electronic structures of coordination compounds of gold(I).

The isolobal analogy between the proton and the gold cation can naturally be extended to silver and copper cations.[25b] Arguably, the silver cation, due to a larger energy gap between its valence d orbitals and its unoccupied s orbital and therefore less mixing of d character into its lowest unoccupied orbital, is even better approximated as a pure σ-acceptor than gold. In fact, energy decomposition analyses of (NHC)Ag complexes indicate that π-interations account for only about 6% of the attractive forces between the NHC ligand and silver, which is less than in analogous copper and gold systems.[28] Certainly π-interactions are not negligible, but the covalent component of the interactions between NHC ligands and group 11 metals, especially silver, is dominated by σ-donation from the NHC to the metal. It is therefore likely that the strength of the metal-ligand bond correlates with the σ-bascity of the NHC ligands used in this work (5Dipp, 6Dipp, and 7Dipp), increasing with ring size.

1.4 Notes and References

1 For an overview of NHCs and their complexes of silver, see: (a) M. N. Hopkinson, C. Richter, M. Schedler, F. Glorius, *Nature* **2014**, *510*, 485–496. (b) S. Gaillard, C. S. J. Cazin, S. P. Nolan, *Acc. Chem. Res.* **2012**, *45*, 778–787. (c) T. Dröge, F. Glorius, *Angew. Chem. Int. Ed.* **2010**, *49*, 6940–6952. (d) O. Schuster, L. Yang, H. G. Raubenheimer, M. Albrecht, *Chem. Rev.* **2009**, *109*, 3445–3478. (e) J. C. Garrison, W. J. Youngs, *Chem. Rev.* **2005**, *105*, 3978−4008. (f) I. J. B. Lin, C. S. Vasam, *Comments Inorg. Chem.* **2004**, *25*, 75–129. (g) P. Arnold. *Heteroatom. Chem*. **2002**, *13*, 534.

2 H. M. J. Wang, I. J. B. Lin, *Organometallics* **1998**, *17*, 972–975.

3 X. Hu, I. Castro-Rodriguez, K. Olsen, K. Meyer, *Organometallics* **2004**, *23,* 755–764.

4 P. de Frémont, N. M. Scott, E. D. Stevens, T. Ramnial, O. C. Lightbody, C. L. B. Macdonald, J. A. C. Clyburne, C. D. Abernethy, S. P. Nolan, *Organometallics* **2005**, *24,* 6301–6309.

5 (a) B. K. Tate, J. T. Nguyen, J. Bacsa, J. P. Sadighi, *Chem. Eur. J.* **2015**, *21*, 10160–10169. (b) B. K. Tate, C. M. Wyss, J. Bacsa, K. Kluge, L. Gelbaum, J. P. Sadighi, *Chem. Sci.* **2013**, *4*, 3068–3074. (c) C. M. Wyss, B. K. Tate, J. Bacsa, M. Wieliczko, J. P. Sadighi, *Polyhedron* **2014**, *84*, 87–95. (d) D. S. Laitar, Ph.D. thesis, Massachusetts Institute of Technology (Cambridge), **2006**, http://dspace.mit.edu/handle/1721.1/36268.

6 (a) D. V. Partyka, T. J. Robilotto, J. B. Updegraff III, M. Zeller, A. D. Hunter, T. G. Gray, *Organometallics* **2009**, *28*, 795–801. (b) P. de Frémont, N. M. Scott, E. D. Stevens, S. P. Nolan, *Organometallics* **2005**, *24*, 2411–2418.

7 A. J. Ardeungo, H. V. R. Dias, J. C. Calabrese, F. Davidson, *Organometallics* **1993**, *12*, 3405–3409.

8 A. J. Arduengo, R. Krafczyk, R. Schmutzler, *Tetrahedron* **1999**, *55*, 14523–14534.

9 A. C. Hillier, W. J. Sommer, B. S. Yong, J. L. Petersen, L. Cavallo, S. P. Nolan, *Organometallics* **2003,** *22,* 4322–4326.

10 A. M. Magill, K. J. Cavell, B. F. Yates, *J. Am. Chem. Soc.* **2004**, *126*, 8717–8724.

11 (a) E. L. Kolychev, I. A. Portnyagin, V. V. Shuntikov, V. N. Khrustalev, M. S. Nechaev, *J. Organomet. Chem.* **2009**, *694*, 2454–2462 (b) M. Iglesias, D. J. Beetstra, J. C. Knight, L.-L. Ooi, A. Stasch, S. Coles, L. Male, M. B. Hursthouse,

K. J. Cavell, A. Dervisi, I. A. Fallis, *Organometallics* **2008**, *27*, 3279–3289.

12 W. A. Herrmann, S. K. Schneider, K. Öfele, M. Sakamoto, E. Herdtweck, *J. Organomet. Chem.* **2004**, *689*, 2441–2449.

13 N. Phillips, T. Dodson, R. Tirfoin, J. I. Bates, S. Aldridge, *Chem. Eur. J.* **2014**, *20*, 16721–16731.

14 See also Section 4.2.3.

15 C. A. Tolman, *Chem. Rev.* **1977**, *77*, 313–348.

16 H. Clavier, S. P. Nolan, *Chem. Commun.* **2010**, *46*, 841–861.

17 R. Dorta, E. D. Stevens, N. M. Scott, C. Costabile, L. Cavallo, C. D. Hoff, S. P. Nolan, *J. Am. Chem. Soc.* **2005**, *127*, 2485–2495.

18 (a) J. J. Dunsford, K. J. Cavell, B. M. Kariuki, *Organometallics* **2012**, *31*, 4118−4121. (b) P. de Frémont, N. M. Scott, E. D. Stevens, S. P. Nolan, *Organometallics* **2005**, 24, 2411–2418. (c) M. R. Fructos, T. R. Belderrain, P. de Frémont, N. M. Scott, S. P. Nolan, M. M. Díaz-Requejo, P. J. Pérez, *Angew. Chem.* **2005**, 117, 5418–5422.

19 (a) R. Tonner, G. Frenking, *Organometallics* **2009**, *28*, 3901–3905. (b) M. Iglesias, D. J. Beetstra, A. Stasch, P. N. Horton, M. B. Hursthouse, S. J. Coles, K. J. Cavell, A. Dervisi, I. A. Fallis, *Organometallics* **2007**, *26,* 4800–4809.

20 A. Bondi, *J. Phys. Chem.* **1964**, *68*, 441–451.

21 Cyclic alkyl(amino)carbenes extend this range by ~5 cm^{-1}. Abnormal, remote, and acyclic carbenes, and other synthetically intensive carbenes extend the range by up to 30 cm^{-1}. See ref. 1c.

22 A. M. Magill, K. J. Cavell, B. F. Yates, *J. Am. Chem. Soc.* **2004**, *126*, 8717–8724.

23 (a) J. J. Dunsford, D. S. Tromp, K. J. Cavell, C. J. Elsevierb. B. M. Kariuki, *Dalton Trans.* **2013**, *42*, 7318. (b) D. G. Gusev, *Organometallics* **2009**, *28*, 6458–6461.

24 J. W. Lauher, K. Wald, *J. Am. Chem. Soc.* **1981**, *103*, 7648–7650.

25 (a) G. A. Hutchings, M. Brust, H. Schmidbaur, *Chem. Soc. Rev.* **2008**, *37*, 1747–1758. (b) F. G. A. Stone, *Angew. Chem., Int. Ed.* **1984**, *23*, 89–99. (c) R. Hoffmann, *Angew. Chem., Int. Ed*. **1982**, *21*, 711–724. (d) M. Elian, M. M.-L. Chen, D. M. P. Mingos, R. Hoffmann, *Inorg. Chem.* **1976**, *15*, 1148–1155.

26 (a) P. Pyykkö, J. P. Desclaux, *Acc. Chem. Res.* **1979**, *12*, 276–281. (b) P. Pyykkö, *Angew. Chem., Int. Ed.* **2004**, *43*, 4412–4456. (c) P. Pyykkö, M. Patzschke, J. Suurpere, *Chem. Phys. Lett.* **2003**, *381*, 45–52.

27 H. G. Raubenheimer, H. Schmidbaur, *Organometallics* **2012**, *31*, 2507−2522.

28 (a) D. Nemcsok, K. Wichmann, G. Frenking, *Organometallics* **2004**, *23,* 3640–3646. (b) X. Hu, I. Castro-Rodriguez, K. Olsen, K. Meyer, *Organometallics* **2004**, *23,* 755–764.

CHAPTER 2

AN NHC-SUPPORTED DISILVER HYDRIDE

2.1 Background

Hydride complexes of the group 11 metals have excited considerable interest, in both their bonding and their reactivity. Copper hydride itself was first reported in 1844, but its existence and composition were controversial for decades.[1] Halpern and coworkers, studying the reduction of transition metal ions by dihydrogen, provided kinetic evidence for the formation of copper and silver hydride intermediates through a heterolytic mechanism.[2] Caulton and coworkers, studying model complexes for the catalytic hydrogenation of carbon monoxide, showed the remarkable hydrogenolysis of copper alkoxides to form (phosphine)copper(I) hydride clusters.[3] In the 1980s, Stryker and others began to demonstrate the versatility of such complexes in organic synthesis;[4] applications in synthesis,[5,6] and more recently in solar energy storage,[7] continue to emerge rapidly. Discrete gold hydride complexes are rare,[8] but appear relevant to gold-catalyzed reduction processes.[8b,c] Isolable silver hydride clusters have been described only recently by Liu, Saillard and co-workers.[9] We sought to explore the potential of silver hydrides, the least explored of the coinage metal hydride complexes, as platforms for carbon dioxide reduction under mild conditions.[10–12]

Silver hydride clusters have been studied in the gas phase by mass spectroscopy[13] and vibrational spectroscopy.[14] Polynuclear silver hydrides, formed through the chemisorption of hydrogen on silver-exchanged zeolites, have been characterized in the

solid state using magic-angle spinning (MAS) ^{1}H NMR spectroscopy.[15] The Ag_2H^+ fragment has been proposed as an intermediate in heterogeneous processes such as the activation of methane in zeolites[15a] and the coupling of allyl halides on silver surfaces.[16] Theoretical studies of Ag_2H^+ have produced divergent structural predictions, including both a linear $[Ag–H–Ag]^+$ arrangement[13a] and the three-center, two-electron system favored by more recent studies.[13b,14a,17]

A number of isolated complexes feature a hydride bridging between silver and another transition metal.[18] In cases where the other metal contains a spin-active nucleus, the magnitude of dipolar coupling between that nucleus and $^{107/109}$Ag often implies substantial metal–metal bonding. Recently Liu,[9] Saillard,[9a,c,e] Fackler[9b] and coworkers studied silver-only hydride clusters $[Ag_7H]$,[9a] $[Ag_8H]$[9b,d,e] and $[Ag_{11}(\mu^4\text{-}H)]$[9c] stabilized by dichalcogenophosphate[9a,c–e] or ethylenedithiolate[9b] ligands. Structural and NMR spectroscopic characterization show close contacts between the hydrides in these clusters and numerous silver atoms.

N-Heterocyclic carbene (NHC) ligands have been shown to stabilize a number of unusual hydride complexes of group 11 metals, including a copper(I) hydride dimer,[19] terminal gold(I) hydrides[8b,e] and a hydride-bridged digold cation.[8e] Numerous (NHC)silver complexes are known,[20] but in many of these the silver–carbon bond is labile, and carbene transfer between the silver centers readily forms $[(NHC)_2Ag]^+$ cations. Certain NHC ligands are slow to transfer from silver;[21] we expected that the use of a sufficiently inert ligand would inhibit the formation of homoleptic species, and allow the isolation of silver hydrides.

This chapter describes the synthesis of the dinuclear silver(I) hydride complexes $\{[(5Dipp)Ag]_2(\mu\text{-}H)\}^+X^-$, **1a,** [5Dipp = 1,3-bis-(2,6-diisopropylphenyl)imidazolin-2-ylidene; $X^- = CF_3SO_3^-$ or BF_4^-]. Structural and spectroscopic data suggest considerable three-center, two-electron bonding in the $[Ag_2H]^+$ core. Although generally inert, the disilver hydride cation reacts rapidly with a Lewis base adduct of carbon dioxide, a reaction with implications for potential catalytic reduction processes.

2.2 Results and Discussion

2.2.1 Synthesis and Structure of $\{[(5Dipp)Ag]_2(\mu\text{-}O^tBu)\}^+$ Salts

The starting complex (5Dipp)silver(I) chloride, **2**,[8e,20d] reacts readily with sodium *tert*-butoxide to form (5Dipp)silver(I) *tert*-butoxide, **3a**, (Scheme 2.1a).[22] Treatment of this complex with (5Dipp)AgOTf (**4**; OTf = trifluoromethanesulfonate, or triflate) results in formation of the *tert*-butoxide-bridged $\{[(5Dipp)Ag]_2(\mu\text{-}O^tBu)\}^+$ as its OTf^- salt (**5a**[OTf], Scheme 2.1b). Diffusion of hexanes into a THF solution of **5a**[OTf] affords crystals suitable for X-ray diffraction. The resulting structure (Figure 2.1) reveals a nearly trigonal arrangement about the oxygen, with an Ag–O–Ag angle of 122.4(1)°.[23] The silver centers are nearly linear, with C_{NHC}–Ag–O angles of 173.74(9)° and 170.77(9)°. The silver–silver distance is 3.6409(4) Å, more than twice the van der Waals radius of 1.72 Å.[24]

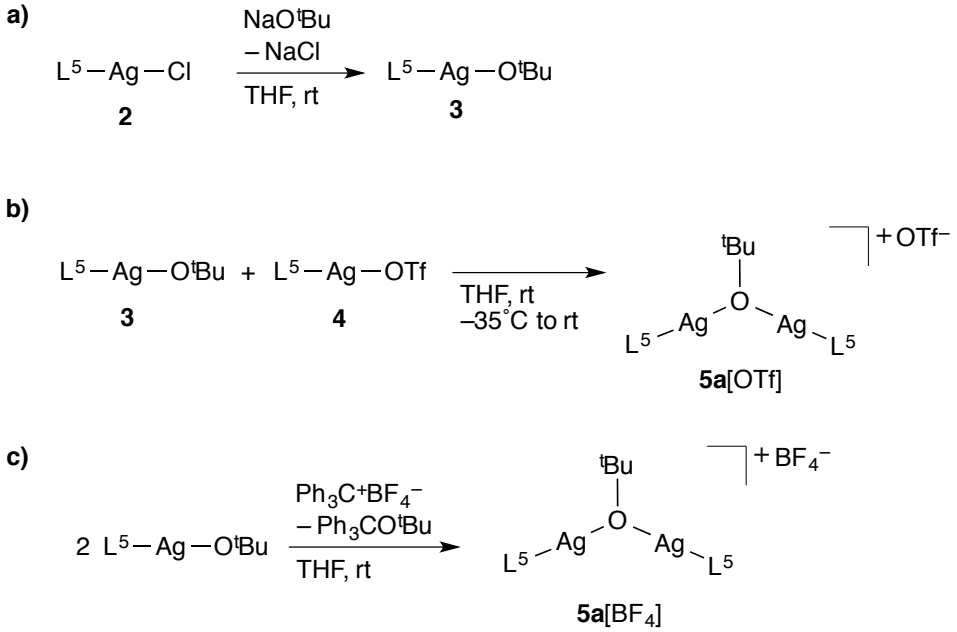

Scheme 2.1. Synthesis of *tert*-butoxide silver complexes **3**, **5a**[OTf], and **5a**[BF_4].

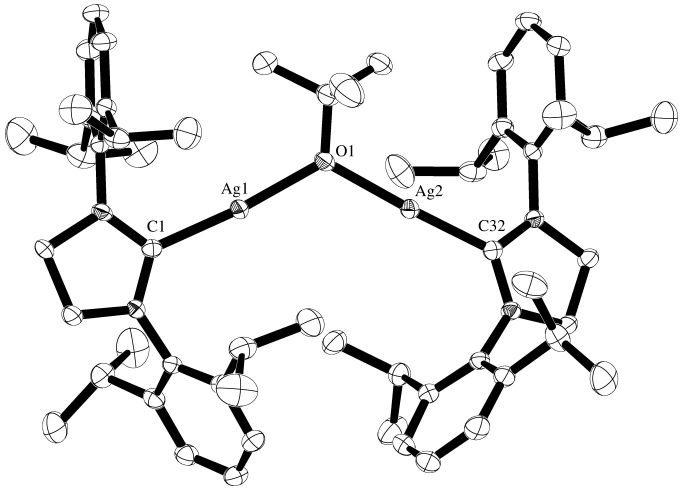

Figure 2.1. Solid-state structure of **5a**[OTf], 50% probability ellipsoids. Anion and co-crystallized solvent omitted for clarity. Selected interatomic distances (Å) and angles (deg): Ag(1)–Ag(2), 3.6409(5); Ag(1)–C(1), 2.066(2); Ag(1)–O(1), 2.080(2); Ag(2)–O(1), 2.076(2); Ag(2)–C(32), 2.061(2); C(1)–Ag(1)–O(1), 173.66(9); Ag(1)– O(1)–Ag(2), 122.3(1); O(1)–Ag(2)–C(32), 170.76(9).

The same cation may also be synthesized by treatment of the neutral silver alkoxide with a suitable Lewis acid. The reaction of (5Dipp)silver *tert*-butoxide with one-

half equivalent of $Ph_3C^+BF_4^-$ affords $\{[(5Dipp)Ag]_2(\mu\text{-}O^tBu)\}^+BF_4^-$, **5a**[$BF_4$], which is easily separated from the neutral byproduct Ph_3CO^tBu (Scheme 2.1c).[25]

2.2.2 Synthesis and Characterization of $[(5Dipp)Ag]_2(\mu\text{-}H)\}^+$ Salts

The reaction of **5a**[OTf] with phenylsilane (Scheme 2.2) proceeds smoothly in THF-d_8 solution, affording a single new 5Dipp-containing species as judged by ^{1}H NMR spectroscopy. The striking spectral feature of the product complex is an apparent triplet of triplets, each roughly 1:2:1, centerd at δ –1.13 ppm (δ –1.18 ppm in CD_2Cl_2), suggesting the formation of a hydride-bridged disilver cation. Integration of this multiplet relative to the 5Dipp ligand resonances is consistent with the formation of a product complex $\{[(5Dipp)Ag]_2(\mu\text{-}H)\}^+OTf^-$ (**1a**[OTf]). The tetrafluoroborate salt $\{[(5Dipp)Ag]_2(\mu\text{-}H)\}^+BF_4^-$, **1a**[$BF_4$] is likewise formed by reaction of **5a**[BF_4] with phenylsilane; its ^{1}H NMR spectrum is essentially identical to that of **1a**[OTf].

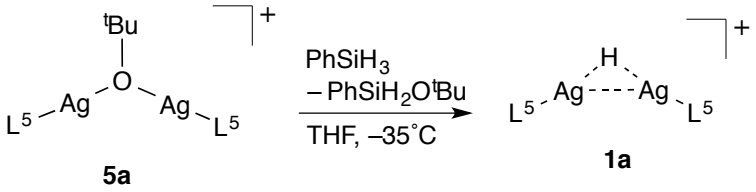

5a 1a

Scheme 2.2. Synthesis of hydride-bridged disilver cation **1a**.

The observed pattern arises from the superimposition of three resonances, each that of an isotopologue in which the hydrogen couples to two silver centers (Figure 2.2a). Naturally occurring silver consists of *ca.* 52% ^{107}Ag and 48% ^{109}Ag, each with a nuclear spin of ½.[26] A hydride-bridged disilver cation therefore comprises a mixture of roughly 1:2:1 (27:50:23) of [^{107}Ag–H–^{107}Ag], [^{107}Ag–H–^{109}Ag] and [^{109}Ag–H–^{109}Ag]. Given

inequivalent J_{H-Ag} coupling constants, each homonuclear isotopologue gives rise to a 1:2:1 triplet, with the central peaks coincident. In the heteronuclear isotopologue, the resonance for the hydride is split into a doublet by the ^{109}Ag nucleus, then further into a doublet of doublets by the ^{107}Ag nucleus.

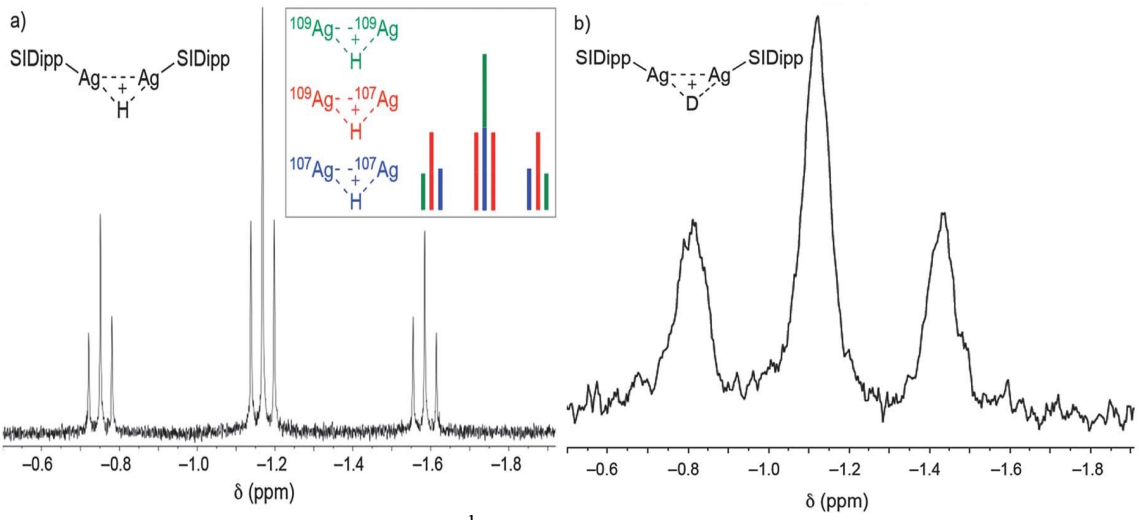

Figure 2.2. (a) Hydride region of ^{1}H NMR spectrum for **1a**[BF_4] in CD_2Cl_2 solution. Inset: interpretation of signals from each isotopologue. (b) Deuteride region of ^{2}H NMR spectrum for **1a**-*d*[BF_4] in CD_2Cl_2 solution.

The measured $^{1}J_{H-Ag}$ values are 134 Hz and 116 Hz, directly proportional to the gyromagnetic ratios of ^{109}Ag and ^{107}Ag. Well-resolved coupling to ^{107}Ag and ^{109}Ag has been observed in the ^{13}C NMR spectra of (NHC)silver complexes,[20d,21b] and in the ^{1}H NMR spectra of heteronuclear Ag–H–M clusters.[18] In the fluxional silver hydride clusters reported by Liu, Saillard and coworkers, multiplet resonances reflect averaged silver–hydrogen coupling constants, but decoupling experiments establish the ^{1}H–^{107}Ag and ^{1}H–^{109}Ag coupling constants separately.[9]

We prepared the deuteride-bridged analogue of **1a**[BF_4], **1a**-*d*[BF_4], by reaction of **5a**[BF_4] with $PhSiD_3$.[27] Comparing the infrared spectra of **1a**[BF_4] and **1a**-*d*[BF_4], we

could discern no obvious silver–hydrogen or silver–deuterium stretching bands (Figure 2.17). However, the ^{1}H NMR spectrum of **1a**-*d*[BF_4] is identical to that of **1a**[BF_4] except for the absence of the hydride resonance. The ^{2}H NMR spectrum of **1a**-*d*[BF_4] (Figure 2.2b) displays a triplet resonance at δ –1.12 ppm, with an observed ^{2}H–Ag coupling constant of 18.7 Hz. Broader linewidths and smaller coupling constants, relative to those in the ^{1}H NMR spectra of the hydride, do not permit differentiation between the ^{2}H–^{107}Ag and the ^{2}H–^{109}Ag coupling.

The ^{109}Ag NMR spectrum[28] of **1a**[OTf] displays an apparent doublet of triplets, actually a doublet superimposed on a doublet of doublets, centered at δ 519.3 ppm (Figure 2.3a). The [^{107}Ag–H–^{107}Ag] isotopologue gives rise to no signal. In the [^{109}Ag–H–^{109}Ag] isotopologue, the two silver nuclei are magnetically equivalent, and their resonance is split into a doublet by the bridging hydrogen. In the [^{109}Ag–H–^{107}Ag] isotopologue, the signal for the ^{109}Ag nucleus is split into a doublet by the hydrogen, then into a doublet of doublets by the ^{107}Ag nucleus. This analysis confirms the assignment of the ^{109}Ag–^{1}H coupling constant as 134 Hz, and provides the ^{109}Ag–^{107}Ag coupling constant of 113 Hz. In the ^{109}Ag NMR spectrum of **1a**-*d*[BF_4] (Figure 2.3b), coupling between ^{109}Ag and ^{2}H (nuclear spin = 1) gives rise to a 1:1:1 triplet, which ^{107}Ag splits into a 1:1 doublet of 1:1:1 triplets. This pattern reflects the large ^{109}Ag–^{107}Ag coupling and the smaller ^{109}Ag–^{2}H coupling. In contrast, the ^{109}Ag NMR spectrum of the *tert*-butoxide-bridged **5a**[OTf] shows a singlet resonance at δ 541.4 ppm: no coupling is observed between ^{109}Ag and ^{107}Ag. The magnitude of silver–silver coupling in **1a**[OTf] suggests a significant bonding interaction.[29]

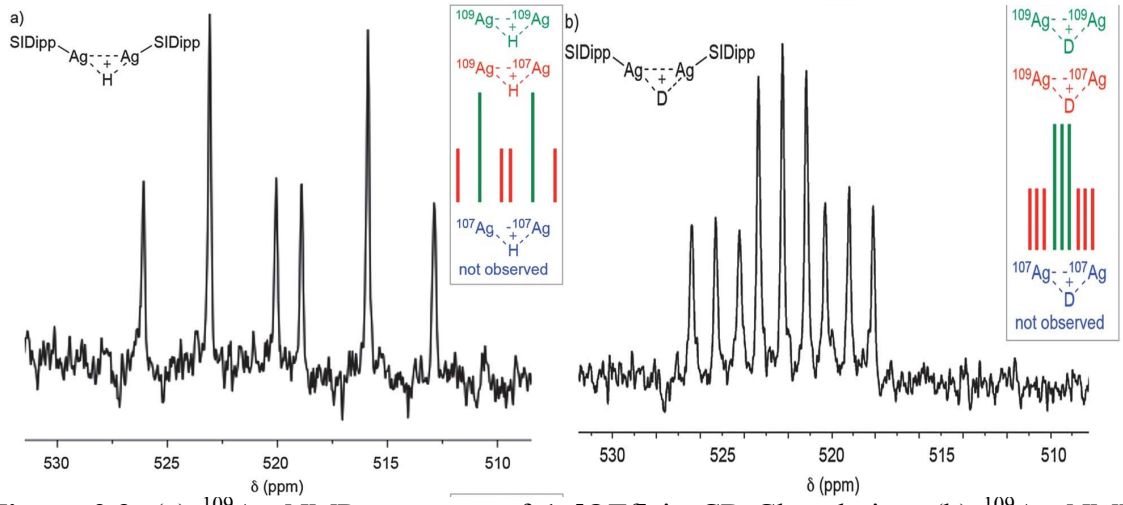

Figure 2.3. (a) ^{109}Ag NMR spectrum of **1a**[OTf] in CD_2Cl_2 solution. (b) ^{109}Ag NMR spectrum of **1a**-*d*[BF_4] in CD_2Cl_2 solution. Insets: interpretation of signals from each isotopologue.

Slow diffusion of pentane into a THF solution of **1a**[OTf] afforded crystals suitable for X-ray diffraction. Complex **1a**[OTf] crystallizes in the *P*21/*c* space group, with two disordered THF molecules in the asymmetric unit. Both solvent molecules and the triflate anion are located well outside the metal coordination spheres.

The solid-state structure (Figure 2.4) shows a notably short silver–silver distance of 2.8087(4) Å, suggesting the contribution of a three-center, two-electron bond to the description of the $[Ag_2H]^+$ core. The silver-bound hydride was located, and the silver–hydrogen distances were found to be 1.69(4) Å and 1.71(3) Å. For $[Ag_2H]^+$ in the gas phase, DeKock and coworkers calculated a silver–silver distance of 2.86 Å, with silver–hydrogen distances of 1.69 Å.[13b] In a gold analogue of **1a**[OTf], $\{[(IDipp)Au]_2(\mu\text{-}H)\}^+OTf^-$ (IDipp = 1,3-bis(2,6-diisopropylphenyl)imidazol-2-ylidene), the hydride could not be located, but the gold–gold distance of 2.7099(4) Å likewise implied considerable metal–metal bonding.[8e] The silver–carbon distances, 2.108(3) Å and 2.104(3) Å, are slightly longer than those in *tert*-butoxide-bridged **5a**[OTf].

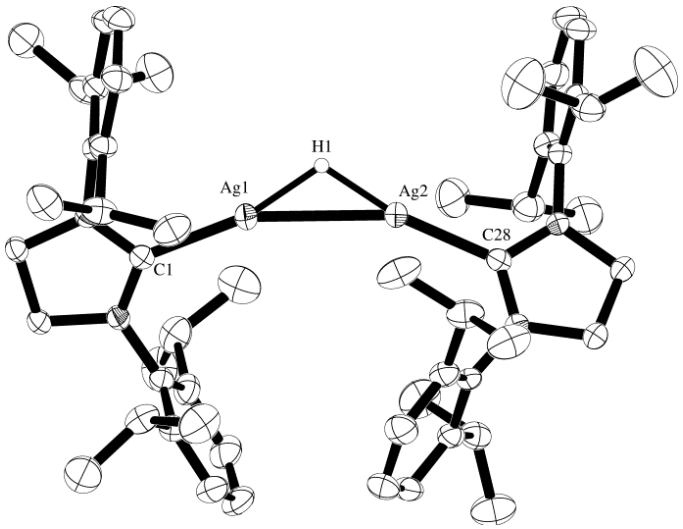

Figure 2.4. Solid-state structure of **1a**[OTf], 50% probability ellipsoids. Anion and co-crystallized solvent omitted for clarity. Selected bond lengths (Å) and angles (˚): Ag(1)–C(1), 2.108(3); Ag(2)–C(28), 2.104(3); Ag(1)–Ag(2), 2.8087(4); Ag(1)–H(1), 1.69(4); Ag(2)–H(1), 1.71(3); C(1)–Ag(1)–Ag(2), 158.88(8); Ag(1)–Ag(2)–C(28), 155.46(8); C(1)–Ag(1)–H(1), 166(1); C(28)–Ag(2)–H(1), 170(1).

2.2.3 Stability and Reactivity of $\{[(5Dipp)Ag]_2(\mu\text{-}H)\}^+$ Salts

The $\{[(5Dipp)Ag]_2(\mu\text{-}H)\}^+$ salts **1a**[OTf] and **1a**[BF_4] are soluble in THF and show moderate stability at ambient temperature. In THF-d_8 solution after 24 hours, ^{1}H NMR spectroscopy indicates 54% decomposition to salts of the homoleptic $[(5Dipp)_2Ag]^+$, with a peak for dihydrogen at δ 4.55 ppm,[30] and a silver mirror is visible on the inner wall of the NMR tube. Decomposition occurs more slowly in CD_2Cl_2 solution, to the extent of roughly 8% after 24 h, and produces a new, as yet unidentifed 5Dipp-containing species as well as those observed previously. No (5Dipp)AgCl, potentially formed by reaction with CD_2Cl_2, is observed after several weeks. In contrast, the *tert*-butoxide-bridged cation **5a** forms significant (7%) (5Dipp)AgCl after three hours in CD_2Cl_2 solution, and the more basic (5Dipp)AgO^tBu decomposes quantitatively within minutes.

The observed decomposition of $\{[(5Dipp)Ag]_2(\mu\text{-}H)\}^+$ is consistent with solvent-assisted dissociation of the cluster to form an unstable terminal hydride (5Dipp)AgH, not observed, plus the solvated cation $[(5Dipp)Ag(solv)]^+$. Several efforts to prepare the terminal hydride independently led to rapid decomposition. Moreover, **1a**[OTf] and **1a**[BF_4] decompose completely within hours in CD_3CN solution, or in CD_2Cl_2 solution in the presence of added triphenylphosphine (1 equiv.). These observations are consistent with a Lewis-base-assisted decomposition pathway (Scheme 2.3), in which a Lewis base, B, coordinates to **1a**, forming a terminal hydridosilver complex (Scheme 2.3a), which undergoes bimolecular disproportionation to produce hydrogen, elemental silver, and free 5Dipp (Scheme 2.3b). Free 5Dipp then displaces the weaker Lewis base or coordinated solvent, forming the observed decomposition product $[(5Dipp)_2Ag]^+$ (Scheme 2.3c). This results in an overall process characterized by the formation of $[(5Dipp)_2Ag]^+$, elemental silver, and hydrogen (Scheme 2.3.d). Interestingly, **1a** does not react with D_2O to produce H–D (Scheme 2.3e), although D_2O can act as a Lewis base to facilitate decomposition.

Solutions of **1a**[OTf] and **1a**[BF_4] in CD_2Cl_2 exhibit only partial decomposition, 25% in 24 h, after exposure to the atmosphere. The addition of a drop of D_2O to these solutions did not greatly affect the decomposition: the same products were formed, the rate was similar (33% after 24 h), and the only form of dihydrogen observed by ^1H NMR spectroscopy was $^1H_2$. The 1:1:1 triplet resonance of H–D,[31] which would arise from direct deuterolysis of the hydride, was not observed.

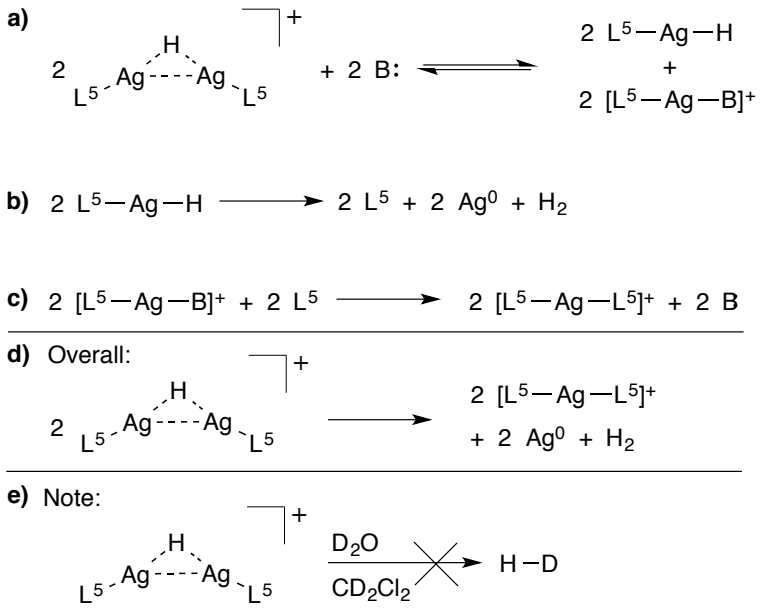

Scheme 2.3. Possible sequence for decomposition of **1a**. (a) Lewis base, B, coordinates to silver, forming a terminal hydridosilver complex. (b) Terminal hydridosilver complex undergoes bimolecular disproportionation, producing hydrogen, elemental silver, and free 5Dipp. (c) Free 5Dipp displaces the weaker Lewis base, forming the observed decomposition product $[(5Dipp)_2Ag]^+$. (d) The overall decomposition reaction. (e) **1a** does not react with D_2O to produce H–D; however, D_2O does increase the rate of Lewis-base-assisted decomposition.

Next we examined the reactivity of the cationic disilver hydride with various carbonyl-containing substrates. No reaction was observed between **1a**[BF_4] and benzaldehyde or benzophenone in CD_2Cl_2 solution at ambient temperature, and gradual decomposition was observed on heating. Exposure of **1a**[BF_4] in CD_2Cl_2 solution to an atmosphere of ^{13}C-labeled carbon dioxide led to a very slow reaction (Scheme 2.4a), accompanied by considerable decomposition. The key new feature in the spectrum was a doublet resonance centerd at δ 8.0 ppm ($^1J_{C–H}$ = 195 Hz), and a set of 5Dipp resonances integrating to two ligands for each newly formed C–H bond. The ^{13}C NMR spectrum of the reaction mixture, obtained without the use of decoupling, showed a doublet resonance at δ 167.9 ppm ($^1J_{C–H}$ = 194 Hz). These resonances are consistent with the assignment of

this species as a formate-bridged disilver complex. The reaction was highly incomplete, with roughly 5% conversion after four days.

Reduction to formic acid derivatives represents an important method for catalytic carbon dioxide fixation.[10] The key step in such catalysis, the net addition of H^- to CO_2 to produce a metal formate, occurs for a variety of metal hydrides.[32] Mechanistic studies and computations show that this reaction depends on the Lewis-basic character of the hydride,[33] and so the observation of any C–H bond formation between CO_2 and the rather inert **1a** was surprising. This process was clearly impractical, however, in light of the low conversion and accompanying decomposition over long reaction times.

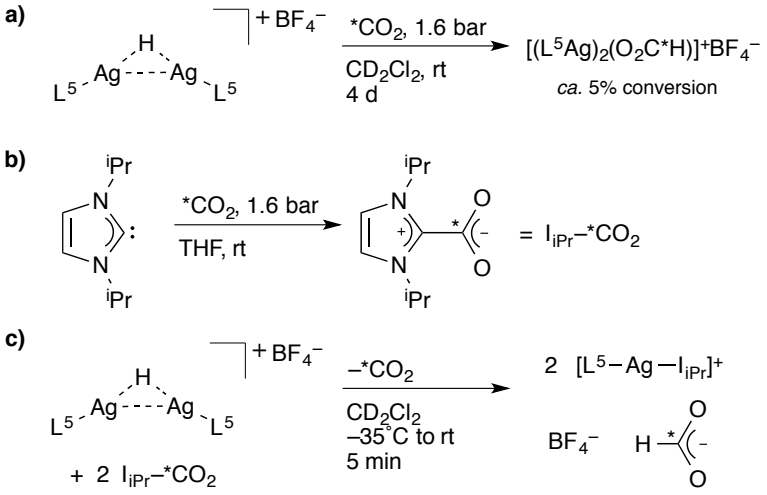

Scheme 2.4. Reactions of **1a** with CO_2. (a) Reaction of **1a** with free CO_2. (b) Formation of NHC–CO_2 adduct. (c) Reaction of **1a** with NHC–CO_2 adduct.

Reasoning that the sluggishness of this reaction stemmed from the poor Lewis basicity of the cationic disilver hydride toward the Lewis-acidic CO_2, we examined the reaction between **1a**[BF_4] and a Lewis-basic derivative of CO_2, the imidazolium-2-carboxylate formed by the reversible reaction of a free NHC with CO_2 (Scheme 2.4b).

Such NHC–CO_2 adducts are key intermediates in the transition-metal-free NHC-catalyzed reduction of CO_2 with silanes.[11k,o] The reduction of an NHC–CO_2 adduct by a late transition metal hydride, in which the metal centers form far weaker bonds to oxygen than does silicon, would represent a step toward catalytic processes using milder reducing agents.

Addition of 1,3-diisopropylimidazolium-2-^{13}C-carboxylate[34] (I_{iPr}–$^{13}CO_2$) to a solution of **1a**[BF_4] in CD_2Cl_2, precooled to –35˚C and containing 4,4′-dimethylbiphenyl as an internal standard, led to visible evolution of gas within one minute after mixing. The resulting solution was allowed to warm to ambient temperature, and its ^{1}H NMR spectrum was recorded five minutes after carboxylate addition. This spectrum showed the complete consumption of the starting hydride, and the formation of a new 5Dipp-containing complex, accounting for 95% of the starting 5Dipp as judged by integration relative to the internal standard. The appearance of a doublet resonance centered at δ 8.67 ppm, with $^1J_{C–H}$ = 178 Hz, is consistent with the conversion of one equivalent of CO_2 to the formate anion, HCO_2^-. The ^{13}C NMR spectrum, recorded immediately afterward, likewise displayed a strong doublet resonance (δ 167 ppm, $^1J_{C–H}$ = 178 Hz) assigned to the formate anion. The ^{1}H NMR resonances for the new silver complex are identical to those of [(5Dipp)Ag(I_{iPr})]$^+BF_4^-$ prepared independently, suggesting that the formate ion interacts weakly, if at all, with the silver center in solution.

A balanced reaction between **1a**[BF_4] and I_{iPr}–$^{13}CO_2$ to form [(5Dipp)Ag(I_{iPr})]$^+$ and formate should release half of the NHC-bound $^{13}CO_2$ (Scheme 2.4c). The signal for free CO_2 is not observed in the ^{13}C NMR spectrum of the reaction mixture at ambient temperature. Because [(5Dipp)Ag(I_{iPr})]$^+$ is formed nearly quantitatively, we believe that

most of the liberated CO_2 is present in the headspace of the NMR tube; a spectrum obtained after cooling the tube to –78˚C showed a singlet resonance at δ 125.1 ppm. A maximum conversion of 50% is of course undesirable in a stoichiometric reduction of CO_2, but the incorporation of this reaction into a catalytic cycle would lead to recapture of the lost CO_2 as the reaction proceeded. Studies of possible catalytic turnover steps are currently underway (see Chapters 4 and 5).

2.3 Conclusion

The hydride-bridged disilver cation, studied in the gas phase and implicated in heterogeneous catalytic processes, has been stabilized using an N-heterocyclic carbene ligand. The core of this complex adopts a triangular structure, with a silver–silver distance shorter than that of silver metal. Strong dipolar coupling between silver nuclei is observed using ^{109}Ag NMR spectroscopy, further suggesting silver–silver bonding consistent with a three-center, two-electron bond. The disilver hydride cation reacts extremely slowly with an atmosphere of carbon dioxide. The addition of carbon dioxide in the form of a Lewis base adduct, reversing the polarity of the substrate, leads to rapid hydride transfer without the concomitant formation of a metal–oxygen bond. This process is being studied as a key step in potential catalytic cycles.

2.4 Experimental

2.4.1 General Considerations

Unless otherwise indicated, manipulations were performed in an MBraun glovebox under an inert atmosphere of nitrogen, or in sealable glassware on a Schlenk line under an atmosphere of argon. Glassware and magnetic stir bars were dried in a

ventilated oven at 160˚C and were allowed to cool under vacuum. Compounds of silver were stored in the dark as a precaution against photodegradation, and glassware was covered with aluminum foil during manipulations to minimize exposure to light.

Dichloromethane (BDH), diethyl ether (EMD Millipore Omnisolv), hexane (EMD Millipore Omnisolv), tetrahydrofuran (THF, EMD Millipore Omnisolv), and toluene (EMD Millipore Omnisolv) were sparged with ultra high purity argon (NexAir) for 30 minutes prior to first use, dried using an MBraun solvent purification system, transferred to Straus flasks, degassed using three freeze-pump-thaw cycles, and stored under nitrogen or argon. Anhydrous benzene (EMD Millipore Drisolv) and anhydrous pentane (EMD Millipore Drisolv), both sealed under a nitrogen atmosphere, were used as received and stored in a glovebox. Tap water was purified in a Barnstead International automated still prior to use.

Dichloromethane-d_2 (Cambridge Isotope Labs) and acetonitrile-d_3 (Cambridge Isotope Labs) were dried over excess calcium hydride overnight, vacuum-transferred to an oven-dried sealable flask, and degassed by successive freeze-pump-thaw cycles. Tetrahydrofuran-d_8 (Cambridge Isotope Labs) was dried over sodium benzophenone ketyl, vacuum-transferred to an oven-dried sealable flask, and degassed by successive freeze-pump-thaw cycles. Deuterium oxide (Cambridge Isotope Labs), chloroform-*d* (Cambridge Isotope Labs), and methanol-d_1 (Cambridge Isotope Labs) were used as received.

Sodium *tert*-butoxide (TCI America), potassium *tert*-butoxide (Alfa-Aesar), silver trifluoromethanesulfonate (Alfa-Aesar), silver nitrate (Alfa-Aesar), triphenylcarbenium tetrafluoroborate (Alfa-Aesar), sodium trimethylsilanolate (Sigma-Aldrich),

tetrafluoroboric acid (50% w/w aqueous solution, Sigma-Aldrich), 1,3-diisopropylimidazolium chloride (Sigma-Aldrich), 1,3-diisopropylimidazolium tetrafluoroborate (Sigma-Aldrich), trichlorophenylsilane (Sigma-Aldrich), lithium aluminum deuteride (Sigma-Aldrich), magnesium sulfate (Alfa-Aesar), sodium metal (Alfa-Aesar), benzophenone (Alfa-Aesar), calcium hydride (Alfa-Aesar), $^{13}CO_2$ (Cambridge Isotope Labs), potassium bromide (anhydrous, spectroscopic grade, Sigma-Aldrich), nitrogen (NexAir), and argon (both industrial and ultra high purity grades, NexAir) were used as received. Phenylsilane (Sigma-Aldrich) was degassed using three freeze-pump-thaw cycles prior to use. 5Dipp·HCl·$(EtO)_3CH$[35] and (5Dipp)AgCl[36] were prepared according to literature protocols and were characterized by ^{1}H NMR spectroscopy. Phenylsilane-d_3 was prepared by the reaction of trichlorophenylsilane with lithium aluminum deuteride in analogy to a published protocol for the preparation of alkylsilanes.[37] *N,N*-Dimethylanilinium tetrafluoroborate was prepared according to a published procedure.[38]

^{1}H, ^{2}H, ^{13}C, and ^{109}Ag NMR spectra were obtained using a Bruker DSX 400 MHz spectrometer, and ^{19}F NMR spectra were obtained using a Varian Vx 400 MHz spectrometer. ^{1}H and ^{13}C NMR chemical shifts are referenced with respect to solvent signals[30] and are reported relative to tetramethylsilane. ^{2}H NMR chemical shifts are referenced to solvent signals, with the assumption that the ^{2}H chemical shifts of deuterated solvents are identical to the ^{1}H chemical shifts of their protiated isotopologues. ^{109}Ag NMR chemical shifts were referenced with respect to an external solution of 4.00 M silver nitrate (Alfa-Aesar) in deuterium oxide (defined as δ 0 ppm). ^{19}F NMR chemical

shifts were referenced to external neat hexafluorobenzene (Alfa-Aesar, δ −164.90 ppm) and are reported with respect to trichlorofluoromethane.

Samples for infrared spectroscopy were prepared as pellets in potassium bromide, using a pellet die which was dried in a ventilated oven at 160˚C and cooled under vacuum prior to use. The pellets were prepared in the glovebox under an atmosphere of dry nitrogen, and were exposed to air as briefly as possible prior to data collection. Spectra were recorded using a Perkin Elmer Spectrum 1000 infrared spectrometer.

Elemental analyses were performed by Atlantic Microlab in Norcross, Georgia.

2.4.2 Synthetic Procedures

2.4.2.1 (5Dipp)Ag(O^{t}Bu) (**3a**)

(5Dipp)Ag(O^{t}Bu) was prepared by a modification of the reported procedure.[39] Sodium *tert*-butoxide (0.360 g, 3.74 mmol) was added to a suspension of (5Dipp)AgCl (2.000 g, 3.746 mmol) in THF (10 mL) with stirring. The reaction flask was covered with foil to exclude light. After stirring for 2 hours, the reaction mixture was filtered through Celite, and the filter pad was washed with two portions of THF (5 mL each). The solvent was removed from the filtrate under vacuum, and the residue was dried in the dark for 16 hours at 40˚C under vacuum, affording the product as a white powder (2.283 g, 3.47 mmol, 93%). In anhydrous CH_2Cl_2, (5Dipp)Ag(O^{t}Bu) rapidly decomposes to (5Dipp)AgCl and *tert*-butanol. The product hydrolyzes readily in the presence of atmospheric moisture. ^{1}H NMR (400 MHz, THF-d_8): δ (ppm) 7.35 (t, J = 7.8 Hz, 2H, *para*-C*H*), 7.26 (d, J = 7.8 Hz, 4H, *meta*-C*H*), 4.06 (s, 4H, NCH_2), 3.15 (sept, J = 6.9 Hz, 4H, C*H*(CH$_3$)$_2$), 1.35 (d, J = 6.9 Hz, 12H, CH(CH_3)$_2$), 1.31 (d, J = 6.9 Hz, 12H, CH(CH_3)$_2$), 0.66 (s, 9H, OC(CH_3)$_3$). ^{13}C{^{1}H} NMR (100 MHz, THF-d_8): δ (ppm) 209.0

(app dd, $J(^{13}C\text{-}^{109}Ag)$, = 218 Hz, $J(^{13}C\text{-}^{107}Ag)$ = 190 Hz, N*C*Ag), 147.5 (*ortho-C*), 136.4 (*ipso-C*), 129.9 (*para-C*), 124.9 (*meta-C*), 68.5 (O*C*$(CH_3)_3$), 54.5 (d, $J(^{13}C\text{-Ag})$, = 7 Hz, N*C*H_2), 37.13 (OC(*C*$H_3)_3$), 29.3 (*C*H$(CH_3)_2$), 25.5 (CH(*C*$H_3)_2$), 24.2 (CH(*C*$H_3)_2$). ^{109}Ag NMR (18.6 MHz, THF-d_8): δ (ppm) 677.2 (s). IR: ν (cm^{-1}) 3071 (w), 2981 (s), 2930, 2870, 1941 (w), 1871 (w), 1800 (w), 1706 (w), 1655 (w), 1489 (s), 1467 (s), 1459 (s), 1384, 1388, 1342, 1327, 1274 (s), 1249, 1216, 1190 (s), 1180, 1116, 1103, 1060, 1017, 961 (s), 935, 913, 878, 804 (s), 757 (s), 711, 620, 563, 547, 516, 445. Elemental analysis calculated for $C_{31}H_{47}N_2AgO$: C, 65.14; H, 8.29; N, 4.90. Found: C, 64.54; H, 8.13; N, 4.59. Note: Attempts to purify this complex further, via filtration or recrystallization, have failed to result in satisfactory carbon analyses. Both complexes prepared directly from this one, **1**[OTf] and **1**[BF_4], were nonetheless isolated in analytically pure form. The purity of the (5Dipp)Ag(O^{t}Bu) reported here is unsatisfying, but sufficient for practical purposes.

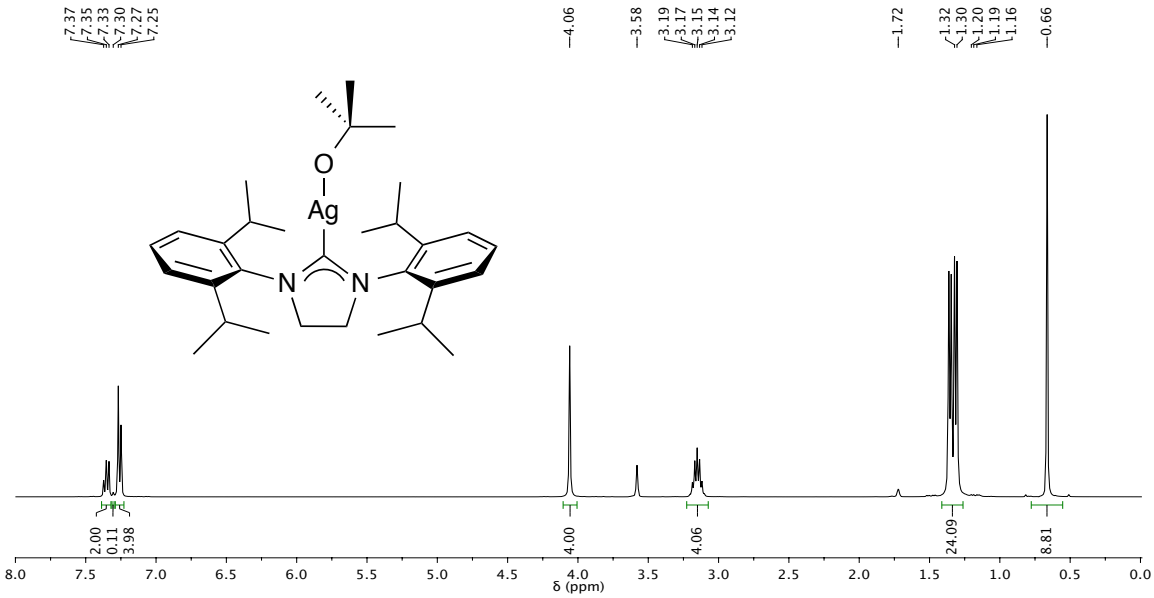

Figure 2.5. ^{1}H NMR (400 MHz, THF-d_8) spectrum of (5Dipp)Ag(O^{t}Bu). A trace of benzene (δ 7.30 ppm)[30] is present as the result of benzophenone ketyl decomposition.

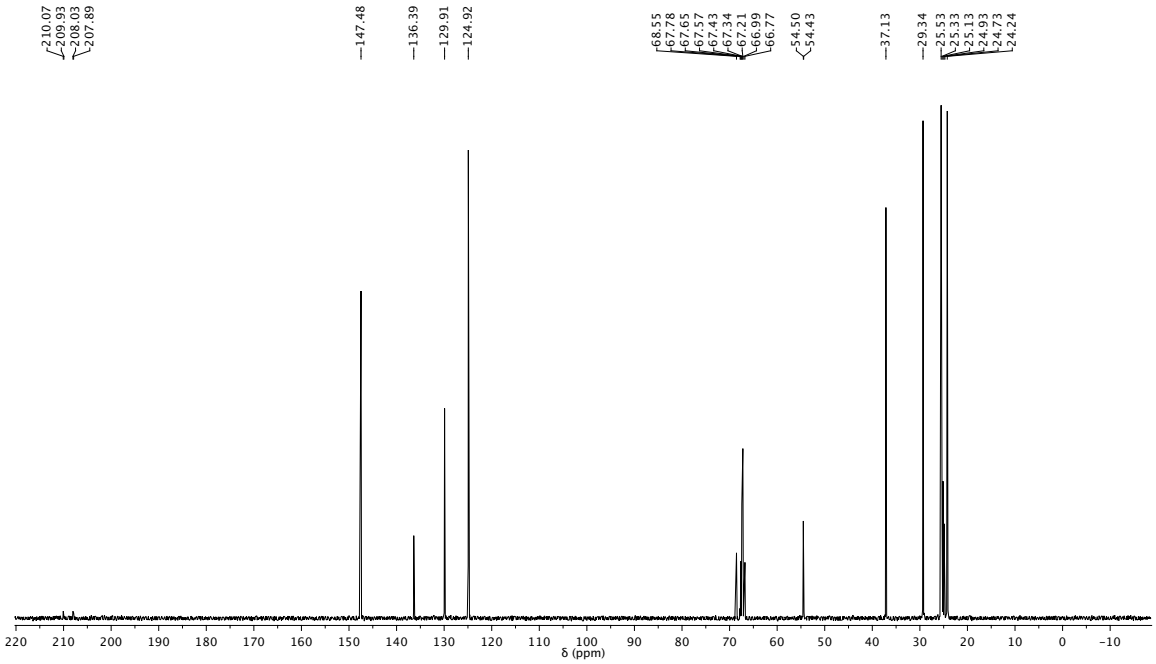

Figure 2.6. $^{13}C\{^{1}H\}$ NMR (100 MHz, THF-d_8) spectrum of (5Dipp)Ag(O^{t}Bu).

2.4.2.2 (5Dipp)AgOTf (**4**)

(5Dipp)AgOTf was prepared by a procedure analogous to that reported for [1,3-bis(2,6-diisopropylphenyl)imidazole-2-ylidene]gold(I) trifluoromethanesulfonate.[40] A solution of silver trifluoromethanesulfonate (0.962 g, 3.74 mmol) in THF (2 mL) was added to a suspension of (5Dipp)AgCl (2.000 g, 3.746 mmol) in THF (15 mL). The reaction flask was covered with foil to exclude light, and the mixture was stirred at room temperature for 1 hour, producing a white silver chloride precipitate. The precipitate was removed by filtration through Celite, and the filter pad was rinsed with two portions of THF (5 mL each). The solvent was removed from the filtrate under vacuum, and the residue was dried in the dark at 40˚C for 4 hours under vacuum, affording the product as a white powder (2.164 g, 3.342 mmol, 89%). ^{1}H NMR (400 MHz, CD_2Cl_2): δ (ppm) 7.45 (t, J = 7.8 Hz, 2H, *para*-C*H*), 7.28 (d, J = 7.8 Hz, 4H, *meta*-C*H*), 4.11 (s, 4H, NCH_2),

3.02 (sept, J = 6.9 Hz, 4H, C*H*(CH_3)$_2$), 1.34 (d, J = 6.9 Hz, 12H, CH(C*H*$_3$)$_2$), 1.25 (d, J = 6.9 Hz, 12H, CH(C*H*$_3$)$_2$). $^{13}C\{^1H\}$ NMR (100 MHz, CD_2Cl_2): δ (ppm) 205.3 (app dd, J(^{13}C-^{109}Ag), = 304 Hz, J(^{13}C-^{107}Ag) = 264 Hz, N*C*Ag), 147.1 (*ortho-C*), 134.7 (*ipso-C*), 130.4 (*para-C*), 125.1 (*meta-C*), 120.4 (q, J(^{13}C-^{19}F) = 320 Hz, O_3SCF_3), 54.5 (d, J(^{13}C-Ag), = 10 Hz, N*C*H$_2$), 29.1 (*C*H(CH_3)$_2$), 25.5 (CH(*C*H$_3$)$_2$), 24.2 (CH(*C*H$_3$)$_2$). ^{19}F NMR (375 MHz, CD_2Cl_2): δ (ppm) −76.9 (s). ^{109}Ag NMR (18.6 MHz, CD_2Cl_2): δ (ppm) 386.7 (s). IR: ν (cm^{-1}) 3071 (w), 2981 (s), 2930, 2870, 1590, 1491 (s), 1467 (s), 1460 (s), 1384, 1364, 1342, 1327, 1274 (s), 1233 (s), 1205 (s), 1170 (s), 1061, 1018 (s), 936, 915, 808 (s), 760 (s), 709, 637 (s), 620, 580, 569, 548, 515, 447. Elemental analysis calculated for $C_{28}H_{38}N_2AgF_3O_3S$: C, 51.93; H, 5.91; N, 4.33. Found: C, 51.73; H, 5.91; N, 4.27.

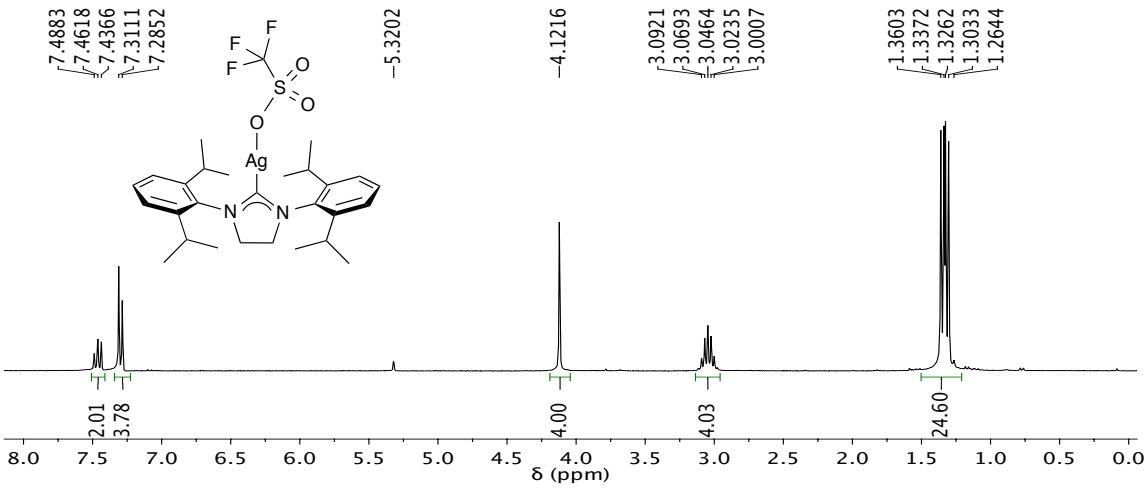

Figure 2.7. ^{1}H NMR (400 MHz, CD_2Cl_2) spectrum of (5Dipp)AgOTf.

2.4.2.3 {[(5Dipp)Ag]$_2$(μ-O^{t}Bu)}$^+$[OTf]$^-$ (**5a**[OTf])

A solution of (5Dipp)AgOTf (0.650 g, 1.00 mmol, 1.00 equiv) in 3 mL THF and a solution of (5Dipp)Ag(O^{t}Bu) (0.600 g, 1.05 mmol, 1.05 equiv) in THF (3 mL) were cooled to −35˚C. The (5Dipp)Ag(O^{t}Bu) solution was added via pipette to the

(5Dipp)AgOTf solution with stirring, and the reaction flask was covered with foil to exclude light. The reaction mixture was allowed to warm to room temperature. After 20 minutes, a layer of toluene (19 mL) was carefully added above the THF solution. The THF and toluene layers were allowed to mix by diffusion at −35˚C for 10 hours, resulting in the formation of colorless crystals. The mother liquor was decanted. Two portions of toluene (5 mL each) were successively added to the residue and decanted. The residue was dissolved in THF (3 mL) and the product was precipitated by the addition of pentane (15 mL). The precipitate was collected on a fritted glass filter and was washed with three portions of pentane (5 mL each). The filtrand was dried in the dark under vacuum at 40˚C for 16 hours, affording the product as a white powder (0.971 g, 0.796 mmol, 80%). The product hydrolyzes readily in the presence of atmospheric moisture. ^{1}H NMR (400 MHz, THF-d_8): δ (ppm) 7.39 (t, J = 7.8 Hz, 4H, *para*-C*H*), 7.23 (d, J = 7.8 Hz, 8H, *meta*-C*H*), 4.15 (s, 8H, NCH_2), 3.08 (sept, J = 6.9 Hz, 8H, C*H*(CH_3)$_2$), 1.29 (d, J = 6.9 Hz, 24H, CH(CH_3)$_2$), 1.11 (d, J = 6.9 Hz, 24H, CH(CH_3)$_2$), 0.31 (s, 9H, O(CH_3)$_3$). ^{13}C{^{1}H} NMR (100 MHz, THF-d_8): δ (ppm) 205.3 (app dd, J(^{13}C-^{109}Ag) = 265 Hz, J(^{13}C-^{107}Ag) = 229 Hz, N*C*Ag), 147.5 (*ortho*-*C*), 136.1 (*ipso*-*C*), 130.2 (*para*-*C*), 125.1 (*meta*-*C*), 122.4 (q, J(^{13}C-^{19}F) = 321.4 Hz, O_3SCF_3), 72.2 (O*C*(CH_3)$_3$, 55.0 (d, J(^{13}C-Ag), = 9 Hz, N*C*H_2), 29.1 (*C*H(CH_3)$_2$), 25.6 (CH(*C*H_3)$_2$), 24.0 (CH(*C*H_3)$_2$). ^{19}F NMR (375 MHz, THF-d_8): δ (ppm) −77.6 (s). ^{109}Ag NMR (18.6 MHz, THF-d_8): δ (ppm) 541.4 (s). IR: ν (cm^{-1}): 3071 (w) 2964 (s), 2926, 2870, 1591 (w), 1492 (s), 1460 (s), 1384, 1363, 1327, 1272 (s), 1220, 1176, 1148, 1101, 1056, 1032, 931, 805, 757, 706, 637 (s), 572, 548, 513, 447. Elemental analysis calculated for $C_{59}H_{85}N_4Ag_2F_3O_4S$: C, 58.13; H, 7.03; N, 4.60. Found: C, 58.11; H, 6.91; N, 4.49.

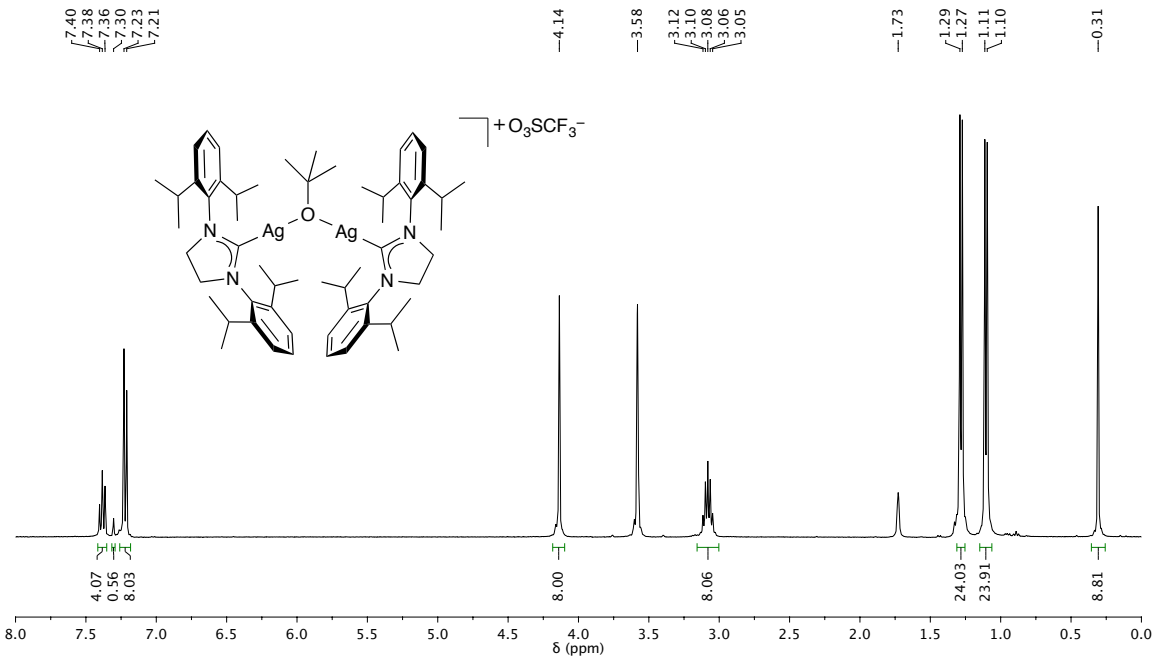

Figure 2.8. ^{1}H NMR (400 MHz, THF-d_8) spectrum of **5a**[OTf]. Benzene (δ 7.30 ppm)[30] is present as the result of benzophenone ketyl decomposition.

2.4.2.4 {[(5Dipp)Ag]$_2$(μ-H)}$^+$[OTf]$^-$ (**1a**[OTf])

A solution of {[(5Dipp)Ag]$_2$(μ-O^{t}Bu)}$^+$[OTf]$^-$ (0.600 g, 0.492 mmol) in THF (2 mL) and a solution of phenylsilane (0.061 mL, 0.053 g, 0.49 mmol) in THF (2 mL) were cooled to −35˚C. The phenylsilane solution was added dropwise via pipette to the {[(5Dipp)Ag]$_2$(μ-O^{t}Bu)}$^+$[OTf] $^-$ solution with stirring, and the resultant mixture was stored in the dark at −35˚C for 2 hours. A layer of pentane (12 mL) was carefully added over the THF solution, and the layers were allowed to mix by diffusion at −35˚C for 16 hours, resulting in the formation of colourless crystals. The mother liquor was decanted, and the crystals were collected on a fritted glass filter. The crystals were triturated, then washed with three portions of pentane (2 mL each) and dried in the dark under vacuum at 40˚C for 16 hours, affording the product as a white powder (0.490 g, 0.427 mmol, 87%). The product is stable toward brief exposure to air and moisture. ^{1}H NMR (400 MHz,

CD_2Cl_2): δ (ppm) 7.41 (t, *J* = 7.8 Hz, 2H, *para*-C*H*), 7.19 (d, *J* = 7.8 Hz, 4H, *meta*-C*H*), 4.02 (s, 4H, NCH_2), 2.92 (sept, *J* = 6.9 Hz, 4H, C*H*(CH_3)$_2$), 1.29 (d, *J* = 6.9 Hz, 12H, CH(CH_3)$_2$), 1.03 (d, *J* = 6.9 Hz, 12H, CH(CH_3)$_2$), −1.18 (app tt, 1H, *J*(^{1}H-^{109}Ag), = 134 Hz, *J*(^{1}H-^{107}Ag) = 116 Hz, Ag*H*Ag). ^{13}C{^{1}H} NMR (100 MHz, CD_2Cl_2): δ (ppm) 208.3 (m, N*C*Ag), 147.0 (*ortho*-*C*), 134.5 (*ipso*-*C*), 130.3 (*para*-*C*), 124.9 (*meta*-*C*), 121.5 (q, *J*(^{13}C-^{19}F) = 319.4 Hz, O_3SCF_3), 54.5 (m, N*C*H_2), 29.0 (*C*H(CH_3)$_2$), 25.7 (CH(*C*H_3)$_2$), 23.9 (CH(*C*H_3)$_2$). ^{19}F NMR (375 MHz, CD_2Cl_2): δ (ppm) −77.6 (s). ^{109}Ag NMR (18.6 MHz, CD_2Cl_2): δ (ppm) 519.3 (app dt, *J*(^{109}Ag-^{1}H) = 134 Hz, *J*(^{109}Ag-^{107}Ag) = 113 Hz). IR: ν (cm^{-1}) 3068 (w), 3049 (w), 2963 (s), 2924, 2869, 1591, 1486 (s), 1461 (s) 1383, 1362, 1327, 1272 (s), 1223, 1181, 1147, 1105, 1059, 1032 (s), 938, 907, 806, 754, 709, 637 (s), 619, 572, 545, 514, 449, 420. Elemental analysis calculated for $C_{55}H_{77}N_4Ag_2F_3O_3S$: C, 57.59; H, 6.77; N, 4.88. Found: C, 57.41; H 6.79; N, 4.95.

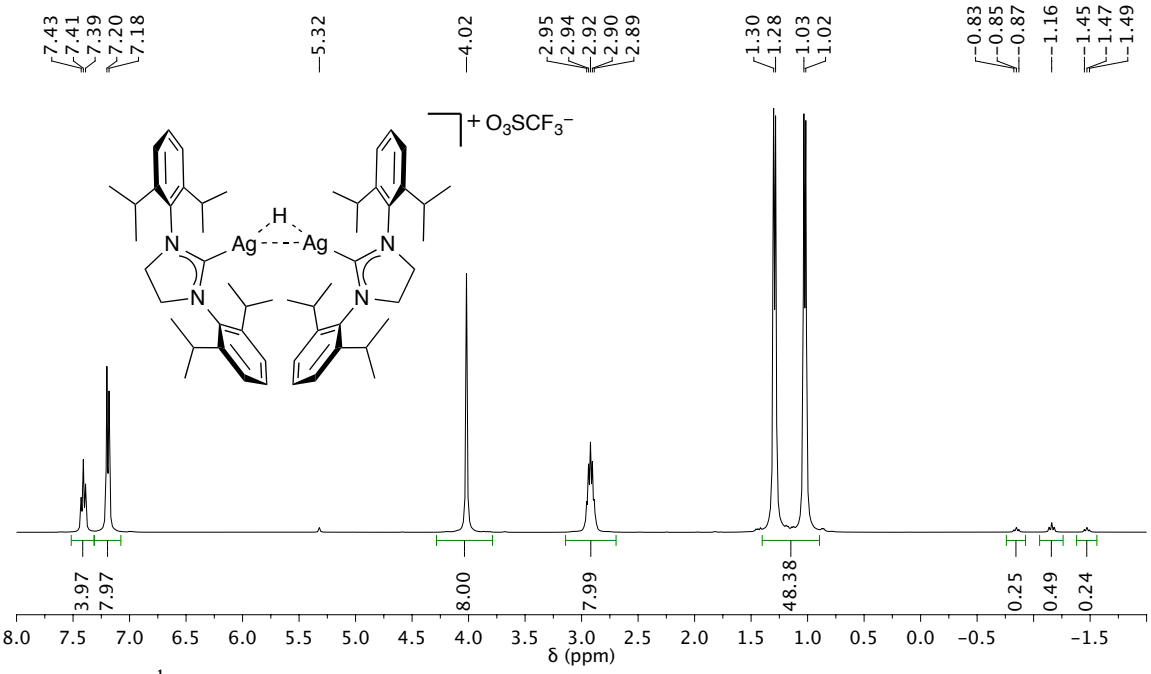

Figure 2.9. ^{1}H NMR (400 MHz, CD_2Cl_2) spectrum of **1a**[OTf].

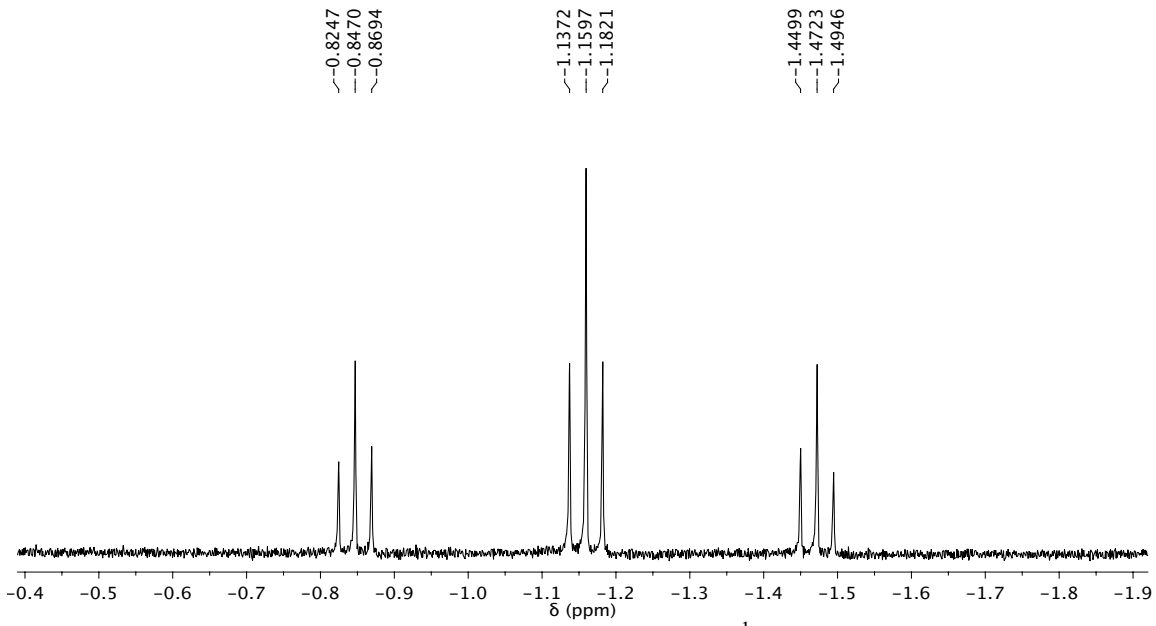

Figure 2.10. Detail of the hydride resonance in the ^{1}H NMR (400 MHz, CD_2Cl_2) spectrum of **1a**[OTf]. The splitting pattern, which appears to be a triplet of triplets, is more accurately described as three coincident resonances for each of three isotopologues of the complex: ^{107}Ag–^{107}Ag (triplet, 27% abundance), ^{109}Ag–^{109}Ag (triplet, 24% abundance), and ^{107}Ag–^{109}Ag (doublet of doublets, 50% abundance), where $J(^{1}\text{H}\text{-}^{107}\text{Ag})$ = 116 Hz and $J(^{1}\text{H}\text{-}^{109}\text{Ag})$ = 134 Hz.

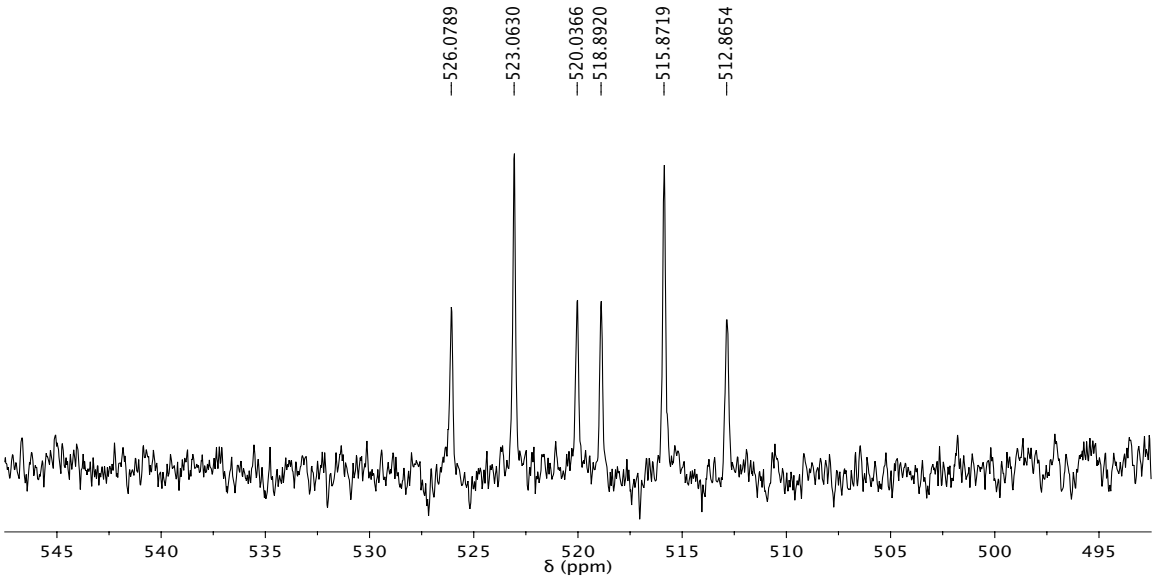

Figure 2.11. ^{109}Ag NMR (18.6 MHz, CD_2Cl_2) spectrum of **1a**[OTf]. The splitting pattern, which appears to be a doublet of triplets, is more accurately described as two coincident resonances for each of two ^{109}Ag-containing isotopologues of the complex: ^{109}Ag–^{109}Ag (doublet, 24% abundance), and ^{107}Ag–^{109}Ag (doublet of doublets, 50% abundance), where $J(^{109}\text{Ag}\text{-}^{1}\text{H})$ = 134 Hz and $J(^{109}\text{H}\text{-}^{107}\text{Ag})$ = 113 Hz.

2.4.2.5 {[(5Dipp)Ag]$_2$(μ-O^{t}Bu)}$^+$[BF$_4$]$^-$ (**5a**[BF$_4$])

Triphenylcarbenium tetrafluoroborate (0.200 g, 0.606 mmol) was added to a solution of (5Dipp)Ag(O^{t}Bu) (0.700 g, 1.22 mmol) in THF (4 mL). The reaction flask was covered with foil to exclude light, and the mixture was stirred for 4 hours. A layer of toluene (12 mL) was carefully added over the THF solution. The layers were allowed to mix by diffusion at −35˚C for 16 hours, resulting in the formation of colorless crystals from which the mother liquor was decanted. Two portions of toluene (10 mL) were successively added and decanted. The crystals were collected on a fritted glass filter and were washed with pentane (5 mL). The crystals were dissolved in THF (2 mL) and were precipitated by the addition of pentane (12 mL). The precipitate was collected on a fritted glass filter and was washed with three portions of pentane (5 mL each). Residual solvents were removed in the dark under vacuum at 40˚C for 16 hours, affording the product as a white powder (0.603 g, 93%). The product hydrolyzes readily in the presence of atmospheric moisture. ^{1}H NMR (400 MHz, THF-d_8): δ (ppm) 7.38 (t, J = 7.8 Hz, 2H, *para*-C*H*), 7.22 (d, J = 7.8 Hz, 4H, *meta*-C*H*), 4.14 (s, 4H, NCH_2), 3.08 (sept, J = 6.8 Hz, 4H, C*H*(CH$_3$)$_2$), 1.28 (d, J = 6.8 Hz, 12H, CH(CH_3)$_2$), 1.10 (d, J = 6.8 Hz, 12H, CH(CH_3)$_2$), 0.31 (s, 9H, O(CH_3)$_3$). ^{13}C{^{1}H} NMR (100 MHz, THF-d_8): δ (ppm) 205.3 (app dd, J(^{13}C-^{109}Ag) = 265 Hz, J(^{13}C-^{107}Ag) = 229 Hz, N*C*Ag), 147.5 (*ortho*-*C*), 136.1 (*ipso*-*C*), 130.2 (*para*-*C*), 125.1 (*meta*-*C*), 72.2 (O*C*(CH$_3$)$_3$, 55.0 (d, J(^{13}C-Ag), = 9 Hz, NCH$_2$), 29.1 (*C*H(CH$_3$)$_2$), 25.6 (CH(*C*H$_3$)$_2$), 24.0 (CH(*C*H$_3$)$_2$). ^{19}F NMR (375 MHz, THF-d_8): δ (ppm) −152.30 (s, ^{10}BF$_4^-$), −152.35 (s, ^{11}BF$_4^-$). IR: ν (cm^{-1}) 3071 (w), 2981 (s), 2930, 2870, 1590, 1488 (s), 1459 (s), 1384, 1364, 1327, 1274 (s), 1180, 1099, 1064 (s),

1017, 932, 913, 809, 763, 625, 550, 522, 450. Elemental analysis calculated for $C_{58}H_{85}N_4Ag_2BF_4O$: C, 60.22; H, 7.41; N, 4.84. Found: C, 60.35; H, 7.50; N, 4.83.

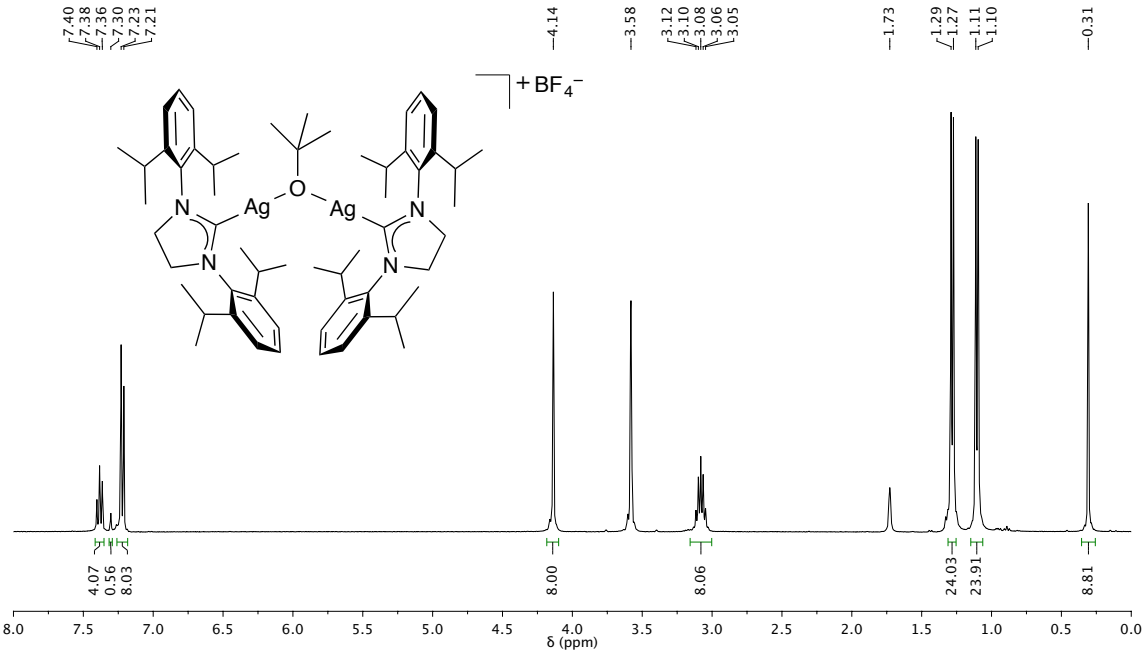

Figure 2.12. ^{1}H NMR (400 MHz, THF-d_8) spectrum of **5a**[BF_4]. Benzene (δ 7.30 ppm)[30] is present as the result of benzophenone ketyl decomposition.

2.4.2.6 {[(5Dipp)Ag]$_2$(μ-H)}$^+$[BF_4]$^-$ (**1a**[BF_4])

A solution of {[(5Dipp)Ag]$_2$(μ-O^{t}Bu)}$^+$[BF_4]$^-$ (0.800 g, 0.692 mmol) in THF (2 mL) and a solution of phenylsilane (0.085 mL, 0.075 g, 0.693 mmol) in THF (2 mL) were cooled to −35˚C. The phenylsilane solution was added dropwise via pipette to the {[(5Dipp)Ag]$_2$(μ-O^{t}Bu)}$^+$[OTf]$^-$ solution with stirring, and the resultant mixture was stored in the dark at −35˚C for 2 hours. A layer of pentane (12 mL) was carefully added over the THF solution, and the layers were allowed to mix by diffusion at −35˚C for 16 hours, resulting in the formation of colourless crystals. The mother liquor was decanted, and the crystals were collected on a fritted glass filter. The crystals were ground to a

powder and were washed with three portions of pentane (2 mL each). Residual solvents were removed in the dark under vacuum at 40˚C for 16 hours, affording the product as a white powder (0.600 g, 0.553 mmol, 92%). The product is stable toward brief exposure to air and moisture. ^{1}H NMR (400 MHz, CD_2Cl_2): δ (ppm) 7.42 (t, *J* = 7.8 Hz, 2H, *para*-C*H*), 7.19 (d, *J* = 7.8 Hz, 4H, *meta*-C*H*), 4.02 (s, 4H, NCH_2), 2.92 (sept, *J* = 6.9 Hz, 4H, C*H*(CH_3)$_2$), 1.29 (d, *J* = 6.9 Hz, 12H, CH(CH_3)$_2$), 1.03 (d, *J* = 6.9 Hz, 12H, CH(CH_3)$_2$), −1.18 (app tt, 1H, *J*(^{1}H-^{109}Ag), = 134 Hz, *J*(^{1}H-^{107}Ag) = 116 Hz, Ag*H*Ag). ^{13}C{^{1}H} NMR (100 MHz, CD_2Cl_2): δ (ppm) 208.3 (m, N*C*Ag), 147.0 (*ortho*-*C*), 134.5 (*ipso*-*C*), 130.3 (*para*-*C*), 124.9 (*meta*-*C*), 54.5 (m, N*C*H_2), 29.0 (*C*H(CH_3)$_2$), 25.7 (CH(*C*H_3)$_2$), 23.9 (CH(*C*H_3)$_2$). ^{19}F NMR (375 MHz, CD_2Cl_2): δ (ppm) −152.30 (s, $^{10}BF_4^-$), −152.35 (s, $^{11}BF_4^-$). IR: ν (cm^{-1}) 3071 (w), 2981 (s), 2930, 2870, 1941 (w), 1871 (w), 1800 (w), 1706 (w), 1655 (w), 1489 (s), 1467 (s), 1459 (s), 1384, 1388, 1342, 1327, 1274 (s), 1249, 1216, 1190 (s), 1180, 1116, 1103, 1060, 1017, 961 (s), 935, 913, 878, 804 (s), 757 (s), 711, 620, 563, 547, 516, 445. Elemental analysis calculated for $C_{54}H_{77}N_4Ag_2B_1F_4$: C, 59.79; H, 7.15; N, 5.16. Found: C, 59.53; H, 7.22; N, 5.09.

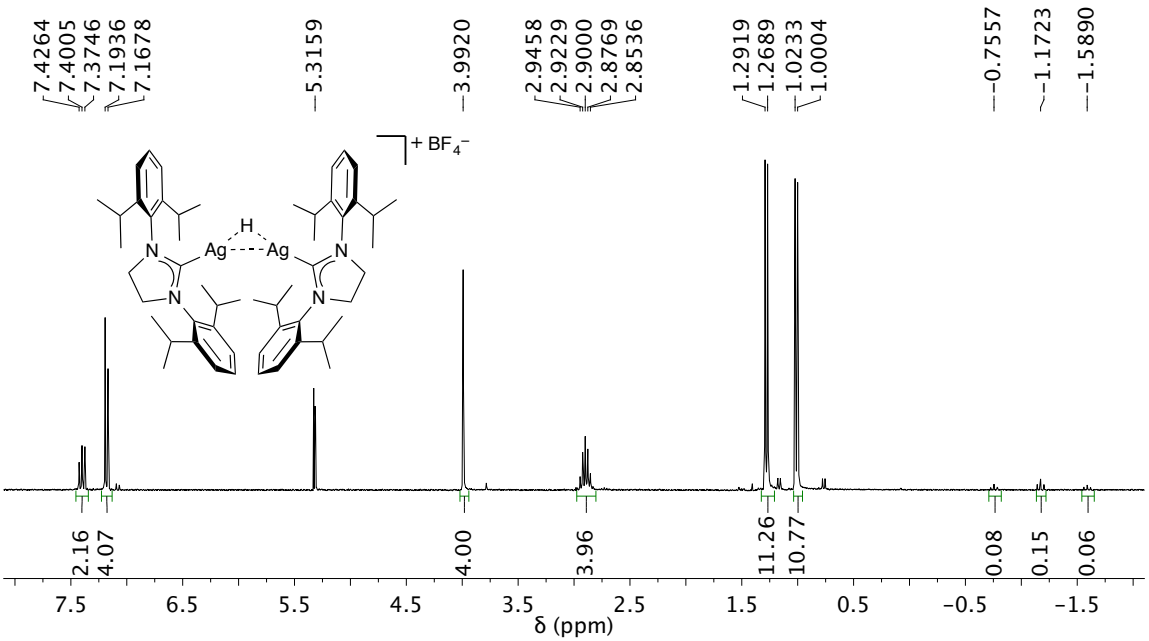

Figure 2.13 ^{1}H NMR (400 MHz, CD_2Cl_2) spectrum of **1a**[BF_4].

2.4.2.7 {[(5Dipp)Ag]$_2$(μ-^{2}H)}$^+$[BF_4]$^-$ (**1a**-*d*[BF_4])

The deuteride complex was prepared by analogy to the hydride, using phenylsilane-d_3 as the deuteride source. ^{1}H NMR (400 MHz, CD_2Cl_2): δ (ppm) 7.42 (t, J = 7.8 Hz, 2H, *para*-C*H*), 7.20 (d, J = 7.8 Hz, 4H, *meta*-C*H*), 4.03 (s, 4H, NCH_2), 2.93 (sept., J = 6.9 Hz, 4H, C*H*(CH_3)$_2$), 1.30 (d, J = 6.9 Hz, 12H, CH(CH_3)$_2$), 1.03 (d, J = 6.9 Hz, 12H, CH(CH_3)$_2$). ^{13}C{^{1}H} NMR (100 MHz, CD_2Cl_2): δ (ppm) 208.3 (m, N*C*Ag), 147.0 (*ortho*-*C*), 134.5 (*ipso*-*C*), 130.3 (*para*-*C*), 124.9 (*meta*-*C*), 54.5 (m, N*C*H_2), 29.0 (*C*H(CH_3)$_2$), 25.7 (CH(*C*H_3)$_2$), 23.9 (CH(*C*H_3)$_2$). ^{19}F NMR (375 MHz, CD_2Cl_2): δ (ppm) −152.30 (s, $^{10}BF_4^-$), −152.35 (s, $^{11}BF_4^-$). ^{2}H NMR (30.0 MHz, CD_2Cl_2): δ (ppm) −1.12 (t, J(^{2}H-$^{107/109}$Ag) = 18.7 Hz) ^{109}Ag NMR (18.6 MHz, CD_2Cl_2): δ (ppm) 522.2 (app tt, 1:1:1:2:2:2:1:1:1, J(^{109}Ag-^{107}Ag) = 114 Hz), J(^{109}Ag-^{2}H) = 20.5 Hz). IR: ν (cm^{-1}) 3071 (w), 2981 (s), 2930, 2870, 1941 (w), 1871 (w), 1800 (w), 1706 (w), 1655 (w), 1489 (s),

1467 (s), 1459 (s), 1384, 1388, 1342, 1327, 1274 (s), 1249, 1216, 1190 (s), 1180, 1116, 1103, 1060, 1017, 961 (s), 935, 913, 878, 804 (s), 757 (s), 711, 620, 563, 547, 516, 445.

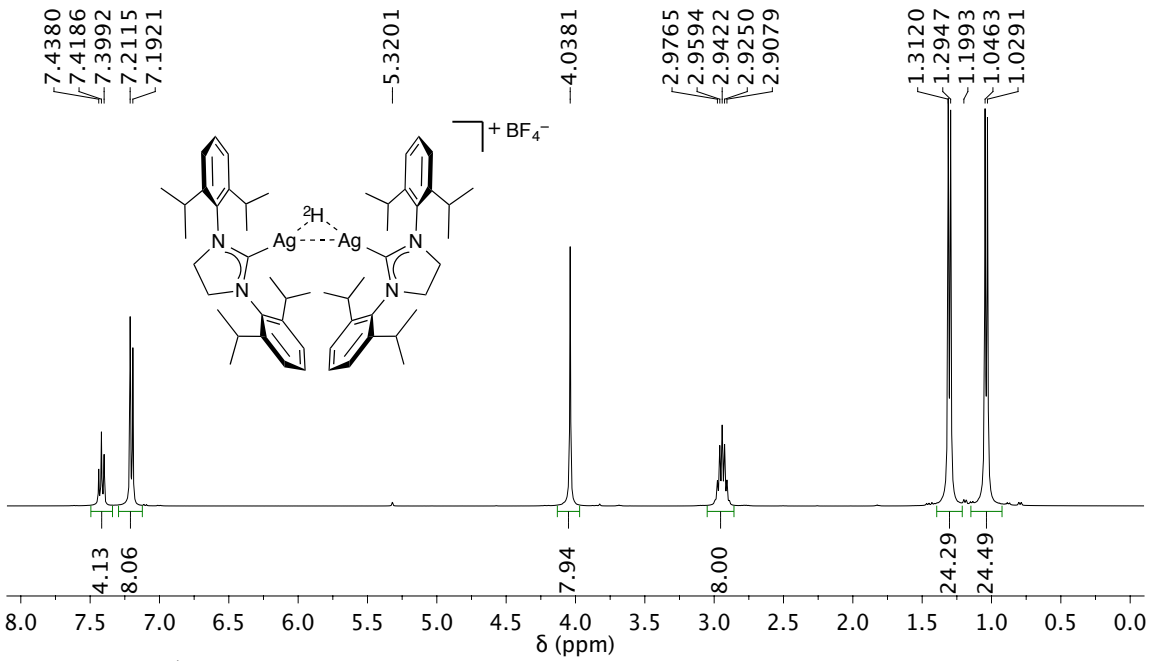

Figure 2.14. ^{1}H NMR (400 MHz, CD_2Cl_2) spectrum of **1a**-*d*[BF_4].

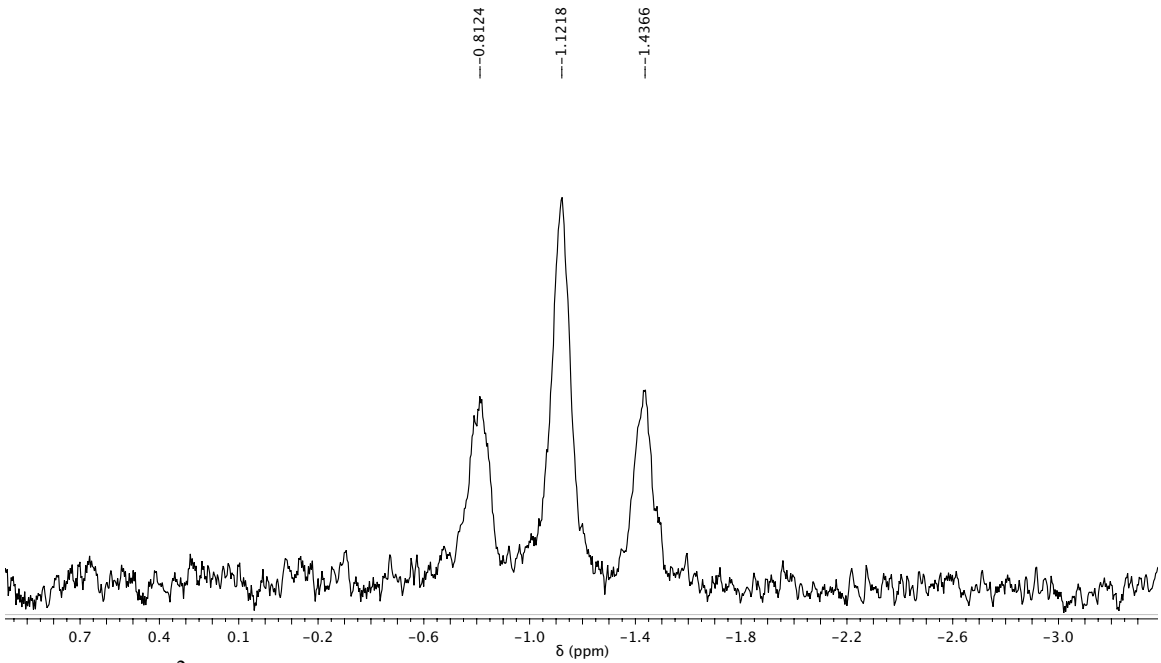

Figure 2.15. ^{2}H NMR (30.0 MHz, CD_2Cl_2) spectrum of **1a**-*d*[BF_4].

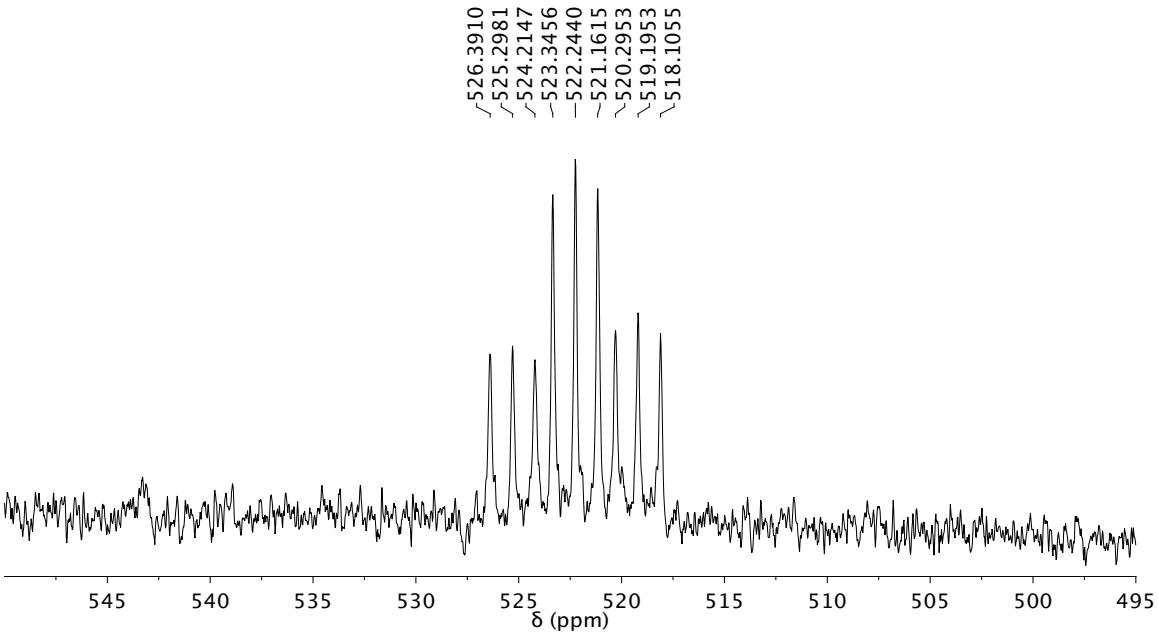

Figure 2.16. ^{109}Ag NMR (18.6 MHz, CD_2Cl_2) spectrum of **1a**-*d*[BF_4]. The multiplet, which has the appearance of a 1:2:1 triplet of 1:1:1 triplets, is attributable to coincident signals from each of the two ^{109}Ag-containing isotopologues of the complex: ^{109}Ag–^{109}Ag (1:1:1 triplet, 23% abundance) and ^{107}Ag–^{109}Ag (1:1 doublet of 1:1:1 triplets, 50% abundance), where $J(^{109}\text{Ag}\text{-}^{107}\text{Ag})$ = 114 Hz and $J(^{109}\text{Ag}\text{-}^{2}\text{H})$ = 20.5 Hz.

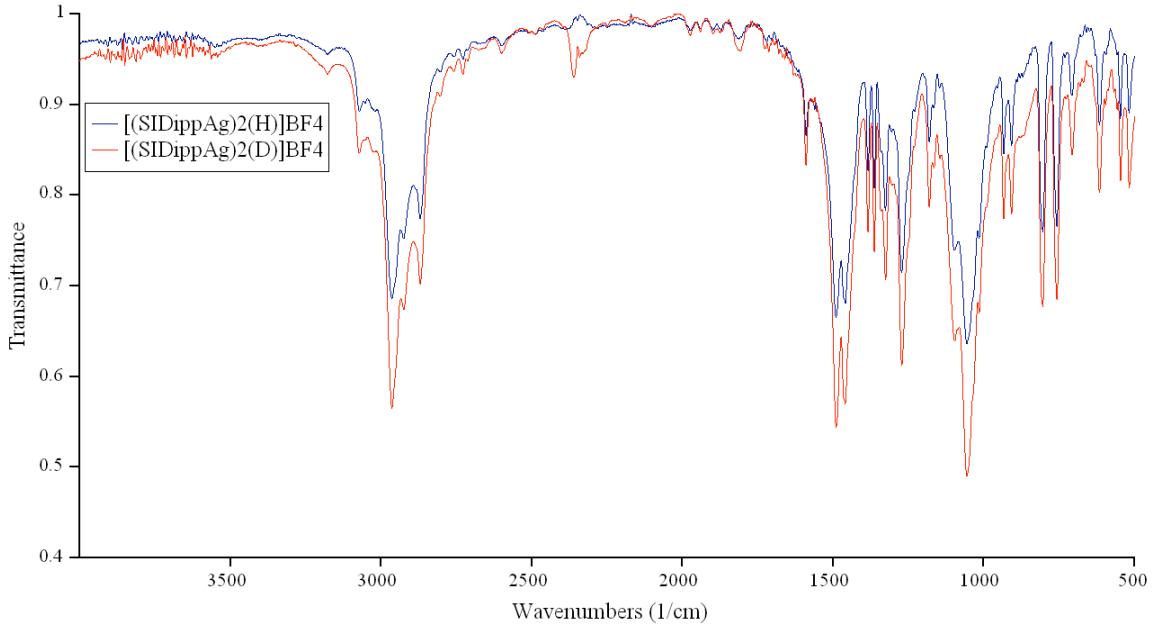

Figure 2.17. Overlay of the infrared absorption spectra of the hydride **1a**[BF_4] (blue spectrum) and deuteride **1a**-*d*[BF_4] (red spectrum). No discernible hydride or deuteride stretching resonances are observed. The feature at ν = 2360 cm^{-1} is attributable to fluctuations in CO_2 concentration in the sample chamber of the spectrometer.

2.4.2.8 $[(5Dipp)_2Ag]^+BF_4^-$

A solution of (5Dipp)Ag($OSiMe_3$) (0.150 g, 0.255 mmol) in CH_2Cl_2 (1.5 mL) was prepared in a Schlenk flask equipped with a stir bar, and the flask was sealed with a rubber septum. A solution of 5Dipp·HBF_4 (0.122 g, 0.255 mmol) in CH_2Cl_2 (1.5 mL) was added dropwise via syringe through the septum, with stirring. The reaction flask was covered with foil to exclude light. After stirring for 30 minutes, the flask was opened to air and no further attempt was made to maintain anhydrous conditions. The diffusion of a layer of hexane into the solution at −20˚C for 24 hours resulted in the formation of colorless crystals. The mother liquor was decanted, and residual solvent was removed under vacuum in the dark at 50˚C for 6 hours, affording the product as a white solid (0.160 g, 0.164 mmol, 64%). The product is stable in the presence of air and moisture. ^{1}H NMR (400 MHz, CD_2Cl_2): δ (ppm) 7.38 (t, J = 7.8 Hz, 2H, *para*-C*H*), 7.08 (d, J = 7.8 Hz, 4H, *meta*-C*H*), 3.80 (s, 4H, NCH_2), 2.75 (sept., J = 6.9 Hz, 4H, C*H*(CH_3)$_2$), 1.17 (d, J = 6.9 Hz, 12H, CH(CH_3)$_2$), 0.77 (d, J = 6.9 Hz, 12H, CH(CH_3)$_2$). ^{13}C{^{1}H} NMR (100 MHz, CD_2Cl_2): δ (ppm) 205.8 (d, J(^{13}C-^{109}Ag) = 178 Hz, N*C*Ag), 146.6 (*ortho-C*), 134.9 (*ipso-C*), 130.3 (*para-C*), 124.8 (*meta-C*), 54.5 (m, N*C*H_2), 28.8 (*C*H(CH_3)$_2$), 25.5 (CH(*C*H_3)$_2$), 24.1 (CH(*C*H_3)$_2$). ^{19}F NMR (375 MHz, CD_2Cl_2): δ (ppm) −152.30 (s, $^{10}BF_4^-$), −152.35 (s, $^{11}BF_4^-$). ^{109}Ag NMR (18.6 MHz, CD_2Cl_2): δ (ppm) 386.7 (s). IR: ν (cm^{-1}) 3072 (w), 2966 (s), 2926, 2870, 1591, 1479 (s), 1459 (s), 1381, 1365, 1324, 1271 (s), 1246, 1184, 1094, 1054 (s), 938, 903, 806 (s), 762 (s), 735, 711, 618, 548, 517, 445, 419. Elemental analysis calculated for $C_{54}H_{76}N_4AgBF_4$: C, 66.46; H, 7.85; N, 5.74. Found: C, 66.33; H, 7.84; N, 5.72.

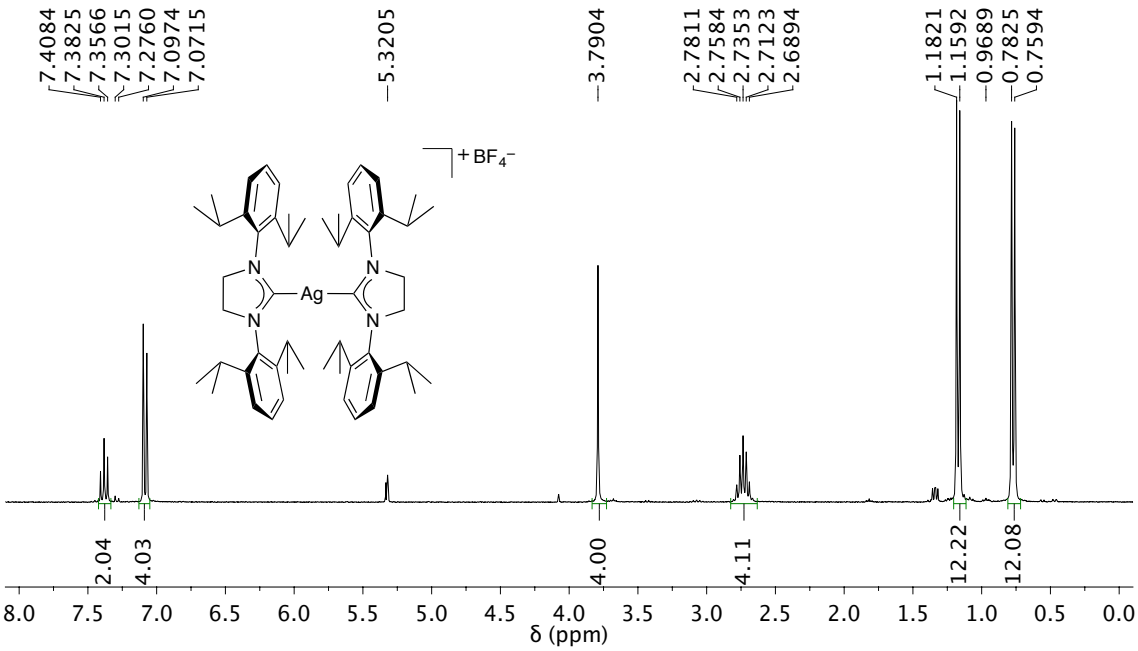

Figure 2.18. ^{1}H NMR (300 MHz, CD_2Cl_2) spectrum of $[(5Dipp)_2Ag]^+BF_4^-$.

2.4.2.9 $[(5Dipp)Ag(I_{iPr})]^+BF_4^-$

A solution of (5Dipp)Ag($OSiMe_3$) (0.150 g, 0.255 mmol) in CH_2Cl_2 (2 mL) was prepared in a Schlenk flask equipped with a stir bar, and the flask was sealed with a rubber septum. A solution of $I_{iPr}\cdot HBF_4$ (0.050 g, 0.25 mmol) in CH_2Cl_2 (2 mL) was added dropwise via syringe with stirring. The reaction flask was covered with foil to exclude light. After stirring for 30 minutes, the reaction mixture was dried in the dark under vacuum at 80˚C for 16 hours to remove the water and hexamethyldisiloxane byproducts. The residue was dissolved in CH_2Cl_2 (2 mL) and was filtered through Celite. A layer of diethyl ether (10 mL) was added over the filtrate. The layers were allowed to mix by diffusion at −35˚C for 16 hours, resulting in the formation of colorless crystals. The crystals were collected on a fritted glass filter, were washed with diethyl ether (2 mL), and were ground to a fine powder. Residual solvents were removed in the dark under vacuum at 40˚C for 16 hours, affording the product as a white powder (0.109 g,

0.148 mmol, 59%). ^{1}H NMR (400 MHz, CD_2Cl_2): δ (ppm) 7.48 (t, *J* = 7.6 Hz, 2H, *para*-C*H*), 7.31 (d, *J* = 7.6 Hz, 4H, *meta*-C*H*), 6.90 (d, *J*(^{1}H-Ag) = 1.8 Hz, 2H, NC*H*C*H*N), 4.24 (s, 4H, NCH_2), 3.50 (sept , *J* = 6.7 Hz, 2H, I_{iPr} C*H*$(CH_3)_2$), 3.13 (sept., *J* = 6.7 Hz, 4H, 5Dipp C*H*$(CH_3)_2$), 1.38 (d, *J* = 6.7 Hz, 12H, 5Dipp CH(C$H_3)_2$), 1.29 (d, *J* = 6.7 Hz, 12H, CH(C$H_3)_2$), 1.02 (d, *J* = 6.7 Hz, 12H, I_{iPr} CH(C$H_3)_2$). ^{13}C{^{1}H} NMR (100 MHz, CD_2Cl_2): δ (ppm) 208.6 (app dd, *J*(^{13}C-^{109}Ag), = 218 Hz, *J*(^{13}C-^{107}Ag) = 194 Hz, 5Dipp N*C*Ag), 175.3 (app dd, *J*(^{13}C-^{109}Ag), = 209 Hz, *J*(^{13}C-^{107}Ag) = 180 Hz, I_{iPr} N*C*Ag), 147.6 (*ortho*-*C*), 135.0 (*ipso*-*C*), 130.3 (*para*-*C*), 125.0 (*meta*-*C*), 118.6 (d, *J*(^{13}C -Ag) = 6 Hz, N*C*H), 54.4 (d, *J*(^{13}C-Ag), = 5 Hz, N*C*H_2), 29.2 (5Dipp *C*H$(CH_3)_2$), 25.6 (5Dipp CH(*C*$H_3)_2$), 24.2 (5Dipp CH(*C*$H_3)_2$) 23.7 (I_{iPr} CH(*C*$H_3)_2$). ^{19}F NMR (375 MHz, CD_2Cl_2): δ (ppm) −152.30 (s, $^{10}BF_4^-$), −152.35 (s, $^{11}BF_4^-$). ^{109}Ag NMR (18.6 MHz, CD_2Cl_2): δ (ppm) 684.0 (s). IR: ν (cm^{-1}) 3168, 3139, 3072 (w), 2966 (s), 2926, 2870, 1591 (w), 1558 (w), 1491, 1466, 1460, 1397, 1381, 1365, 1324, 1271 (s), 1216 (s), 1184, 1109, 1064 (s), 935, 916, 811 (s), 764, 744, 681, 606, 621, 548, 522, 444. Elemental analysis calculated for $C_{36}H_{54}N_4AgBF_4$: C, 58.63 ; H, 7.38; N, 7.60. Found: C, 58.66; H, 7.25; N, 7.50.

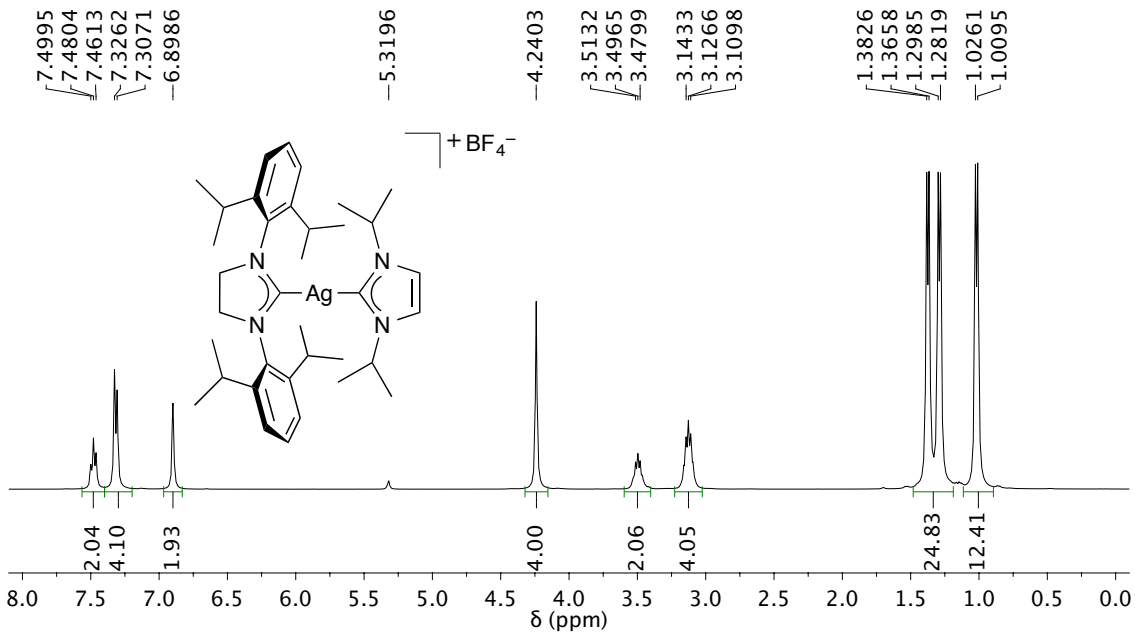

Figure 2.19. ^{1}H NMR (300 MHz, CD_2Cl_2) spectrum of $[(5Dipp)Ag(I_{iPr})]^{+}BF_4^{-}$.

2.4.2.10 (5Dipp)Ag($OSiMe_3$)

Sodium trimethylsilanolate (0.210 g, 1.87 mmol) was added to a suspension of (5Dipp)AgCl (1.000 g, 1.873 mmol) in THF (2 mL) with stirring. The reaction flask was covered with foil to exclude light. After stirring for 2 hours, the reaction mixture was filtered through Celite into a Schlenk flask. The solvent was removed from the filtrate under vacuum. The residue was dissolved in 10 mL toluene and was filtered once more through Celite into a Schlenk flask. The solvent was again removed from the filtrate under vacuum. The residue was dissolved in 2 mL CH_2Cl_2, and a layer of 18 mL diethyl ether was added. The layers were allowed to mix in the dark at −35˚C for 72 hours, resulting in the formation of colourless crystals. The crystals were collected on a fritted glass filter and were ground to a fine powder. The product was washed with diethyl ether (2 mL). Residual solvents were removed in the dark for 16 hours at 40˚C under vacuum, affording the product as a white powder (0.531 g, 0.605 mmol, 48%). The product

hydrolyzes readily in the presence of atmospheric moisture. ^{1}H NMR (400 MHz, CD_2Cl_2): δ (ppm) 7.43 (t, *J* = 7.8 Hz, 2H, *para*-C*H*), 7.28 (d, *J* = 7.8 Hz, 4H, *meta*-C*H*), 4.07 (s, 4H, NCH_2), 3.09 (sept, *J* = 6.9 Hz, 4H, C*H*$(CH_3)_2$), 1.37 (d, *J* = 6.9 Hz, 12H, CH(CH_3)$_2$), 1.35 (d, *J* = 6.9 Hz, 12H, CH(CH_3)$_2$), –0.44 (s, 9H, OSi(CH_3)$_3$). ^{13}C{^{1}H} NMR (100 MHz, CD_2Cl_2): δ (ppm) 207.8 (app dd, *J*(^{13}C-^{109}Ag), = 241 Hz, *J*(^{13}C-^{107}Ag) = 208 Hz, N*C*Ag), 147.2 (*ortho*-*C*), 135.4 (*ipso*-*C*), 130.0 (*para*-*C*), 124.8 (*meta*-*C*), 54.2 (d, *J*(^{13}C-Ag), = 8 Hz, N*C*H$_2$), 29.2 (*C*H(CH$_3$)$_2$), 25.5 (CH(*C*H$_3$)$_2$), 24.2 (CH(*C*H$_3$)$_2$), 4.3 (OSi(*C*H$_3$)$_3$). ^{109}Ag NMR (18.6 MHz, CD_2Cl_2): δ (ppm) 645.3 (s). IR: ν (cm^{-1}) 3071 (w), 2981 (s), 2930, 2870, 1590, 1488 (s), 1459 (s), 1384, 1367, 1327, 1274 (s), 1245, 1230 (s) 1180, 1103, 1060, 1017, 984 (s) 935, 824 (s), 808 (s), 763, 736, 663, 620, 550, 439. Elemental analysis calculated for $C_{30}H_{47}N_2AgSiO$: C, 61.31; H, 8.06; N, 4.77. Found: C, 61.07; H, 8.13; N, 4.74.

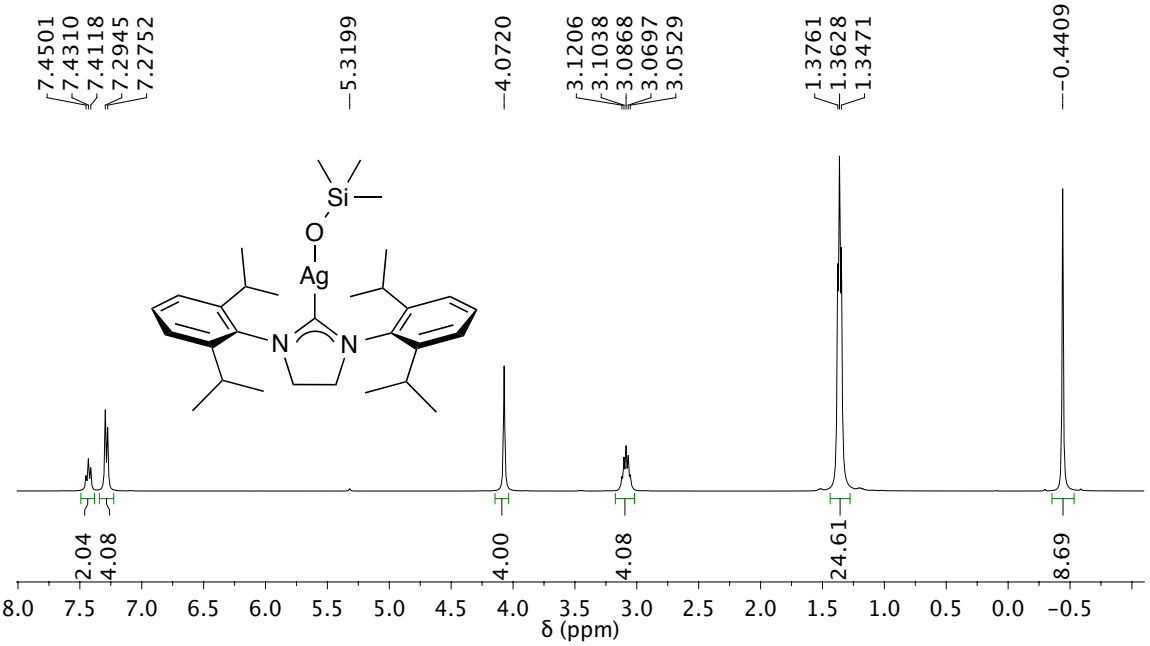

Figure 2.20. ^{1}H NMR (300 MHz, CD_2Cl_2) spectrum of (5Dipp)Ag(OSiMe$_3$).

2.4.2.11 5Dipp·HBF_4

1,3-Bis(2,6-diisopropylphenyl)imidazolinium tetrafluoroborate was prepared in analogy with the literature protocol for the synthesis of 1,3-diarylimidazolium tetrafluoroborate salts.[41] The procedure was conducted in air with solvents and reagents which were neither dried nor degassed, and in glassware which was not oven-dried. A 50% w/w aqueous solution of tetrafluoroboric acid (0.047 mL, 0.382 mmol HBF_4) was added in stoichiometric excess to a solution of 1,3-bis(2,6-diisopropylphenyl)-imidazolinium chloride (added as the triethylorthoformate adduct 5Dipp·HCl·$(EtO)_3CH$, 0.200g, 0.348 mmol) in water (10 mL). The reaction mixture was stirred for 30 minutes, and the product was extracted with three portions of CH_2Cl_2 (5 mL each). The extract was dried over excess magnesium sulfate and filtered through Celite, and the filtrate was concentrated under vacuum to a volume of 2 mL. The diffusion of a layer of diethyl ether (18 mL) at −20˚C for 16 hours resulted in the precipitation of colorless crystals, which were collected in a fritted glass funnel. The crystals were triturated and washed with diethyl ether (5 mL), affording the product as a white solid (0.130 g, 0.781 mmol, 78%). The product was characterized by ^{1}H NMR spectroscopy. Spectral data were in agreement with those reported in the literature.[42] ^{1}H NMR (400 MHz, CD_2Cl_2): δ (ppm) 8.58 (s, 1H, N(C*H*)N), 7.52 (t, *J* = 7.8 Hz, 2H, *para*-C*H*), 7.32 (d, *J* = 7.8 Hz, 4H, *meta*-C*H*), 4.54 (s, 4H, NCH_2), 2.98 (sept, *J* = 6.9 Hz, 4H, C*H*$(CH_3)_2$), 1.38 (d, *J* = 6.9 Hz, 12H, CH$(CH_3)_2$), 1.25 (d, *J* = 6.9 Hz, 12H, CH$(CH_3)_2$).

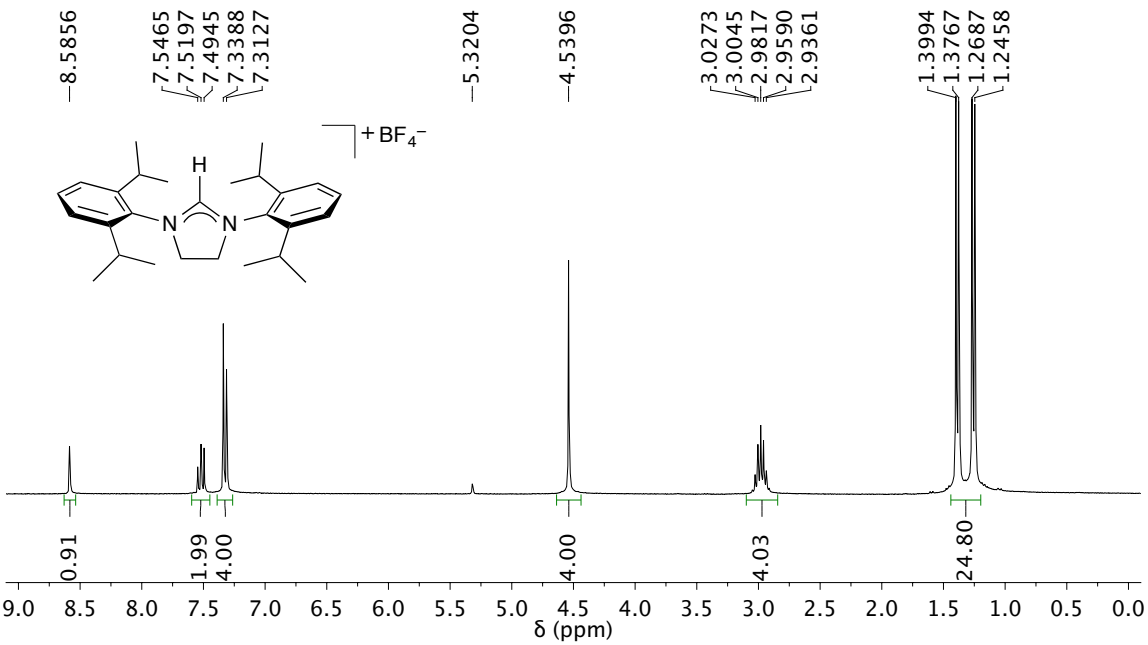

Figure 2.21. ^{1}H NMR (300 MHz, CD_2Cl_2) spectrum of 5Dipp·HBF_4.

2.4.2.12 I_{iPr}·$^{13}CO_2$

Isotopically labeled 1,3-diisopropylimidazolium ^{13}C-carboxylate (I_{iPr}·$^{13}CO_2$) was prepared by an adaptation of a literature protocol for the preparation 1,3-di-*tert*-butylimidazolium-2-carboxylate.[43] Potassium *tert*-butoxide (0.240 g, 2.14 mmol, 1.35 equiv) was added to a suspension of I_{iPr}·HCl (0.300 g, 1.58 mmol, 1.00 equiv) in THF (3 mL) to generate free 1,3-diisopropylimidazol-2-ylidene in solution. After stirring for 2 hours, the reaction mixture was filtered through Celite into a Schlenk flask equipped with a magnetic stir bar. The filtrate was degassed by three freeze-pump-thaw cycles, and the flask was pressurized with 160 kPa ^{13}C-carbon dioxide. The product began to precipitate as a white solid. After stirring for 16 hours under $^{13}CO_2$, the precipitate was collected on a fritted glass filter and was washed with diethyl ether (2 mL), affording the product as a white solid (0.260 g, 1.32 mmol, 83%). The product was characterized by ^{1}H NMR spectroscopy. Spectral data were in agreement with the literature.[44] ^{1}H NMR (400 MHz,

CD_2Cl_2): δ (ppm) 7.11 (d, J(H-^{13}C) = 0.3 Hz, 2H, NC*H*C*H*N), 5.56 (sept, J = 6.8 Hz, 2H, C*H*(CH_3)$_2$), 1.48 (d, J = 6.8 Hz, 12H, CH(C*H*$_3$)$_2$).

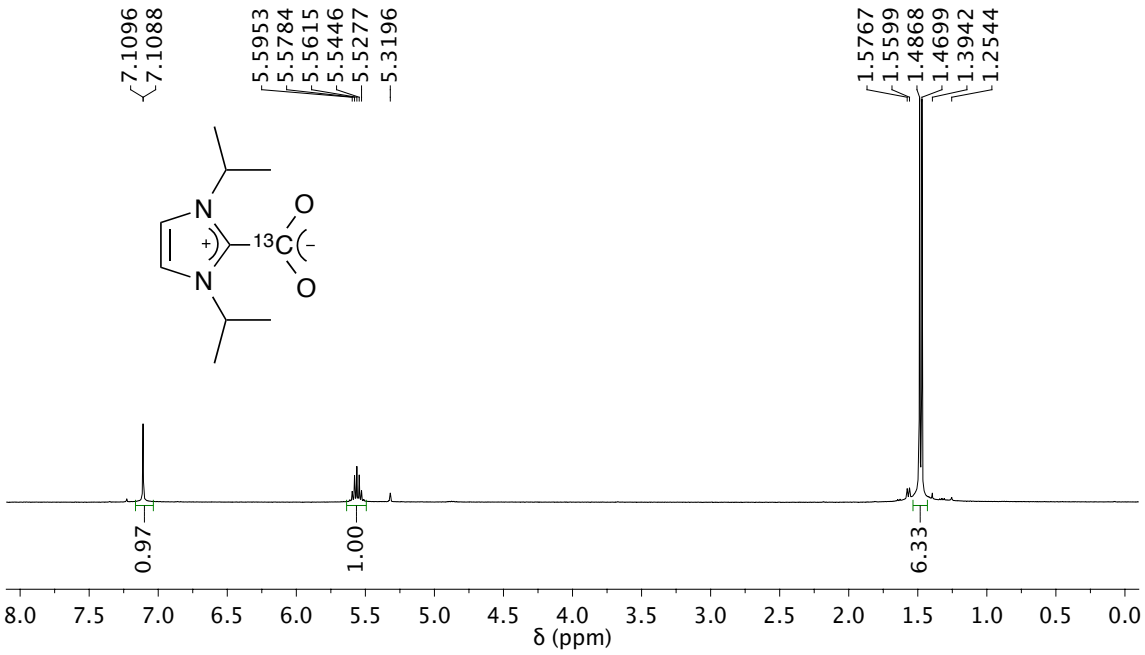

Figure 2.22. ^{1}H NMR (400 MHz, CD_2Cl_2) spectrum of $I_{iPr}{\cdot}^{13}CO_2$.

2.4.3 Reactivity Studies

2.4.3.1 Hydride Delivery to $I_{iPr}{\cdot}CO_2$

A solution of {[(5Dipp)Ag]$_2$(μ-H)}$^+$[BF_4]$^-$ (**1a**[BF_4], 0.030 g, 0.028 mmol, 1.0 equiv) and 4,4′-dimethylbiphenyl (internal standard; 0.010 g, 0.055 mmol) in CD_2Cl_2 was prepared in a sealable NMR tube and was chilled to −35˚C. Isotopically labeled 1,3-diisopropylimidazolium-2-^{13}C-carboxylate ($I_{iPr}{\cdot}^{13}CO_2$, 0.011 g, 0.056 mmol, 2.0 equiv) was added. The reaction tube was quickly capped, and its contents were thoroughly mixed by inversion. Gas evolution was observed immediately and subsided over the course of approximately 60 seconds. The solution was allowed to warm to room

temperature en route to the NMR facility. ^{1}H and ^{13}C NMR spectra were promptly recorded, and a second ^{13}C NMR spectrum was recorded after cooling the NMR tube at −78˚C for 2 hours to increase $^{13}CO_2$ solubility. The components of the product solution were identified as $[(5Dipp)Ag(I_{iPr})]^+$ (0.95 equiv), free ^{13}C-formate ion (0.66 equiv), and $^{13}CO_2$ (not quantified). $[(5Dipp)Ag(I_{iPr})]^+$ and ^{13}C-formate were quantified by integration of peak areas with respect to those of 4,4′-dimethylbiphenyl in the ^{1}H NMR spectrum. No unexpected signals were observed in the ^{19}F NMR spectrum of the product solution, confirming the BF_4^- anion remained unchanged.

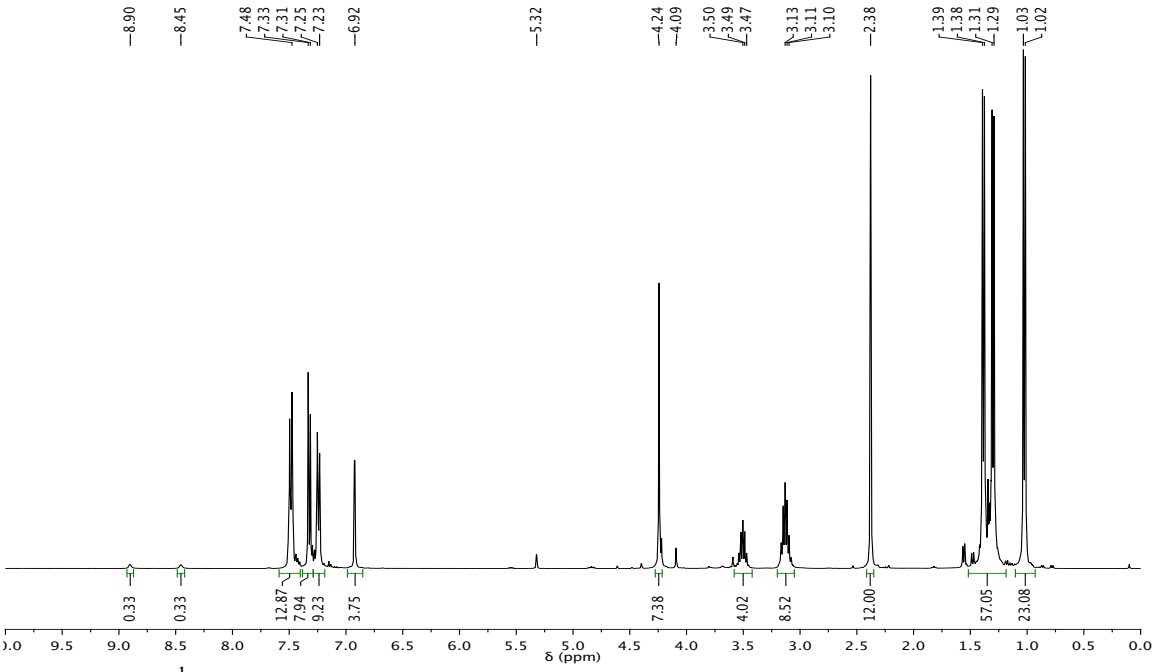

Figure 2.23. ^{1}H NMR (400 MHz, CD_2Cl_2) spectrum of the reaction of **1a**$[BF_4]$ with two equivalents of $I_{iPr}\cdot{}^{13}CO_2$ after 5 minutes. Two equivalents of 4,4′-dimethylbiphenyl [δ (ppm) 7.49 (d, 4H, J = 7.8 Hz), 7.24 (d, 4H, J = 7.8 Hz), 2.38 (s, 6H)] are present as an internal standard.

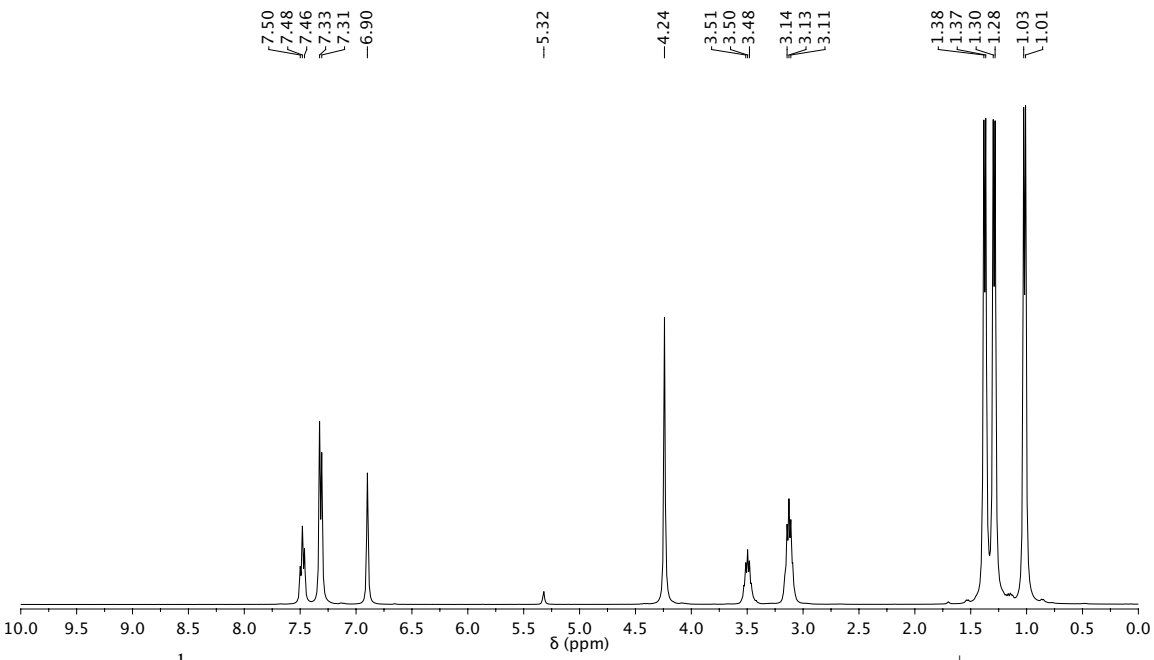

Figure 2.24. ^{1}H NMR (400 MHz, CD_2Cl_2) spectrum of $[(5Dipp)Ag(I_{iPr})]^{+}BF_4^{-}$, prepared independently by the treatment of (5Dipp)Ag($OSiMe_3$) with IiPr·HBF_4.

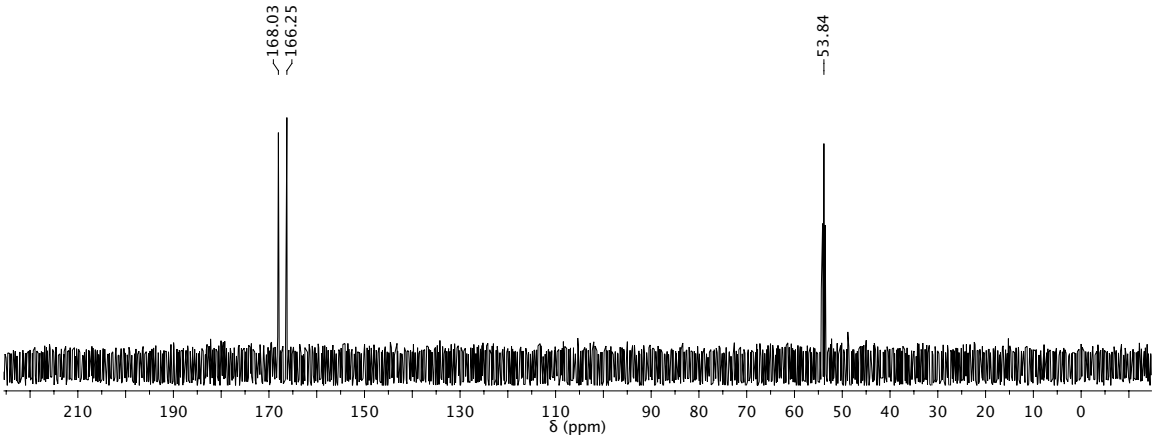

Figure 2.25. ^{13}C NMR (100 MHz, CD_2Cl_2, ^{1}H-nondecoupled) spectrum of the reaction of **2**[BF_4] with two equivalents of I_{iPr}·$^{13}CO_2$ after 7 minutes, showing the production of ^{13}C-formate.

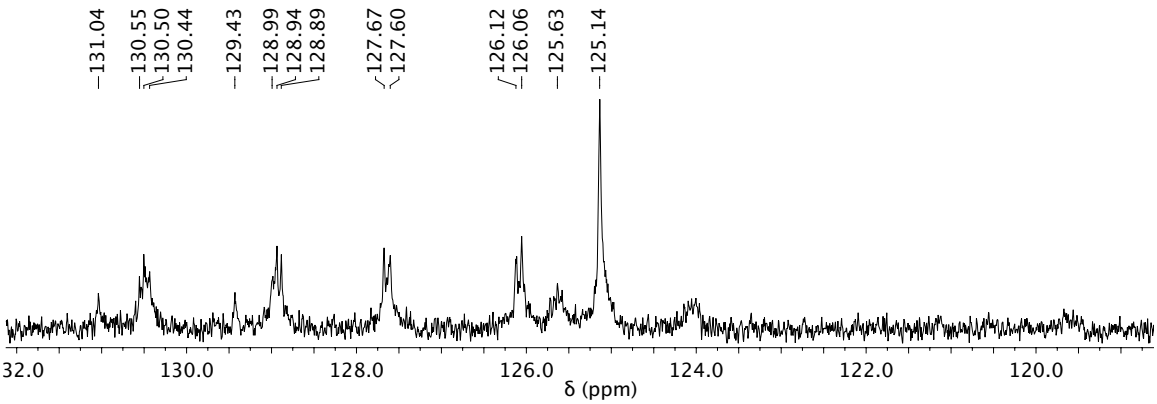

Figure 2.26. Detail of the $^{13}CO_2$ resonance (δ 125.14 ppm) in the ^{13}C NMR spectrum (75.5 MHz, CD_2Cl_2, ^1H-nondecoupled, after cooling to –78˚C) of the reaction of **2**[BF_4] with two equivalents of $I_{iPr}{\cdot}^{13}CO_2$. Resonances arising from the aryl groups of 5Dipp and 4,4′-dimethylbiphenyl are also visible.

2.4.3.2 Reaction of $\{[(5Dipp)Ag]_2(\mu\text{-}H)\}^+$ with free CO_2

A solution of $\{[(5Dipp)Ag]_2(\mu\text{-}H)\}[BF_4]$ (**2**[BF_4], 0.020 g) in CD_2Cl_2 (0.7 mL) in a NMR tube equipped with a J. Young valve was degassed by three freeze-pump-thaw cycles and, at room temperature, was pressurized with $^{13}CO_2$ (*ca.* 160 kPa). The tube was wrapped in foil and was agitated continuously to ensure mixing. The reaction was monitored by ^1H and ^{13}C NMR spectroscopy at intervals over four days. Over time, the tube became opaque as the result of silver(0) deposition on the interior walls. Slow hydride delivery to $^{13}CO_2$ was observed by NMR (less than 5% conversion of hydride in four days). The decomposition of **2**[BF_4] to $[(5Dipp)_2Ag]^+$ and $5DippH^+$ occurred more rapidly than the formation of ^{13}C-formate.

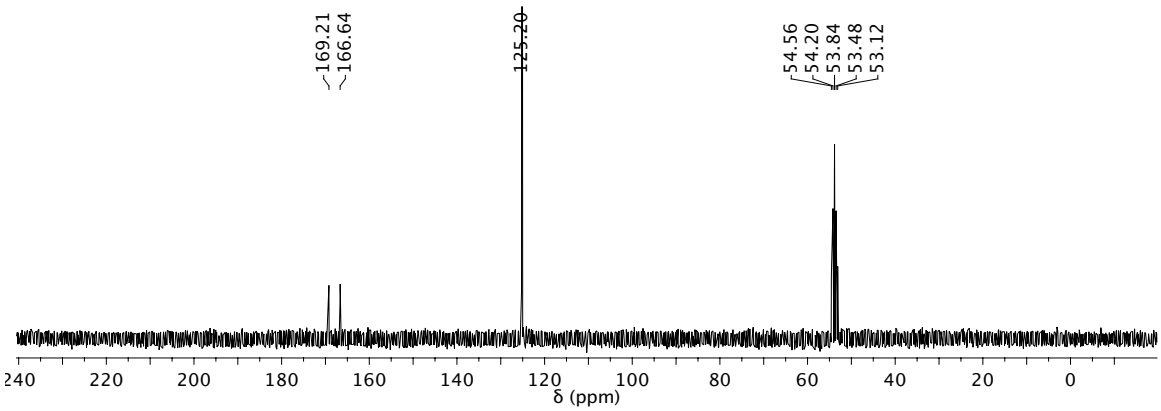

Figure 2.27. ^{13}C NMR spectrum (75.5 MHz, CD_2Cl_2, ^{1}H-nondecoupled) of the reaction of **2**[BF_4] with 160 kPa $^{13}CO_2$ after 4 days. The doublet at δ 167.9 ppm ($J(^{13}C\text{-}^{1}H)$ = 194 Hz) is believed to indicate ^{13}C-formate complexed with silver. The intense singlet at δ 125.2 ppm corresponds to $^{13}CO_2$.[30]

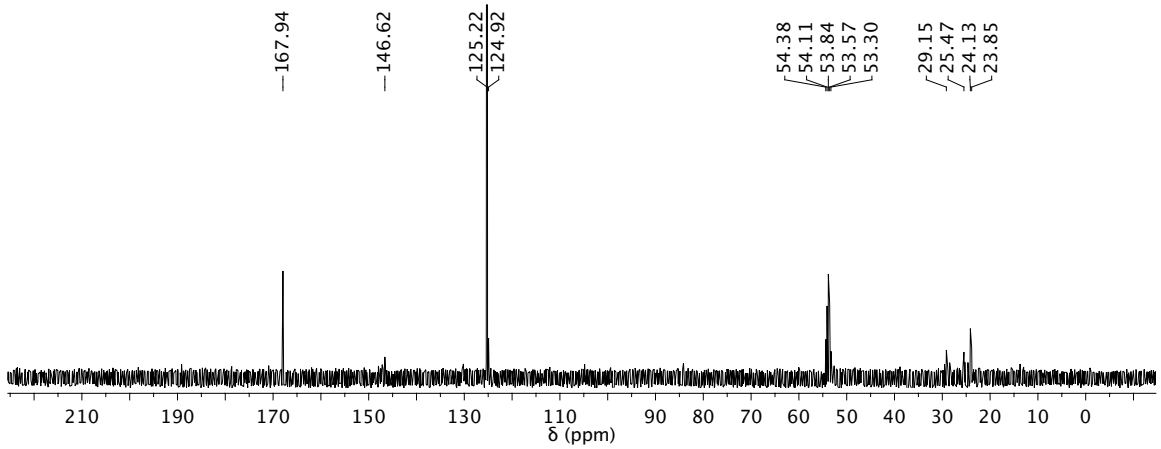

Figure 2.28. $^{13}C\{^{1}H\}$ NMR spectrum (75.5 MHz, CD_2Cl_2) of the reaction of **2**[BF_4] with 160 kPa $^{13}CO_2$ after 4 days. ^{1}H decoupling reduces the ^{13}C-formate signal at δ 167.9 ppm to a singlet. The intense singlet at δ 125.2 ppm corresponds to $^{13}CO_2$.[30] ^{1}H decoupling also enhances unlabeled 5Dipp-derived resonances, which are observed at δ 146.6 ppm and 124.9 ppm and in the range of 29.2–23.9 ppm.

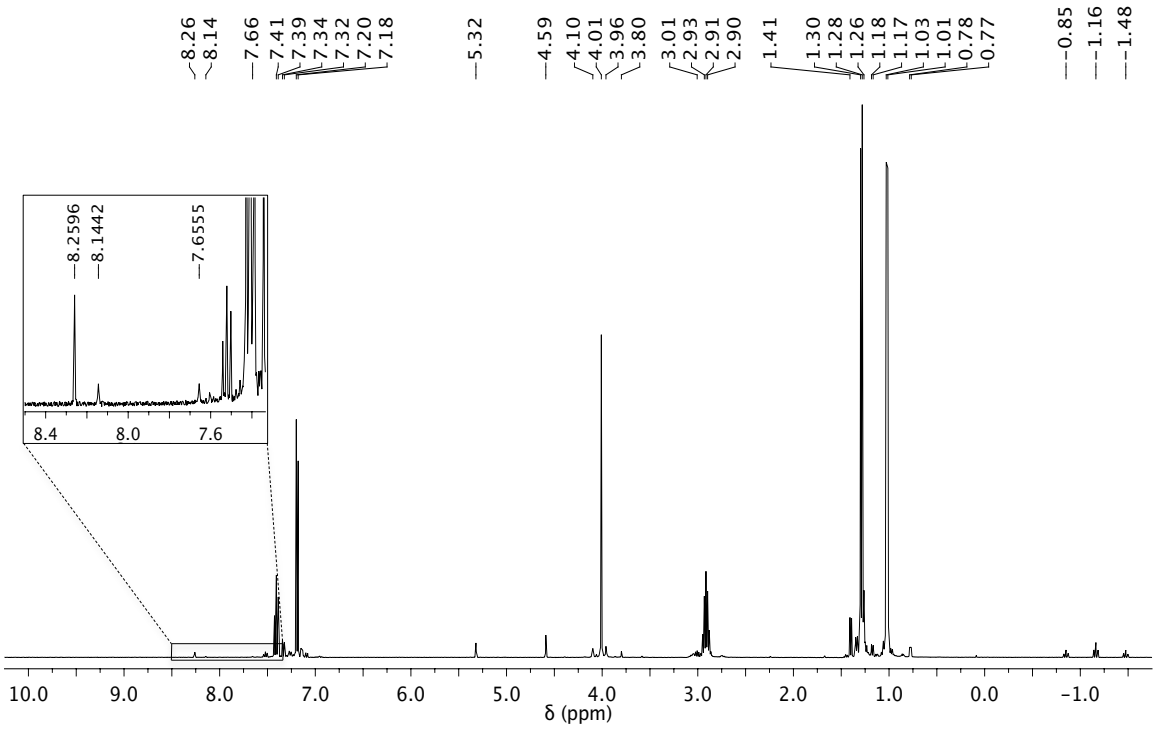

Figure 2.29. ^{1}H NMR spectrum (400 MHz, CD_2Cl_2, ^{13}C-nondecoupled) of the reaction of **2**[BF_4] with 160 kPa $^{13}CO_2$ after 4 days. In addition to ^{13}C-formate, indicated by a doublet ($J(^{1}H\text{-}^{13}C)$ = 195 Hz) at δ 7.90 ppm, decomposition products including $[(5Dipp)_2Ag]^+$ and $5DippH^+$ are also observed.

2.4.3.3 Acidolysis of $\{[(5Dipp)Ag]_2(\mu\text{-}H)\}^+$

No attempt to maintain anhydrous or air-free conditions was made in the investigation of the reactivity of **1a** with potential proton donors.

The treatment of **1a**[BF_4] with either methanol-d_1, 2,4,6-trimethylphenol, or *N*,*N*-dimethylanilinium tetrafluoroborate in $CDCl_3$ solution resulted in no reaction as discerned by ^{1}H NMR spectroscopy.

Treatment of **1a**[BF_4] (0.025 g, 0.023 mmol) with benzoic acid (0.003 g, 0.02 mmol) in CD_2Cl_2 resulted in the evolution of hydrogen gas (δ 4.61 ppm),[30] the deposition of silver(0), and a mixture of unreacted **1a** (accounting for 39% of the 5Dipp derivatives

in solution, quantified by the integration of ^{1}H NMR peak area), 5DippH^{+} (31%), an unidentified 5Dipp derivative (28%), and [(5Dipp)$_2$Ag]$^{+}$ (2%).

2.4.4 X-Ray Diffraction Studies

2.4.4.1 {[(5Dipp)Ag]$_2$(μ-O^{t}Bu)}$^{+}$[OTf]$^{-}$ (**5a**[OTf])

Diffraction-quality crystals were grown by the diffusion of hexane vapor into a solution of **5a**[OTf] in THF at −35˚C.

A suitable crystal was selected from the sample and mounted quickly onto a nylon fibre with paratone oil and placed under a cold stream at −100˚C. Single crystal X-ray data were collected on a Bruker APEX2 diffractometer with 1.6 kW graphite monochromated Mo radiation. The detector-to-crystal distance was 5.1 cm. The data collection was performed using a combination of sets of ω scans yielding data in the θ range 1.81˚ to 32.10˚ with an average completeness of 97.7%. The frames were integrated with the SAINT v7.68a.[45] A multi-scan absorption correction was carried out using the program SADABS V2008-1.[46] The structure was solved with JANA2006[47] and refined with Olex2[48] and SHELX.[49]

The crystal structure contains a {[(5Dipp)Ag]$_2$(μ-O^{t}Bu)}$^{+}$ complex, a triflate anion and two THF molecules of crystallization. One THF molecule is badly disordered, and was modelled using two components each with similarity restraints in SHELX. However, the disorder of this molecule is severe and the electron density ill-defines such that the locations of the O atoms cannot be identified with certainty (these too are probably disordered).

2.4.4.2 {[(5Dipp)Ag]$_2$(μ-H)}$^+$[OTf]$^-$ (**1a**[OTf])

Diffraction-quality crystals were grown by the diffusion of pentane vapor into a solution of **1a**[OTf] in THF at −35˚C.

A suitable crystal was selected from the sample and mounted quickly onto a nylon fibre with paratone oil and placed under a cold stream at −100˚C. Single crystal X-ray data were collected on a Bruker APEX2 diffractometer with 1.6 kW graphite monochromated Mo radiation. The detector-to-crystal distance was 5.1 cm. The data collection was performed using a combination of sets of ω scans yielding data in the θ range 1.39˚ to 29.61˚ with an average completeness of 99.6%. The frames were integrated with the SAINT v7.68a.[45] A multi-scan absorption correction was carried out using the program SADABS V2008-1.[46] The structure was solved with JANA2006[47] and refined with Olex2[48] and SHELX.[49]

The crystal structure contains a {[(5Dipp)Ag]$_2$(μ-H)}$^+$ complex, a triflate anion and two THF molecules of crystallization. Both solvent molecules are disordered, and were modelled using two components each with similarity restraints in SHELX.

2.5 Acknowledgements

This research was supported by the Georgia Institute of Technology, through the College of Science and the School of Chemistry & Biochemistry. We thank Prof. Seth R. Marder and his group for the use of their FT-IR spectrometer. Mr. Joel A. Starch kindly provided a sample of phenylsilane-d_3. We thank Mr. J. Kevin Busa for helpful discussions, and for the preparation of SIDipp•HCl and (SIDipp)AgCl. We thank Dr. Thomas J. Robilotto for helpful discussions and for technical assistance.

2.6 Notes and References

1 (a) A. Wurtz, *C. R. Hebd. Seances Acad. Sci.* **1880**, *90*, 22–25; (b) M. Berthelot, *C. R. Hebd. Seances Acad. Sci.* **1879**, *89*, 1097–1099; (c) A. Wurtz, *C. R. Hebd. Seances Acad. Sci.* **1844**, *18*, 702–704.

2 (a) J. Halpern, G. Czapski, J. Jortner, G. Stein, *Nature* **1960**, *186*, 629–630; (b) J. Halpern, *J. Phys. Chem.* **1959**, *63*, 398–403; (c) A. H. Webster, J. Halpern, *J. Phys. Chem.* **1957**, *61*, 1245–1248; (d) A. H. Webster, J. Halpern, *J. Phys. Chem.* **1957**, *61*, 1239–1245; (e) J. Halpern, E. R. Macgregor, E. Peters, *J. Phys. Chem.* **1956**, *60*, 1455–1456.

3 (a) G. V. Goeden, J. C. Huffman, K. G. Caulton, *Inorg. Chem.* **1986**, *25*, 2484–2485; (b) T. H. Lemmen, K. Folting, J. C. Huffman, K. G. Caulton, *J. Am. Chem. Soc.* **1985**, *107*, 7774–7775; (c) G. V. Goeden, K. G. Caulton, *J. Am. Chem. Soc.* **1981**, *103*, 7354–7355.

4 (a) J. F. Daeuble, C. McGettigan, J. M. Stryker, *Tetrahedron Lett.* **1990**, *31*, 2397–2400; (b) D. M. Brestensky, J. M. Stryker, *Tetrahedron Lett.* **1989**, *30*, 5677–5680; (c) W. S. Mahoney, J. M. Stryker, *J. Am. Chem. Soc.* **1989**, *111*, 8818–8823; (d) W. S. Mahoney, D. M. Brestensky, J. M. Stryker, *J. Am. Chem. Soc.* **1988**, *110*, 291–293; (e) H. Brunner, W. Miehling, *J. Organomet. Chem.* **1984**, *275*, c17–c21.

5 Selected recent examples: (a) H. Lv, Y.-B. Cai, J.-L. Zhang, *Angew. Chem., Int. Ed.* **2013**, *52*, 3203–3207; (b) H. Reeker, P.-O. Norrby, N. Krause, *Organometallics* **2012**, *31*, 8024–8030; (c) A. Saxena, B. Choi, H. W. Lam, *J. Am. Chem. Soc.* **2012**, *134*, 8428–8431; (d) K. R. Voigtritter, N. A. Isley, R. Moser, D. H. Aue, B. H. Lipshutz, *Tetrahedron* **2012**, *68*, 3410–3416; (e) P. Hasin, Y. Wu, *Chem. Commun.* **2012**, *48*, 1302–1304; (f) G. D. Frey, B. Donnadieu, M. Soleilhavoup, G. Bertrand, *Chem.–Asian J.* **2011**, *6*, 402–405; (g) R. Moser, Z. V. Boskovic, C. S. Crowe, B. H. Lipshutz, *J. Am. Chem. Soc.* **2010**, *132*, 7852–7853.

6 For a review, see: C. Deutsch, N. Krause, B. H. Lipshutz, *Chem. Rev.* **2008**, *108*, 2916–2927.

7 R. S. Dhayal, J.-H. Liao, Y.-R. Lin, P.-K. Liao, S. Kahlal, J.-Y. Saillard, C. W. Liu, *J. Am. Chem. Soc.* **2013**, *135*, 4704–4707.

8 (a) D.-A. Rosca, D. A. Smith, D. L. Hughes, M. Bochmann, *Angew. Chem., Int. Ed*. **2012**, *51*, 10643–10646; (b) S. Gaillard, A. M. Z. Slawin, S. P. Nolan, *Chem. Commun.* **2010**, *46*, 2742–2744; (c) A. Escalle, G. Mora, F. Gagosz, N. Mezailles, X. F. Le Goff, Y. Jean, P. Le Floch, *Inorg. Chem.* **2009**, *48*, 8415–8422; (d) H. Ito, T. Saito, T. Miyahara, C. Zhong, M. Sawamura, *Organometallics* **2009**, *28*, 4829–4840; (e) E. Y. Tsui, P. Müller, J. P. Sadighi, *Angew. Chem., Int. Ed.* **2008**,

47, 8937–8940.

9 (a) C. W. Liu, Y.-R. Lin, C.-S. Fang, C. Latouche, S. Kahlal, J.-Y. Saillard, *Inorg. Chem.* **2013**, *52*, 2070–2077; (b) P.-K. Liao, K.-G. Liu, C.-S. Fang, C. W. Liu, J. P. Fackler, Jr, Y.-Y. Wu, *Inorg. Chem.* **2011**, *50*, 8410–8417; (c) C. W. Liu, P.-K. Liao, C.-S. Fang, J.-Y. Saillard, S. Kahlal, J.-C. Wang, *Chem. Commun.* **2011**, *47*, 5831–5833; (d) C. W. Liu, H.-W. Chang, C.-S. Fang, B. Sarkar, J.-C. Wang, *Chem. Commun.* **2010**, *46*, 4571–4573; (e) C. W. Liu, H.-W. Chang, B. Sarkar, J.-Y. Saillard, S. Kahlal, Y.-Y. Wu, *Inorg. Chem.* **2010**, *49*, 468–475.

10 Selected recent advances in reduction to formate: (a) W. Sattler, G. Parkin, *J. Am. Chem. Soc.* **2012**, *134*, 17462–17465; (b) J. F. Hull, Y. Himeda, W.-H. Wang, B. Hashiguchi, R. Periana, D. J. Szalda, J. T. Muckerman, E. Fujita, *Nat. Chem.* **2012**, *4*, 383–388; (c) R. K. Yadav, J.-O. Baeg, G. H. Oh, N.-J. Park, K.-j. Kong, J. Kim, D. W. Hwang, S. K. Biswas, *J. Am. Chem. Soc.* **2012**, *134*, 11455–11461; (d) C. W. Li, M. W. Kanan, *J. Am. Chem. Soc.* **2012**, *134*, 7231–7234; (e) C. Das Neves Gomes, O. Jacquet, C. Villiers, P. Thuery, M. Ephritikhine, T. Cantat, *Angew. Chem., Int. Ed.* **2012**, *51*, 187–190; (f) T. J. Schmeier, G. E. Dobereiner, R. H. Crabtree, N. Hazari, *J. Am. Chem. Soc.* **2011**, *133*, 9274–9277; (g) R. Tanaka, M. Yamashita, K. Nozaki, *J. Am. Chem. Soc.* **2009**, *131*, 14168–14169.

11 For recent advances in the deoxygenative reduction of CO_2, see for example: (a) O. Jacquet, X. Frogneux, C. Das Neves Gomes, T. Cantat, *Chem. Sci.* **2013**, *4*, 2127–2131; (b) Y. Chen, C. W. Li, M. W. Kanan, *J. Am. Chem. Soc.* **2012**, *134*, 19969–19972; (c) S. Sato, T. Morikawa, T. Kajino, O. Ishitani, *Angew. Chem., Int. Ed.* **2013**, *52*, 988–992; (d) J. M. Smieja, E. E. Benson, B. Kumar, K. A. Grice, C. S. Seu, A. J. M. Miller, J. M. Mayer, C. P. Kubiak, *Proc. Natl. Acad. Sci. U. S. A.* **2012**, *109*, 15646–15650; (e) S. Park, D. Bézier, M. Brookhart, *J. Am. Chem. Soc.* **2012**, *134*, 11404–11407; (f) K. Teramura, S. Iguchi, Y. Mizuno, T. Shishido, T. Tanaka, *Angew. Chem., Int. Ed.* **2012**, *51*, 8008–8011; (g) S. Wesselbaum, T. vom Stein, J. Klankermayer, W. Leitner, *Angew. Chem., Int. Ed.* **2012**, *51*, 7499–7502; (h) C. Costentin, S. Drouet, M. Robert, J.-M. Savéant, *Science* **2012**, *338*, 90–94; (i) C. A. Huff, M. S. Sanford, *J. Am. Chem. Soc.* **2011**, *133*, 18122– 18125; (j) E. Balaraman, C. Gunanathan, J. Zhang, L. J. W. Shimon, D. Milstein, *Nat. Chem.* **2011**, *3*, 609–614; (k) F. Huang, G. Lu, L. Zhao, H. Li, Z.-X. Wang, *J. Am. Chem. Soc.* **2010**, *132*, 12388–12396; (l) E. B. Cole, P. S. Lakkaraju, D. M. Rampulla, A. J. Morris, E. Abelev, A. B. Bocarsly, *J. Am. Chem. Soc.* **2010**, *132*, 11539–11551; (m) S. Chakraborty, J. Zhang, J. A. Krause, H. Guan, *J. Am. Chem. Soc.* **2010**, *132*, 8872–8873; (n) L. Gu, Y. Zhang, *J. Am. Chem. Soc.* **2010**, *132*, 914–915; (o) S. N. Riduan, Y. Zhang, J. Y. Ying, *Angew. Chem., Int. Ed.* **2009**, *48*, 3322–3325.

12 For reviews, see: (a) P. Markewitz, W. Kuckshinrichs, W. Leitner, J. Linssen, P. Zapp, R. Bongartz, A. Schreiber, T. E. Müller, *Energy Environ. Sci.* **2012**, *5*, 7281–7305; (b) C. Federsal, R. Jackstell, M. Beller, *Angew. Chem., Int. Ed.* **2010**, *49*, 6254–6257; (c) E. E. Benson, C. P. Kubiak, A. J. Sathrum, J. M. Smieja, *Chem. Soc. Rev.* **2009**, *38*, 89–99; (d) M. Rakowski DuBois, D. L. DuBois, *Acc.*

Chem. Res. **2009**, *42*, 1974–1982.

13 (a) R. A. Flurer, K. L. Busch, *J. Am. Chem. Soc.* **1991**, *113*, 3656–3663; (b) R. L. DeKock, R. D. van Zee, T. Ziegler, *Inorg. Chem.* **1987**, *26*, 563–567.

14 (a) R. Mitrić, J. Petersen, A. Kulesza, M. I. S. Röhr, V. Bonačić-Koutecký, C. Brunet, R. Antoine, P. Dugourd, M. Broyer, R. A. J. O'Hair, *J. Phys. Chem. Lett.* **2011**, *2*, 548–552; (b) G. N. Khairallah, R. A. J. O'Hair, *Angew. Chem., Int. Ed.* **2005**, *44*, 728–731; (c) G. N. Khairallah, R. A. J. O'Hair, *Dalton Trans.* **2005**, 2702–2712.

15 (a) T. Baba, H. Sawada, T. Takahashi, M. Abe, *Appl. Catal., A* **2002**, *231*, 55–63; (b) T. Baba, Y. Tohjo, T. Takahashi, H. Sawada, Y. Ono, *Catal. Today* **2001**, *66*, 81–89; (c) T. Baba, N. Komatsu, H. Sawada, Y. Yamaguchi, T. Takahashi, H. Sugisawa, Y. Ono, *Langmuir*, **1999**, *15*, 7894–7896.

16 F. Q. Wang, G. N. Khairallah, R. A. J. O'Hair, *Int. J. Mass Spectrom.* **2009**, *283*, 17–25.

17 (a) S. Zhao, Z.-P. Liu, Z.-H. Li, W.-N. Wang, K.-N. Fan, *J. Phys. Chem. A* **2006**, *110*, 11537–11542; (b) R. Gáspár, I. Tamássy-Lentei, *Acta Phys. Acad. Sci. Hung.* **1981**, *50*, 343–347.

18 (a) M. Gorol, N. C. Mösch-Zanetti, H. W. Roesky, M. Noltemeyer, H.-G. Schmidt, *Chem. Commun.* **2003**, 46–47; (b) T. Beringhelli, G. D'Alfonso, M. G. Garavaglia, M. Panigati, P. Mercandelli, A. Sironi, *Organometallics* **2002**, *21*, 2705–2714; (c) H. Brunner, D. Mijolovic, B. Wrackmeyer, B. Nuber, *J. Organomet. Chem.* **1999**, *579*, 298–303; (d) R. Carreno, V. Riera, M. A. Ruiz, A. Tiripicchio, M. Tiripicchio-Camellini, *Organometallics* **1994**, *13*, 993–1004; (e) A. Albinati, S. Chaloupka, F. Demartin, T. F. Koetzle, H. Ruegger, L. M. Venanzi, M. K. Wolfer, *J. Am. Chem. Soc.* **1993**, *115*, 169–175; (f) L. F. Rhodes, J. C. Huffman, K. G. Caulton, *Inorg. Chim. Acta* **1992**, *198–200*, 639–649; (g) A. Albinati, C. Anklin, P. Janser, H. Lehner, D. Matt, P. S. Pregosin, L. M. Venanzi, *Inorg. Chem.* **1989**, *28*, 1105–1111; (h) S. S. D. Brown, P. J. McCarthy, I. D. Salter, P. A. Bates, M. B. Hursthouse, I. J. Colquhoun, W. McFarlane, M. Murray, *J. Chem. Soc., Dalton Trans*. **1988**, 2787–2796; (i) L. F. Rhodes, J. C. Huffman, K. G. Caulton, *J. Am. Chem. Soc*. **1984**, *106*, 6874–6876; (j) A. T. Hutton, P. G. Pringle, B. L. Shaw, *Organometallics* **1983**, *2*, 1889–1891; (k) M. Green, A. G. Orpen, I. D. Salter, F. G. A. Stone, *J. Chem. Soc., Chem. Commun.* **1982**, 813–814.

19 N. P. Mankad, D. S. Laitar, J. P. Sadighi, *Organometallics* **2004**, *23*, 3369–3371. For a related complex, see ref. 5f.

20 See for example: (a) Z. Lu, S. A. Cramer, D. M. Jenkins, *Chem. Sci.* **2012**, *3*, 3081–3087; (b) U. Hintermair, U. Englert, W. Leitner, *Organometallics* **2011**, *30*, 3726– 3731; (c) D. V. Partyka, N. Deligonul, *Inorg. Chem.* **2009**, *48*, 9463–9475; (d) D. V. Partyka, T. J. Robilotto, J. B. Updegraff, III, M. Zeller, A. D. Hunter, T.

G. Gray, *Organometallics*, **2009**, *28*, 795–801; (e) P. de Fremont, N. M. Scott, E. D. Stevens, T. Ramnial, O. C. Lightbody, C. L. B. Macdonald, J. A. C. Clyburne, C. D. Abernethy, S. P. Nolan, *Organometallics* **2005**, *24*, 6301–6309; (f) D. J. Nielsen, K. J. Cavell, M. S. Viciu, S. P. Nolan, B. W. Skelton, A. H. White, *J. Organomet. Chem.* **2005**, *690*, 6133–6142; (g) X. Hu, I. Castro-Rodriguez, K. Olsen, K. Meyer, *Organometallics* **2004**, *23*, 755–764; (h) H. M. J. Wang, I. J. B. Lin, *Organometallics* **1998**, *17*, 972–975.

21 (a) D. S. Laitar, P. Müller, T. G. Gray, J. P. Sadighi, *Organometallics* **2005**, *24*, 4503–4505; (b) W. A. Herrmann, S. K. Schneider, K. Öfele, M. Sakamoto, E. Herdtweck, *J. Organomet. Chem.* **2004**, *689*, 2441–2449.

22 D. S. Laitar, Ph.D. thesis, Massachusetts Institute of Technology (Cambridge), **2006**, http://dspace.mit.edu/handle/ 1721.1/36268.

23 Analogous $\{[(NHC)Au]_2OH\}^+$ complexes are known: (a) A. Gómez-Suárez, Y. Oonishi, S. Meiries, S. P. Nolan, *Organometallics* **2013**, *32*, 1106–1111; (b) A. Zhdanko, M. Ströbele, M. E. Maier, *Chem.–Eur. J.* **2012**, *18*, 14732–14744; (c) R. S. Ramón, S. Gaillard, A. Poater, L. Cavallo, A. M. Z. Slawin, S. P. Nolan, *Chem.–Eur. J.* **2011**, *17*, 1238–1246.

24 A. Bondi, *J. Phys. Chem.* **1964**, *68*, 441–451.

25 Treatment of (IDipp)AuOH with one-half equivalent of $Et_2O{\bullet}HBF_4$ likewise affords $\{[(IDipp)Au]_2OH\}^+BF_4^-$; see ref. 23c.

26 G. H. Penner, X. Liu, *Prog. Nucl. Magn. Reson. Spectrosc.* **2006**, *49*, 151–167.

27 Prepared from $PhSiCl_3$ and $LiAlD_4$ by analogy to the procedure for $PhSiH_3$: A. E. Finholt, A. C. Bond, Jr, K. E. Wilzbach, H. I. Schlesinger, *J. Am. Chem. Soc.* **1947**, *69*, 2692–2696.

28 For a solid-state ^{109}Ag NMR study of an (NHC)AgCl complex, see: T. Ramnial, C. D. Abernethy, M. D. Spicer, I. D. McKenzie, I. D. Gay, J. A. C. Clyburne, *Inorg. Chem.* **2003**, *42*, 1391–1393.

29 Dipolar coupling between ^{109}Ag and ^{195}Pt has been interpreted as a measure of the metal–metal interaction: A. F. M. J. van der Ploeg, G. van Koten, C. Brevard, *Inorg. Chem.* **1982**, *21*, 2878–2881.

30 G. R. Fulmer, A. J. M. Miller, N. H. Sherden, H. E. Gottlieb, A. Nudelman, B. M. Stoltz, J. E. Bercaw, K. I. Goldberg, *Organometallics* **2010**, *29*, 2176–2179.

31 B. D. Nageswara Rao, L. R. Anders, *Phys. Rev.* **1965**, *140*, A112–A117.

32 See for example: (a) D. J. Darensbourg, *Inorg. Chem.* **2010**, *49*, 10765–10780; (b) D. H. Gibson, *Coord. Chem. Rev.* **1999**, 185–186, 335–355; (c) X. Yin, J. R. Moss, *Coord. Chem. Rev*. **1999**, *181*, 27–59.

33 (a) D. J. Darensbourg, H. Pickner Wiegreffe, P. W. Wiegreffe, *J. Am. Chem. Soc.* **1990**, *112*, 9252–9257; (b) S. Sakaki, K. Ohkubo, *Inorg. Chem.* **1989**, *28*, 2583–2590; (c) D. J. Darensbourg, A. Rokicki, M. Y. Darensbourg, *J. Am. Chem. Soc.* **1981**, *103*, 3223–3224.

34 B. R. Van Ausdall, J. L. Glass, K. M. Wiggins, A. M. Aarif, J. Louie, *J. Org. Chem.* **2009**, *74*, 7935–7942.

35 A. J. Arduengo III, R. Krafczyk, R. Schmutzler, *Tetrahedron* **1999**, *55*, 14523–14534.

36 D. S. Laiter, P. Müller, T. G. Gray, J. P. Sadighi, *Organometallics* **2005**, *24,* 4503–4505.

37 A. E. Finholt., C. Bond Jr., K. E. Wilzbach, H. I. Schlesinger, *J. Am. Chem. Soc.* **1947**, *69*, 2692.

38 F. G. Bordwell, D. L. Hughes, *J. Am. Chem. Soc.* **1986**, *108*, 7300.

39 D. S. Laitar, "Synthetic and catalytic studies of Group 11 N-heterocyclic carbene complexes," Ph.D. Thesis, Massachusetts Institute of Technology (Cambridge), 2006; http://dspace.mit.edu/handle/1721.1/36268

40 E. Y. Tsui, P. Müller, J. P. Sadighi, *Angew. Chem. Int. Ed.* **2008**, *47*, 8937–8940.

41 X. Bantreil, S. P. Nolan, *Nature Protocols,* **2011**, *6*, 69–77.

42 E. M. Higgins, J. A. Sherwood, A. G. Lindsay, J. Armstrong, R. S. Massey, R. W. Alder, A. C. O'Donoghue, *Chem. Commun.* **2011**, *47*, 1559–1561.

43 Y. Kayaki, M. Yamamoto, T. Ikariya, *Angew. Chem. Int. Ed.* **2009**, *48*, 4194–4197.

44 M. Fèvre, P. Coupillaud, K. Miqueu, J. Sotiropoulos, J. Vignolle, D. Taton, *J. Org. Chem.* **2012**, *77*, 10135–10144.

45 Bruker (**2009**), SAINT V7.68a, BRUKER AXS Inc., Madison, WI, USA.

46 Bruker (**2008**), SADABS V2008-1, BRUKER AXS Inc., Madison, WI, USA.

47 V. Petricek, M. Dusek, L. Palatinus (**2006**), Jana2006, The crystallographic computing system, Institute of Physics, Prague, Czech Republic.

48 O. V. Dolomanov, L. J. Bourhis, R. J. Gildea, J. A. K. Howard, H. Puschmann, OLEX2: a complete structure solution, refinement and analysis program. See: (a) *J. Appl. Cryst.* **2009**, *42*, 339. (b) *Supramol. Chem.* **2001***, 1,* 189–191.

49 G. M. Sheldrick, *Acta Cryst.* **2008**, *A64*, 112.

CHAPTER 3

FLUORIDE-BRIDGED COMPLEXES OF THE GROUP 11 METALS

3.1 Note on Collaborative Efforts

This chapter describes a collaborative project that contributes significantly to this thesis as well as that of Chelsea M. Wyss.[1] The experimental data presented in both documents is the same, but the discussion is adapted to the context of each thesis.

3.2 Background

Fluorides of the monovalent group 11 metals exhibit interesting reactivity, in part due to their extreme hard-soft mismatch.[2] Binary silver(I) salts of chloride, bromide, and iodide have remarkably low solubility in water and organic solvents, rendering them largely chemically inert, and their precipitation is often used as a driving force for halide abstraction in chemical synthesis.[3] In contrast, silver(I) fluoride is highly soluble in water and somewhat soluble in some polar, coordinating organic solvents such as alcohols and acetonitrile.[3] Silver(I) fluoride exhibits a broad range of reactivity, forming complexes with nitriles, amines, and phosphines,[4b,5] and serving as a fluoride source in organic and inorganic syntheses.[6] The reaction of AgF with perfluoroolefins or organosilanes produces perfluoroalkyl complexes of silver,[4b] which are synthetically useful carbanion synthons.[7] The NHC-supported fluorosilver complex (5Dipp)AgF, is spectroscopically and structurally characterized,[8] but prior to our investigation of its reaction with hydrogen (See Chapter 4),[9] very little was known about its reactivity.

Although silver(I) fluoride is stable as a simple salt, copper(I) fluoride readily disproportionates to elemental copper and copper(II) fluoride,[10] while gold(I) fluoride has only been observed transiently in the gas phase.[11] While fluoride complexes of gold(III) have demonstrated utility in C–F and C–C bond formation,[12] fluorides complexes of copper(I) and gold(I), for which one would expect a larger degree of hard-soft mismatch compared to the higher oxidation states, were limited until recently to phosphine-supported copper fluorides,[13] though little is known about their reactivity. Recently, NHC-supported copper(I) and gold(I) fluorides, as well as the related bifluoride complexes, have garnered attention due to their involvement in catalytic fluorination, silylation, and C–C coupling reactions.[14]

Interest in dinuclear cationic complexes of the group 11 metals, especially gold, has grown recently due to the observation that the second metal center can alter or enhance reactivity in stoichiometric or catalytic processes. The coordination of a cationic gold fragment to an olefin or terminal alkyne, for instance, increases the acidity of the organic substrate, thereby promoting C–H functionalization under mild conditions.[15] Due to the potential for cooperative reactivity in dinuclear complexes and the synthetic expertise which our group has acquired in the preparation of dinuclear group 11 systems,[9,16] we proposed a series of NHC-supported dinuclear fluorides of the monovalent group 11 metals. This chapter describes the synthesis and characterization of these fluoride-bridged complexes of copper, silver, and gold, as well as some interesting observations of reactivity and characterization of the reaction products, include halogen exchange with dichloromethane and insertion of a cumulated diene.

3.3 Results and Discussion

3.3.1 Alternative Syntheses of Terminal Fluorides

Published procedures for the preparation of terminal group 11 fluorides (5Dipp)CuF (**6**),[8] (5Dipp)AgF (**7**),[8] and (5Dipp)AuF[14h] (**8**) (M = Cu, Ag, Au) call for triethylamine trihydrofluoride (Et_3NH^+ $H_2F_3^-$ or treat-HF) as a source of fluoride ion. This HF synthon is far less hazardous than gaseous HF, can be handled in glass vessels, although glass is not ideal for long-term storage, and has been used in the preparation of other fluoride complexes of transition-metals.[17] The treatment of alkoxide precursor (5Dipp)CuO^{t}Bu (**9**), (5Dipp)AgO^{t}Bu (**3**), or (5Dipp)AuO^{t}Bu (**10**) with one-third equivalent of treat-HF results in the precipitation of **6**, **7**, or **8**. Unfortunately, use of the highly hygroscopic reagent treat-HF resulted in the formation of metal-triethylamine adducts as side-products, reducing the yield of **6**–**8**, and introduced moisture, which forms hydrogen bonds with **6**–**8** and is difficult to completely remove (Scheme 3.1a).

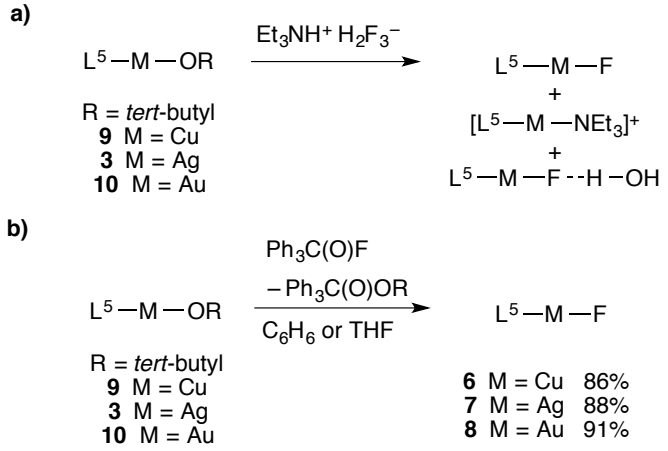

Scheme 3.1. (a) The preparation of terminal fluoride complexes **6–8** via treat-HF, potentially resulting in impurities such as metal-triethylamine complexes and hydrated fluorides. (b) The preparation of terminal fluoride complexes **9–11** via benzoyl fluoride.

We found, however, that the aprotic fluoride source benzoyl fluoride, dried over calcium hydride, reacts smoothly with group 11 alkoxides **9, 3,** and **10** in benzene to produce group 11 fluorides **6–8** rigorously in rigorously anhydrous conditions (Scheme 3.1b). Like treat-HF, benzoyl fluoride is a relatively benign HF synthon but has the advantage that it may be throroughly dried and stored in a resealable glass container to prevent absorption of atmospheric moisture. Furthermore, the by-product *tert*-butyl benzoate is benzene-soluble and does not tend to form adducts with the metal complexes, allowing convenient collection of the fluoride products by filtration and resulting consistently in high yields and high purity.

3.3.2 Syntheses of Fluoride-Bridged Dinucelar Cations

In analogy to the preparation of alkoxide-bridged dinuclear cations of copper[16a] and silver,[16b] treatment of terminal fluorides **6–8** with one-half equivalent of triphenylcarbenium tetrafluoroborate ($Ph_3C^+BF_4^-$) in THF results in the abstraction of one-half equivalent of fluoride, and the formation of fluoride-bridged dinuclear cations $\{[(5Dipp)Cu]_2(\mu\text{-}F)\}^+$ (**11**), $\{[(5Dipp)Ag]_2(\mu\text{-}F)\}^+$ (**12**), and $\{[(5Dipp)Au]_2(\mu\text{-}F)\}^+$ (**13**) (Scheme 3.2). Fluorides **11–13** can be precipitated as colorless tetrafluoroborate salts by the addition of a nonpolar solvent, affording convenient separation from the hydrocarbon-soluble fluorotriphenylmethane byproduct.

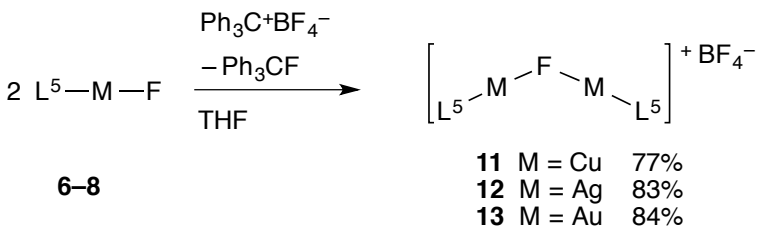

Scheme 3.2. The synthesis of fluoride-bridged dinuclear complexes **11–13**.

The fluoride-bridged complexes **11–13** hydrolyze rapidly upon exposure to moisture, forming hydroxide-bridged dinuclear complexes, as one might predict according to hard/soft acid-base principles. The sensitivity of **11–13** to moisture necessitates conscientious exclusion of air during manipulations and thorough drying of glassware and solvents.

3.3.3 ^{19}F NMR Spectroscopic Characterization

Close inspection of the ^{19}F NMR characteristics of fluoride complexes **6–8** and especially **11–13** reveals some interesting implications about the behavior of the complexes in solution. The broadness of the ^{19}F NMR signal of **7** shows a dependence on hydration, while the ^{19}F NMR chemical shifts of **11–13** are significantly solvent-dependent. The ^{19}F NMR data of these complexes is summarized in Table 3.1.

The ^{19}F NMR resonances of the terminal fluorides **6–8** appear in the range of δ –238.5 to –247.2 ppm in CD_2Cl_2. While the ^{19}F NMR resonances of **6** and **8** are singlets, as expected due to the quadrupolar nature of the ^{63}Cu, ^{65}Cu, and ^{197}Au nuclei, the resonance of **7** features ^{19}F–$^{107/109}$Ag coupling. Because the two isotopes of silver are unresolved, the resonance is observed as an apparent doublet with $J(^{19}F\text{-}^{107/109}Ag)$ = 163 Hz. After a brief exposure to atmospheric moisture, the ^{19}F NMR signal of **7** broadens to the extent that coupling can no longer be distinguished. Likewise, a sample of **7** prepared using hydrated treat-HF exhibits a broad singlet resonance. This dependence of the broadness of the ^{19}F NMR resonance of **7** suggests that even traces of moisture interact with **7** in solution, as one might expect due to the potential of fluoride to participate in hydrogen-bonds.

Table 3.1. ^{19}F NMR chemical shifts of fluoride complexes **6–8** and **11–13**.

Metal	L^5–M–F (CD_2Cl_2)	$[(L^5–M)_2(\mu\text{-}F)]^+$ (CD_2Cl_2)	$[(L^5–M)_2(\mu\text{-}F)]^+$ (THF-d_8)
Cu	–238.5	–311.1	–291.1
Ag	–243.1	–308.5	–302.9
Au	–247.2	–318.5	–272.6

Relative to those of the terminal fluorides, the ^{19}F NMR resonances of the bridging fluorides **11–13** appear much farther upfield, i.e. at more negative chemical shifts, in the range of δ –308.5 to –318.5 ppm in CD_2Cl_2, and are very broad, even after our most conscientious precautions to exclude moisture. No ^{19}F–$^{107/109}$Ag coupling is resolved in **12**. Intentional yet brief exposure to atmospheric moisture causes the signals of **11–13** to broaden to the extent that they can no longer be resolved from the spectral baseline, even for samples which still appear pristinely pure by ^{1}H NMR spectroscopy.

Interestingly, in THF-d_8 solution, the chemical shifts of the ^{19}F NMR resonances of **11–13** appear in the range of δ –272.6 to –302.9 ppm, significantly upfield of their positions in CD_2Cl_2 and nearer to the chemical shifts of the terminal fluorides **6–8**. We suspect that this phenomenon may be due to the rapidly reversible coordination of THF to one metal center of the dinuclear complex, resulting in an equilibrium concentration of terminal fluoride plus solvated $[(5Dipp)Ag]^+$ ion (Scheme 3.3). The solvent dependence of the chemical shift of the silver complex **12** is substantial, shifting 5.6 ppm between CD_2Cl_2 THF-d_8, and for the copper and gold complexes **11** and **13**, the solvent dependence is astonishing, with a difference of 20 ppm and 46 ppm, respectively. We speculate that each ^{19}F NMR resonance observed in THF-d_8 is a weighted average of the resonances of the terminal and bridging fluorides, in rapid equilibrium. Despite this

apparently significant coordination of THF to **11–13**, removal of THF under vacuum allows full recovery of solvent-free compounds.

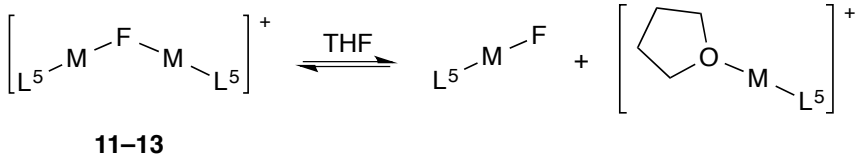

11–13

Scheme 3.3. The proposed coordination of THF to fluoride-bridged complexes **11–13**.

3.3.4 Crystallographic Characterization

The fluoride-bridged complexes **11–13** crystallize as their tetrafluoroborate salts with identical connectivity and other similar characteristics such as linear coordination about each metal and slightly bent geometry about fluorine. Key metrics are summarized in Table 3.2. In all three complexes, the BF_4^- anion lies well outside the metal coordination sphere, and M–C distances are comparable to those of the corresponding terminal fluorides (**6–8**). In contrast to their hydride-bridged analogues, which exhibit varying degrees of metal-metal bonding, the distance between metal centers in **11–13** is significantly greater than twice the van der Waals radius of each metal, precluding the possibility of both metal-metal bonding, which has been observed in hydride- and carbanion-bridged analogs (see Chapters 2, 4, and 5),[16] and closed-shell metallophilic interactions, which have been observed in other halide-bridged complexes of gold.[18]

Table 3.2. Selected bond lengths (Å) and angles (˚) for fluoride-bridged complexes **11**–**13**.

M	M–C	M–F	M···M	C–M–F	M–F–M
Cu	1.868(3)	1.843(2)	3.5130(7)	176.5(1)	142.99(17)
	1.876(3)	1.862(2)		172.5(1)	
Cu	1.850(3)	1.836(2)	3.4522(7)	174.5(1)	140.96(16)
	1.863(3)	1.827(3)		178.4(1)	
Ag	2.053(3)	2.0672(7)	4.0589(4)	176.60(11)	158.09(17)
		2.0671(7)			
Au	1.944(3)	2.060(1)	3.9495(5)	179.64(11)	146.93(10)

The asymmetric unit of the structure of copper complex **11** contains two crystallographically distinct molecules, one of which is shown in Figure 1.1. The Cu–F distances range from 1.827(3) to 1.862(2) Å, remarkably comparable to that of the terminal fluoride **6** (1.8426(10) Å). The M–F–M angles of **6** (140.96(16)˚ and 142.99(17)˚) are smaller than those of **7** and **8**, even though the smaller size of copper results in the greatest potential for steric clashes between 5Dipp ligands.

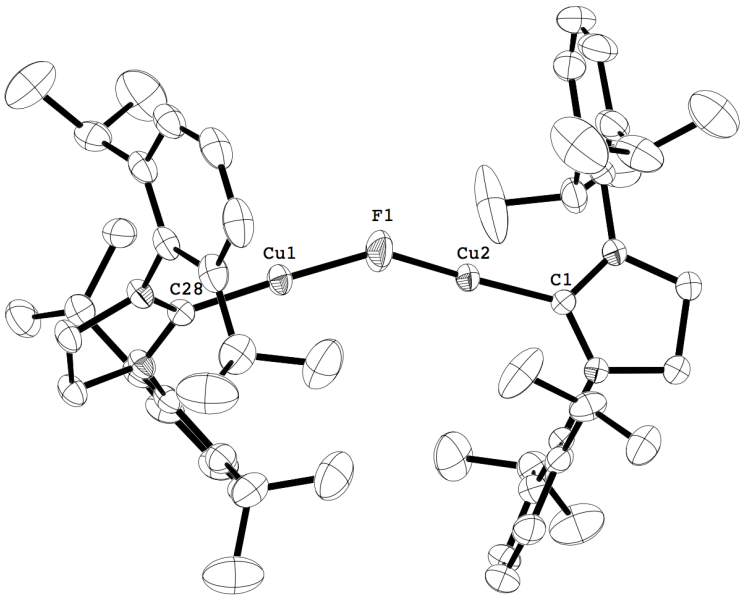

Figure 3.1. Solid-state structure of fluoride-bridged dicopper complex **11**. One of two crystallographically distinct molecules is shown. Hydrogen atoms, cocrystallized solvent, and BF_4^- counterion omitted for clarity.

The structure of the silver complex **12**, shown in Figure 2.2 features Ag–F distances of 2.0671(7) Å and 2.0672(7) Å, which are very similar to the Ag–F distances in the terminal analogue **7** (201682(13) Å). The M–F–M angle of **12** (158.09(17)˚) is larger than that of its group 11 congeners, approaching linear coordination about fluorine, which one would expect in a system featuring purely ionic bonding. The large Ag–F–Ag angle may reflect a larger degree of ionic character in **12** relative to **11** and **13**, although it is also possible that a shallow potential energy barrier for bending about fluorine allows crystal packing forces to dominate the M–F–M angles.

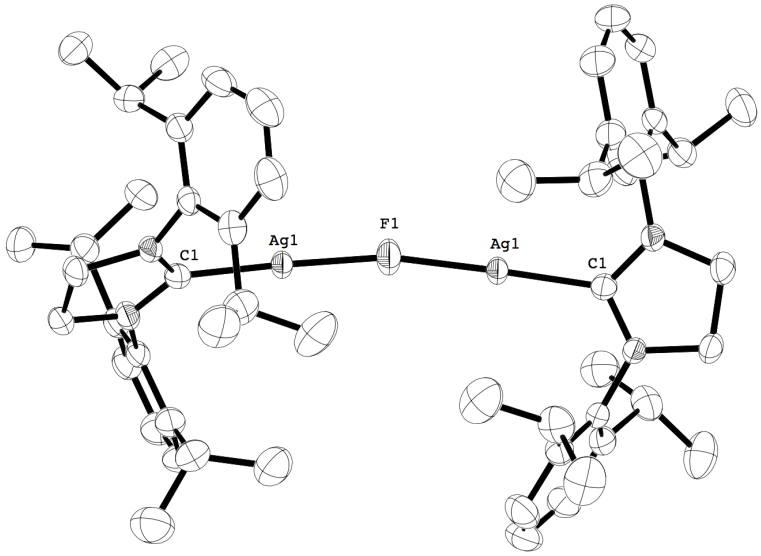

Figure 3.2. Solid-state structure of fluoride-bridged disilver complex **12**. Hydrogen atoms, cocrystallized solvent, and BF_4^- counterion omitted for clarity.

The Au–F distances of the gold complex **13** (both 2.060(1) Å) are subtly shorter than those of silver complex **12**. This similarity is not surprising considering that despite gold's greater atomic mass, its atomic radius is approximately the same as that of silver

due to a combination of the lanthanide contraction and relativistic effects. The M–F–M angle of **13** (146.93(10)˚) lies between that of **11** and **12**.

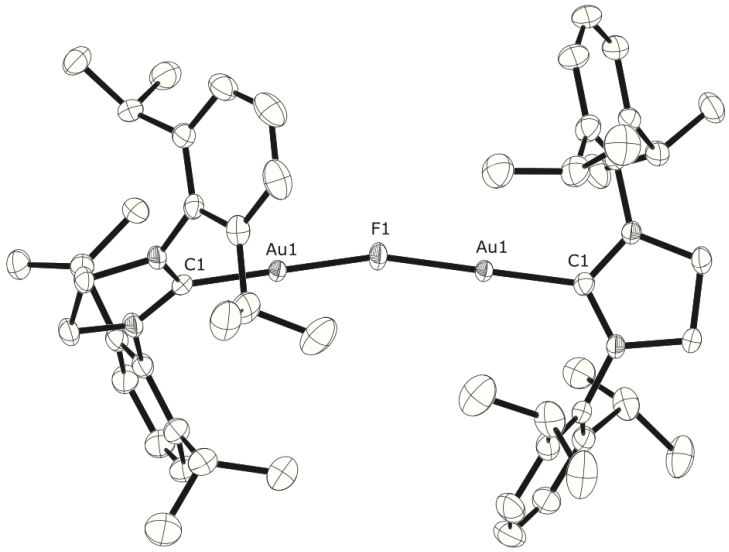

Figure 3.3. Solid-state structure of fluoride-bridged digold complex **13**. Hydrogen atoms and BF_4^- counterion omitted for clarity.

3.3.5 Reactions of Fluoride-Bridged Dinuclear Complexes

The hydrolysis of the fluoride-bridged complexes **11–13** exemplifies their chemical behavior from the perspective of the hard-soft acid and base model of reactivity. The fluoride ion has far less affinity for a proton than hydroxide does.[19] One would expect a proton transfer equilibrium to lie many orders of magnitude in favor of H_2O and F^-, rather than HF and OH^-. However, clearly H–OH bond breaking and H–F bond formation do not account for the full hydrolysis of **11–13**. The breaking of weak M–F bonds and formation of relatively strong M–OH bonds is the apparent driving force of the observed hydrolyses. The hard-soft mismatches between the monovalent group 11 metals

and the fluoride ion are quenched, resulting in the formation of less mismatched acid-base pairs. In addition to their propensity to hydrolyze upon exposure to moisture, the fluoride-bridged complexes exhibit further chemical behavior consistent with their high degree of hard/soft mismatch.

We initially recorded NMR spectra in CD_2Cl_2 solution in order to mitigate the apparent dissociation of the fluoride-bridged complexes that was encountered in more strongly coordinating solvents, and **11–13** seemed to be inert during the time required to collect NMR spectra. In fact, silver complex **12** does not seem to react with CD_2Cl_2 at all. After 24 h in CD_2Cl_2 solution, only trace decomposition of **12** to the homoleptic complex $[(5Dipp)_2Ag]^+$ was observed by ^1H NMR spectroscopy. Likewise, copper complex **11** is stable in CD_2Cl_2 overnight. However, after revisiting a solution of the gold complex **13** after 24 h in CD_2Cl_2 solution, quantitative conversion of **13** to the chloride-bridged complex $\{[(5Dipp)Au]_2(\mu\text{-}Cl)\}^+$ was observed by ^1H NMR spectroscopy. Since the solvent was the only source of chloride present, we anticipated that halogen exchange between **13** and CD_2Cl_2 had occurred (Scheme 3.4). Indeed, analysis of the solution by ^{19}F NMR revealed the presence of CD_2ClF and CD_2F_2. Similar halide exchange processes have been observed for fluoride complexes of palladium(II).[20]

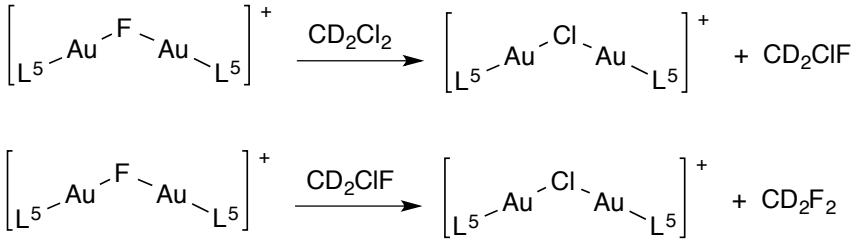

Scheme 3.4. Reaction of fluoride-bridged digold complex **13** with CD_2Cl_2.

New methods for the selective and efficient fluorination of organic substrates are of interest due to the prevalence of fluorine-containing pharmaceuticals as well as the need for rapid preparation of ^{18}F-enriched tracers for positron emission tomography. The insertion of an unsaturated organic substrate into a M–F bond could constitute a key step in these fluorination processes or potentially in the formation of fluorinated polymers.[14,21] We therefore investigated the reactivity of the fluoride-bridged group 11 complexes towards unsaturated C–C bonds and discovered that the gold complex **13** rapidly and quantitatively adds across the substituted double bond of the allene 3-methyl-1,3-butadiene in THF-d_8 solution (Scheme 3.5). ^{1}H and ^{19}F NMR characterization of the insertion product suggested fluorination of the fully substituted carbon in the 3-position and auration of the carbon in the 2-position. Although only one set of 5Dipp resonances in the ^{1}H NMR suggested equivalence of the 5Dipp ligands, it was unclear based on NMR spectroscopy whether the doubly aurated fluorovinyl carbanion was bound to the gold centers in a symmetrical three-centered, two-electron binding mode. Another possibility was an asymmetrical σ,π-binding mode[15] in which one 5DippAg fragment forms a σ-bond to the carbanion while the other forms a π-bond to the remaining C=C double bond. This σ,π-binding mode would require rapid exchange of the 5DippAg fragments in order to account for the NMR equivalence of the 5Dipp ligands. The allene insertion product crystallized as its tetrafluoroborate salt with a significant degree of disorder, especially in the 5Dipp ligands, but the connectivity of the gold atoms and the bridging fluorovinyl carbanion were determined with confidence via X-ray diffraction crystallography, confirming the complex adopts the asymmetrical σ,π-binding mode in the solid state.

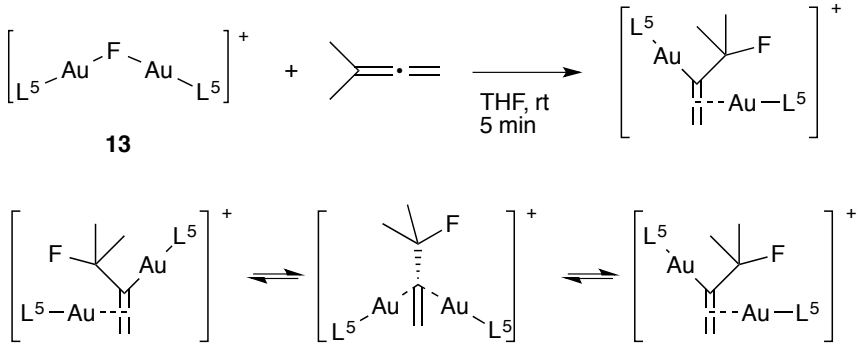

Scheme 3.5. Reaction of fluoride-bridged digold complex **13** with 3-methyl-1,3-butadiene and proposed exchange of 5DippAu fragments in the resulting fluorovinyl digold complex.

No sign of reaction between the silver complex **12** and 3-methyl-1,3-butadiene was detected by ^{1}H NMR spectrscopy after 24 h in CD_2Cl_2. Under similar conditions the copper complex **11** reacts with the allene, giving rise after 30 min to a doublet in its ^{1}H NMR spectrum at δ 0.10 ppm, consistent with the formation of a fluorovinyl species, and a new set of 5Dipp resonances. Integration of peak areas suggest the new species accounts for less than 10% conversion of the starting complex, and the reaction was not found to proceed further after several hours, suggesting that an equilibrium had been reached, in which **11** is favored over the insertion product even in the presence of a significant excess of the allene.

The reactions of silver complexes **7** and **12** with hydrogen likewise reflect behavior consistent with their hard-soft mismatched Ag–F bonds and are described in Chapter 5.

3.4 Conclusion

Dinculear fluoride-bridged complexes of copper, silver, and gold, supported by the NHC ligand 5Dipp, were prepared by partial abstraction of fluoride from known

mononuclear terminal fluoride complexes. ^{19}F NMR characterization suggests that coordination of solvent may cause dissociation of the complexes. The structures of the fluoride-bridged complexes were confirmed by X-ray diffraction studies, which suggest varying degrees of ionic versus covalent character in the metal-fluorine bonds, with the copper complex having the most covalent character and silver the most ionic. The fluoride-bridged complexes exhibit reactivity consistent with the hard-soft mismatch between the soft monovalent group 11 metals and the hard fluoride ion. Their tendency to hydrolyze required the development of a new reliably moisture-free synthesis of the mononuclear precursors, which was achieved through the substitution of benzoyl fluoride for treat-HF as the source of fluoride. Other reactions include the exchange of halide between the digold fluoride and CD_2Cl_2 as well as the addition of the digold fluoride to an allene to produce a diaurated fluorovinyl complex, which was found to adopt an asymmetric σ,π-binding mode in the solid state.

3.5 Experimental

3.5.1 General Considerations

Unless otherwise indicated, manipulations were performed in an MBraun glovebox under an inert atmosphere of nitrogen, or in resealable glassware on a Schlenk line under an atmosphere of argon. Glassware and magnetic stir bars were dried in a ventilated oven at 160˚C and were allowed to cool under vacuum. Compounds of silver were stored in the dark as a precaution against photodegradation, and glassware was covered with aluminum foil during manipulations to minimize exposure to light.

^{1}H, ^{13}C, ^{19}F, NMR spectra were obtained using a Bruker DSX 400 MHz spectrometer, a Varian Vx 400 MHz spectrometer, and a Varian Mercury 300

spectrometer. ^{1}H and ^{13}C NMR chemical shifts are referenced with respect to solvent signals[22] and are reported relative to tetramethylsilane. ^{19}F NMR chem- ical shifts were referenced to external neat hexafluorobenzene (Alfa-Aesar, δ –164.90 ppm) and are reported with respect to fluorotrichloromethane.

Samples for infrared spectroscopy were prepared as pellets in potassium bromide, using a pellet die which was dried in a ventilated oven at 160˚C and cooled under vacuum prior to use. The pellets were prepared in the glovebox under an atmosphere of dry nitrogen, and were exposed to air as briefly as possible prior to data collection. Spectra were recorded using a Perkin Elmer Spectrum 1000 or a Bruker Alpha-P infrared spectrometer.

Elemental analyses were performed by Atlantic Microlab, Inc. in Norcross, GA.

3.5.2 Materials and Methods

Hexanes (EMD Millipore Omnisolv), tetrahydrofuran (THF, EMD Millipore Omnisolv), and toluene (EMD Millipore Omnisolv) were sparged with ultra high purity argon (NexAir) for 30 min prior to first use, and dried using an MBraun solvent purification system. These solvents were further dried over sodium benzophenone ketyl, transferred under vacuum to an oven-dried sealable flask, and degassed by successive freeze–pump–thaw cycles. Anhydrous benzene (EMD Millipore Drisolv) was stored over 3Å molecular sieves (Alfa-Aesar) in a glovebox.

Dichloromethane-d_2 (Cambridge Isotope Laboratories) was dried by stirring overnight over calcium hydride. It was then vacuum-transferred to an oven-dried resealable Schlenk flask, and degassed by successive freeze–pump–thaw cycles. Tetrahydrofuran-d_8 (Cambridge Isotope Laboratories) was dried over sodium

benzophenone ketyl, transferred under vacuum to an oven-dried resealable flask, and degassed by successive freeze–pump–thaw cycles.

Sodium *tert*-butoxide (TCI America), copper(I) chloride (Alfa-Aesar), triphenylcarbenium tetrafluoroborate (Alfa-Aesar), 2,6-diisopropylaniline (Sigma–Aldrich), acetic acid (Alfa-Aesar), glyoxal 40% w/w aqueous solution (Alfa-Aesar), methanol (BDH), acetone (BDH), dichloromethane (BDH) hydrochloric acid (EMD), sodium borohydride (Alfa-Aesar), benzoyl fluoride (Alfa-Aesar), triethyl orthoformate (Alfa-Aesar), formic acid (Alfa-Aesar), potassium carbonate (Alfa-Aesar), 3-methyl-1,2-butadiene (Sigma–Aldrich), silver(I) oxide (Sigma–Aldrich), dimethyl sulfide (Alfa-Aesar), tetrachloroauric acid (Strem), sodium metal (Alfa- Aesar), benzophenone (Alfa-Aesar), calcium hydride (Alfa-Aesar), potassium bromide (Sigma–Aldrich), nitrogen (NexAir), and argon (both industrial and ultra high purity grades, NexAir) were used as received. 5Dipp•HCl,[23] (5Dipp)CuCl,[8] (5Dipp)Cu(O^{t}Bu),[8] (5Dipp)AgCl,[14h] (5Dipp)Ag(O^{t}Bu),[16b] (5Dipp)AuCl,[24] and (5Dipp)Au(O^{t}Bu),[14h] were prepared as described previously, and characterized by ^{1}H NMR spectroscopy.

3.5.2.1 (5Dipp)CuF (**6**)

Benzoyl fluoride (0.089 mL, 0.102 g, 0.818 mmol) was added to a solution of (5Dipp)Cu(O^{t}Bu) (0.287 g, 0.544 mmol) in toluene (4 mL) with stirring. After 3 h, a white precipitate had formed. The precipitate was collected on a fritted glass filter and washed with two portions of toluene (6 mL each) and two portions of hexanes (5 mL each). Residual solvents were removed under vacuum at 40˚C over 18 h, affording the product as a white powder (0.221 g, 0.467 mmol, 86%). ^{1}H NMR (400 MHz, CD_2Cl_2): δ

(ppm) 7.45 (t, J = 7.8 Hz, 2H, *para*-C*H*), 7.30 (d, J = 7.8 Hz, 4H, *meta*-C*H*), 4.01 (s, 4H, NC*H*2), 3.07 (sept, J = 6.9 Hz, 4H, C*H*$(CH_3)_2$), 1.36 (d, J = 6.8 Hz, 12H, CH(C*H*$_3)_2$), 1.35 (d, J = 6.8 Hz, 12H, CH(C*H*$_3)_2$). $^{13}C\{^1H\}$ NMR (100 MHz, CD_2Cl_2): δ (ppm) 203.7 (br N*C*Cu), 147.2 (*ortho*-*C*), 135.1 (*ipso*-*C*), 130.0 (*para*-*C*), 124.9 (*meta*-*C*), 54.1 (N*C*H_2), 29.2 (*C*H$(CH_3)_2$), 25.5 (CH(*C*$H_3)_2$), 24.0 (CH(*C*$H_3)_2$). ^{19}F NMR (375 MHz, CD_2Cl_2): δ (ppm) –238.5. IR: ν (cm^{-1}) 3075 (w), 2962 (s), 2924, 2867, 1591 (w), 1482 (s), 1458 (s), 1421, 1384, 1361, 1327, 1300, 1269 (s), 1180 (w), 1164 (w), 1099 (w), 1061, 1017 (w), 993 (w), 936, 925, 807 (s), 766, 708 (w), 619 (w), 560, 543, 504 (w), 477 (w), 449, 425 (w), 398 (w). Elemental analysis calculated for $C_{27}H_{38}N_2CuF$: C, 68.54; H, 8.10; N, 5.92; F, 4.02. Found: C, 68.21; H, 7.98; N, 5.79; F, 3.96.

3.5.2.2 $\{[(5Dipp)Cu]_2(\mu\text{-}F)\}^+BF_4^-$ (**11**[BF_4])

Triphenylcarbenium tetrafluoroborate (0.025 g, 0.076 mmol) was added to a solution of (5Dipp)CuF (0.072 g, 0.152 mmol) in THF (3 mL) with stirring. After 1 h, hexanes (15 mL) were added to the reaction mixture, resulting in the formation of a white precipitate. The mother liquor was decanted, and the residual solvents were removed under vacuum at 35˚C over 18 h, affording the product as a white powder (0.059 g, 0.058 mmol, 77%). ^1H NMR (400 MHz, CD_2Cl_2): δ (ppm) 7.42 (t, J = 7.8 Hz, 4H, *para*-C*H*), 7.20 (d, J = 7.8 Hz, 8H, *meta*-C*H*), 3.99 (s, 8H, NC*H*2), 2.90 (sept, J = 6.9 Hz, 8H, C*H*$(CH_3)_2$), 1.30 (d, J = 6.8 Hz, 24H, CH(C*H*$_3)_2$), 1.06 (d, J = 6.8 Hz, 24H, CH(C*H*$_3)_2$). $^{13}C\{^1H\}$ NMR (100 MHz, CD_2Cl_2): δ (ppm) 200.7 (br, N*C*Cu), 147.1 (*ortho*-*C*), 134.6 (*ipso*-*C*), 130.3 (*para*-*C*), 125.0 (*meta*-*C*), 54.5 (N*C*H2), 29.1 (*C*H$(CH_3)_2$), 25.6 (CH(*C*$H_3)_2$), 24.0 (CH(*C*$H_3)_2$). ^{19}F NMR (375 MHz, CD_2Cl_2): δ (ppm) –153.26 (s,

$^{10}BF_4^-$), –153.31 (s, $^{11}BF_4^-$), –311.11 (br s, Cu*F*Cu). IR: ν (cm^{-1}) 3074 (w), 2963 (s), 2924, 2867, 1490 (s), 1459 (s), 1384, 1363, 1329, 1273 (s), 1176 (w), 1057 (s), 931 (w), 806, 761, 620 (w), 448 (w). Elemental analysis calculated for $C_{54}H_{76}N_4Cu_2BF_5$: C, 63.96; H, 7.55; N, 5.52; F, 9.37. Found: C, 63.62; H, 7.60; N, 5.37; F, 9.04. ^{1}H NMR (400 MHz, THF-d_8): δ (ppm) 7.35 (t, J = 7.6 Hz, 4H, *para*-C*H*), 7.21 (d, J = 8.0 Hz, 8H, *meta*-C*H*), 4.09 (s, 8H, NCH_2), 3.08 (sept, J = 6.8 Hz, 8H, C*H*$(CH_3)_2$), 1.28 (d, J = 6.8 Hz, 24H, CH(CH_3)$_2$), 1.12 (d, J = 6.8 Hz, 24H, CH(CH_3)$_2$). ^{19}F NMR (375 MHz, THF-d_8): δ (ppm) –152.79 (s, $^{10}BF_4^-$), –152.84 (s, $^{11}BF_4^-$), –291.14 (br s, Cu*F*Cu). Diffraction-quality crystals were grown by layering toluene onto a THF solution of **11**.

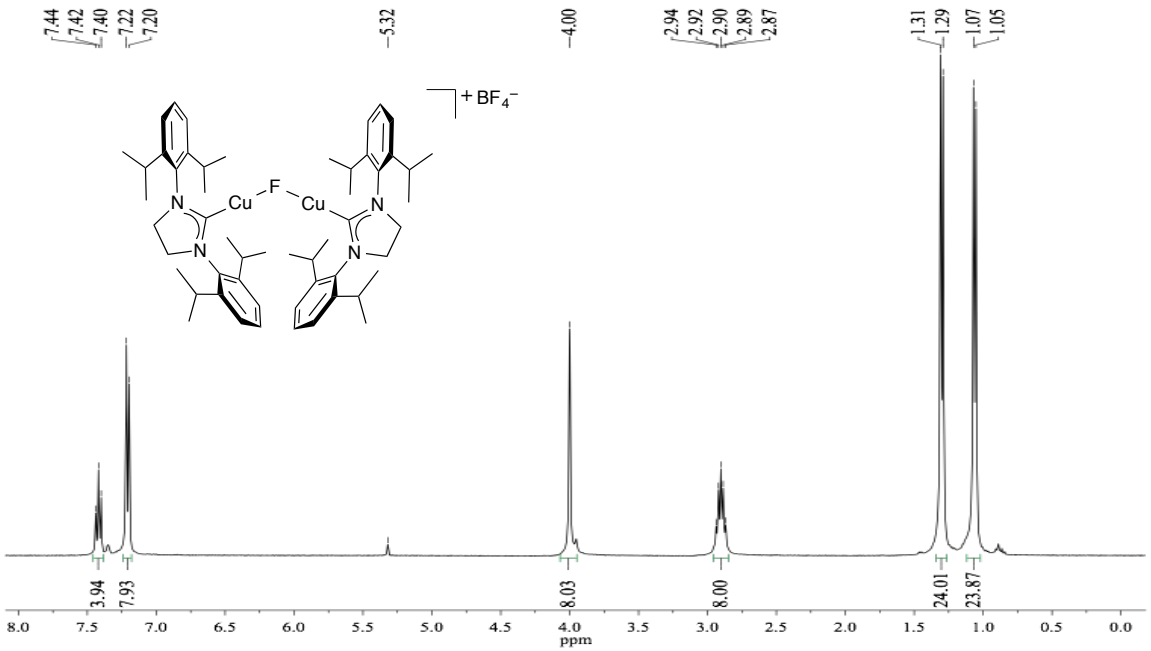

Figure 3.4. ^{1}H NMR (400 MHz, CD_2Cl_2) spectrum of **11**[BF_4].

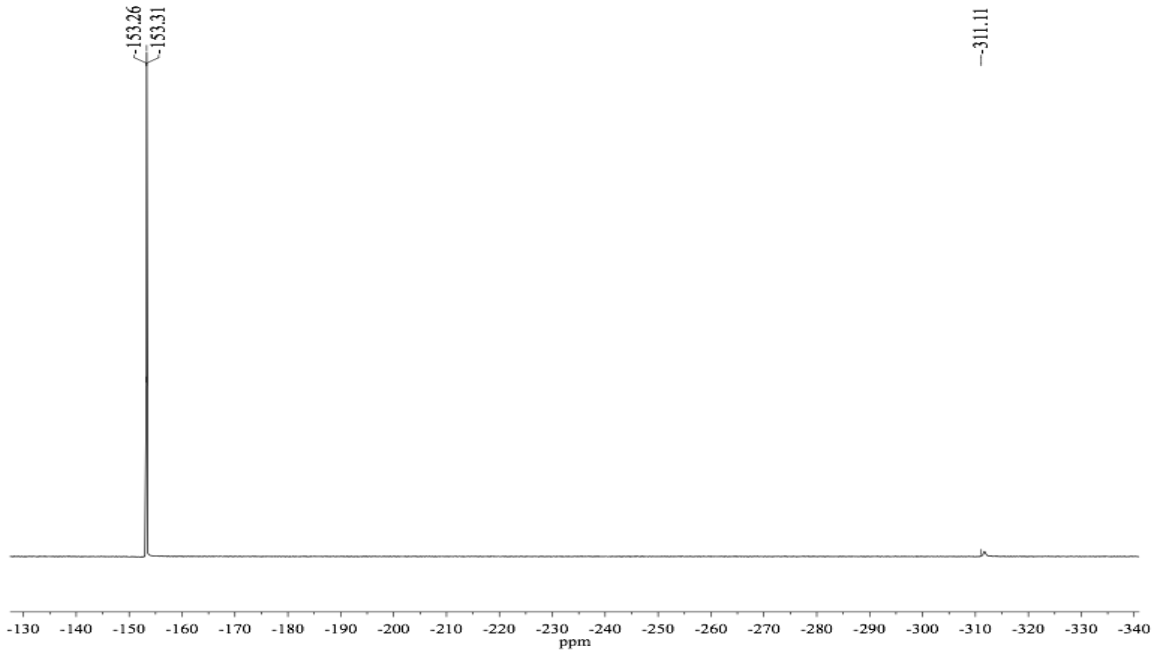

Figure 3.5. ^{19}F NMR (375 MHz, CD_2Cl_2) spectrum of **11**[BF_4].

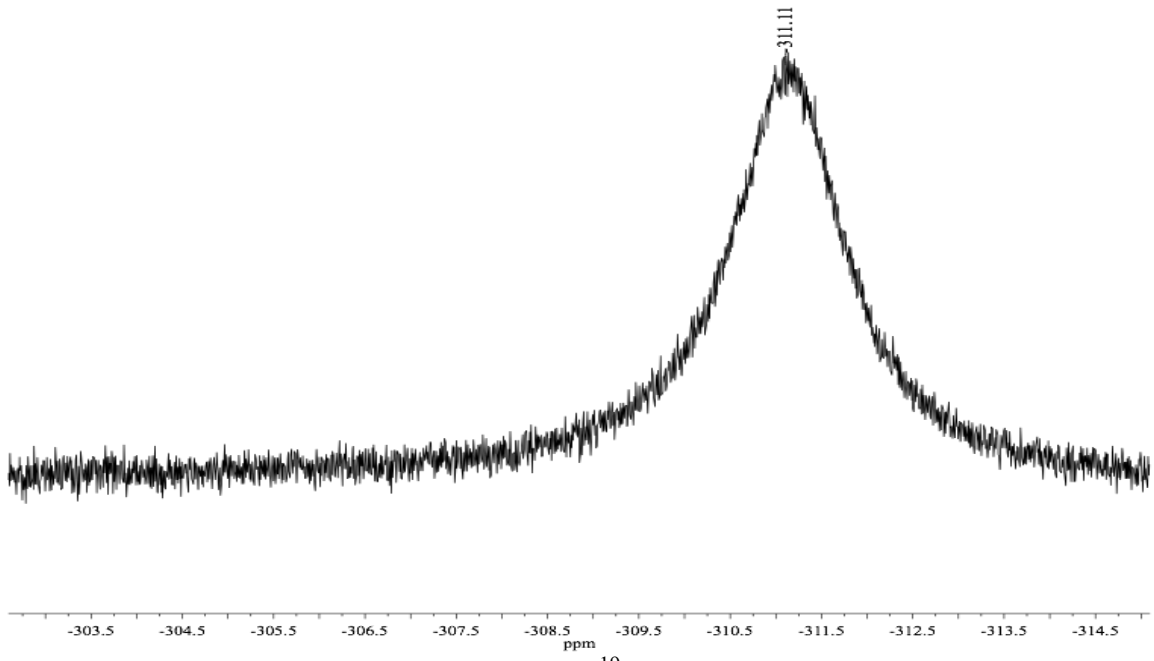

Figure 3.6. Detail of μ-fluoride resonance of ^{19}F NMR (375 MHz, CD_2Cl_2) spectrum of **11**[BF_4].

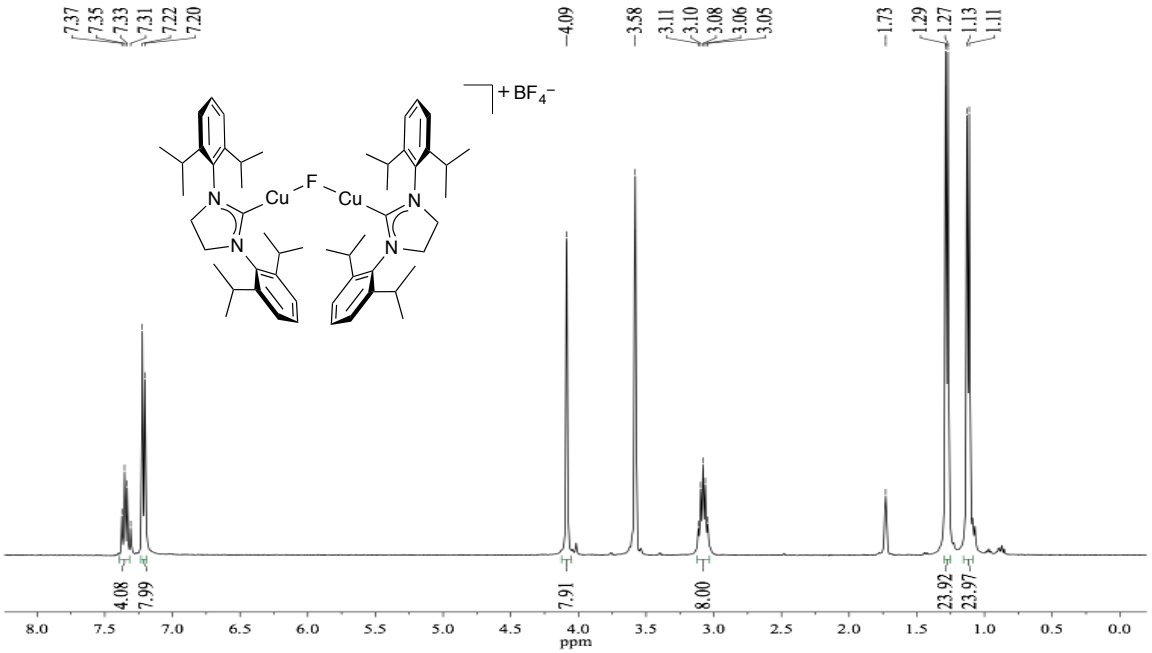

Figure 3.7. ^{1}H NMR (400 MHz, THF-d_8) spectrum of **11**[BF_4]. A trace of benzene (δ 7.31 ppm) is present as the result of benzophenone ketyl decomposition.

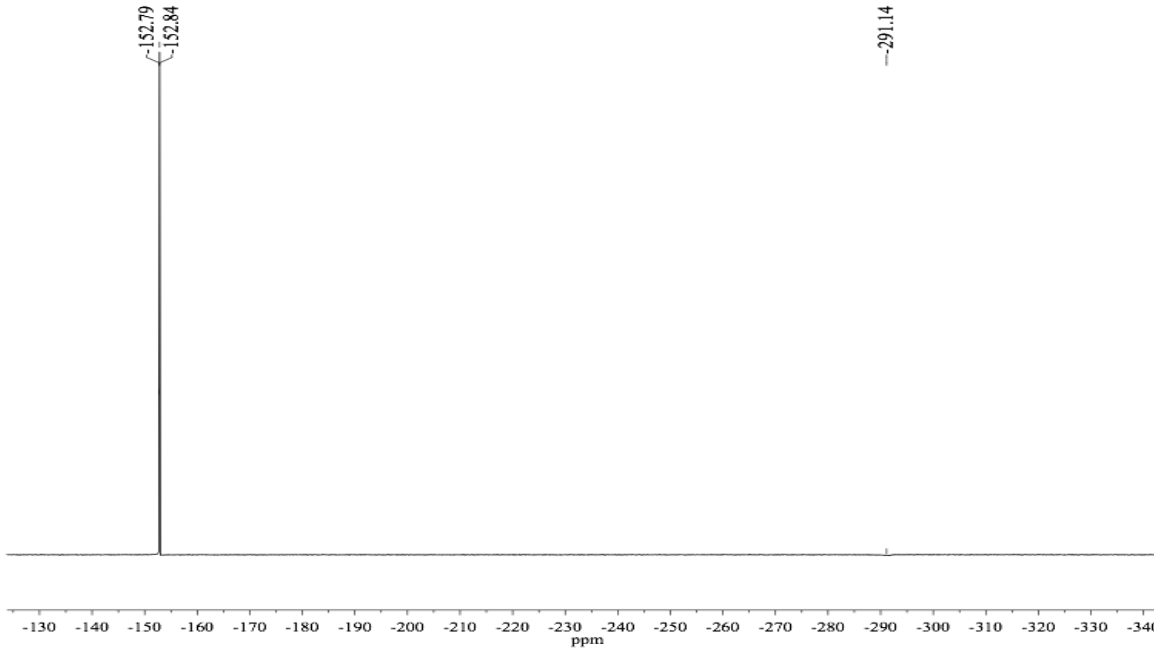

Figure 3.8. ^{19}F NMR (375 MHz, THF-d_8) spectrum of **11**[BF_4].

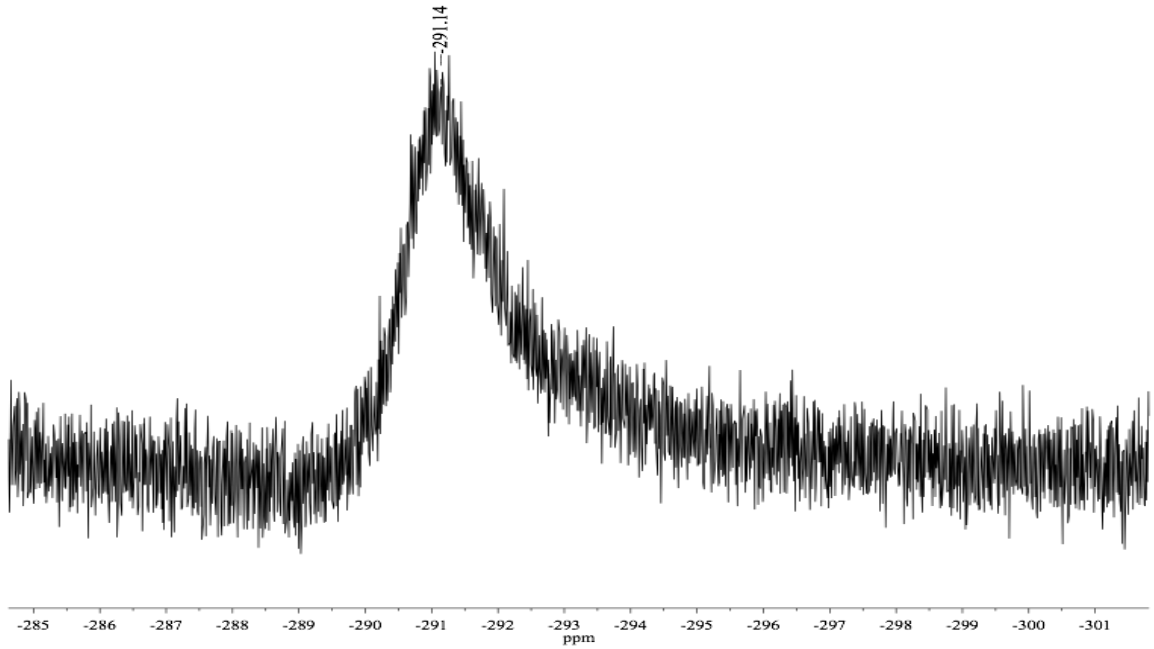

Figure 3.9. Detail of μ-fluoride resonance of ^{19}F NMR (375 MHz, THF-d_8) spectrum of **11**[BF_4].

3.5.2.3 (5Dipp)AgF (**7**)

Benzoyl fluoride (0.374 mL, 0.426 g, 3.43 mmol) was added to a solution of (5Dipp)Ag(O^{t}Bu) (1.308 g, 2.288 mmol) in benzene (4 mL). The reaction flask was covered with foil to exclude light, and the mixture was stirred for 3 h. The resulting white precipitate was collected on a fritted glass filter and washed with three portions of benzene (2 mL each). Residual solvents were removed in the dark under vacuum at 40˚C for 16 h, affording the product as a white powder (1.045 g, 2.019 mmol, 88%). ^{1}H NMR (400 MHz, CD_2Cl_2): δ (ppm) 7.45 (t, J = 7.8 Hz, 2H, *para*-C*H*), 7.29 (d, J = 7.8 Hz, 4H, *meta*-C*H*), 4.07 (s, 4H, NCH_2), 3.06 (sept, J = 6.9 Hz, 4H, CH(CH_3)$_2$), 1.34 (d, J = 6.9 Hz, 12H, CH(CH_3)$_2$), 1.33 (d, J = 6.9 Hz, 12H, CH(CH_3)$_2$). ^{13}C{^{1}H} NMR (100 MHz, CD_2Cl_2): δ (ppm) 206.3 (app. dd, J(^{13}C-^{109}Ag) = 271 Hz, J(^{13}C-^{107}Ag) = 240 Hz, N*C*Ag), 147.1 (*ortho*-*C*), 135.2 (*ipso*-*C*), 130.2 (*para*-*C*), 125.0 (*meta*-*C*), 54.3 (d, J(^{13}C-$^{107/109}$Ag)

= 9 Hz N*C*H$_2$), 29.1 (*C*H(CH$_3$)$_2$), 25.5 (CH(*C*H$_3$)$_2$), 24.1 (CH(*C*H$_3$)$_2$). ^{19}F NMR (375 MHz, CD_2Cl_2): δ (ppm) –243.13 (d, J(^{19}F-$^{107/109}$Ag) = 163 Hz). IR: ν (cm^{-1}) 3073 (w) 3036 (w), 2963 (s), 2943, 2868, 1965 (w), 1820 (w), 1718 (w), 1591 (w), 1486 (s), 1477 (s), 1384, 1364, 1326, 1269, 1180, 1103, 1058, 936, 914, 807, 763, 683, 619, 548, 448. Elemental analysis calculated for $C_{27}H_{38}N_2AgF$: C, 62.67; H, 7.40; N, 5.41; F, 3.67. Found: C, 62.48; H, 7.31; N, 5.32; F, 3.40.

3.5.2.4 {[(5Dipp)Ag]$_2$(μ-F)}$^+$BF$_4^-$ (**12**[BF$_4$])

Triphenylcarbenium tetrafluoroborate (0.064 g, 0.19 mmol) was added to a solution of (5Dipp)AgF (0.200 g, 0.386 mmol) in THF (4 mL). The reaction flask was covered with foil to exclude light, and the mixture was stirred for 2 h. A layer of hexanes (12 mL) was carefully added over the THF solution, and the layers were allowed to mix by diffusion at –35 °C for 16 h, resulting in the formation of colorless crystals. The mother liquor was decanted, and the crystals were washed with two portions of hexanes (2 mL each). Residual solvents were removed in the dark under vacuum at 40˚C for 16 h, affording the product as a white powder (0.177 g, 0.160 mmol, 83%). ^{1}H NMR (400 MHz, CD_2Cl_2): δ (ppm) 7.43 (t, J = 7.8 Hz, 2H, *para*-C*H*), 7.24 (d, J = 7.8 Hz, 4H, *meta*-C*H*), 4.07 (s, 4H, NC*H*$_2$), 2.98 (sept, J = 6.9 Hz, 4H, C*H*(CH$_3$)$_2$), 1.32 (d, J = 6.9 Hz, 12H, CH(C*H*$_3$)$_2$), 1.17 (d, J = 6.9 Hz, 12H, CH(C*H*$_3$)$_2$). ^{13}C{^{1}H} NMR (100MHz, CD_2Cl_2): δ (ppm) 204.9 (app. dd, J(^{13}C-^{109}Ag) = 300 Hz, J(^{13}C-^{107}Ag) = 261 Hz, N*C*Ag), 147.0 (*ortho*-*C*), 134.9 (*ipso*-*C*), 130.3 (*para*-*C*), 125.0 (*meta*-*C*), 54.4 (d, J(^{13}C-$^{107/109}$Ag) = 10 Hz, N*C*H$_2$), 29.1 (*C*H(CH$_3$)$_2$), 25.5 (CH(*C*H$_3$)$_2$), 24.0 (CH(*C*H$_3$)$_2$). ^{19}F NMR (375 MHz, CD_2Cl_2): δ (ppm) –153.60 (s, ^{10}B*F*$_4^-$), –153.65 (s, ^{11}B*F*$_4^-$), –308.5 (br s, Ag*F*Ag).

IR: ν (cm^{-1}) 3073 (w), 2966 (s), 2945, 2871, 1590 (w), 1489 (s), 1462 (s), 1385, 1365, 1327, 1275 (s), 1183, 1103, 1062 (s), 936, 932, 807, 759, 711, 620, 548, 520, 449. Elemental analysis calculated for $C_{54}H_{76}N_4Ag_2BF_5$: C, 58.81; H, 6.95; N, 5.08; F, 8.61. Found: C, 59.07; H, 7.13; N, 5.07; F, 8.38. ^{1}H NMR (400 MHz, THF-d_8): δ (ppm) 7.38 (mult, J = 7.8 Hz, 2H, *para*-C*H*), 7.25 (mult, J = 7.8 Hz, 4H, *meta*-C*H*), 4.18 (s, 4H, NCH_2), 3.13 (sept, J = 6.9 Hz, 4H, CH(CH_3)$_2$), 1.32 (d, J = 6.9 Hz, 12H, CH(CH_3)$_2$), 1.19 (d, J = 6.9 Hz, 12H, CH(CH_3)$_2$). ^{19}F NMR (375 MHz, THF): δ (ppm) –154.23 (s, ^{10}BF_4^-), –154.28 (s, ^{11}BF_4^-), –302.9 (br s, AgFAg). Diffraction-quality crystals were grown by cautious layering of toluene onto a THF solution of **12** followed by diffusion in the dark at –35˚C.

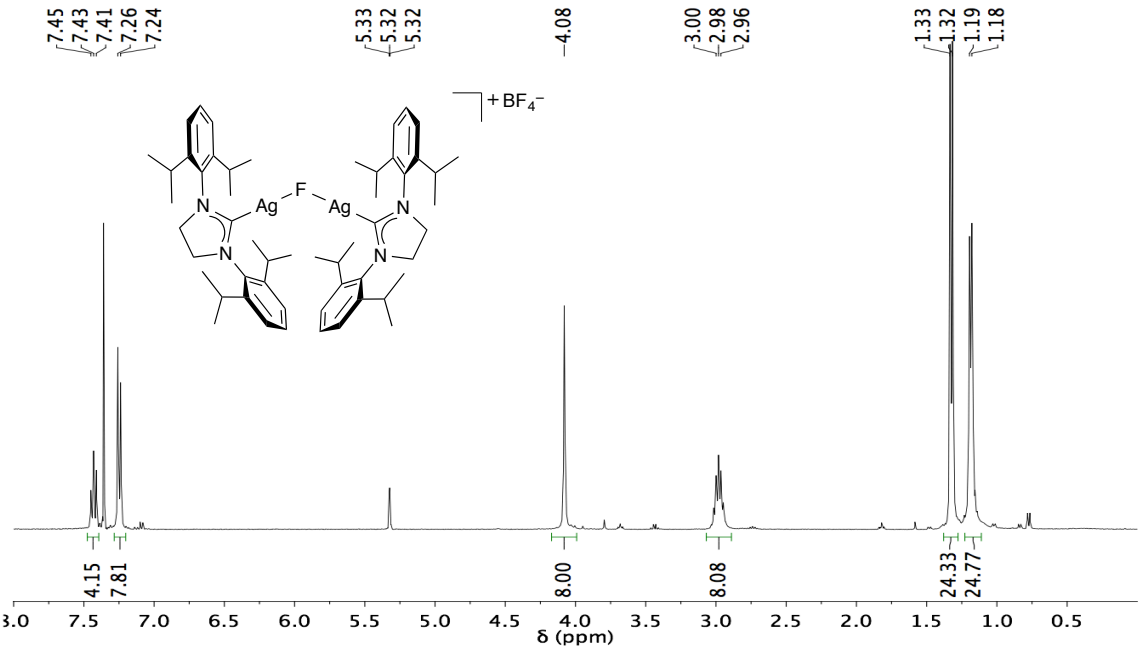

Figure 3.10. ^{1}H NMR (400 MHz, CD_2Cl_2) spectrum of **12**[BF_4]. Adventitious benzene (δ 7.31 ppm) and a trace of the known complex [(5Dipp)$_2$Ag]$^+$ are present.

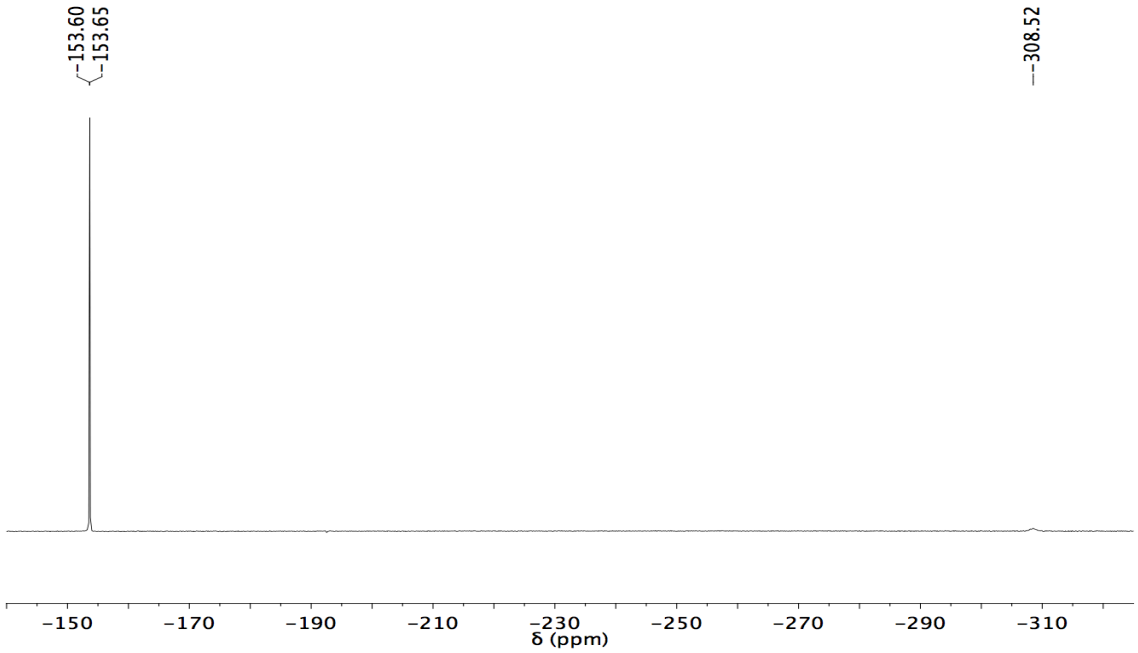

Figure 3.11. ^{19}F NMR (375 MHz, CD_2Cl_2) spectrum of **12**[BF_4].

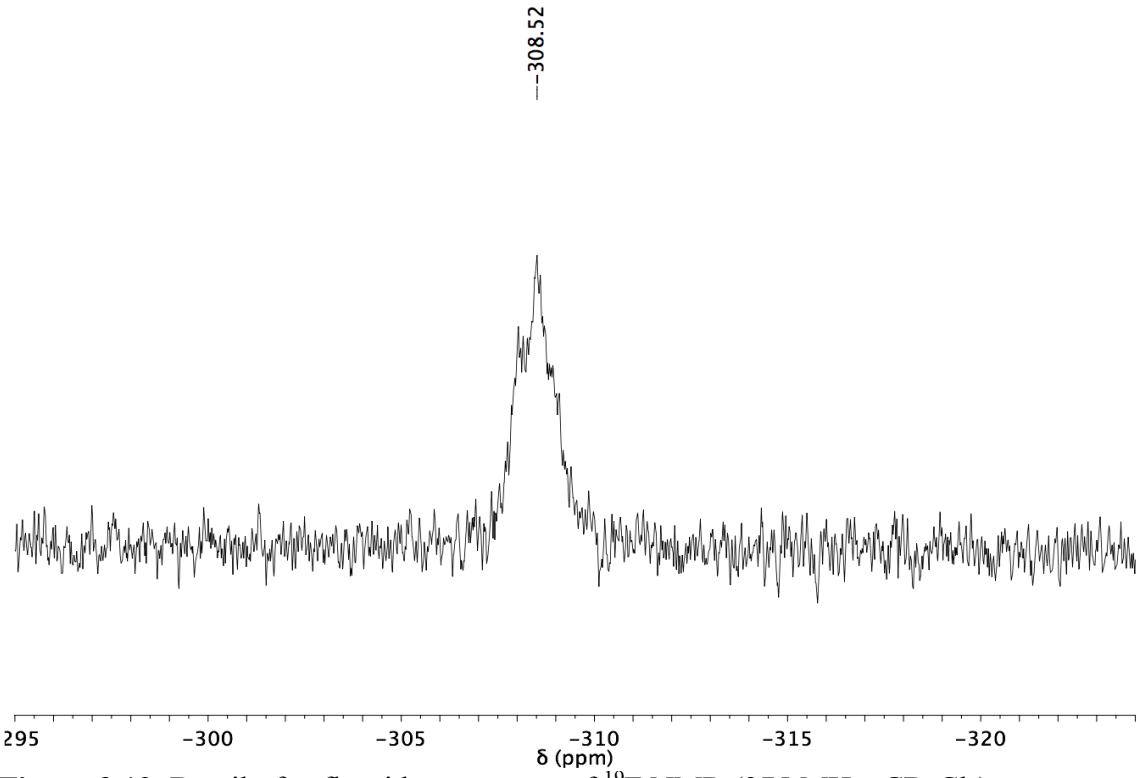

Figure 3.12. Detail of μ-fluoride resonance of ^{19}F NMR (375 MHz, CD_2Cl_2) spectrum of **12**[BF_4].

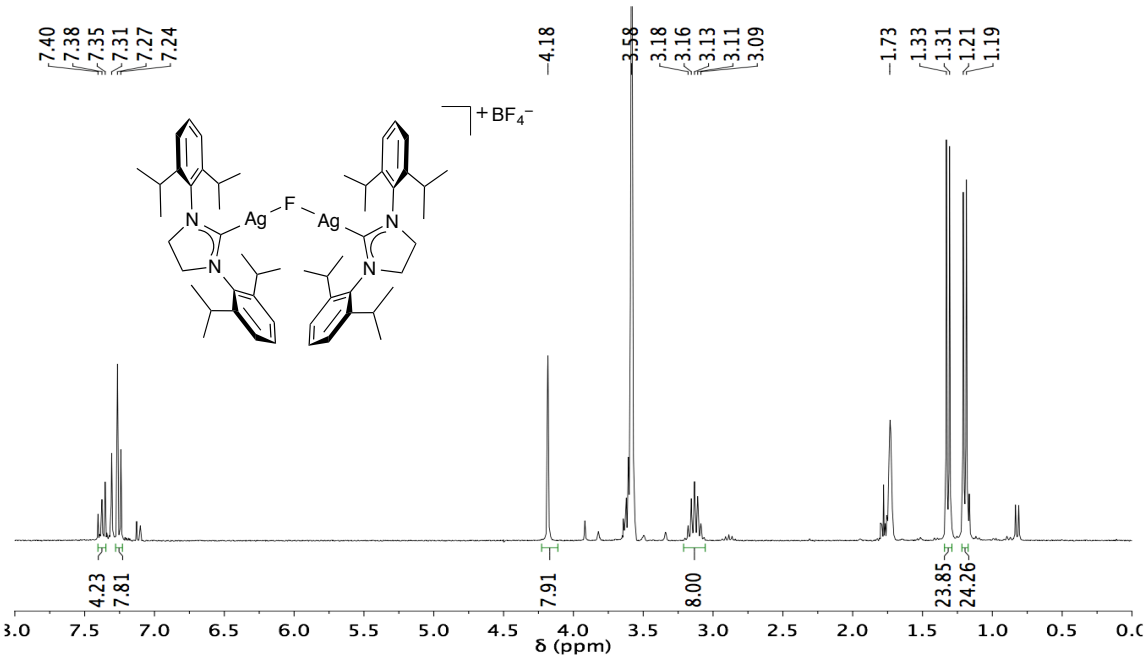

Figure 3.13. ^{1}H NMR (400 MHz, THF-d_8) spectrum of **12**[BF_4]. Adventitious benzene (δ 7.31 ppm) and a trace of the known complex $[(5Dipp)_2Ag]^+$ are present.

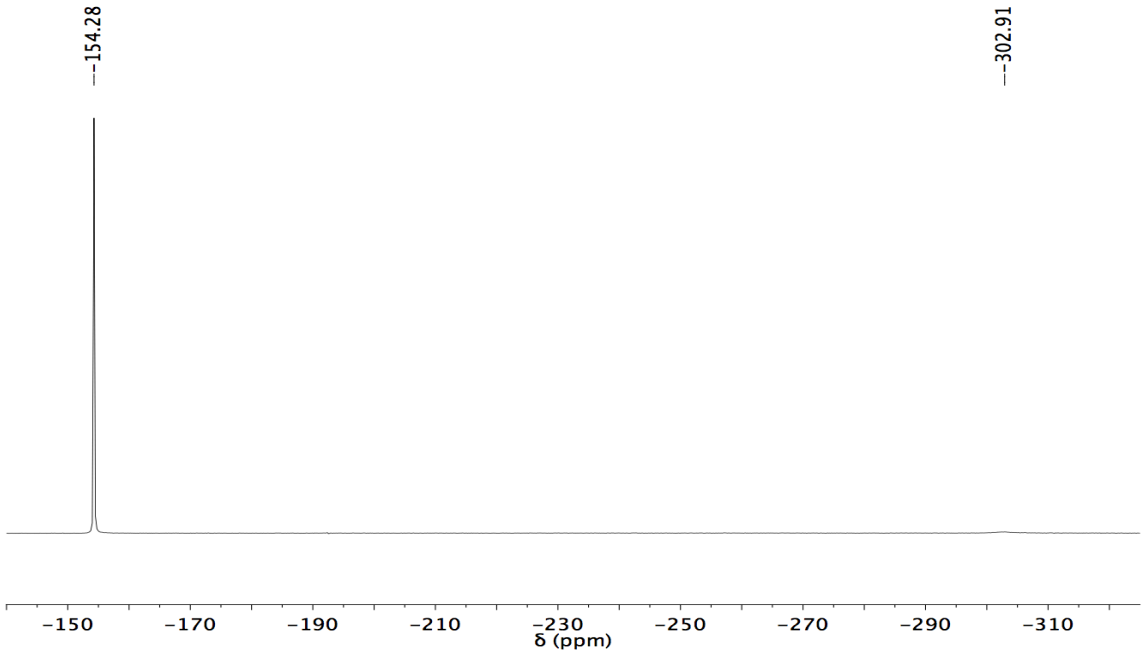

Figure 3.14. ^{19}F NMR (375 MHz, THF-d_8) spectrum of **12**[BF_4].

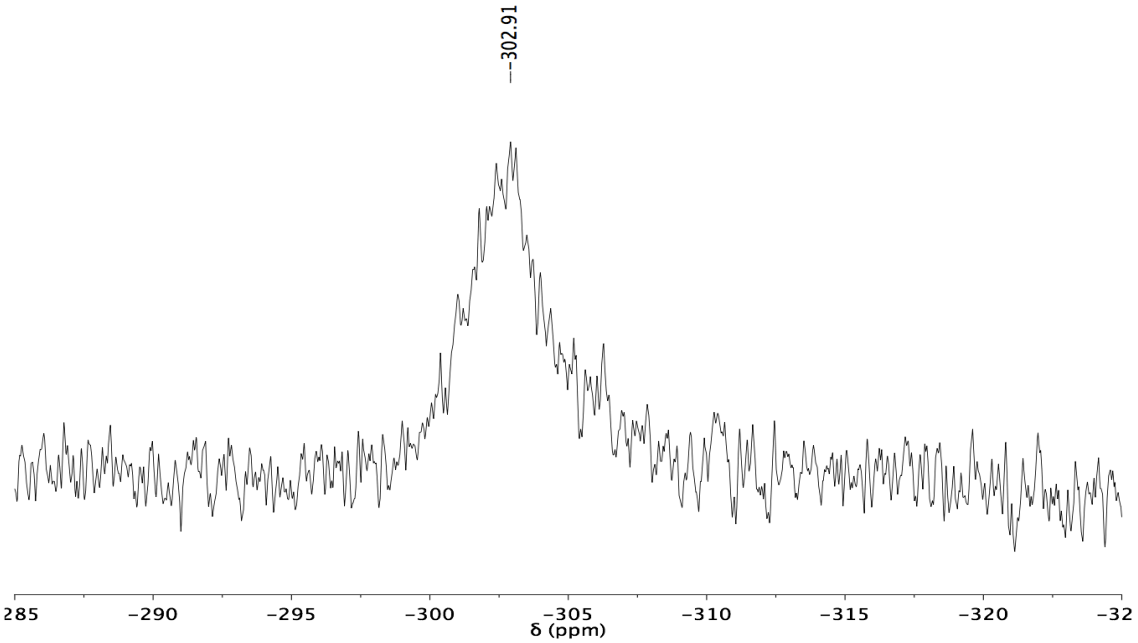

Figure 3.15. Detail of μ-fluoride resonance of ^{19}F NMR (375 MHz, CD_2Cl_2) spectrum of **12**[BF_4].

3.5.2.5 (5Dipp)AuF (**8**)

Benzoyl fluoride (0.065 mL, 0.074 g, 0.597 mmol) was added to a solution of (5Dipp)Au(O^{t}Bu) (0.265 g, 0.401 mmol) in toluene (4 mL) with stirring. After 3 h, a white precipitate had formed. The precipitate was collected on a fritted glass filter and washed with two portions of toluene (6 mL each) and two portions of hexanes (5 mL each). Residual solvents were removed under vacuum at 35˚C over 18 h, affording the product as a white powder (0.216 g, 0.356 mmol, 91%). ^{1}H NMR (400 MHz, CD_2Cl_2): δ (ppm) 7.47 (t, J = 7.8 Hz, 2H, *para*-C*H*), 7.29 (d, J = 7.6 Hz, 4H, *meta*-C*H*), 4.05 (s, 4H, NCH_2), 3.04 (sept, J = 6.9 Hz, 4H, C*H*(CH_3)$_2$), 1.41 (d, J = 6.8 Hz, 12H, CH(CH_3)$_2$), 1.34 (d, J = 6.8 Hz, 12H, CH(CH_3)$_2$). ^{19}F NMR (375 MHz, CD_2Cl_2): δ (ppm) –247.16. The ^{1}H and ^{19}F NMR spectra for this sample match those of (5Dipp)AuF prepared according to the previously published method.[14h]

3.5.2.6 {[(5Dipp)Au](μ-F)}$^{+}BF_4^{-}$ (**13**)

Triphenylcarbenium tetrafluoroborate (0.019 g, 0.058 mmol) was added to a solution of (5Dipp)AuF (0.070 g, 0.115 mmol) in THF (4 mL) in a flame-dried resealable flask with stirring. The flask was sealed, removed from the glovebox and brought out to the Schlenk line. After 1 h, the solution was concentrated to a volume of about 1 mL. Hexanes (ca. 20 mL) were transferred under vacuum from a solution of sodium benzophenone ketyl into the reaction mixture, resulting in the formation of a white precipitate. The mother liquor was decanted via cannula, and the residual solvents were removed over 18 h under vacuum at 35˚C, affording the product as a white powder (0.063 g, 0.049 mmol, 84%). ^{1}H NMR (400 MHz, THF-d_8): δ (ppm) 7.39 (t, J = 7.8 Hz, 4H, *para*-C*H*), 7.24 (d, J = 8.0 Hz, 8H, *meta*-C*H*), 4.21 (s, 8H, NCH_2), 3.13 (sept, J = 6.8 Hz, 8H, C*H*(CH_3)$_2$), 1.30 (d, J = 6.8 Hz, 48H, CH(CH_3)$_2$). ^{13}C{^{1}H} NMR (75 MHz, THF-d_8): δ (ppm) 182.2 (br N*C*Au), 147.7 (*ortho-C*), 135.1 (*ipso-C*), 130.5 (*para-C*), 125.1 (*meta-C*), 54.6 (N*C*H_2), 29.3 (*C*H(CH_3)$_2$), 25.5 (CH(*C*H_3)$_2$), 24.1 (CH(*C*H_3)$_2$). ^{19}F NMR (375 MHz, THF-d_8): δ (ppm) –154.44 (s, ^{10}B*F*$_4^-$), □154.49 (s, ^{11}B*F*$_4^-$), –272.60 (br s, Au*F*Au). IR: ν (cm^{-1}) 3072 (w), 3026 (w), 2967 (s), 2931, 2868, 1595, 1500 (s), 1467 (s), 1391, 1365, 1345, 1329, 1309 (w), 1280 (s), 1234 (w), 1181, 1102, 1063 (s), 1020, 941, 809 (s), 760 (s), 704 (w), 664 (w), 625, 588, 549, 526 (w), 451. Elemental analysis calculated for $C_{54}H_{76}N_4Au_2BF_5$: C, 50.63; H, 5.98; N, 4.37; F, 7.42. Found: C, 50.35; H, 5.83; N, 4.18; F, 7.13. ^{1}H NMR (400 MHz, CD_2Cl_2): δ (ppm) 7.45 (t, J = 7.8 Hz, 4H, *para*-C*H*), 7.23 (d, J = 8.0 Hz, 8H, *meta*-C*H*), 4.10 (s, 8H, NCH_2), 2.90 (sept, J = 6.8 Hz, 8H, C*H*(CH_3)$_2$), 1.31 (d, J = 6.8 Hz, 24H, CH(CH_3)$_2$), 1.21 (d, J = 6.8 Hz, 24H, CH(CH_3)$_2$). ^{19}F NMR (375 MHz, CD_2Cl_2): δ (ppm) –153.50 (s, ^{10}B*F*$_4^-$), –153.55 (s,

$^{11}BF_4^-$), –318.45 (br s, Au*F*Au). Diffraction-quality crystals were grown by cautious layering of toluene onto a THF solution of **13**.

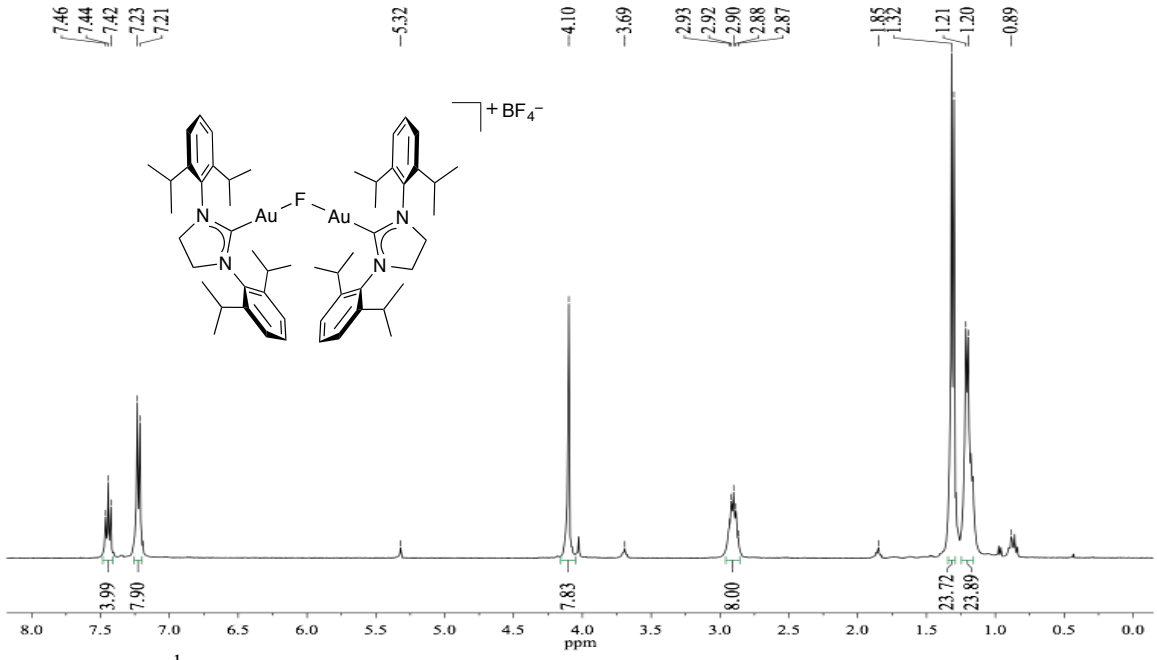

Figure 3.16. ^{1}H NMR(400 MHz, CD_2Cl_2) spectrum of **13**[BF_4]. Traces of residual THF (δ 3.69 and 1.85 ppm) and hexane (δ 0.89) are present.

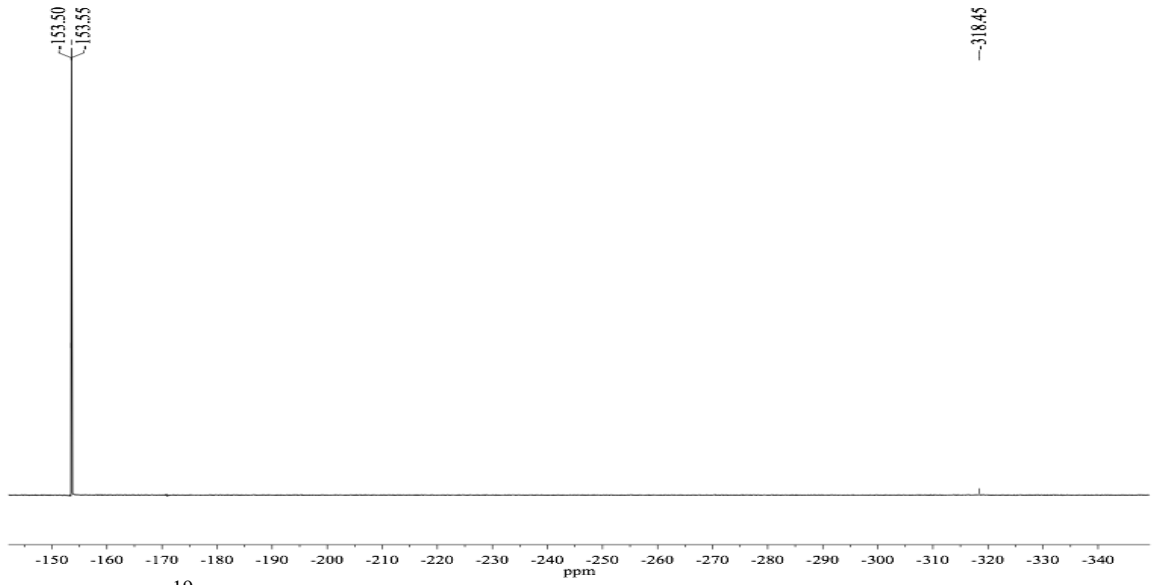

Figure 3.17. ^{19}F NMR (375 MHz, CD_2Cl_2) spectrum of **13**[BF_4].

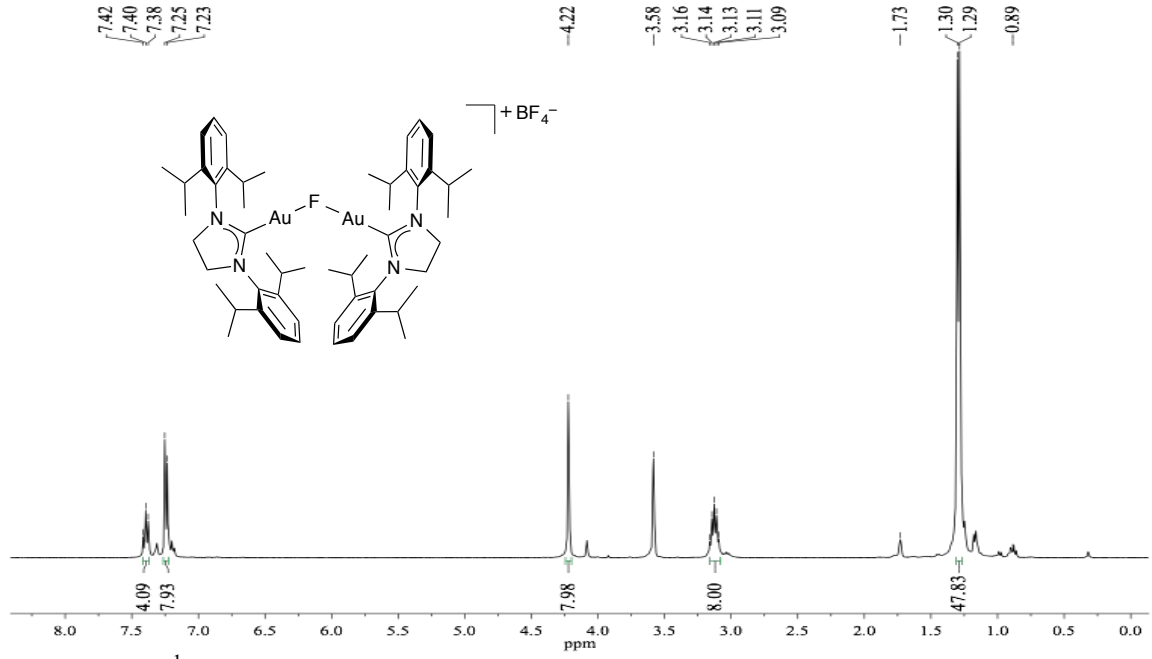

Figure 3.18. ^{1}H NMR (400 MHz, THF-d_8) spectrum of **12**[BF_4]. A trace of residual hexane (δ 0.89) is present.

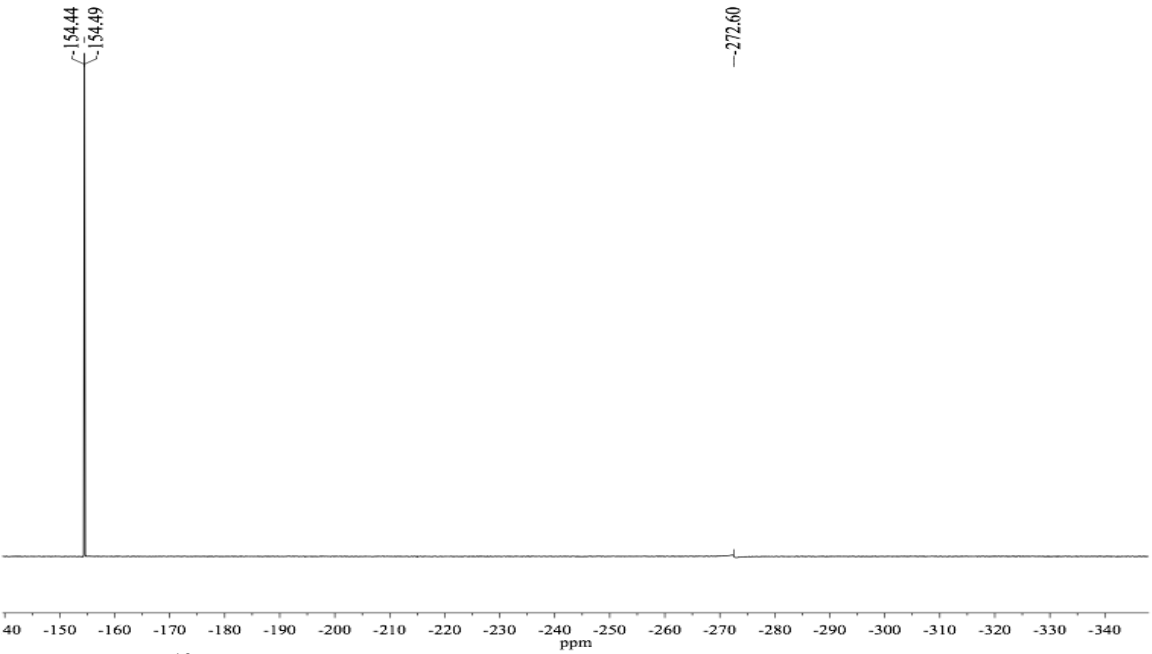

Figure 3.19. ^{19}F NMR (375 MHz, THF-d_8) spectrum of **13**[BF_4].

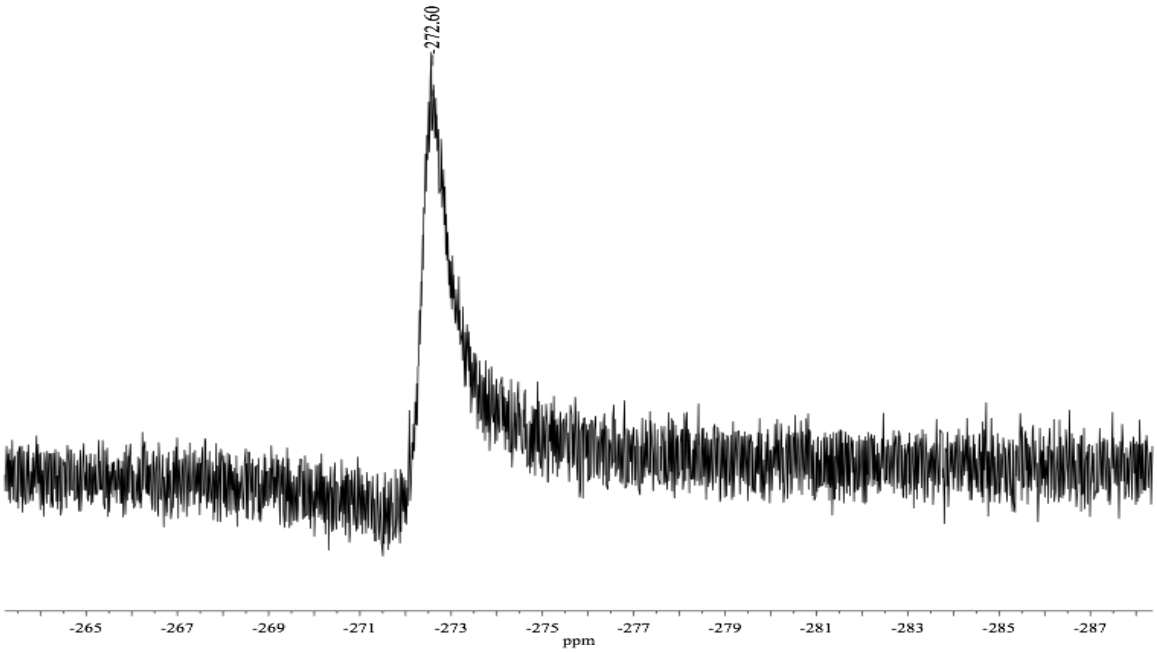

Figure 3.20. Detail of μ-fluoride resonance of ^{19}F NMR (375 MHz, THF-d_8) spectrum of **13**[BF_4].

3.5.2.7 Halide Exchange Between {[(5Dipp)Au]$_2$(μ-F)}$^+$$BF_4^-$ and CD_2Cl_2

A solution of {[(5Dipp)Au]$_2$(μ-F)}$^+$$BF_4^-$ (0.060 g, 0.047 mmol) in CD_2Cl_2 (0.7 mL) was transferred to an NMR tube equipped with a J. Young valve. After 24 h, the solution had turned yellow, and the starting complex had been completely consumed as judged by ^{1}H NMR and ^{19}F NMR spectroscopy. New resonances in the ^{1}H and ^{19}F spectra were assigned to {[(5Dipp)Au]$_2$(μ-Cl)}$^+$$BF_4^-$, CD_2ClF, and CD_2F_2. ^{1}H NMR (300 MHz, CD_2Cl_2): δ (ppm) 7.44 (t, J = 7.8 Hz, 4H, *para*-C*H*), 7.22 (d, J = 7.8 Hz, 8H, *meta*-C*H*), 4.10 (s, 8H, NCH_2), 2.92 (sept, J = 6.7 Hz, 8H, C*H*(CH_3)$_2$), 1.31 (d, J = 6.9 Hz, 24H, CH(CH_3)$_2$), 1.17 (d, J = 6.9 Hz, 24H, CH(CH_3)$_2$). ^{19}F NMR (375 MHz, CD_2Cl_2): δ (ppm) –144.10 (quin, CD_2F_2), –153.44 (s, ^{10}BF_4^-), –153.50 (s, ^{11}BF_4^-), –170.85 (quin, CD_2ClF).

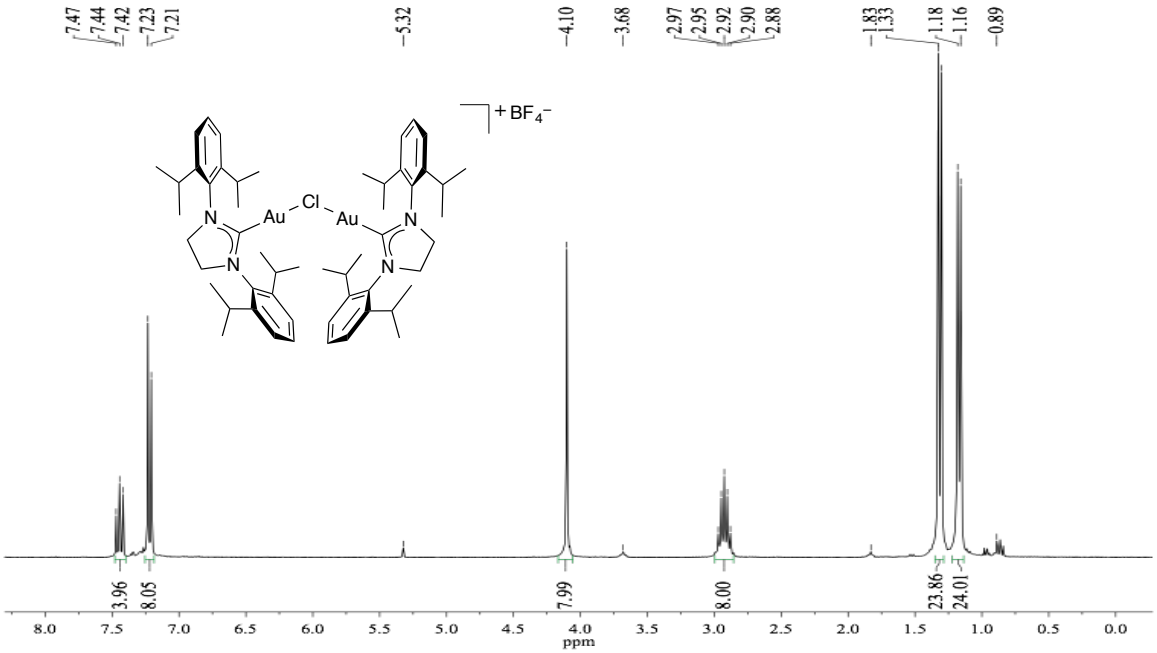

Figure 3.21. ^{1}H NMR (300 MHz, CD_2Cl_2) spectrum of halide exchange between **13**[BF_4] and CD_2Cl_2. Traces of residual THF (δ 3.68 and 1.83 ppm) and hexane (δ 0.89) are present.

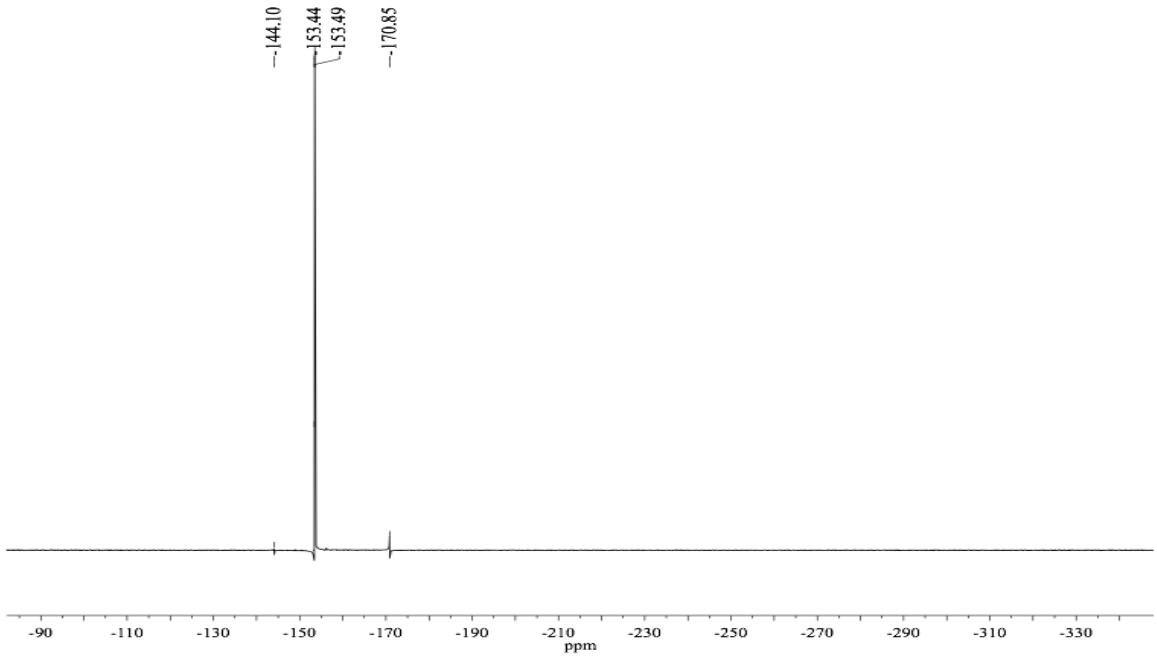

Figure 3.22. ^{19}F NMR (375 MHz, CD_2Cl_2) spectrum of the halide exchange between **13**[BF_4] and CD_2Cl_2.

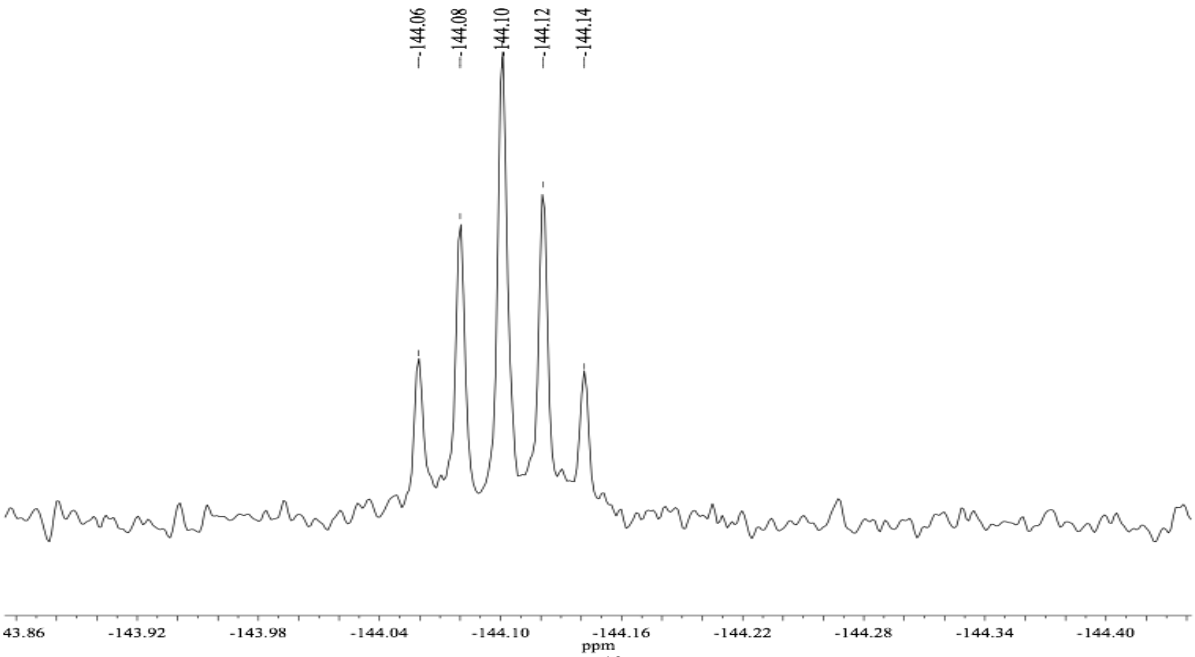

Figure 3.23. Detail of CD_2F_2 resonance in the ^{19}F NMR (375 MHz, CD_2Cl_2) spectrum of the halide exchange between **13**[BF_4] and CD_2Cl_2.

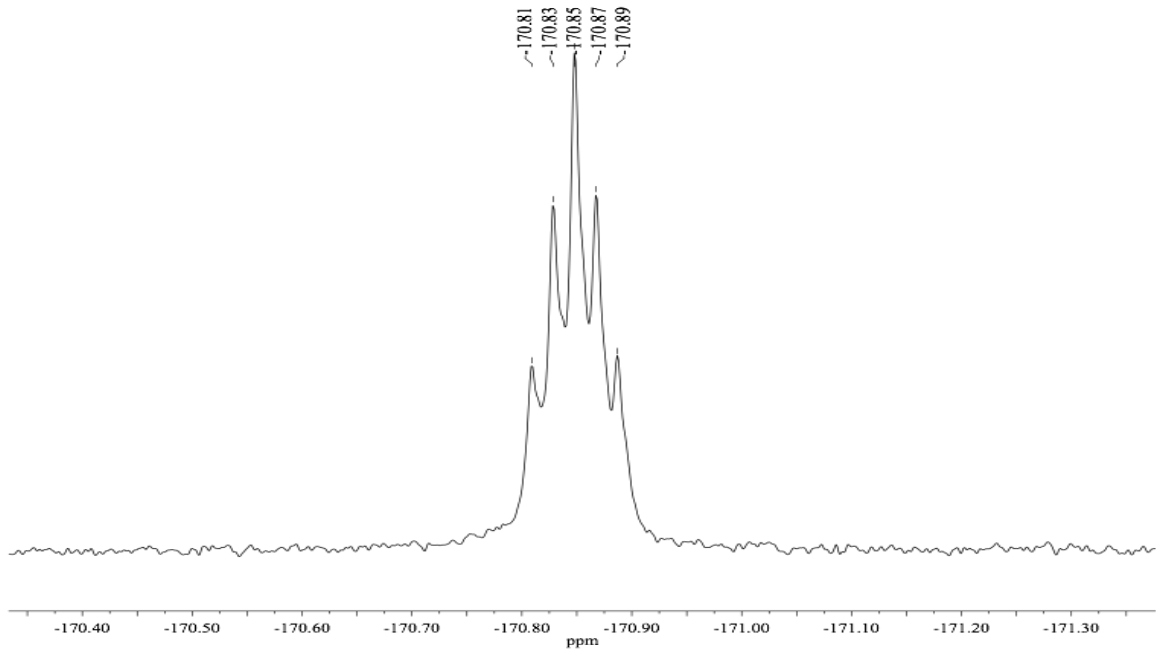

Figure 3.24. Detail of CD_2ClF resonance in the ^{19}F NMR (375 MHz, CD_2Cl_2) spectrum of the halide exchange between **13**[BF_4] and CD_2Cl_2.

3.5.2.8 Reaction of $\{[(5Dipp)Au]_2(\mu\text{-}F)\}^+BF_4^-$ with 3-Methyl-1,2-butadiene

A solution of $\{[(5Dipp)Au]_2(\mu\text{-}F)\}^+BF_4^-$ (0.063 g, 0.049 mmol) in THF-d_8 (0.7 mL) was transferred to an NMR tube equipped with a J. Young valve. The tube was then opened, and 3-methyl-1,2-butadiene (4.8 μL, 0.049 mmol) was added. After 5 min, the starting complex had been completely consumed as judged by ^{1}H NMR and ^{19}F NMR spectroscopy. New resonances in the ^{1}H and ^{19}F spectra were assigned to $\{[(5Dipp)Au]_2[\mu\text{-}C(=CH_2)CF(CH_3)_2]\}^+BF_4^-$. ^{1}H NMR (400 MHz, THF-d_8): δ (ppm) 7.37 (t, J = 7.8 Hz, 4H, *para*-C*H*), 7.20 (mult, 8H, *meta*-C*H*), 4.89 (d, J = 4.8 Hz, 1H, CCH_2), 4.22 (mult, 1H, CCH_2), 4.15 (s, 8H, NCH_2), 3.06 (sept, J = 6.8 Hz, 8H, CH(CH$_3$)$_2$), 1.26 (mult, 24H, CH(CH_3)$_2$), 1.18 (d, J = 6.8 Hz, 12H, CH(CH_3)$_2$), 1.11 (d, J = 6.8 Hz, 12H, CH(CH_3)$_2$), 0.31 (d, J = 20.4 Hz, 6H, CF(CH_3)$_2$). ^{13}C{^{1}H} NMR (75 MHz, THF-d_8): δ (ppm) 205.8 (br N*C*Au), 184.5 (br Au*C*Au), 147.6 (*ortho*-*C*), 140.7 (CCH2), 135.3 (*ipso*-*C*), 130.6 (*C*(CH$_3$)$_2$F), 130.3 (*para*-*C*), 125.2 (*meta*-*C*), 125.0 (*meta*-*C*), 54.9 (N*C*H$_2$), 35.3 (C(*C*H$_3$)$_2$F), 28.8 (C(*C*H$_3$)$_2$F, 29.4 (*C*H(CH$_3$)$_2$), 29.2 (CH(*C*H$_3$)$_2$), 25.5 (CH(*C*H$_3$)$_2$), 25.4 (CH(*C*H$_3$)$_2$), 23.9 (CH(*C*H$_3$)$_2$). ^{19}F NMR (375 MHz, THF-d_8): δ (ppm) –128.40 (sept, J = 20.6 Hz, C(CH$_3$)$_2$*F*), –152.73 (s, ^{10}B*F*$_4^-$), –152.78 (s, ^{11}B*F*$_4^-$). Crystals were grown by vapor diffusion of hexanes into a THF solution of $\{[(5Dipp)Au]_2(\mu\text{-}C(=CH_2)CF(CH_3)_2)\}^+BF_4^-$.

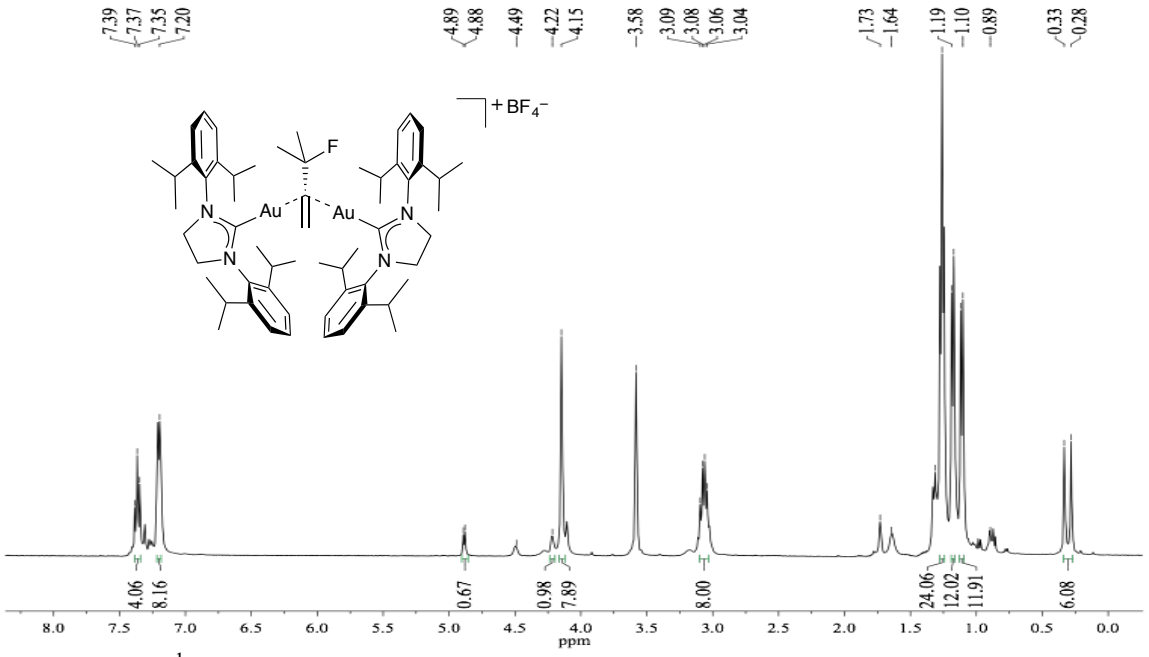

Figure 3.25. ^{1}H NMR (400 MHz, THF-d_8) spectrum of the reaction of **13**[BF_4] with 3-methyl-1,2-butadiene. A trace of residual hexane (δ 1.31 and 0.89) and a slight excess of 3-methyl-1,2-butadiene (δ 4.49 and 1.64) are present.

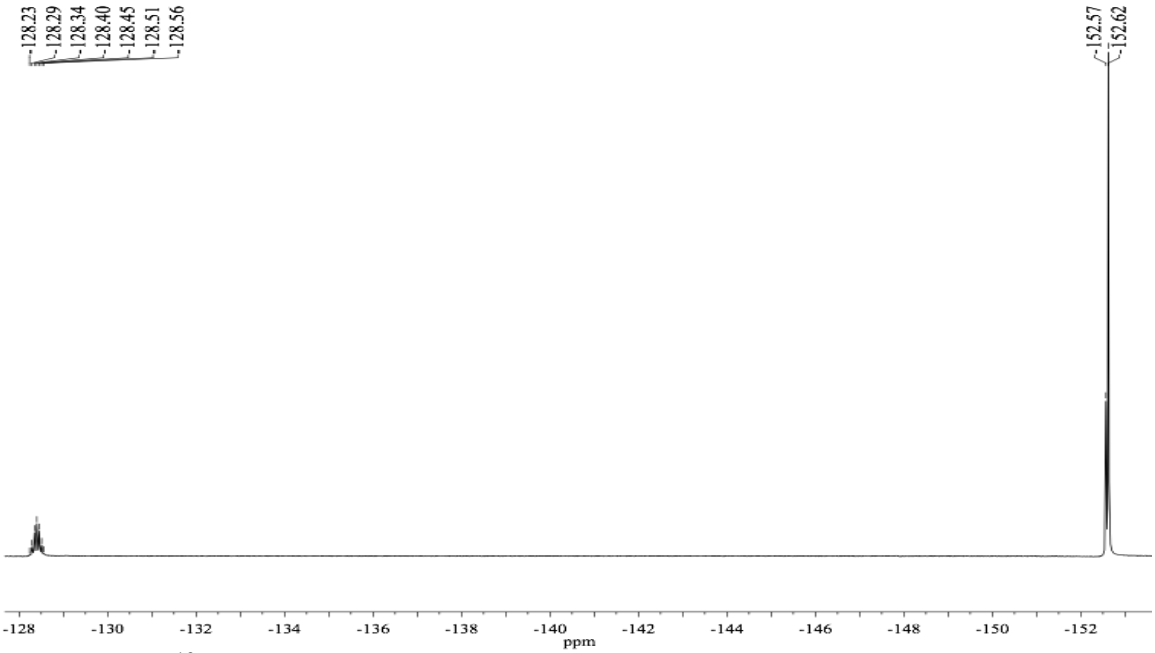

Figure 3.26. ^{19}F NMR spectrum (375 MHz, THF-d_8) of the reaction of **13**[BF_4] with 3-methyl-1,2-butadiene.

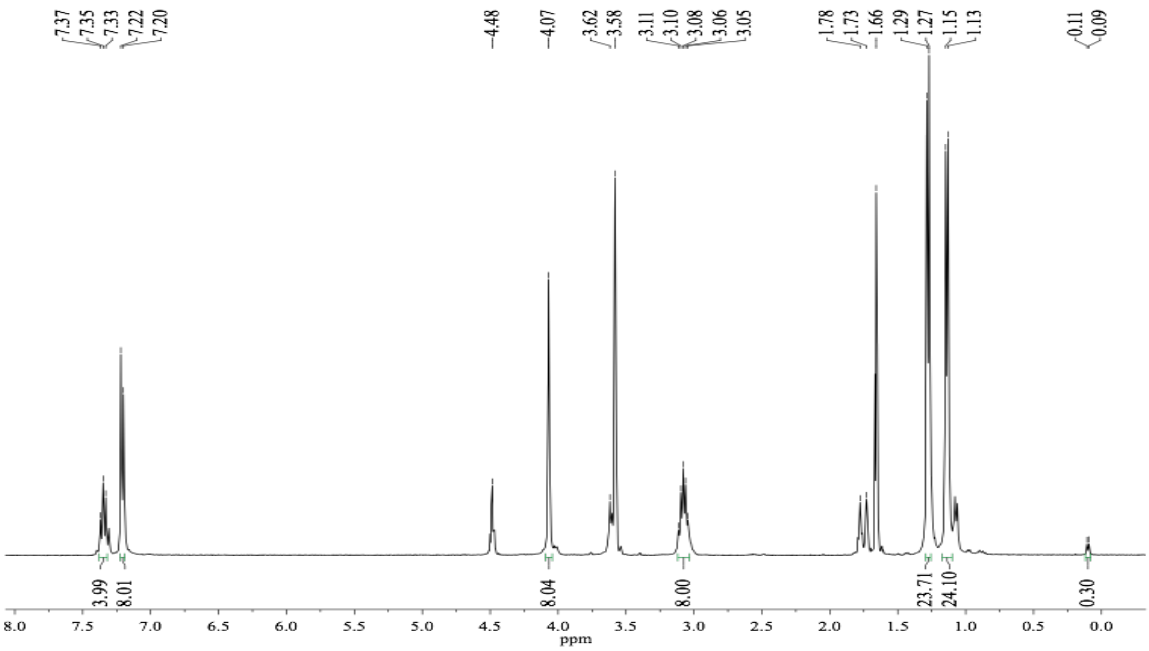

Figure 3.27. ^{1}H NMR spectrum (400 MHz, THF-d_8) of the reaction of **11**[BF_4] with 3-methyl-1,2-butadiene. A trace of residual THF (δ 3.62 and 1.78) and 3-methyl-1,2-butadiene (δ 4.48 and 1.66) are present.

3.5.3 X-Ray Diffraction Studies

For each complex, a suitable crystal was selected and mounted on a loop with Paratone oil on an ApexII Mo diffractometer (MoKa radiation, k = 0.71073 Å). The crystal was maintained at low temperature during data collection. Using Olex2,[25] the structure was solved with the Superflip[26] structure solution program, using the Charge Flipping solution method. The model was refined with the SHELXL[26] refinement package using Least Squares minimization.

Refinement of the crystal data for $\{[(5Dipp)Au]_2(\mu\text{-}F)\}^{+}BF_4^{-}$ gave rise to large difference peaks, ascribed to ghost peaks from the gold atoms. The largest peak lies along the Au–Au vector, and the distance from this peak to the crystallographic unique Au atom (3.95 Å) coincides with the Au–Au distance. These peaks probably arise from

undetected twinning and translational disorder. This contribution, however, is small and difficult to detect: A search for twinning and/or supersymmetry yielded no results.

The crystal structure of $\{[(5Dipp)Au]_2(\mu\text{-}C(=CH_2)CF(CH_3)_2)\}^+BF_4^-$. exhibits substantial disorder. In addition to the normal degree of translational disorder, the crystal is made of molecules with small differences in orientations. This disorder affects all the Au atoms, which were refined as split atoms with two different positions for each atom. The distance between split Au atoms was about 0.7 Å. The large peaks close to the Au atoms are due to unresolved disorder. No further modeling of this disorder was attempted. The structure was modeled after removal of the BF_4^- anion, co-crystallized solvent and part of the disorder of the main molecules, and after the masking of reflections resulting from this disorder. This analysis does not support a detailed discussion of metrics in this complex, but it allows confirmation of the assigned connectivity, and affords insight into the binding mode of the vinyl anion.

3.6 Acknowledgements

We thank the U.S. National Science Foundation (CHE-1300659) and the Georgia Institute of Technology for support. We are indebted to Professors Seth R. Marder and Jake D. Soper, and their groups, for the use of their FT-IR spectrometers. Dr. Thomas J. Robilotto carried out helpful preliminary experiments on the hydrolysis of $[Au_2(\mu\text{-}F)]^+$ complexes.

3.7 Notes and References

1 (a) Wyss, C. M. "Synthesis, Structure and Reactivity Studies of Dinuclear Group 11 N-Heterocyclic Carbene Complexes," Ph.D. Thesis, Georgia Institute of Technology (Atlanta), **2015**. (b) See Appendix A for a breakdown of collaborator contributions.

2 R.G. Pearson, *J. Am. Chem. Soc.* **1963**, *85*, 3533–3539.

3 D. C. Luehrs, R. T. Iwamoto, J. Kleinberg. *Inorg. Chem.* **1966**, *5*, 201–204.

4 (a) M. F. C. Ladd, W. H. Lee *Trans. Faraday Soc.* **1958**, *54*, 34–39. (b) W. T. Miller, R. J. Burnard. *J. Am. Chem. Soc.* **1968**, *90*, 7367–7368.

5 (a) E. L. Muetterties, C. W. Alegranti, *J. Am. Chem. Soc.* **1972**, *94*, 6386. (b) Q.-M. Wang, T. C. W. Mak, *J. Am. Chem. Soc.* **2000**, *122*, 7608. (c) P. J. Steel, C. J. Sumby, *Chem. Commun.* **2002** 322. (d) D. Rais, D. M. P. Mingos, R. Vilar, A. J. P. White, D. J. Williams, *J. Organomet. Chem.* **2002**, *652*, 87. (e) Q.-M. Wang, G.-C. Guo, T. C. W. Mak, *Polyhedron* **2002**, *22*, 217. (f) A. Yanagisawa, T. Touge, T. Arai, *Angew. Chem., Int. Ed.* **2005**, *44*, 1546. (g) A. Yanagisawa, H. Kageyama, Y. Nakatsuka, K. Asakawa, Y. Matsumoto, H. Yamamoto. *Angew. Chem. Int. Ed.* **1999**, *38*, 3701–3703.

6 (a) *Silver in Organic Chemistry*. M. Harmata, Ed. John Wiley & Sons Inc., **2010**. ISBN 978-0470466117. (b) J.-M. Weibel, A. Blanc, P. Pale, *Chem. Rev.* **2008**, *108*, 3149–3173.

7 Dubot, G.; Mansuy, D.; Lecolier, S.; Normant, J. F. *J. Organomet. Chem.* **1972**, 42.

8 D. S. Laitar. "Synthetic and catalytic studies of Group 11 N-heterocyclic carbene complexes," Ph.D. Thesis, Massachusetts Institute of Technology (Cambridge), **2006**; http://dspace.mit.edu/ handle/1721.1/36268

9 B. K. Tate, J. T. Nguyen, J. Bacsa, J. P. Sadighi, *Chem. Eur. J.* **2015**, *21*, 10160–10169.

10 A. Walsh, C. R. A. Catlow, R. Galvelis, D. O. Scanlon, F. Schiffmann, A. A. Sokol, S. M. Woodley, *Chem. Sci.* **2012**, *3*, 2565–2569.

11 (a) D. Schröder, J. Hrušák, I. C. Tornieporth-Oetting, T. M. Klapötke, H. Schwarz. *Angew. Chem., Int. Ed. Engl.* **1994**, *33*, 212. (b) C. J. Evans, M. C. L. Gerry. *J. Am. Chem. Soc.* **2000**, *122*, 1560. (c) J. M. Thomas, N. R. Walker, S. A. Cooke, M. C. L. Gerry. *J. Am. Chem. Soc.* **2004**, *126*, 1235. (d) S. A. Cooke, M. C. L. Gerry. *J. Am. Chem. Soc.* **2004**, *126*, 17000. (e) C. J. Evans, L. M. Reynard, M. C. L. Gerry. *Inorg. Chem.* **2001**, *40*, 6123.

12 (a) N. P. Mankad, F. D. Toste, *J. Am. Chem. Soc.* **2010**, *132*, 12859. [34] V. J. Scott, J. A. Labinger, J. E. Bercaw, *Organometallics* **2010**, *29*, 4090. (b) N. P. Mankad, F. D. Toste, *Chem. Sci.* **2012**, *3*, 72.

13 (a) D. J. Gulliver, W. Levason, M. Webster, *Inorg. Chim. Acta* **1981**, *52*, 153. (b) P. C. Healy, J. V. Hanna, J. D. Kildea, B. W. Skelton, A. H. White, *Aust. J. Chem.* **1991**, *44*, 427. (c) M. K. Chaudhuri, S. S. Dhar, N. Vijayashree, *Transition Met. Chem.* **2000**, *25*, 559. (d) B. F. Straub, F. Rominger, P. Hofmann, *Inorg. Chem*. **2000**, *39*, 2113.

14 (a) S. K. Gurung, S. Thapa, A. Kafle, D. A. Dickie, R. Giri, *Org. Lett.* **2014**, *16*, 1264. (b) T. Vergote, F. Nahra, D. Peeters, O. Riant, T. Leyssens, *J. Organomet. Chem.* **2013**, *730*, 95. (c) T. Vergote, F. Nahra, A. Welle, M. Luhmer, J. Wouters, N. Mager, O. Riant, T. Leyssens, *Chem. Eur. J.* **2012**, *18*, 793. (d) T. Fujihara, T. Xu, K. Semba, J. Terao, Y. Tsuji, *Angew. Chem., Int. Ed.* **2011**, *50*, 523. (e) J. R. Herron, V. Russo, E. J. Valente, Z. T. Ball, *Chem. Eur. J.* **2009**, *15*, 8713. (f) J. R. Herron, Z. T. Ball, *J. Am. Chem. Soc.* **2008**, *130*, 16486. (g) J. A. Akana, K. X. Bhattacharyya, P. Müller, J. P. Sadighi, *J. Am. Chem. Soc.* **2007**, *129*, 7736. (h) D. S. Laitar, P. Müller, T. G. Gray, J. P. Sadighi, *Organometallics* **2005**, *24*, 4503–4505.

15 (a) J. Bucher, T. Wurm, K. S. Nalivela, M. Rudolph, F. Rominger, A. S. K. Hashmi, *Angew. Chem. Int. Ed.* **2014**, *53*, 3854–3858. (b) K. Graf, P. D. Hindenberg, Y. Tokimizu, S. Naoe, M. Rudolph, F. Rominger, H. Ohno, A. S. K. Hashmi, *ChemCatChem*, **2014**, *6*, 199–204. (c) T. J. Brown, R. A. Widenhoefer, *Organometallics* **2011**, *30*, 6003−6009.

16 (a) C. M. Wyss, B. K. Tate, J. Bacsa, T. G. Gray, J. P. Sadighi. *Angew. Chem. Int. Ed.* **2013**, *52*, 12920–12923. (b) B. K. Tate, C. M. Wyss, J. Bacsa, K. Kluge, L. Gelbaum, J. P. Sadighi. *Chem. Sci.* **2013**, *4*, 3068–3074. (c) E. Y. Tsui, P. Müller, J. P. Sadighi. *Angew. Chem. Int. Ed.* **2008**, *47*, 8937–8940.

17 (a) S. L. Fraser, M. Yu. Antipin, V. N. Khroustalyov, V. V. Grushin, *J. Am. Chem. Soc.* **1997**, *119*, 4769. (b) M. K. Whittlesey, R. N. Perutz, B. Greener, M. H. Moore, *Chem. Commun.* **1997**, 187.

18 (a) H. Schmidbaur, A. Schier, *Chem. Soc. Rev.* **2012**, *41*, 370. (b) P. G. Jones, G. M. Sheldrick, R. Uson, A. Laguna, *Acta Crystallogr., Sect. B* **1980**, *36*, 1486.

19 F. G. Bordwell, *Acc. Chem. Res.* **1988**, *21*, 456–463.

20 J. P. Flemming, M. C. Pilon, O. Ya. Borbulevitch, M. Yu. Antipin, V. V. Grushin, *Inorg. Chim. Acta* **1998**, *280*, 87.

21 A. Corma, A. Leyva-Pérez, M. J. Sabater, *Chem. Rev.* **2011**, *111*, 1657.

22 G. R. Fulmer, A. J. M. Miller, N. H. Sherden, H. E. Gottlieb, A. Nudelman, B. M. Stoltz, J. E. Bercaw, K. I. Goldberg, *Organometallics* **2010**, *29*, 2176–2179.

23 A. J. Arduengo III, R. Krafczyk, R. Schmutzler, H. A. Craig, J. R. Goerlich, W. J. Marshall, M. Unverzagt, *Tetrahedron* **1999**, *55*, 14523–14534.

24 A. Collado, A. Gómez-Suárez, A. R. Martin, A. M. Z. Slawin, S. P. Nolan, *Chem. Commun.* **2013**, *49*, 5541.

25 O. V. Dolomanov, L. J. Bourhis, R. J. Gildea, J. A. K. Howard, H. Puschmann, *J. Appl. Crystallogr.* **2009**, *42*, 339.

26 SHELXS-97 (Sheldrick, **2008**).

CHAPTER 4

HYDROGEN ACTIVATION BY HARD-SOFT MISMATCHED SILVER COMPLEXES

4.1 Background

Activation of dihydrogen is a key step in the catalytic hydrogenation of alkenes, carbonyl compounds, and other substrates.[1] Oxidative addition to suitable transition metal complexes represents the most thoroughly studied mechanism for dihydrogen activation in solution.[2] The heterolysis of H_2 by Frustrated Lewis Pairs, systems in which reactive Lewis acids and Lewis bases coexist, affords active hydrogenation catalysts through non-redox mechanisms.[3] Such pathways are also known for a number of transition metal complexes. The hydrogenolysis of ruthenium(II) fluorides has been observed spectroscopically in solution.[4] More recently, the hydrogenolysis of palladium(II) hydroxides, alkoxides and aryloxides has been studied in detail.[5] The catalysts developed by Noyori[6] and Shvo[7] for the hydrogenation of C=O and C=N bonds operate through outer-sphere mechanisms[8] in which the heterolysis of hydrogen is a key step.

Among the earliest detailed studies of H_2 activation in homogeneous solution are those of Halpern and coworkers, who examined the reduction of aqueous copper(II), silver(I) and other metal cations.[9] Kinetic evidence suggests the formation of $[(\eta^2\text{-}H_2)M]$ cations, followed by rapid deprotonation to generate reactive metal hydrides. These[9f] and subsequent[10] studies indicated that fluoride ion serves as a notably effective promoter of

the heterolysis. Caulton and coworkers used the hydrogenolysis of tetrameric copper(I) *tert*-butoxide in the presence of phosphines to synthesize a series of (phosphine)copper(I) hydride oligomers.[11] The reaction of a copper(I)-oxygen bond with dihydrogen is the key step in several copper-catalyzed hydrogenation processes.[12]

Copper[13] and silver[14] hydride clusters have recently been shown to undergo photo-induced H_2 release. Such complexes could potentially serve as catalysts for the release of H_2 from promising storage media such as formic acid.[15] Examining the reverse reaction, we have demonstrated hydride transfer from a dinuclear silver complex[16] to Lewis-base-activated carbon dioxide, but the hydride was derived from energy-intensive phenylsilane. Other isolable silver hydrides have been synthesized using borohydrides as the hydride source.[17] Combinations of silver salts with certain phosphines, in contrast, catalyze the hydrogenation of aldehydes in water at elevated temperatures and pressures,[18] probably via silver hydride intermediates formed through heterolysis of dihydrogen.[19]

This chapter describes the hydrogenolysis of silver(I) alkoxide and fluoride complexes to form isolable hydrides. An alkoxy-bridged disilver cation reacts to form a (μ-hydrido)disilver cation plus the free alcohol; neutral silver fluorides afford (μ-hydrido)disilver cations as their bifluoride salts. The kinetics of these reactions are first-order in both silver and H_2. This reaction represents a key step in potential new catalysis relating to energy storage.

4.2 Results and Discussion

4.2.1 Hydrogenolysis of an Alkoxide-Bridged Disilver Cation

While exploring the chemistry of $\{[(5Dipp)Ag]_2(\mu\text{-}H)\}^+$ salts[16] (5Dipp = 1,3-bis(2,6-diisopropylphenyl)imidazolin-2-ylidene[20,21]), we observed no reaction of the cation with *tert*-butanol, and inferred that its protonolysis to form alkoxide and H_2 might be thermodynamically unfavorable. After exposing $\{[(5Dipp)Ag]_2(\mu\text{-}O^tBu)\}^+[BF_4]^-$ (**5a**$[BF_4]$) in CD_2Cl_2 solution to H_2 (3.0 bar), we observed by ^1H NMR spectroscopy the appearance of $\{[(5Dipp)Ag]_2(\mu\text{-}H)\}^+[BF_4]^-$ (**1a**$[BF_4]$) plus free *tert*-butanol. Although promising, this reaction was not preparatively useful: Decomposition of the product to $[(5Dipp)_2Ag]^+$, Ag^0, and H_2 became competitive with hydrogenolysis as the reaction proceeded (Scheme 4.1). Running the reaction at 0˚C minimized this decomposition, but slowed the hydrogenolysis so much that only 55% conversion was observed after 14 days. More strongly coordinating solvents such as THF-d_8 or CD_3CN accelerated the decomposition of the hydride relative to hydrogenolysis.

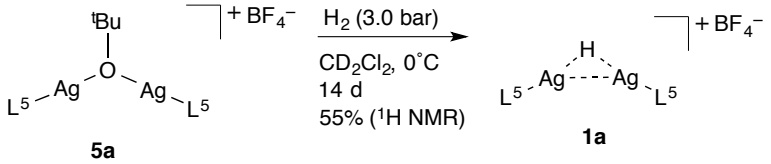

Scheme 4.1. Partial hydrogenolysis of alkoxide-bridged complex **5a**.

4.2.2 Hydrogenolysis of Silver Fluorides

Fluoride is markedly less basic than alkoxides, and so might be expected to react more slowly in a heterolytic cleavage of H_2. The reaction of ruthenium(II) fluorides with

H_2,[4] however, is believed to be thermodynamically driven, and silver(I) fluoride itself reacts readily with H_2 to form unstable hydrides.[10] Fluoride-bridged dinuclear cations of the group 11 metals display considerable basicity despite their overall positive charge.[22] We hoped that the hard/soft acid-base mismatch[23] of the Ag(I)–F bond, and the strength of the resulting H–F bond,[24] would facilitate hydrogenolysis both kinetically and thermodynamically. Indeed, the fluoride-bridged complex $\{[(5Dipp)Ag]_2(\mu\text{-}F)\}^+$ BF_4^- reacted with H_2 (3.0 atm) in CD_2Cl_2 solution, resulting in partial formation of **1a**[BF_4]. We did not observe the inferred byproduct HF by ^1H or ^{19}F NMR spectroscopy; it might have reacted with the borosilicate glass surface. Regardless, decomposition of the product hydride complex to elemental silver, homoleptic $[L_2Ag]^+$ and hydrogen again proved competitive with hydrogenolysis.

Hoping to accelerate the formation of hydride with respect to its decomposition, we reasoned that the formation of a hydrogen bond from HF to a suitable base might facilitate the desired reaction, depending on the mechanism of hydrogenolysis. The strongest known hydrogen bond, really a three-center covalent bond,[25] results from the interaction of fluoride with HF to form the bifluoride anion, $[HF_2]^-$.

A free fluoride ion seemed an unlikely counterion to $\{[(5Dipp)Ag]_2(\mu\text{-}F)\}^+$; the equilibrium should lie far on the side of two equivalents of (5Dipp)AgF.[26] We therefore investigated the potential for (5Dipp)AgF to act as a surrogate for $\{[(5Dipp)Ag]_2(\mu\text{-}F)\}^+$ and F^-. Indeed, two equivalents of the terminal, neutral fluoride (5Dipp)AgF (**7**) react with H_2 to form the (μ-hydrido)disilver cation as its bifluoride salt (**1a**[HF_2], Scheme 4.2). This reaction proceeds to a greater extent than those of $\{[(5Dipp)Ag]_2(\mu\text{-}O^tBu)\}^+$ or $\{[(5Dipp)Ag]_2(\mu\text{-}F)\}^+$, reaching 72% conversion after 14 days under H_2 (3.0 atm) in

CD_2C_{l2} solution at 0˚C. The apparent reaction rate is too low to be of practical use, however, particularly at low concentrations of silver fluoride.

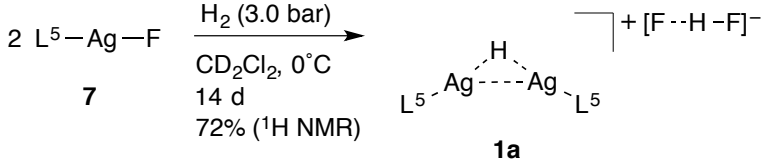

Scheme 4.2. Partial hydrogenolysis of fluoride complex **7**.

4.2.3 Synthesis of Expanded-Ring (NHC)Silver Complexes

Expanded-ring NHCs, including those derived from six- and seven-membered cyclic amidinium salts, are stronger σ-donors than imidazolylidenes,[27] and their bonds to silver(I) are less labile than those of five-membered NHCs.[28] Six-membered NHCs support the formation of rhodium(I) fluorides,[29] and of μ-hydrido- and μ-chlorodigold cations formed via strongly electrophilic $[(NHC)Au]^+$ equivalents.[30] We hoped that a more inert NHC–Ag bond would suppress the formation of homoleptic $[L_2Ag]^+$ from the $[(LAg)_2(\mu\text{-}H)]^+$ cation.

Silver(I) bromide complexes (**14a-b**) bearing expanded-ring NHCs have been described.[31] These ligands impose a greater steric demand, resulting from the wider N–C–N angle, than their five-membered analogues. The tendency of these ligands to form homoleptic $[(NHC)_2Ag]^+$ cations depends on their *N*-substituents. We found that (6Dipp)AgBr and (7Dipp)AgBr (6Dipp = (1,3-bis(2,6-diisopropylphenyl)-3,4,5,6-tetrahydropyrimidin-2-ylidene; 7Dipp = 1,3-bis(2,6-diisopropylphenyl)-4,5,6,7-tetrahydro-1,3-diazepin-2-ylidene) did not react with sodium *tert*-butoxide or sodium *tert*-pentoxide under conditions used to prepare (5Dipp)silver(I) alkoxides from the

corresponding chloride. The readily prepared (NHC)AgOTs complexes (**15a-b**), however, react smoothly with sodium *tert*-pentoxide (NaO^{t}Pent) in THF solution to form (6Dipp)Ag(O^{t}Pent) (**3b**) and (7Dipp)Ag(O^{t}Pent) (**3c**) (Scheme 4.3). Addition of equimolar (6Dipp)AgOTf (OTf = trifluoromethanesulfonate) to (6Dipp)Ag(O^{t}Pent) (**3b**) formed the alkoxide-bridged $\{[(6Dipp)Ag]_2(\mu\text{-}O^tPent)\}^+[OTf]^-$ (**5b**[OTf]), in analogy to the synthesis of $\{[(5Dipp)Ag]_2(\mu\text{-}O^tBu)\}^+[OTf]^-$ (**5a**[OTf]).[16]

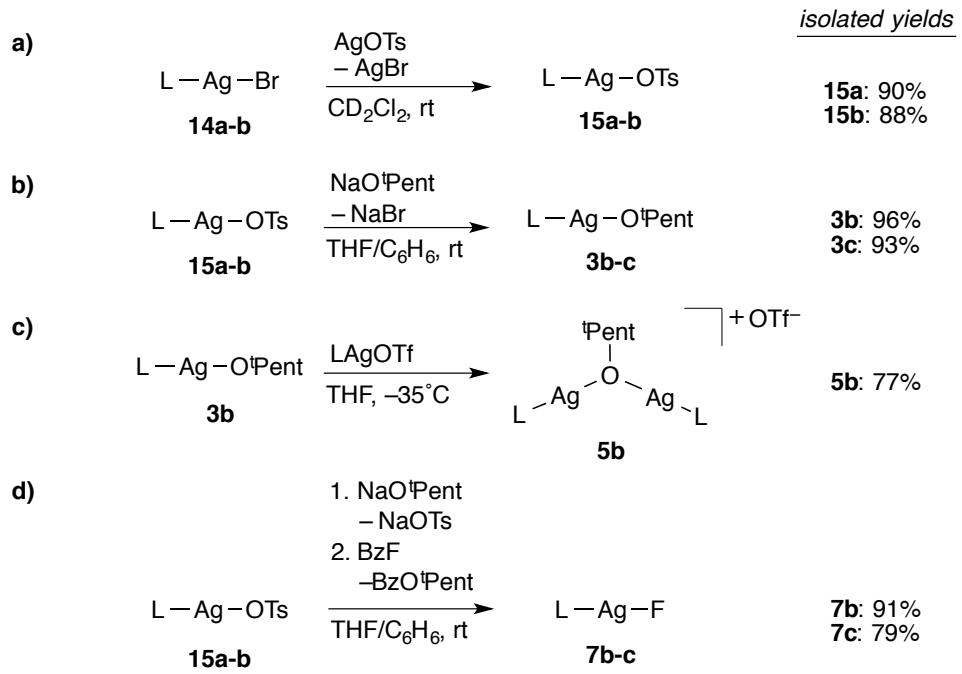

Scheme 4.3. Syntheses of expanded-ring NHC complexes **15a**, **15b**, **3b**, **3c**, **5b**, **7b**, and **7c**.

The neutral alkoxides react rapidly with benzoyl fluoride in THF solution, resulting in the precipitation of fluoride complexes (6Dipp)AgF (**7b**) and (7Dipp)AgF (**7c**). We have been unable to prepare molecular silver fluorides bearing NHC ligands with less sterically demanding substituents such as 2,6-xylyl or *tert*-butyl; all attempts to date have resulted in the formation of homoleptic $[(NHC)_2Ag]^+$ complexes.

Fluoride complexes **7b** and **7c** exhibit sharp ^{19}F NMR resonances at chemical shifts similar to that of **7** (Table 4.1). In contrast to the latter, well-defined $^{19}F–^{109}Ag$ and $^{19}F–^{107}Ag$ coupling results in an apparent doublet of doublets for each. The presence of trace moisture broadens the ^{19}F NMR signals to either doublets or broad singlets.

Table 4.1. ^{19}F NMR data for (NHC)AgF complexes.

	7	**7b**	**7c**
δ, ppm	–243.13	–246.03	–246.16
J ($^{19}F–^{109}Ag$), Hz	163[a]	176	173
J ($^{19}F–^{107}Ag$), Hz		152	150

[a] $^{19}F–^{109}Ag$ and $^{19}F–^{107}Ag$ coupling are unresolved; the resonance appears as an apparent doublet.

4.2.4 Hydrogenolysis of Expanded-Ring NHC Complexes

The alkoxide-bridged salt **5b**[OTf] reacts with hydrogen in CD_2Cl_2 solution to produce **1b**[OTf] and *tert*-pentanol (Scheme 4.4a). Nearly quantitative conversion was observed after 4 days under 4.0 bar H_2 in CD_2Cl_2. Addition of hexanes precipitates **1b**[OTf] as an analytically pure solid in 57% isolated yield.

The hydrogenolysis of fluoride **7b** in CD_2Cl_2 solution proceeds more rapidly than that of **7** (Scheme 4.4b), and does not result in the formation of $[(6Dipp)_2Ag]^+$ and silver metal at room temperature. In contrast, **1a**[BF_4] undergoes roughly 25% decomposition in CD_2Cl_2 solution within 24 h. Virtually quantitative conversion to $\{[(6Dipp)Ag]_2(\mu\text{-}H)\}^+[HF_2]^-$ (**1b**[HF_2]) was observed after 4 days under H_2 (4.4 bar) in CD_2Cl_2 solution, allowing its isolation as colorless microcrystals in 61% yield.

Hydrogenolysis of **7c** likewise proceeds at ambient temperature in CD_2Cl_2 solution (Scheme 4.4b), without detectable formation of homoleptic byproduct. As shown in Figure 4.1, conversion to $\{[(7Dipp)Ag]_2(\mu\text{-}H)\}^+[HF_2]^-$ (**1c**$[HF_2]$) is nearly (>95%) complete after four days under H_2 (4.4 bar), and recrystallization affords analytically pure product in 59% yield.

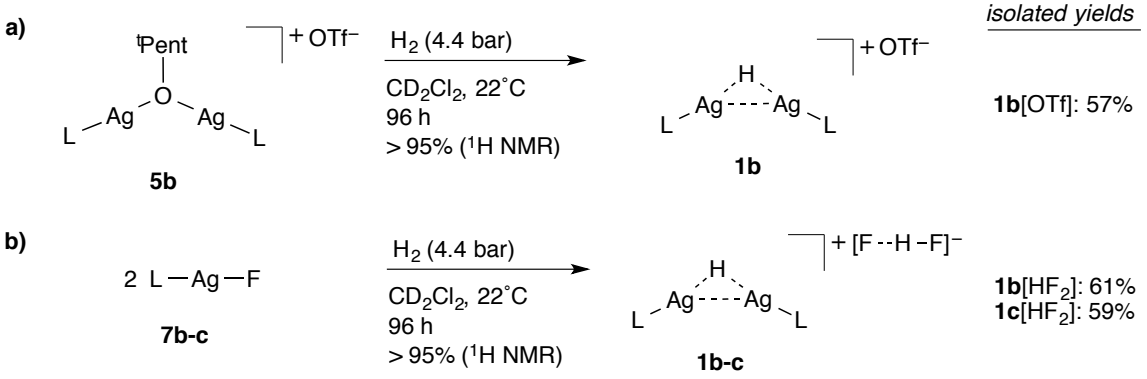

Scheme 4.4. Preparative hydrogenolyses of fluoro- and alkoxysilver complexes **5b**, **7b**, and **7c**.

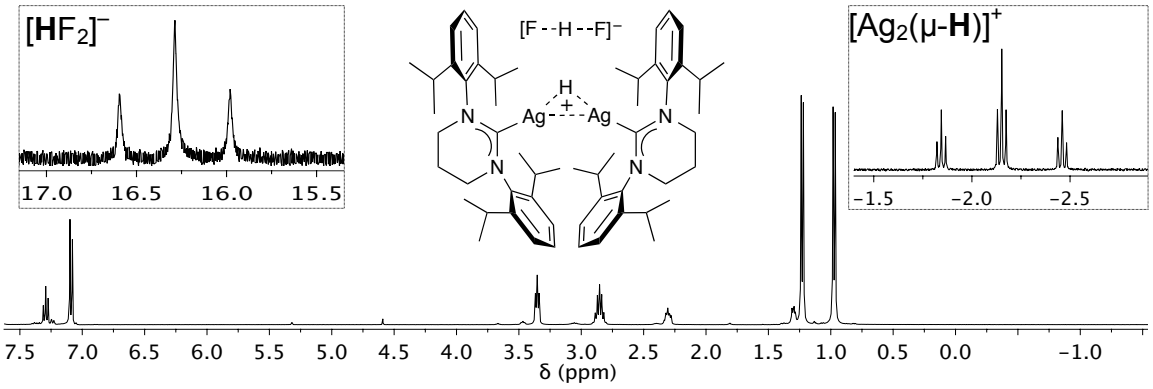

Figure 4.1. ^{1}H NMR spectrum of crude (6Dipp)AgF hydrogenolysis product in CD_2Cl_2. Insets are expanded to show bifluoride and bridging hydride resonances clearly.

4.2.8 Characterization of Hydrogenolysis Products

The ^{1}H NMR spectra of hydride-bridged complexes **1a-c** (Table 4.2) exhibit hydride resonances upfield of tetramethylsilane, with well-resolved ^{1}H–^{109}Ag and ^{1}H–^{107}Ag coupling. The hydride resonance appears at higher field as the NHC ring size expands, shifting from δ –1.18 ppm for the 5Dipp complex to δ –2.15 ppm for 6Dipp and δ –2.46 ppm for 7Dipp. This trend is consistent with increased shielding of the hydride nucleus in the expanded-ring NHC complexes resulting from greater electron density about the hydrides, but may result from increased crowding of the hydride by the ligand aryl groups.[32] The magnitude of ^{1}H–^{109}Ag and ^{1}H–^{107}Ag coupling varies trivially among the three hydride-bridged cations. In rigorously anhydrous environments, the bifluoride counterion exhibits a sharp, well-resolved triplet ($^{1}J_{H–F}$ = 123 Hz) at δ 16.28 ppm.

The ^{109}Ag NMR resonances of the hydride complexes shift downfield with increasing NHC ring size, from δ 519.3 ppm for **1a** to δ 524.6 ppm for **1b** to δ 532.0 ppm for **1c**. These resonances display well-resolved coupling to both ^{1}H and ^{109}Ag; the ^{109}Ag–^{107}Ag coupling constant decreases from 113 Hz for **1a** to 108 Hz for the expanded-ring NHC complexes **1b** and **1c**, possibly reflecting slightly weaker Ag–Ag interactions.

Table 4.2. Selected NMR data for $[(LAg)_2(\mu\text{-}H)]^+$ complexes.[a]

	1a[OTf]	**1b**[HF_2]	**1c**[HF_2]
δ (^{1}H, hydride), ppm	–1.18	–2.15	–2.46
δ (^{109}Ag), ppm	519.3	524.6	532.0
δ (^{13}C), ppm	208.3	207.1	217.4
J (^{1}H–^{109}Ag), Hz	134	132	134
J (^{1}H–^{107}Ag), Hz	116	115	116
J (^{109}Ag–^{107}Ag), Hz	113	108	108

[a] Complete data are given here for **1a**[OTf] because **1a**[HF_2] has not been isolated; however, observed ^{1}H NMR chemical shifts for **1a** and **1b** are unchanged (≤0.01 ppm) between their [OTf] and [HF_2] salts.

The ^{19}F NMR spectra of rigorously anhydrous samples of the bifluoride salts exhibit a doublet at δ –157.3 ppm in the ^{19}F spectra, with a ^{1}H–^{19}F coupling constant matching that observed in the corresponding ^{1}H NMR spectra. Typically the crude hydrogenolysis products also exhibit a sharp singlet at δ –127 ppm, which we ascribe to the formation of hexafluorosilicate through slow etching of the borosilicate NMR tubes by bifluoride. Integration of peak areas suggests that SiF_6^{2-} accounts for less than 2% of the fluorine in the crude product.

Crystals suitable for X-ray diffraction were obtained by diffusion of hexane into a CH_2Cl_2 solution of **1b**[HF_2]. The complex forms monoclinic crystals in the *P*21/*c* space group, with five CH_2Cl_2 molecules in the asymmetric unit. The methylene carbon of one of these lies 3.1(1) Å from the position calculated for the hydride, consistent with a weak attractive interaction between the δ+ C–H bonds and the silver-bound hydride (Figure 4.2).

The structure of cation **1b** is similar to that of **1a**,[16] and metrics for the (6Dipp)Ag fragments are very close to those reported in the structure of (6Dipp)AgBr.[31] The Ag–Ag distance of 2.8948(9) Å is longer than that of 2.8087(4) Å in **1a**[OTf], consistent with the smaller ^{109}Ag–^{107}Ag nuclear spin coupling constant measured by ^{109}Ag NMR spectroscopy. The bifluoride ion of **1b**[HF_2] rests between the 6Dipp backbone and several cocrystallized CH_2Cl_2 molecules, well outside the silver coordination spheres, with a closest approach to silver of nearly 8 Å. The fluorine-fluorine distance is 2.290(10) Å, essentially equal to that in KHF_2 (2.277(6) Å)[33] and shorter than in many complexes featuring metal-bound bifluoride.[34,35]

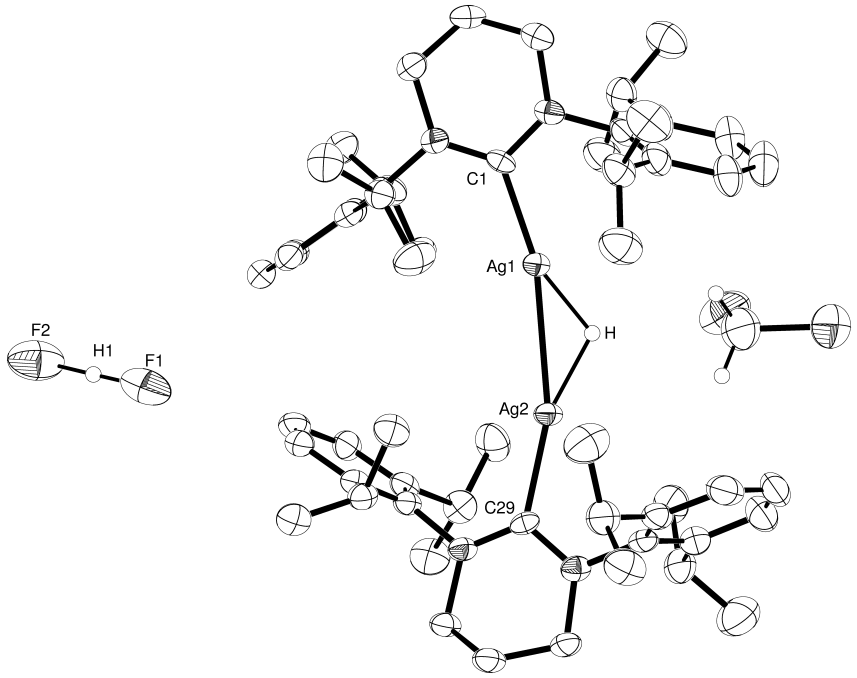

Figure 4.2. Solid-state structure of **1b**[HF_2], shown as 50% probability ellipsoids. Four co-crystallized CH_2Cl_2 molecules omitted for clarity. Selected interatomic distances (Å) and angles (˚): Ag(1)–Ag(2), 2.8948(9); Ag(1)–C(1), 2.126(6); Ag(2)–C(29), 2.127(6); F(1)–F(2), 2.290(10); C(1)–Ag(1)–Ag(2), 165.00(17); Ag(1)–Ag(2)–C(29), 160.39(16).

4.2.9 Hydrogenolysis Kinetics

The hydrogenolysis of **5b**[OTf] in CD_2Cl_2 solution follows first-order kinetics with respect to starting disilver complex (Figure 4.3). The calculated pseudo-first-order rate constants are directly proportional to H_2 concentration. Overall the reaction follows the second-order rate expression $-d[\mathbf{5b}]/dt = k[\mathbf{5b}][H_2]$, where $k = 7.0(\pm 0.2)\ M^{-1}\cdot s^{-1}$.

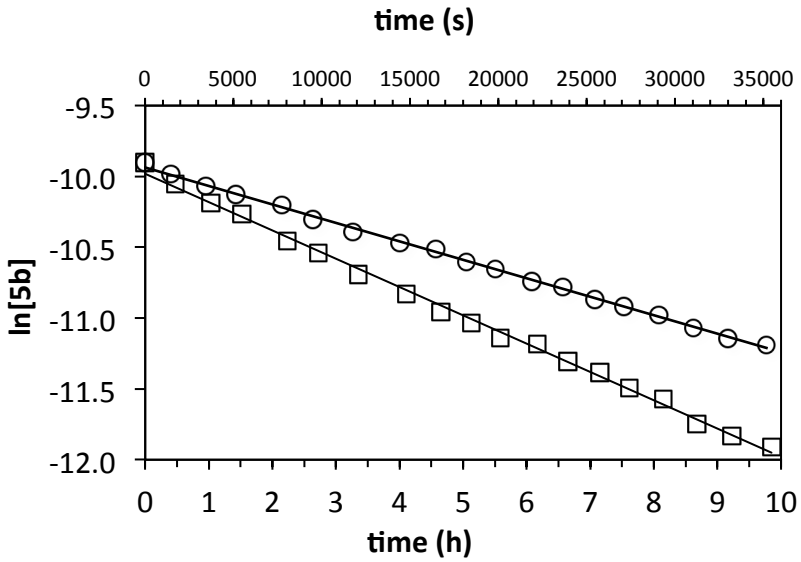

Figure 4.3. Pseudo-first-order kinetic plot for the hydrogenolysis of $\{[(6Dipp)Ag]_2(\mu\text{-}O^tPent)\}^+$ OTf^- (**5b**[OTf]) in CD_2Cl_2: □ $[H_2]$ = 7.9(3) μM, R^2 = 0.998; ○ $[H_2]$ = 5.21(09) μM, R^2 = 0.997.

A mechanism involving the concerted activation of H_2 by an intact $[(LAg)_2(\mu\text{-}OR)]_+$ cation is consistent with this behavior. A plausible alternative (Scheme 4.5) involves the reversible breakup of **5b** to form the dihydrogen complex[36] $[(6Dipp)Ag(\eta^2\text{-}H_2)]^+$ plus the terminal *tert*-pentoxide complex (6Dipp)Ag(O^tPent). Subsequent deprotonation of coordinated H_2[37] would afford the μ-hydrido complex plus *tert*-pentanol. Because both intermediates would be formed together from the starting complex, the steady-state approximation leads to a prediction of overall second-order kinetics, first-order in silver, regardless of the relative rates of dissociation versus deprotonation of coordinated H_2.

We also investigated the kinetics of fluoride hydrogenolysis to gain insight into the activation of dihydrogen by two silver fluorides (Figure 4.4). The kinetics for consumption of **7b** and **7c** are each first-order with respect to silver; again, the pseudo-first-order rate constants are directly proportional to H_2 concentration.

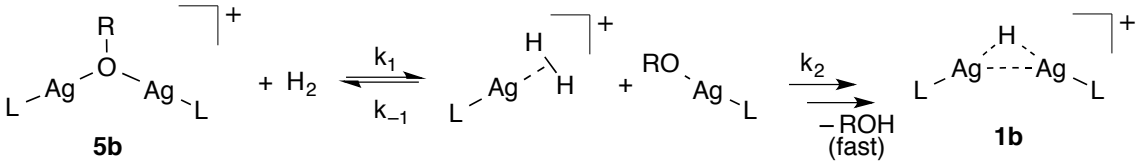

$$\text{If } k_{-1} >> k_2: \quad \frac{d[\mathbf{1b}]}{dt} \approx k_2 K_{eq}[\mathbf{5b}][H_2] \quad (K_{eq} = k_1/k_{-1})$$

$$\text{If } k_2 >> k_{-1}: \quad \frac{d[\mathbf{1b}]}{dt} \approx k_1[\mathbf{5b}][H_2]$$

Scheme 4.5. Possible sequential pathway for the activation of H_2 by $\{[(6Dipp)Ag]_2(\mu\text{-}OR)\}^+OTf^-$ (**5b**[OTf]; L = 6Dipp, R = *tert*-pentyl). Rate law derivations are provided in Section 4.8.

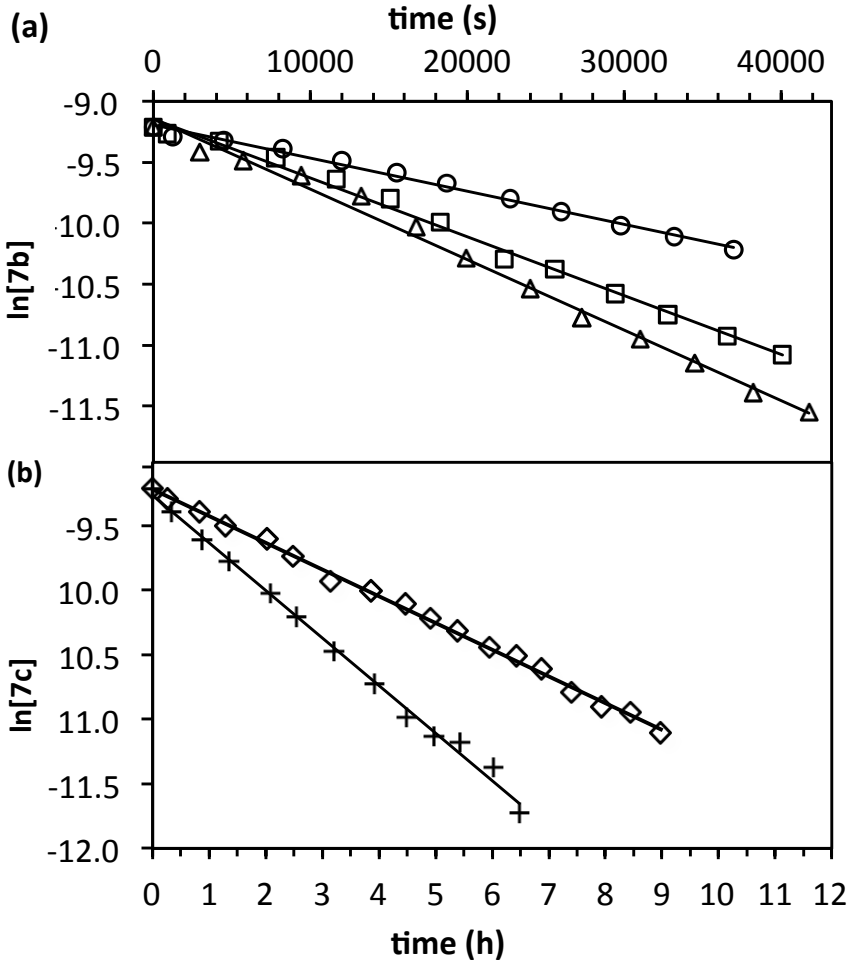

Figure 4.4. Pseudo-first-order kinetic plots for the hydrogenolysis of (NHC)AgF in CD_2Cl_2 where $[H_2]$ is constant. **(a)** (6Dipp)AgF (**7b**): △ $[H_2]$ = 75.7 μM, R^2 = 0.993; □ $[H_2]$ = 65.8 μM, R^2 = 0.994; ○ $[H_2]$ = 36.6 μM, R^2 = 0.993. **(b)** (7Dipp)AgF (**7c**): + $[H_2]$ = 63.5 μM, R^2 = 0.997; ◇ $[H_2]$ = 37.3 μM, R^2 = 0.995.

Despite the greater steric encumbrance of 7Dipp relative to 6Dipp,[31] the hydrogenolysis of **7c** ($k = 13.6(\pm 0.4)\ M^{-1}\cdot s^{-1}$) proceeds somewhat more rapidly than that of **7b** ($k = 7.5\ (\pm\ 0.3)\ M^{-1}\cdot s^{-1}$). This difference suggests a stronger trans-labilizing effect for the 7Dipp ligand than for 6Dipp. Because the ^{19}F NMR chemical shifts and silver-fluorine coupling constants in **7b** and **7c** are remarkably similar (see Table 4.1), such an effect probably does not reflect a weaker silver–fluoride bond in the ground state of **7c**.

Several plausible pathways for the silver fluoride hydrogenolysis are outlined in Scheme 4.6. The first-order rate dependence on both LAgF and H_2 rules out the formation of a disilver complex, such as $[(LAg)_2(\mu\text{-}F)]^+$ or $[(LAg)_2(\mu\text{-}F)_2]$, prior to the activation of H_2 (Scheme 4.6a). A concerted termolecular process[38] in which two LAgF molecules cooperatively cleave H_2 (Scheme 4.6b) is likewise inconsistent with the rate law. These pathways should exhibit second-order rate dependence on silver fluoride concentration. The observed results are consistent with hydrogen activation through the fast, reversible coordination of H_2 to a single molecule of LAgF, followed by heterolysis to afford LAgH[39] and HF (Scheme 4.6c). Formation of a hydride bridge, through displacement of fluoride from a second equivalent of LAgF, and protonation of fluoride to form bifluoride could occur as rapid subsequent steps.

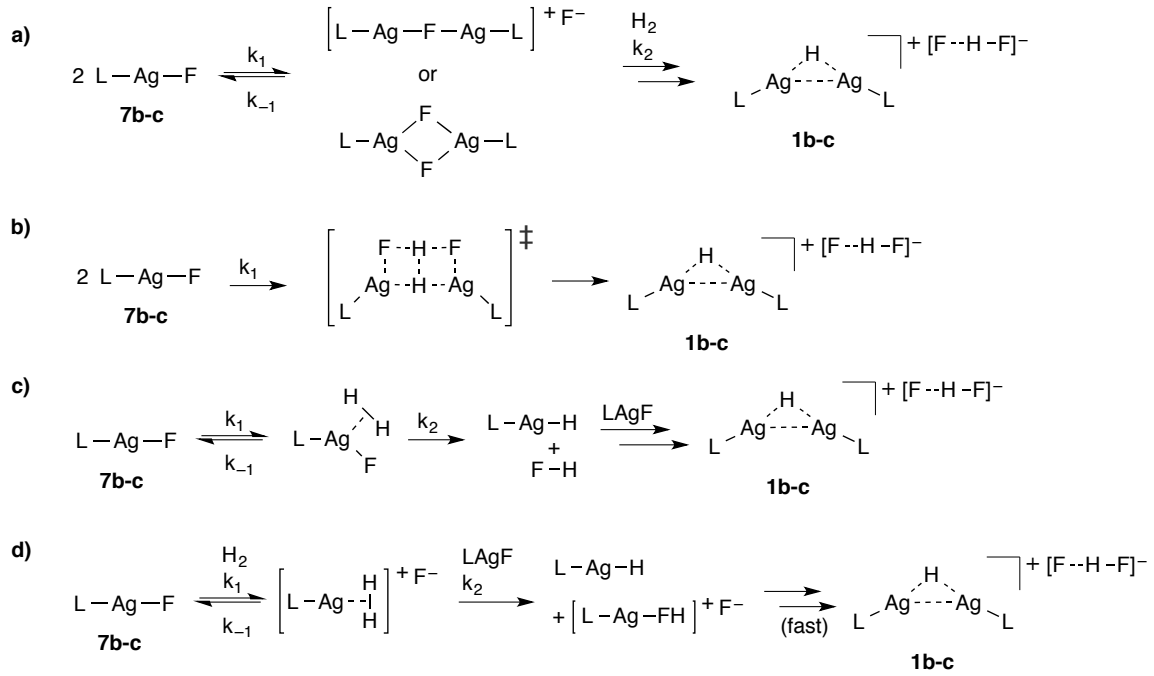

Scheme 4.6. Hypothetical pathways for the hydrogenolysis of neutral silver fluorides. a) Intermediate fluoride-bridged disilver complex: $-d[\mathbf{7b\text{-}c}]/dt \propto [LAgF]^2$ if $k_2 >> k_{-1}$, $-d[\mathbf{7b\text{-}c}]/dt \propto [LAgF]^2[H_2]$ if $k_{-1} >> k_2$; b) concerted termolecular process: $-d[\mathbf{7b\text{-}c}]/dt \propto [LAgF]^2[H_2]$; c) 1:1 reaction of terminal fluoride with H_2: $-d[\mathbf{7b\text{-}c}]/dt \propto [LAgF][H_2]$; d) intermediate h^2-H_2 complex: $-d[\mathbf{7b\text{-}c}]/dt = [LAgF][H_2]$ if $k_2 >> k_{-1}$, $-d[\mathbf{7b\text{-}c}]/dt \propto [LAgF]^2[H_2]$ if $k_{-1} >> k_2$. Rate law derivations are provided in Schemes 4.9 and 4.10.

Alternatively, we considered a sequence in which dihydrogen displaces fluoride to form a cationic η^2-dihydrogen intermediate. Any such intermediate would be transient: In an effort to observe a silver(η^2-dihydrogen) complex independently, we exposed (6Dipp)AgOTf in CD_2Cl_2 solution to H_2 (4.0 bar), and observed no change in the ligand or H_2 resonances by ^{1}H NMR spectroscopy. The steady-state approximation is again useful in considering the hydrogenolysis kinetics.

If the displaced fluoride acts as a base, the kinetic picture is analogous to that shown in Scheme 4.5, and the overall rate law should be first-order in silver regardless of relative rates. This pathway becomes essentially a variant of Scheme 4.6c. Neutral LAgF, however, is present in far larger concentration than free F^-. If the dihydrogen complex is

deprotonated by a second molecule of LAgF (Scheme 4.6d), the rate law should be first-order in silver only if proton transfer is much more rapid than loss of coordinated H_2, i.e., if $k_2 >> k_{-1}$.

In principle the latter scenario is plausible, but the free energy for dissociation of H_2 from $[(6Me)Au(\eta^2\text{-}H_2)]^+$ (6Me is the *N,N′*-dimethyl analogue of 6Dipp) has been calculated at +9.5 kcal/mol.[30] Because gold–ligand bonds are generally stronger than the corresponding silver–ligand bonds, we regard this figure as a rough upper boundary on the barrier for dissociation of H_2 from $[LAg(\eta^2\text{-}H_2)]^+$.[40] The deprotonation of coordinated dihydrogen, as an intermolecular process, would need to be extraordinarily facile to predominate over dissociation.

4.2.10 Kinetic Isotope Effects in Fluoride Hydrogenolysis

The observed rate data for hydrogenolysis rule out the cooperation of two silver fluorides during or prior to the rate-limiting step, but are consistent with several remaining mechanistic pathways, including scenarios in which H–H bond cleavage is rate–limiting, and in which it would need to be extremely rapid. We undertook an examination of kinetic isotope effects to differentiate further among these possibilities.

The rates of reaction between **7c** and H_2 versus D_2 at two different pressures were compared. At 3.0 bar of hydrogen pressure, the kinetic isotope effect (KIE) k_H/k_D was 1.56(±0.12); at 5.0 bar the ratio was 1.58(±0.10). Although these values are modest, KIE values for reactions in which H–H bond-breaking is likely rate-limiting often fall in the range of k_H/k_D = 1.2–1.6,[41] and significantly higher values are rare.[42] Several explanations, including early transition states[43] and complex new vibrational modes as the transition state is approached,[44] have been invoked for this behavior. The measured

KIE for silver fluoride hydrogenolysis thus appears consistent with rate-limiting H–H bond cleavage.

This does not settle the issue, however, for normal KIEs have been observed for the coordination of H_2 versus D_2 to metal centers.[45] Inverse equilibrium isotope effects have been measured for both binding[46] and oxidative addition[47] of H_2 versus D_2, but the kinetic isotope effects[46,47a–c] are normal: The effect is stronger for the reverse reactions than for the forward reactions, making the ratio k_1/k_{-1} smaller for H_2 than for D_2. If the overall rate of heterolysis were determined by formation of an η^2-dihydrogen complex, as shown in Scheme 4.6d, a KIE near 1.5 would be plausible.

To examine the presumed deprotonation of dihydrogen separately from its coordination to silver, we carried out the heterolysis of H–D[48] by **7c** and assessed the ratio of $\{[(7Dipp)Ag]_2(\mu\text{-}D)\}^+[HF_2]^-$ (**1c**-*d*[HF_2]) to $\{[(7Dipp)Ag]_2(\mu\text{-}H)\}^+[DF_2]^-$ (**1c**[DF_2]) (Scheme 4.7). Because the same η^2-dihydrogen complex, if indeed this were an intermediate, would give rise to both isotopomers, this ratio should reflect the relative rates of H^+ versus D^+ loss. The measured ratio is 1.58(±0.04).

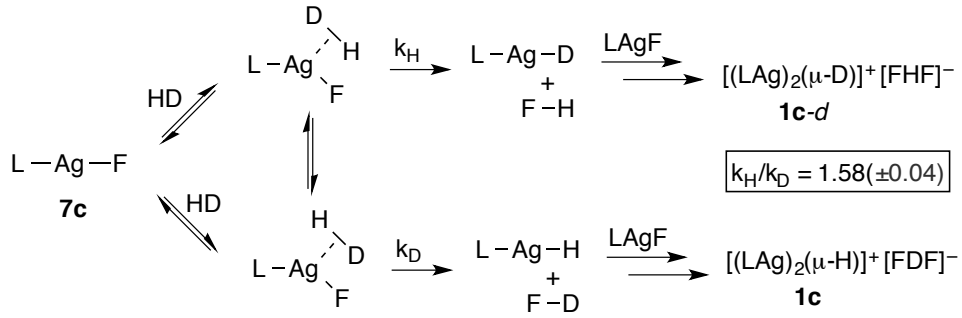

Scheme 4.7. Possible sequence for formation of isotopomers by reaction of HD with (7Dipp)AgF. Reaction carried out in CD_2Cl_2 solution.

The observation of a significant isotope effect in the product ratio does not prove that hydrogen loss is the rate-limiting step. In the second-order case of Scheme 4.6d, even if deprotonation were very fast relative to hydrogen loss, and thus occurred after the rate-limiting step, a normal KIE for this step would be reflected in the product distribution. Other caveats apply: We believe that hydrogen activation is essentially irreversible under these conditions. If the reverse reaction were facile, however, the product distribution would reflect an equilibrium isotope effect rather than a kinetic isotope effect. Finally, we cannot rule out coincidence between the ratio of μ-D and μ-H complexes formed from HD and the ratio of overall reaction rates for H_2 versus D_2. Nonetheless, while the data do not conclusively exclude the second-order case ($k_2 >> k_{-1}$) of Scheme 4.6d, they are consistent with a pathway such as that shown in Scheme 4.6c, in which a single molecule of silver fluoride coordinates dihydrogen rapidly and reversibly, then cleaves it in the rate-limiting step.

4.3 Conclusion

We have explored the formation of hydride-bridged disilver cations through dihydrogen activation. Alkoxide-bridged disilver cations undergo hydrogenolysis with loss of free alcohol. The reaction of two neutral silver fluorides with dihydrogen also affords hydride-bridged disilver cations, generating bifluoride as the counterion. Compared to their five-membered analogues, six- and seven-membered N-heterocyclic carbenes impart remarkable stability to the product complexes, suppressing the formation of homoleptic $[(NHC)_2Ag]^+$ cations and permitting hydrogenolysis to proceed in high yield. In the reactions of dihydrogen with two neutral silver fluoride molecules, kinetics experiments rule out the participation of two silver complexes during or prior to the rate-

limiting step. Although other interpretations remain tenable, the results of hydrogen/ deuterium competition experiments are consistent with rate-limiting deprotonation of coordinated dihydrogen. We are currently exploring the application of these findings to the design of new silver-catalyzed hydrogenation processes.

4.4 Experimental

4.4.1 General Considerations

Unless otherwise indicated, manipulations were performed in an MBraun glovebox under an atmosphere of purified nitrogen, or in sealable glassware on a Schlenk line under an atmosphere of argon. Glassware and magnetic stir bars were dried in a ventilated oven at 160˚C, and allowed to cool under vacuum. Silver complexes were stored in the dark to minimize photodegradation.

Silver *p*-toluenesulfonate (Alfa-Aesar), sodium *tert*-pentoxide (Sigma- Aldrich), benzoyl fluoride (Alfa-Aesar), lithium aluminum hydride (Sigma- Aldrich), 1,4-dimethoxybenzene (Sigma-Aldrich), hydrogen (Sigma- Aldrich), and deuterium (Sigma-Aldrich) were used as received.

(6Dipp)AgBr[52] and (7Dipp)AgBr[53] were prepared according to literature procedures. (6Dipp)AgBr was used without further purification. (7Dipp)AgBr was recrystallized by cooling a saturated solution in methanol from 45˚C to –20˚C. Complexes $\{[(5Dipp)Ag]_2(\mu\text{-}O^tBu)\}^+[BF_4]^-$ (**5a**[BF_4]), (5Dipp)AgF (**7**), $\{[(5Dipp)Ag]_2(\mu\text{-}F\}^+[BF_4]^-$, (**12**) $\{[(5Dipp)Ag]_2(\mu\text{-}H)\}^+[BF_4]^-$ (**1a**[BF_4]) and $\{[(5Dipp)Ag]_2(\mu\text{-}H)\}^+$ OTf^- (**1a**[OTf]) have been described previously.[16,22] In this study these complexes were characterized by ^1H and, in the case of the fluorides, ^{19}F NMR spectroscopy.

Hexanes, tetrahydrofuran (THF), and toluene were purchased from EMD Millipore (OmniSolv grade), sparged with ultra-high purity argon (NexAir) for 45 minutes prior to first use, and dried over activated 3 Å molecular sieves (1/16", Alfa-Aesar), Dichloromethane (BDH) and acetonitrile (EMD Millipore OmniSolv) were dried by stirring overnight with calcium hydride (Alfa-Aesar, coarse powder), degassed by successive freeze-pump-thaw cycles, and vacuum-transferred into oven-dried resealable Schlenk flasks. Anhydrous benzene and anhydrous pentane (EMD Millipore DriSolv) were stored over 3 Å molecular sieves in the glovebox.

Dichloromethane-d_2 and acetonitrile-d_3 (Cambridge Isotope Labs) were dried by stirring overnight with calcium hydride (coarse powder, Alfa- Aesar), degassed by successive freeze-pump-thaw cycles, and vacuum- transferred into oven-dried resealable Schlenk flasks. Tetrahydrofuran-d_8 and benzene-d_6 (Cambridge Isotope Labs) were dried over purple sodium benzophenone, degassed by successive freeze-pump-thaw cycles, and vacuum-transferred into oven-dried resealable Schlenk flasks. Deuterium oxide (Cambridge Isotope Labs) was used as received.

^{1}H, ^{13}C, ^{19}F, and ^{109}Ag NMR spectra were obtained at the Georgia Institute of Technology NMR Center using a Bruker DSX 400 MHz spectrometer, a Varian Vx 400 MHz spectrometer, or a Varian Vx 300 MHz spectrometer. ^{1}H and ^{13}C NMR chemical shifts are referenced with respect to solvent signals and are reported relative to $Si(CH_3)_4$. ^{109}Ag NMR chemical shifts were referenced with respect to an external solution of 4.00 M silver nitrate (Alfa-Aesar) in deuterium oxide (defined as δ 0 ppm). ^{19}F NMR chemical shifts were referenced to external neat C_6F_6 (Alfa-Aesar, δ −164.90 ppm) and are reported relative to $CFCl_3$.

Infrared spectra were collected using microcrystalline samples on a Bruker Alpha-P infrared spectrometer equipped with an attenuated total reflection (ATR) attachment. Samples were exposed to air as briefly as possible prior to data collection.

Elemental analyses were performed by Atlantic Microlab in Norcross, GA. Samples for fluorine analysis were prepared separately from those used for C, H and N analysis, but the same procedures were followed and the resulting ^{1}H NMR spectra for a given complex were identical.

4.4.2 Synthetic Procedures

4.4.2.1 (6Dipp)AgOTs (**15a**)

Silver *p*-toluenesulfonate (AgOTs, 0.407 g, 1.46 mmol) was added to a solution of (6Dipp)AgBr (1.000 g, 1.463 mmol) in CH_2Cl_2 (10 mL) with stirring. The mixture was stirred for 30 min and then filtered through Celite to remove the silver bromide byproduct. The solvent was removed *in vacuo,* and the residue was dried *in vacuo* at 80˚C for 16 h, affording the product as a white powder (1.036 g, 1.32 mmol, 90% yield). ^{1}H NMR (400 MHz, CD_2Cl_2): δ (ppm) = 7.43 (t, *J* = 7.8 Hz, 2H, *para*-C*H*), 7.27 (d, *J* = 7.8 Hz, 4H, *meta*-C*H*), 7.15 (d, *J* = 8.0 Hz, 2H, O_3SCH), 7.04 (d, *J* = 8.0 Hz, 2H, O_3SCHCH) 3.48 (t, *J* = 5.8 Hz, 4H, NCH_2), 3.03 (sep, *J* = 6.9 Hz, 4H, $CH(CH_3)_2$), 2.38 (quin, *J* = 5.8 Hz, 2H, NCH_2CH_2), 2.34 (s, 3H, $O_3S(C4H4)CH_3$), 1.31 (d, *J* = 6.9 Hz, 12H, $CH(CH_3)_2$), 1.28 (d, *J* = 6.9 Hz, 12H, $CH(CH_3)_2$). ^{13}C{^{1}H} NMR (75.5 MHz, CD_2Cl_2): δ (ppm) = 204.4 (app dd, $J(^{13}C\text{-}^{109}Ag)$ = 308 Hz, $J(^{13}C\text{-}^{107}Ag)$ = 267 Hz, N*C*Ag), 145.9 (Dipp-*ortho*-*C*), 143.0 (app d, $J(^{13}C\text{-}^{109/107}Ag)$ = 3 Hz, Dipp-*ipso*-*C*), 141.9 (OTs-*ipso*-*C*), 140.2 (OTs-*para*-*C*), 129.7 (Dipp-*para*-*C*), 128.9 (OTs-*meta*-*C*), 126.1 (OTs-*ortho*-*C*), 125.2 (Dipp-*meta*-*C*), 46.4 (app d, $J(^{13}C\text{-}^{109/107}Ag)$ = 8 Hz, NCH_2), 28.9

($CH(CH_3)_2$), 25.0 ($CH(CH_3)_2$), 24.8 ($CH(CH_3)_2$), 21.4 (NCH_2CH_2), 20.6 ($O_3SC_6H_4CH_3$). IR (ATR): ν (cm^{-1}) = 2957, 2922, 2866, 1520, 1456, 1308, 1264, 1207, 1158, 1111, 1058, 1026, 999, 936, 808, 763, 678, 586, 564, 553, 564, 553, 454, 410. Elemental analysis calculated for $C_{35}H_{47}N_2AgF_3O_3S$: C 61.49, H 6.93, N 4.10. Found: C 61.21, H 6.89, N 4.06.

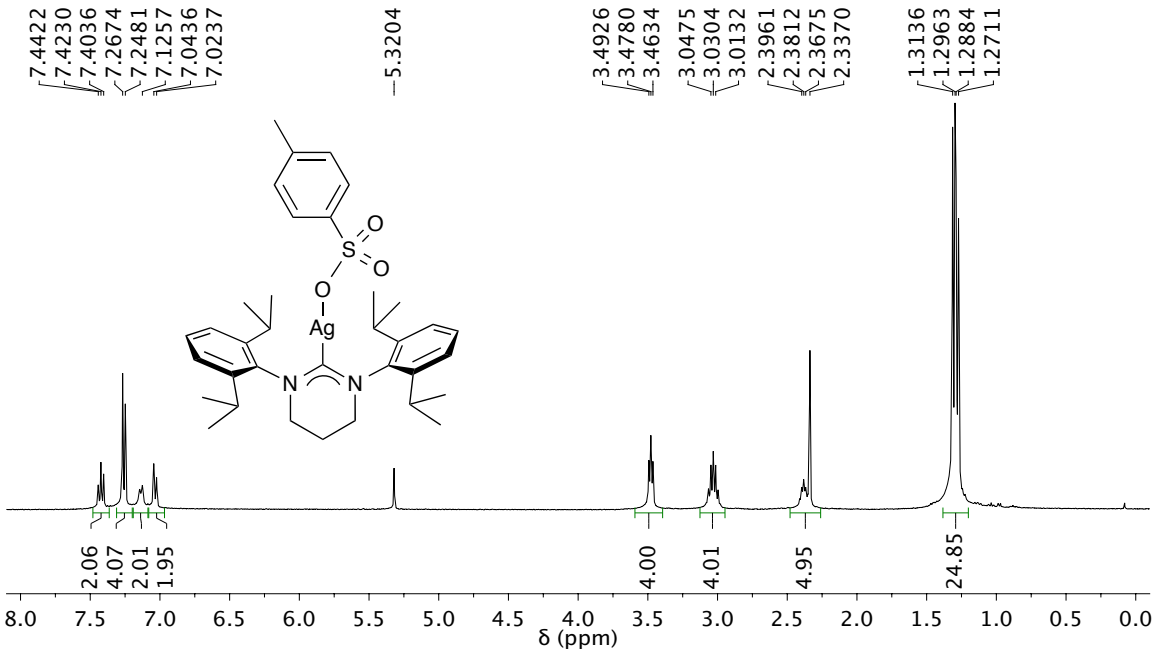

Figure 4.5. ^1H NMR (400 MHz, CD_2Cl_2) spectrum of (6Dipp)AgOTs.

4.4.2.2 (7Dipp)AgOTs (**15b**)

Silver *p*-toluenesulfonate (AgOTs, 0.460 g, 1.65 mmol) was added to a solution of (7Dipp)AgBr (1.000 g, 1.649 mmol) in CH_2Cl_2 (10 mL) with stirring. The mixture was stirred for 30 min and then filtered through Celite to remove the silver bromide byproduct. The solvent was removed *in vacuo*, and the residue was dried *in vacuo* at 80˚C for 16 h, affording the product as a white powder (1.014 g, 1.453 mmol, 88% yield). ^1H NMR (400 MHz, CD_2Cl_2): δ (ppm) = 7.38 (t, J = 7.7 Hz, 2H, *para*-C*H*), 7.24 (d, J =

7.7 Hz, 4H, *meta*-C*H*), 7.11 (d, *J* = 8.0 Hz, 2H, O_3SCH), 7.03 (d, *J* = 8.0 Hz, 2H, O_3SCHCH) 4.02 (mult, 4H, NCH_2), 3.22 (sep, *J* = 6.9 Hz, 4H, $CH(CH_3)_2$), 2.34 (mult, 4H, NCH_2CH_2), 2.34 (s, 3H, $O_3S(C4H4)CH_3$), 1.32 (d, *J* = 6.9 Hz, 12H, $CH(CH_3)_2$), 1.28 (d, *J* = 6.9 Hz, 12H, $CH(CH_3)_2$). $^{13}C\{^1H\}$ NMR (100 MHz, CD_2Cl_2): δ (ppm) = 214.5 (app dd, $J(^{13}C\text{-}^{109}Ag)$ = 308 Hz, $J(^{13}C\text{-}^{107}Ag)$ = 267 Hz, NCAg), 145.7 (app d, $J(^{13}C\text{-}^{109/107}Ag)$ = 3 Hz, Dipp-*ipso*-*C*), 145.3 (Dipp-*ortho*-*C*), 141.9 (OTs-*ipso*-*C*), 140.1 (OTs-*para*-*C*), 129.3 (Dipp-*para*-*C*), 128.8 (OTs-*meta*-*C*), 126.1 (OTs-*ortho*-*C*), 125.3 (Dipp-*meta*-*C*), 54.2 (app d, $J(^{13}C\text{-}^{109/107}Ag)$ = 8 Hz, NCH_2), 29.0 ($CH(CH_3)_2$), 25.4 (NCH_2CH_2), 24.8 ($CH(CH_3)_2$), 24.8 ($CH(CH_3)_2$), 21.4 ($O_3SC_6H_4CH_3$). IR (ATR): ν (cm^{-1}) = 2958, 2962, 2868, 1510, 1454, 1385, 1329, 1307, 1263, 1222, 1207, 1181, 1144, 1104, 1056, 1031, 993, 939, 803, 759, 636, 572, 554, 517, 453. Elemental analysis calculated for $C_{36}H_{49}N_2AgO_3S$: C 61.97, H 7.08, N 4.02. Found: C 62.20, H 7.09, N 4.07.

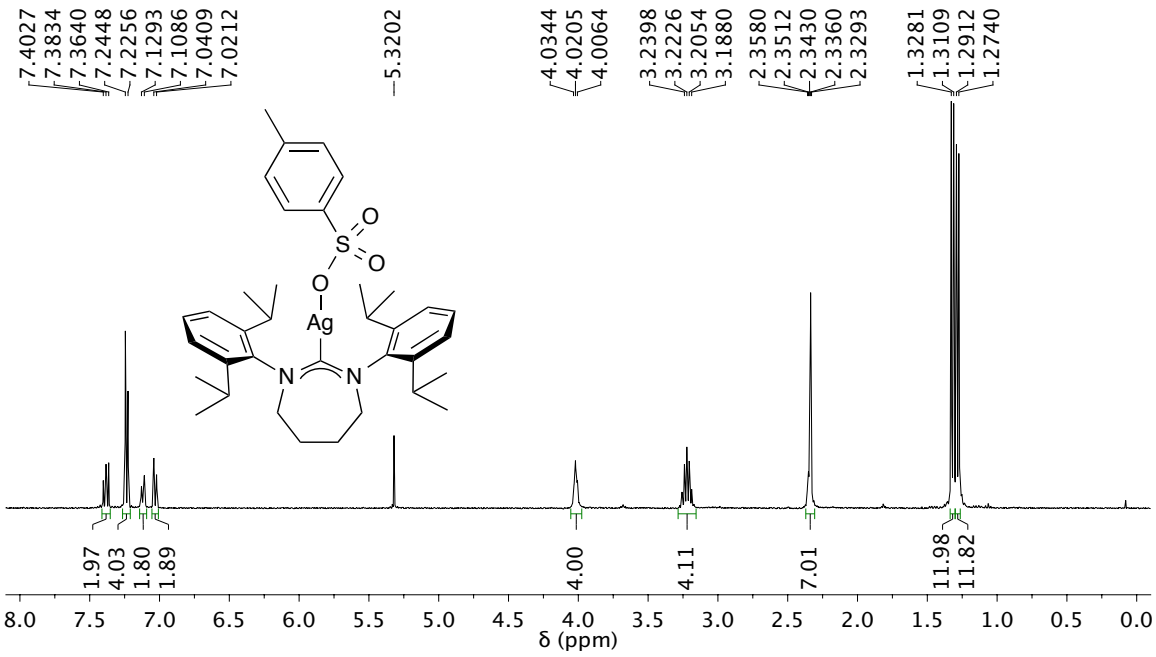

Figure 4.6. ^1H NMR (400 MHz, CD_2Cl_2) spectrum of (7Dipp)AgOTs.

4.4.2.3 (6Dipp)Ag(O^{t}Pent) (**3b**)

A solution of sodium *tert*-pentoxide (0.080 g, 0.73 mmol) in benzene (2 mL) was added dropwise with stirring to a solution of (6Dipp)AgOTs (0.500 g, 0.731 mmol) in THF (10 mL). The mixture was stirred for 1 h and then filtered through Celite to remove the sodium *p*-toluenesulfonate byproduct. Solvent was removed from the filtrate *in vacuo*, and the product was dried *in vacuo* at 70˚C for 16 h, affording the product as a white powder (0.420 g, 0.700 mmol, 96% yield). Note: In anhydrous CH_2Cl_2, (6Dipp)Ag(O^{t}Pent) decomposes rapidly to (6Dipp)AgCl and *tert*-pentanol. In THF-d_8 solution, (6Dipp)Ag(O^{t}Pent) hydrolyzes rapidly after exposure to atmospheric moisture. ^{1}H NMR (400 MHz, C_6D_6): δ (ppm) = 7.16 (t, 2H, *para*-C*H*), 7.03 (d, 4H, *meta*-C*H*), 2.96 (sep, *J* = 6.9 Hz, 4H, C*H*$(CH_3)_2$), 2.70 (t, *J* = 5.8 Hz, 4H, NCH_2), 1.48 (d, *J* = 6.9 Hz, 12H, C*H*$(CH_3)_2$), 1.43 (quin, *J* = 5.8 Hz, 2H, NCH$_2$CH_2), 1.37 (q, *J* = 7.6 Hz, 2H, CH_2CH$_3$), 1.18 (s, 6H, OC(CH_3)$_2$), 1.15 (d, *J* = 6.9 Hz, 12H, C*H*$(CH_3)_2$), 1.10 (t, *J* = 7.6 Hz, 3H CH$_2$CH_3). ^{1}H NMR (400 MHz, THF-d_8): δ (ppm) = 7.16 (mult, 2H, *para*-C*H*), 7.21 (mult, 4H, *meta*-C*H*), 3.44 (t, *J* = 5.8 Hz, 4H, NCH_2), 3.14 (sep, *J* = 6.9 Hz, 4H, C*H*$(CH_3)_2$), 2.29 (quin, *J* = 5.8 Hz, 2H, NCH$_2$CH_2), 1.36 (d, *J* = 6.9 Hz, 12H, C*H*$(CH_3)_2$), 1.29 (d, *J* = 6.9 Hz, 12H, C*H*$(CH_3)_2$), 0.68 (q, *J* = 7.6 Hz, 2H, CH_2CH$_3$), 0.48 (t, *J* = 7.6 Hz, 3H CH$_2$CH_3), 0.44 (s, 6H, OC(CH_3)$_2$). ^{13}C{^{1}H} NMR (100 MHz, THF-d_8): δ (ppm) = 207.4 (app dd, *J*(^{13}C-^{109}Ag) = 227 Hz, *J*(^{13}C-^{107}Ag) = 196 Hz, NCAg), 146.2 (*ortho*-*C*), 144.1 (app d, *J*(^{13}C-$^{109/107}$Ag) = 3 Hz, *ipso*-*C*), 129.4 (*para*-*C*), 125.1 (*meta*-*C*), 69.8 (O*C*$(CH_3)_2$), 46.9 (app d, *J*(^{13}C-$^{109/107}$Ag) = 5 Hz, N*C*H$_2$), 42.2 (*C*H$_2$CH$_3$), 34.5 (OC(*C*H$_3$)$_2$), 29.2 (*C*H$(CH_3)_2$), 24.9 (CH(*C*H$_3$)$_2$), 24.7 (CH(*C*H$_3$)$_2$), 21.1 (NCH$_2$*C*H$_2$), 9.9 (CH$_2$*C*H$_3$). IR (ATR): ν (cm^{-1}) = 2958, 2868, 1511, 1455, 1310, 1261, 1204, 1104, 1055,

961, 880, 802, 758, 727, 556, 452. Elemental analysis calculated for $C_{33}H_{51}N_2AgO$: C 66.10, H 8.57, N 4.67. Found: C 64.68, H 8.66, N 4.44. Note: Attempts to further purify this complex via recrystallization have not resulted in satisfactory carbon analyses. Nonetheless complexes **5b** and **7b,** prepared directly from this one, were isolated in analytical purity.

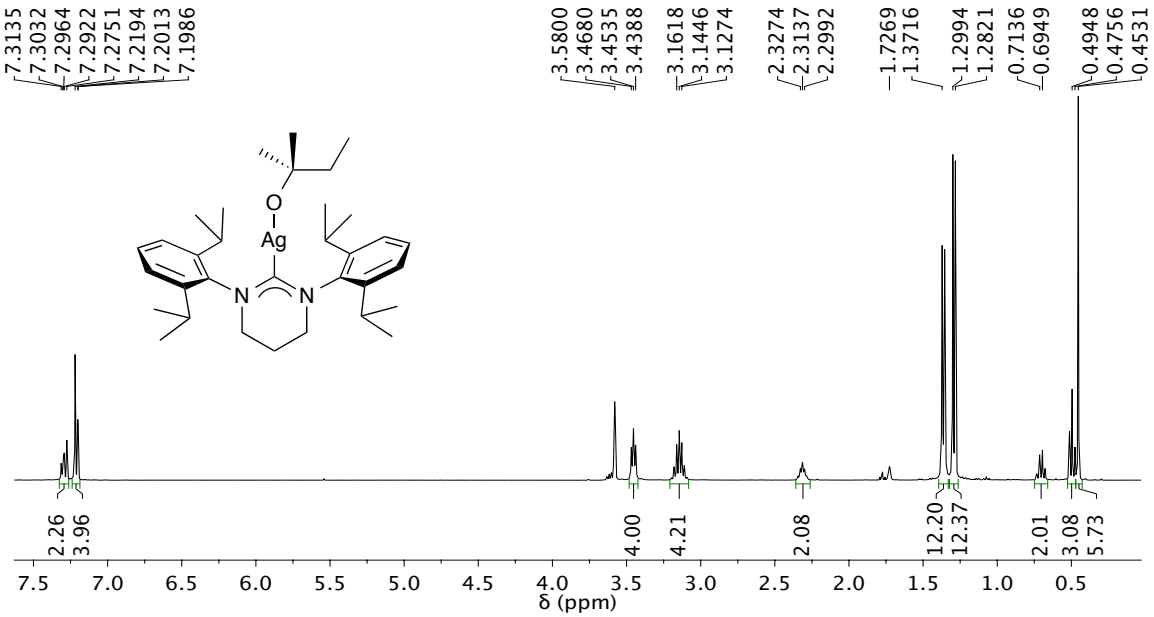

Figure 4.7. ^{1}H NMR (400 MHz, THF-d_8) spectrum of (6Dipp)Ag(O^{t}Pent).

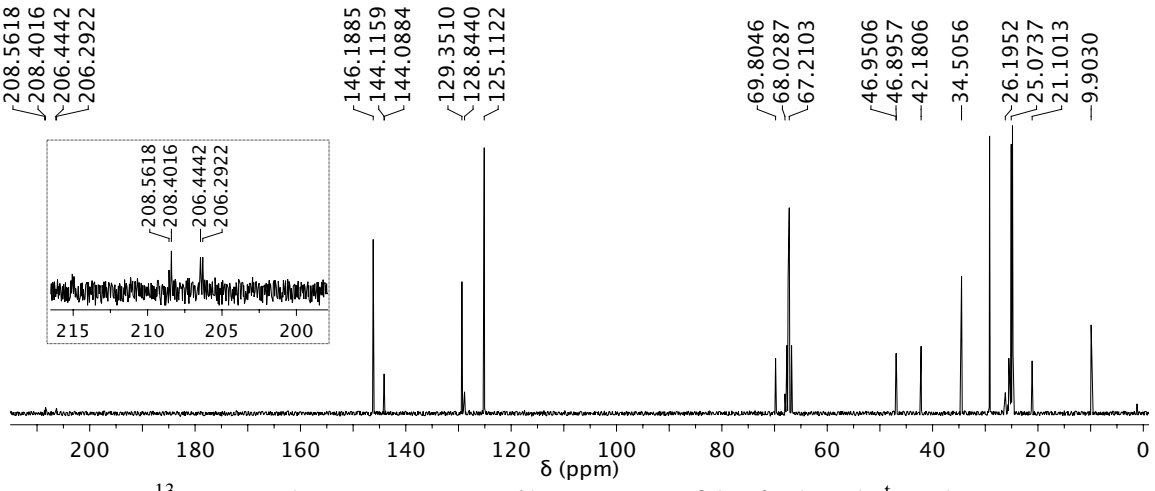

Figure 4.8. ^{13}C NMR (100 MHz, THF-d_8) spectrum of (6Dipp)Ag(O^{t}Pent).

4.4.2.4 (7Dipp)Ag(O^{t}Pent) (**3c**)

A solution of sodium *tert*-pentoxide (0.079 g, 0.72 mmol) in benzene (2 mL) was added dropwise with stirring to a solution of (7Dipp)AgOTs (0.500 g, 0.717 mmol) in THF (10 mL). The mixture was stirred for 1 h and then filtered through Celite to remove the sodium *p*-toluenesulfonate byproduct. Solvent was removed from the filtrate *in vacuo*. The residue was dried *in vacuo* at 70˚C for 16 h, affording the product as a white powder (0.408 g, 0.665 mmol, 93% yield). Note: In anhydrous CH_2Cl_2, (7Dipp)Ag(O^{t}Pent) decomposes rapidly to (7Dipp)AgCl and *tert*-pentanol. In THF-d_8 solution, (7Dipp)Ag(O^{t}Pent) hydrolyzes rapidly after exposure to atmospheric moisture. ^{1}H NMR (400 MHz, C_6D_6): δ (ppm) = 7.16 (t, 2H, *para*-C*H*), 7.02 (d, 4H, *meta*-C*H*), 3.27 (mult, 4H, NCH_2), 3.15 (sep, J = 6.9 Hz, 4H, CH(CH$_3$)$_2$), 1.58 (mult, 4H, NCH$_2$CH_2), 1.50 (d, J = 6.9 Hz, 12H, CH(CH$_3$)$_2$), 1.35 (q, J = 7.6 Hz, 2H, CH_2CH$_3$), 1.17 (d, J = 6.9 Hz, 12H, CH(CH$_3$)$_2$), 1.14 (s, 6H, OC(CH_3)$_2$), 1.09 (t, J = 7.6 Hz, 3H CH$_2$CH_3). ^{13}C{^{1}H} NMR (100 MHz, C_6D_6): δ (ppm) = 217.7 (app dd, J(^{13}C-^{109}Ag) = 228 Hz, J(^{13}C-^{107}Ag) = 199 Hz, N*C*Ag), 145.9 (app d, J(^{13}C-$^{109/107}$Ag) = 9 Hz, Dipp-*ipso*-*C*), 144.8 (Dipp-*ortho*-*C*), 129.0 (Dipp-*para*-*C*), 125.1 (Dipp-*meta*-*C*), 70.2 (O*C*(CH$_3$)$_2$), 53.6 (app d, J(^{13}C-$^{109/107}$Ag) = 7 Hz, N*C*H$_2$), 42.2 (*C*H$_2$CH$_3$), 34.6 (OC(*C*H$_3$)$_2$), 29.0 (*C*H(CH$_3$)$_2$), 25.1 (NCH$_2$*C*H$_2$), 24.8 (CH(*C*H$_3$)$_2$), 10.5 (CH$_2$*C*H$_3$). IR (ATR): ν (cm^{-1}) = 2960, 2928, 2867, 1651, 1589, 1499, 1452, 1434, 1385, 1362, 1344, 1309, 1289, 1262, 1181, 1056, 999, 966, 893, 804, 787, 760, 551, 489, 474, 454. Elemental analysis calculated for $C_{34}H_{53}N_2AgO$: C 66.55, H 8.71, N 4.56. Found: C 64.43, H 8.65, N 4.44. Note: Attempts to further purify this complex via recrystallization have not resulted in

satisfactory carbon analyses. Nonetheless, complex **7c,** which is prepared directly from this one, was isolated in analytical purity.

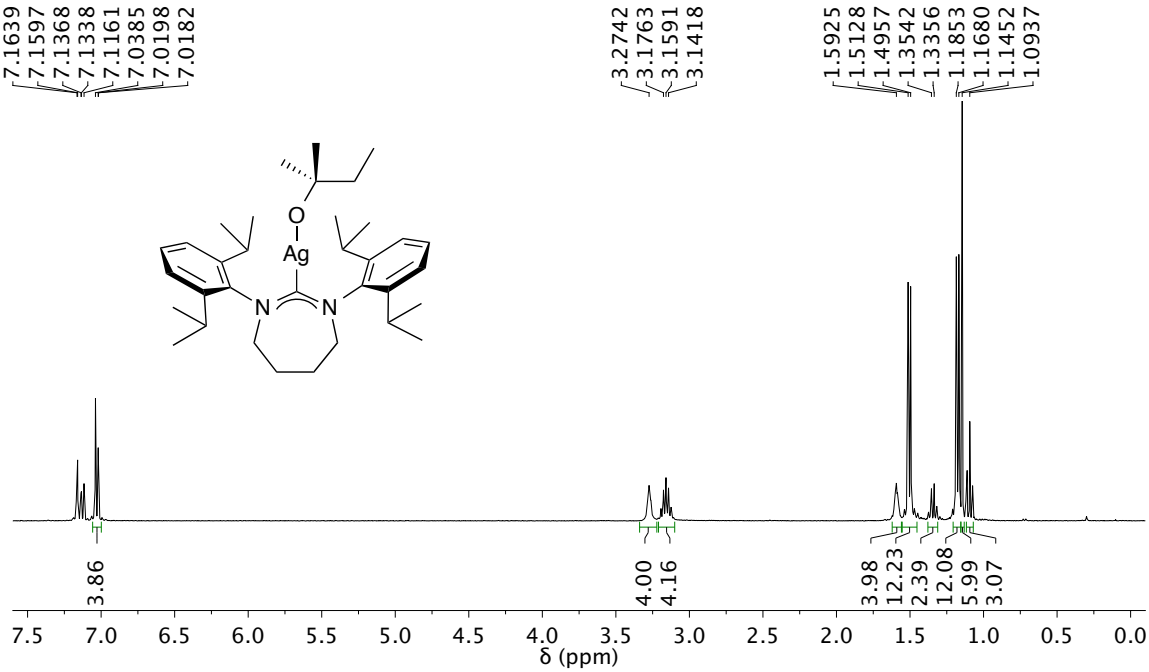

Figure 4.9. ^{1}H NMR (400 MHz, C_6D_6) spectrum of (7Dipp)Ag(O^{t}Pent).

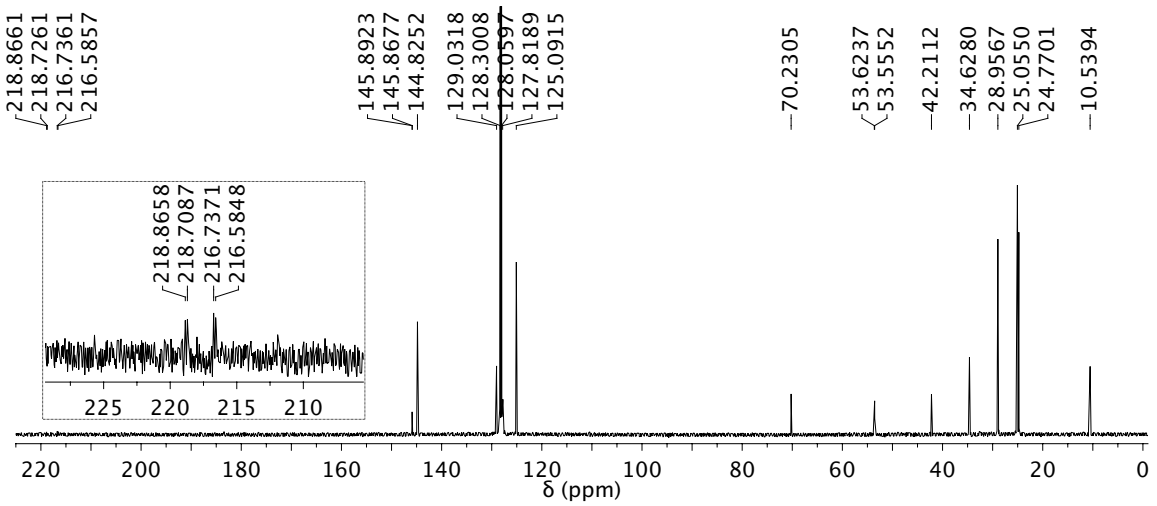

Figure 4.10. ^{13}C NMR (100 MHz, C_6D_6) spectrum of (7Dipp)Ag(O^{t}Pent). **Inset:** Detail of N*C*Ag signal with increased line broadening (2 Hz).

4.4.2.5 (6Dipp)AgOTf

Silver trifluoromethanesulfonate (AgOTf, 0.217 g, 0.845 mmol) was added to a solution of (6Dipp)AgBr (0.500 g, 0.844 mmol) in CH_2Cl_2 (10 mL), and the solution was stirred for 30 minutes. The mixture was filtered through Celite to remove the AgBr byproduct, and the solvent was removed from the filtrate *in vacuo*. The residue was dried under vacuum for 4 hours at 40˚C, affording the product as a white powder (0.479 g, 0.725 mmol, 86% yield). ^{1}H NMR (400 MHz, CD_2Cl_2): δ (ppm) = 7.42 (t, *J* = 7.8 Hz, 2H, *para*-C*H*), 7.26 (d, *J* = 7.8 Hz, 4H, *meta*-C*H*), 3.50 (t, *J* = 5.7 Hz, 4H, NC*H*$_2$), 3.01 (sep, *J* = 6.9 Hz, 4H, C*H*$(CH_3)_2$), 2.39 (quin, *J* = 5.7 Hz, 2H, NCH_2CH_2), 1.31 (d, *J* = 6.9 Hz, 12H, C*H*$(CH_3)_2$), 1.29 (d, *J* = 6.9 Hz, 12H, C*H*$(CH_3)_2$). ^{13}C{^{1}H} NMR (100 MHz, CD_2Cl_2): δ (ppm) = 207.1 (app dd, *J*(^{13}C-^{109}Ag) = 321 Hz, *J*(^{13}C-^{107}Ag) = 278 Hz, N*C*Ag), 145.9 (*ortho*-*C*), 143.0 (app d, *J*(^{13}C-$^{109/107}$Ag) = 2 Hz, *ipso*-*C*), 129.8 (*para*-*C*), 125.3 (*meta*-*C*), 46.5 (app d, *J*(^{13}C-$^{109/107}$Ag) = 8 Hz, N*C*H_2), 29.0 (*C*H$(CH_3)_2$), 25.0 (CH(*C*$H_3)_2$), 24.8 (CH(*C*$H_3)_2$), 20.5 (NCH_2CH_2), O_3SCF_3 not observed. ^{19}F NMR (376 MHz, CD_2Cl_2): δ (ppm) = –78.2 (s, $O_3SCF_3^-$). IR (ATR): ν (cm^{-1}) = 2961, 2927, 2871, 1591, 1520, 1459, 1313, 1232, 1202, 1165, 1033, 1017, 993, 804, 758, 633, 590, 516, 451. Elemental analysis calculated for $C_{29}H_{40}N_2Ag_2F_3O_3S$: C 52.70, H 6.09, N 4.23. Found: C 52.41, H 6.00, N 4.21.

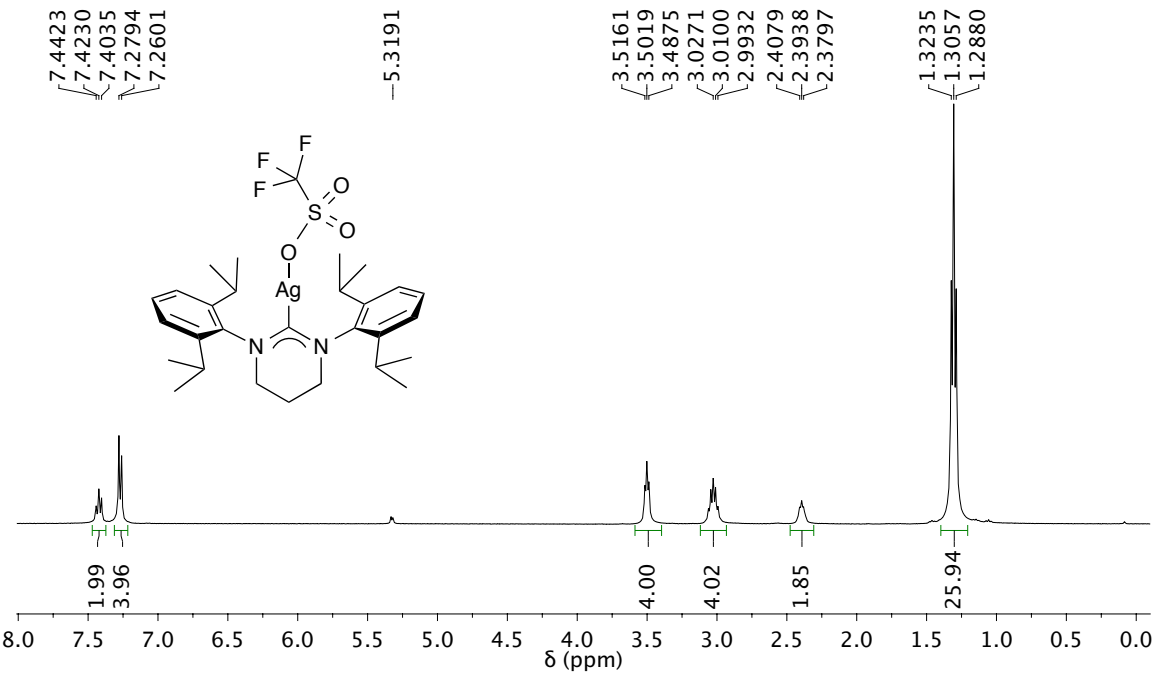

Figure 4.11. ^{1}H NMR (400 MHz, CD_2Cl_2) spectrum of (6Dipp)AgOTf.

4.4.2.6 {[(6Dipp)Ag]$_2$(μ-O^{t}Pent)}$^+$OTf$^-$ (**5b**[OTf])

Solutions of (6Dipp)Ag(OTf) (0.271 g, 0.396 mmol) and of (6Dipp)Ag(O^{t}Pent) (0.250 g, 0.417 mmol) in THF (2 mL each) were prepared and cooled to –35˚C. The (6Dipp)Ag(O^{t}Pent) solution was added dropwise to the (6Dipp)Ag(OTf) solution with stirring, forming a pale yellow mixture with traces of black precipitate. This mixture was stirred for 30 minutes without further cooling, then filtered through Celite. A layer of toluene was carefully added over the filtrate, and the toluene was allowed to diffuse into the THF solution at –35˚C for 48 h, resulting in the formation of colorless crystals. The crystals were collected by filtration, washed with hexanes and dried *in vacuo* at 40˚C for 4 h, affording the product as a white powder (0.403 g, 0.320 mmol, 81%). ^{1}H NMR (400 MHz, CD_2Cl_2): δ (ppm) = 7.31 (mult, 4H, *para*-C*H*), 7.14 (mult, 8H, *meta*-C*H*), 3.39 (t, *J* = 5.8 Hz, 8H, NCH_2), 2.91 (sep, *J* = 6.9 Hz, 8H, CH(CH_3)$_2$), 2.32 (quin, *J* = 5.8 Hz, 4H,

NCH_2CH_2), 1.25 (d, J = 6.9 Hz, 24H, $CH(CH_3)_2$), 1.09 (d, J = 6.9 Hz, 24H, $CH(CH_3)_2$), 0.25 (q, J = 6.4 Hz, 2H, CH_2CH_3), 0.14 (t, J = 6.4 Hz, 3H CH_2CH_3), 0.00 (s, 6H, $OC(CH_3)_2$). $^{13}C\{^1H\}$ NMR (100 MHz, CD_2Cl_2): δ (ppm) = 146.5 (*ortho-C*), 144.0 (app 1:1:1 t, $J(^{13}C\text{-}^{109/107}Ag)$ = 2 Hz, *ipso-C*), 130.5 (*para-C*), 126.1 (*meta-C*), 74.2 ($OC(CH_3)_2$), 48.1 (app 1:1:1 t, $J(^{13}C\text{-}^{109/107}Ag)$ = 3 Hz, NCH_2), 34.5 (CH_2CH_3), 34.5 ($OC(CH_3)_2$), 29.7 ($CH(CH_3)_2$), 25.8 ($CH(CH_3)_2$), 25.8 ($CH(CH_3)_2$), 21.8 (NCH_2CH_2), 11.2 ($CH(CH_3)_2$), N*C*Ag not observed, O_3SCF_3 not observed. ^{19}F NMR (376 MHz, CD_2Cl_2): δ (ppm) = –79.0 (s, $O_3SCF_3^-$). IR (ATR): ν (cm^{-1}) = 2958, 2926, 2868, 1510, 1454, 1385, 1329, 1307, 1263, 1222, 1207, 1181, 1144, 1104, 1056, 1031, 993, 803, 759, 636, 572, 554, 517, 453. Elemental analysis calculated for $C_{62}H_{91}N_4Ag_2F_3O_4S$: C 59.04, H 7.27, N 4.44. Found: C 58.77, H 7.37, N 4.48.

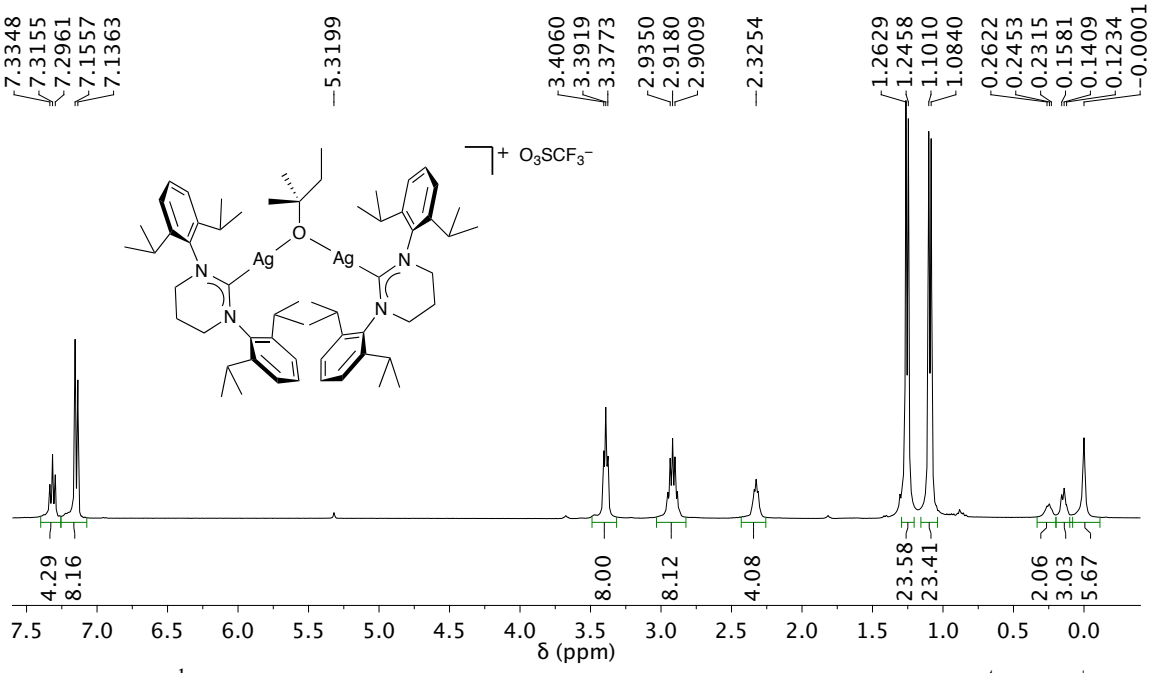

Figure 4.12. ^1H NMR (400 MHz, CD_2Cl_2) spectrum of $\{[(6Dipp)Ag]_2(\mu\text{-}O^tPent)\}^+OTf^-$ (**5b**[OTf]).

4.4.2.7 (6Dipp)AgF (**7b**)

A solution of sodium *tert*-pentoxide (0.161 g, 1.46 mmol) in benzene (2 mL) was added dropwise with stirring to a solution of (6Dipp)Ag(OTs) (1.000 g, 1.463 mmol) in THF (10 mL); the mixture was stirred for 1 h and then filtered through Celite to remove the precipitated sodium *p*-toluenesulfonate. To the filtrate was added excess benzoyl fluoride (0.200 mL, 1.86 mmol), causing the precipitation of the product as a white solid. After stirring for 30 min, the precipitate was collected by filtration. The product was washed with benzene (2 × 5 mL) and dried *in vacuo* at 80˚C overnight, affording the product as a white powder (0.706 g, 1.33 mmol, 91%). (6Dipp)AgF is hygroscopic. ^{1}H NMR (400 MHz, CD_2Cl_2): δ (ppm) = 7.41 (t, *J* = 7.8 Hz, 2H, *para*-C*H*), 7.26 (d, *J* = 7.8 Hz, 4H, *meta*-C*H*), 3.46 (t, *J* = 5.7 Hz, 4H, NCH_2), 3.03 (sep, *J* = 6.9 Hz, 4H, C*H*$(CH_3)_2$), 2.37 (quin, *J* = 5.7 Hz, 2H, NCH_2CH_2), 1.32 (d, *J* = 6.9 Hz, 24H, C*H*$(CH_3)_2$). ^{13}C{^{1}H} NMR (75.5 MHz, CD_2Cl_2): δ (ppm) = 204.5 (app dd, *J*(^{13}C-^{109}Ag) = 295 Hz, *J*(^{13}C-^{107}Ag) = 253 Hz, N*C*Ag), 145.9 (*ortho*-*C*), 143.2 (app d, *J*(^{13}C-$^{109/107}$Ag) = 3 Hz, *ipso*-*C*), 129.6 (*para*-*C*), 125.1 (*meta*-*C*), 46.5 (app d, *J*(^{13}C-$^{109/107}$Ag) = 7 Hz, N*C*H_2), 28.9 (*C*H$(CH_3)_2$), 25.1 (CH(*C*$H_3)_2$), 24.7 (CH(*C*$H_3)_2$), 20.7 (NCH_2CH_2). ^{19}F NMR (376 MHz, CD_2Cl_2): δ (ppm) = −246.03 (app dd, *J*(^{19}F-^{109}Ag) = 176 Hz, *J*(^{19}F-^{107}Ag) = 152 Hz). IR: ν (cm^{-1}) = 2958, 2868, 1514, 1453, 1389, 1333, 1305, 1260, 1208, 1180, 1056, 1033, 804, 761, 558, 500, 452, 427. Elemental analysis calculated for $C_{28}H_{40}N_2AgF$: C 63.27, H 7.59, N 5.27, F 3.57. Found: C 63.04, H 7.56, N 5.17, F 3.57.

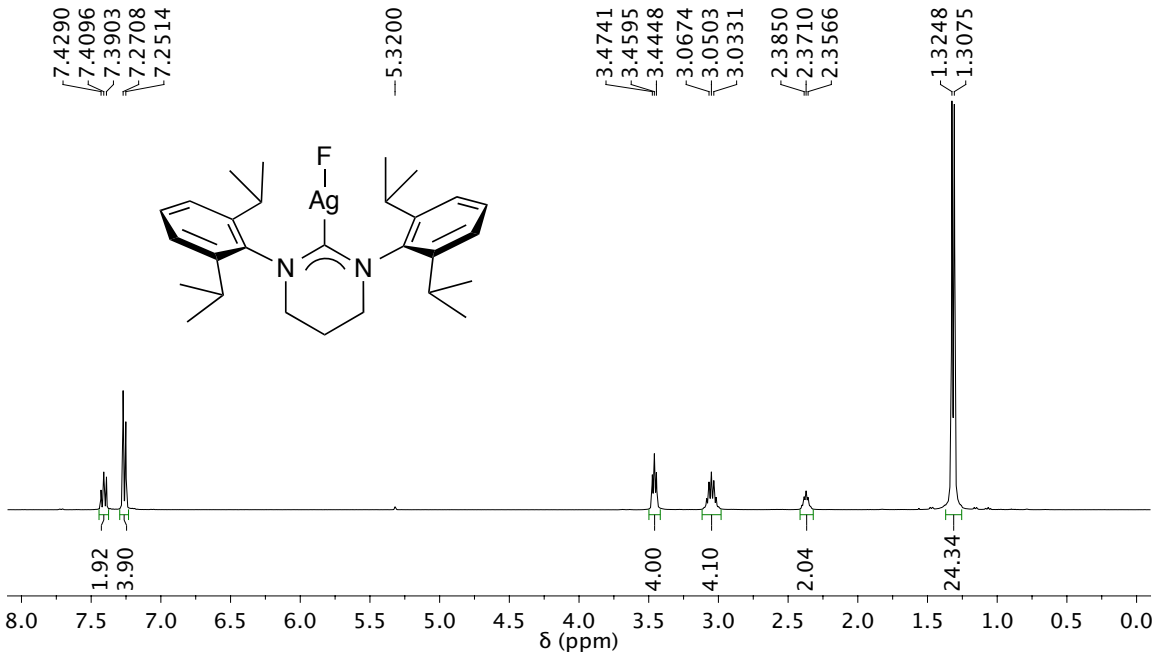

Figure 4.13. ^{1}H NMR (400 MHz, CD_2Cl_2) spectrum of (6Dipp)AgF (**7b**).

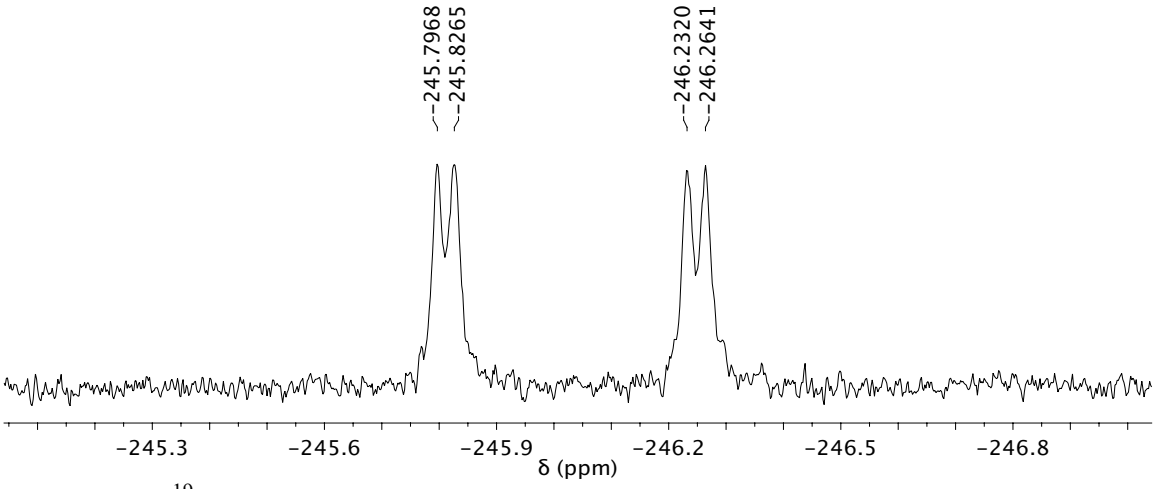

Figure 4.14. ^{19}F NMR (376 MHz, CD_2Cl_2) spectrum of (6Dipp)AgF (**7b**).

4.4.2.8 (7Dipp)AgF (**7c**)

A solution of sodium *tert*-pentoxide (0.079 g, 0.72 mmol) in benzene (2 mL) was added dropwise with stirring to a solution of (7Dipp)Ag(OTs) (0.500 g, 0.717 mmol) in

THF (10 mL); the mixture was stirred for 1 h and then filtered through Celite to remove the precipitated sodium *p*-toluenesulfonate. To the filtrate was added excess benzoyl fluoride (0.100 mL 0.919 mmol), causing the precipitation of the product as a white solid. After stirring for 30 min, the precipitate was collected by filtration. The solid was washed with benzene (2 × 5 mL) and dried *in vacuo* at 40˚C overnight, affording the product as a white powder (0.350 g, 0.642 mmol, 90%). (7Dipp)AgF is hygroscopic. ^{1}H NMR (400 MHz, CD_2Cl_2): δ (ppm) = 7.38 (t, *J* = 7.7 Hz, 2H, *para*-C*H*), 7.24 (d, *J* = 7.7 Hz, 4H, *meta*-C*H*), 4.00 (mult, 4H, NC*H*$_2$), 3.24 (sep, *J* = 6.9 Hz, 4H, C*H*$(CH_3)_2$), 2.33 (mult, 4H, NCH_2CH_2), 1.33 (d, *J* = 6.9 Hz, 12H, $CH(CH_3)_2$), 1.33 (d, *J* = 6.9 Hz, 12H, $CH(CH_3)_2$). ^{13}C{^{1}H} NMR (100 MHz, CD_2Cl_2): δ (ppm) = 215.1 (app dd, *J*(^{13}C-^{109}Ag) = 283 Hz, *J*(^{13}C-^{107}Ag) = 245 Hz, N*C*Ag), 145.8 (app d, *J*(^{13}C-$^{109/107}$Ag) = 3 Hz, *ipso*-*C*), 145.3 (*ortho*-*C*), 129.2 (*para*-*C*), 125.3 (*meta*-*C*), 54.3 (app d, *J*(^{13}C-$^{109/107}$Ag) = 8 Hz, N*C*H_2), 29.1 ($CH(CH_3)_2$), 25.4 (NCH_2CH_2), 24.9 ($CH(CH_3)_2$), 24.7 ($CH(CH_3)_2$). ^{19}F NMR (376 MHz, CD_2Cl_2): δ (ppm) = –246.16 (app dd, *J*(^{19}F-^{109}Ag) = 173 Hz, *J*(^{19}F-^{107}Ag) = 150 Hz). IR (ATR): ν (cm^{-1}) = 3641, 3136, 2964, 2952, 2927, 2866, 1952, 1651, 1589, 1502, 1450, 1385, 1361, 1312, 1291, 1256, 1179, 1095, 1058, 1000, 936, 897, 807, 787, 764, 681, 495, 453, 425, 402. Elemental analysis calculated for $C_{29}H_{42}N_2AgF$: C 63.85, H 7.76, N 5.14. Found: C 63.58, H 7.79, N 5.05.

4.4.3 Preparative Hydrogenolyses

Safety note: Great caution should be used when handling pressurized glassware. Personal protective equipment, especially eye protection, must be worn, and a blast shield is recommended. Pressurized NMR tubes should be transported to the NMR facility in secondary containment.

4.4.3.1 {[(6Dipp)Ag]$_2$(μ-H)}$^+$OTf$^-$ (**3b**[OTf]

A solution of {[(6Dipp)Ag]$_2$(μ-O-*t*- Pent)}$^+$[OTf]$^-$ (0.100 g, 0.079 mmol) in CD_2Cl_2 (1.0 mL) was degassed by two freeze-pump-thaw cycles in an NMR tube equipped with a J. Young valve, and the tube was pressurized with hydrogen (4.4 bar). The reaction was monitored daily by ^{1}H NMR spectroscopy, and nearly quantitative conversion was observed after 96 h. The solution was transferred to Schlenk flask, and the solvent was removed *in vacuo*. The off-white residue was dissolved in CH_2Cl_2 (2 mL) and was precipitated by the addition of hexane (10 mL). The precipitate was collected by vacuum filtration and was washed with hexane. The solid was dried *in vacuo* for 4 h, affording the product as a white powder (0.053 g, 0.045 mol, 57%). ^{1}H NMR (400 MHz, CD_2Cl_2): δ (ppm) = 7.30 (t, *J* = 7.8 Hz, 4H, *para*-C*H*), 7.09 (d, *J* = 7.8 Hz, 8H, *meta*-C*H*), 3.36 (t, *J* = 5.8 Hz, 8H, NC*H*$_2$), 2.82 (sep, *J* = 6.9 Hz, 8H, C*H*(CH$_3$)$_2$), 2.30 (quin, *J* = 5.8 Hz, 4H, NCH$_2$C*H*$_2$), 1.23 (d, *J* = 6.9 Hz, 24H, C*H*(CH$_3$)$_2$), 0.98 (d, *J* = 6.9 Hz, 24H, C*H*(CH3)2), −2.14 (app tt, *J*(^{1}H-^{109}Ag), = 132 Hz, *J*(^{1}H-^{107}Ag) = 115 Hz, Ag*H*Ag). ^{13}C{^{1}H} NMR (100 MHz, CD_2Cl_2): δ (ppm) = 207.1 (mult, N*C*Ag), 145.8 (*ortho*-*C*), 142.1 (app d, *J*(^{13}C-$^{109/107}$Ag) = 1 Hz, *ipso*-*C*), 129.5 (*para*-*C*), 124.8 (*meta*-*C*), 46.5 (app d, *J*(^{13}C-$^{109/107}$Ag) = 8 Hz, N*C*H$_2$), 28.7 (*C*H(CH$_3$)$_2$), 25.2 (CH(*C*H$_3$)$_2$), 24.6 (CH(*C*H$_3$)$_2$), 20.5 (NCH$_2$*C*H$_2$), O$_3$S*C*F$_3$ not observed. ^{19}F NMR (376 MHz, CD_2Cl_2): δ (ppm) = –79.0 (s, O$_3$SC*F*$_3^-$). IR (ATR): ν (cm^{-1}) = 2958, 2926, 2868, 1510, 1454, 1385, 1329, 1307, 1263, 1222, 1207, 1181, 1144, 1104, 1056, 1031, 993, 939, 803, 759, 636, 572, 554, 517, 453. Elemental analysis calculated for $C_{57}H_{81}N_4Ag_2F_3O_3S$: C 58.26, H 6.95, N 4.77. Found: C 57.98, H 6.93, N 4.69.

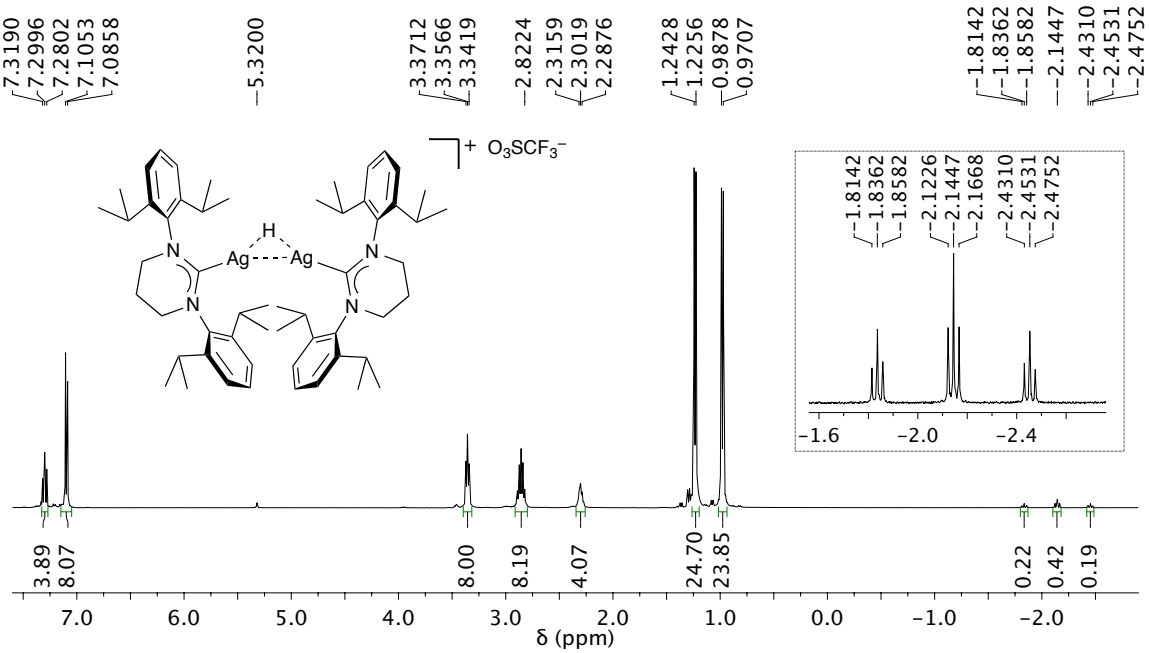

Figure 4.15. ^{1}H NMR (400 MHz, CD_2Cl_2) spectrum of $\{[(6Dipp)Ag]_2(\mu\text{-}H)\}^{+}OTf^{-}$ (**3b**[OTf]). **Inset:** Detail of hydride resonance.

4.4.3.2 $\{[(6Dipp)Ag]_2(\mu\text{-}H)\}^{+}HF_2^{-}$ (**1b**[HF_2])

A solution of (6Dipp)AgF (0.150 g, 0.282 mmol) in CD_2Cl_2 (1.0 mL) was degassed by two freeze-pump-thaw cycles in an NMR tube equipped with a J. Young valve, and the tube was pressurized with hydrogen (4.4 bar). The reaction was monitored daily by ^{1}H NMR spectroscopy, and nearly quantitative conversion was observed after 96 h. The solution was transferred to a vial, and the product was precipitated by the addition of hexane (10 mL). The precipitate was collected by vacuum filtration and was washed with hexane. The solid was dried *in vacuo* for 4 h, affording the product as a white powder (0.092 g, 0.086 mmol, 61%). ^{1}H NMR (400 MHz, CD_2Cl_2): δ (ppm) = 16.28 (t, $J(^{1}H\text{-}^{19}F)$ = 123 Hz, 1H, HF_2^{-}), 7.29 (t, J = 7.8 Hz, 4H, *para*-C*H*), 7.09 (d, J = 7.8 Hz, 8H, *meta*-C*H*), 3.35 (t, J = 5.8 Hz, 8H, NCH_2), 2.82 (sep, J = 6.9 Hz, 8H, $CH(CH_3)_2$), 2.31 (quin, J = 5.8 Hz, 4H, NCH_2CH_2), 1.23 (d, J = 6.9 Hz, 24H, $CH(CH_3)_2$), 0.97 (d, J =

6.9 Hz, 24H, C*H*(CH_3)$_2$), −2.15 (app tt, J(^{1}H-^{109}Ag), = 132 Hz, J(^{1}H-^{107}Ag) = 115 Hz, Ag*H*Ag). ^{13}C{^{1}H} NMR (100 MHz, CD_2Cl_2): δ (ppm) = 207.1 (mult, N*C*Ag), 145.8 (*ortho-C*), 142.1 (app d, J(^{13}C-$^{109/107}$Ag) = 1 Hz, *ipso-C*), 129.5 (*para-C*), 124.8 (*meta-C*), 46.5 (app d, J(^{13}C- $^{109/107}$Ag) = 8 Hz, N*C*H_2), 28.7 (*C*H(CH_3)$_2$), 25.2 (CH(*C*H_3)$_2$), 24.6 (CH(*C*H_3)$_2$), 20.5 (NCH_2*C*H_2). ^{19}F NMR (376 MHz, CD_2Cl_2): δ (ppm) = –157.3 (d, J(^{19}F-^{1}H) = 123 Hz, H*F*$_2^-$). ^{109}Ag NMR (18.6 MHz, CD_2Cl_2): δ (ppm) = 524.6 (app dt, J(^{109}Ag-^{1}H) = 132 Hz, J(^{109}Ag-^{107}Ag) = 108 Hz). IR (ATR): ν (cm^{-1}) = 2958, 2925, 2867, 1658, 1517, 1453, 1399, 1384, 1328, 1307, 1255, 1207, 1180, 1056, 806, 756, 554, 450. Elemental analysis calculated for $C_{57}H_{84}N_4Ag_2F_2$: C 63.15, H 7.76, N 5.26, F 3.57. Found: C 62.97, H 7.76, N 5.26, F 3.52.

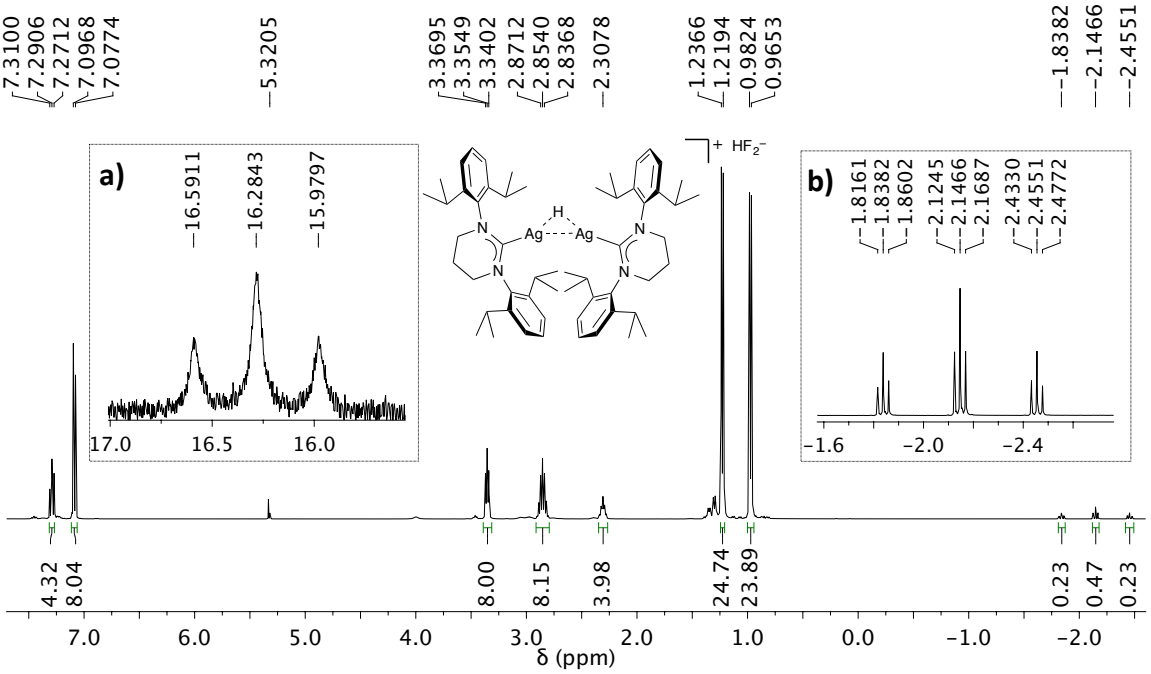

Figure 4.16. ^{1}H NMR (400 MHz, CD_2Cl_2) spectrum of {[(6Dipp)Ag]$_2$(μ-H)}$^+$HF$_2^-$ (**1b**[HF_2]). **a)** Resonance of the HF_2^- ion. **b)** Detail of the hydride resonance.

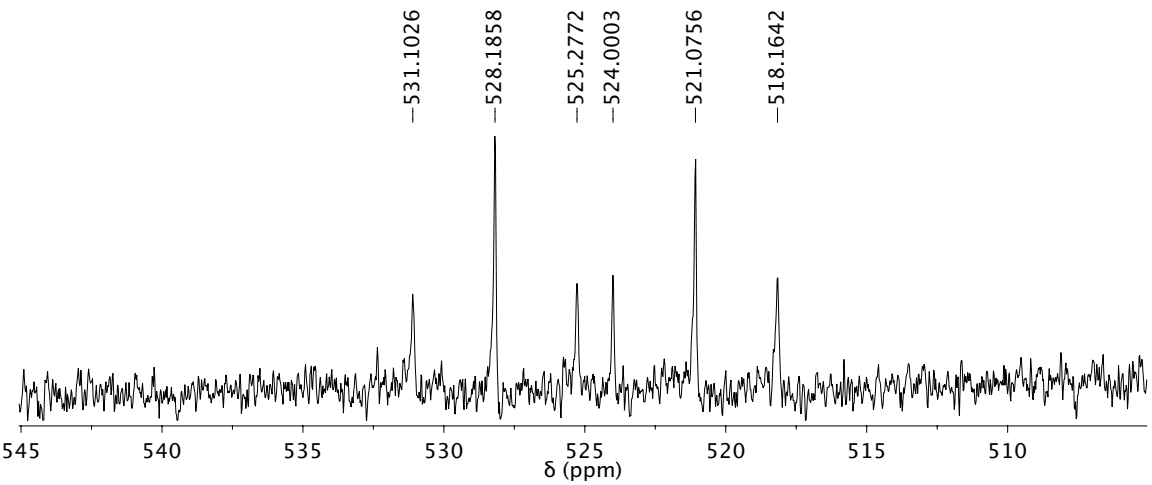

Figure 4.17. ^{109}Ag NMR (18.6 MHz, CD_2Cl_2) spectrum of $\{[(6Dipp)Ag]_2(\mu\text{-}H)\}^+[HF_2]^-$ (**1b**[HF_2]).

4.4.3.3 $\{[(7Dipp)Ag]_2(\mu\text{-}H)\}^+HF_2^-$ (**1c**[HF_2])

A solution of (7Dipp)AgF (0.150 g, 0.275 mmol) in CD_2Cl_2 (1.0 mL) was degassed by two freeze-pump-thaw cycles in an NMR tube equipped with a J. Young valve, and the tube was pressurized with hydrogen (4.4 bar). The reaction was monitored daily by ^{1}H NMR spectroscopy, and nearly quantitative conversion was observed after 96 h. The solution was transferred to a vial, and the product was precipitated by the addition of hexane (10 mL). The precipitate was collected by vacuum filtration and was washed with hexane. The solid was dried *in vacuo* for 4 h, affording the product as a white powder (0.089 g, 0.081 mmol, 59%). ^{1}H NMR (400 MHz, CD_2Cl_2): δ (ppm) = 16.29 (t, $J(^1H\text{-}^{19}F)$ = 123 Hz, 1H, HF_2^-), 7.25 (t, J = 7.7 Hz, 4H, *para*-C*H*), 7.05 (d, J = 7.7 Hz, 8H, *meta*-C*H*), 3.88 (mult, 8H, NCH_2), 3.03 (sep, J = 6.9 Hz, 8H, C$H(CH_3)_2$), 2.25 (mult, 8H, NCH_2CH_2), 1.24 (d, J = 6.9 Hz, 24H, $CH(CH_3)_2$), 0.97 (d, J = 6.9 Hz, 24H, $CH(CH_3)_2$), −2.46 (app tt, $J(^1H\text{-}^{109}Ag)$, = 134 Hz, $J(^1H\text{-}^{107}Ag)$ = 116 Hz, Ag*H*Ag). $^{13}C\{^1H\}$ NMR (100 MHz, CD_2Cl_2): δ (ppm) = 217.4 (mult, N*C*Ag), 145.2 (*ortho*-*C*),

144.9 (*ipso*-*C*), 129.2 (*para*-*C*), 125.0 (*meta*-*C*), 54.4 (app d, $J(^{13}C\text{-}^{109/107}Ag)$ = 6 Hz, NCH_2), 28.8 ($CH(CH_3)_2$), 25.5 (NCH_2CH_2), 24.9 ($CH(CH_3)_2$), 24.7 ($CH(CH_3)_2$). ^{19}F NMR (376 MHz, CD_2Cl_2): δ (ppm) = –157.3 (d, $J(^{19}F\text{-}^{1}H)$ = 123 Hz, HF_2^-). ^{109}Ag NMR (18.6 MHz, CD_3CN): δ (ppm) = 532.0 (app dt, $J(^{109}Ag\text{-}^{1}H)$ = 134 Hz, $J(^{109}Ag\text{-}^{107}Ag)$ = 108 Hz). IR (ATR): ν (cm^{-1}) = 2961, 2927, 2871, 1591, 1520, 1459, 1313, 1232, 1202, 1165, 1033, 1017, 993, 804, 758, 633, 590, 533, 516, 451. Elemental analysis calculated for $C_{58}H_{86}N_4Ag_2F_2$: C 63.73, H 7.93, N 5.13, F 3.48. Found: C 63.48, H 7.85, N 5.08, F 3.47.

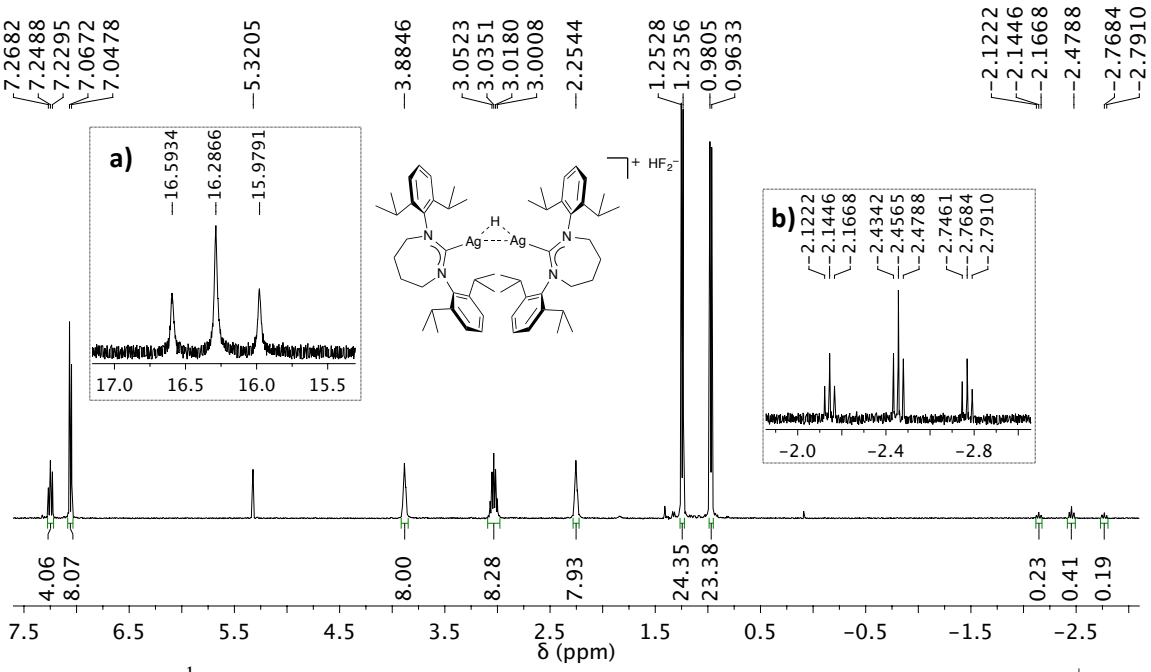

Figure 4.18. ^{1}H NMR (400 MHz, CD_2Cl_2) spectrum of $\{[(7Dipp)Ag]_2(\mu\text{-}H)\}^+HF_2^-$ (**1c**[HF_2]). **a)** Resonance of the HF_2^- ion. **b)** Detail of the hydride resonance.

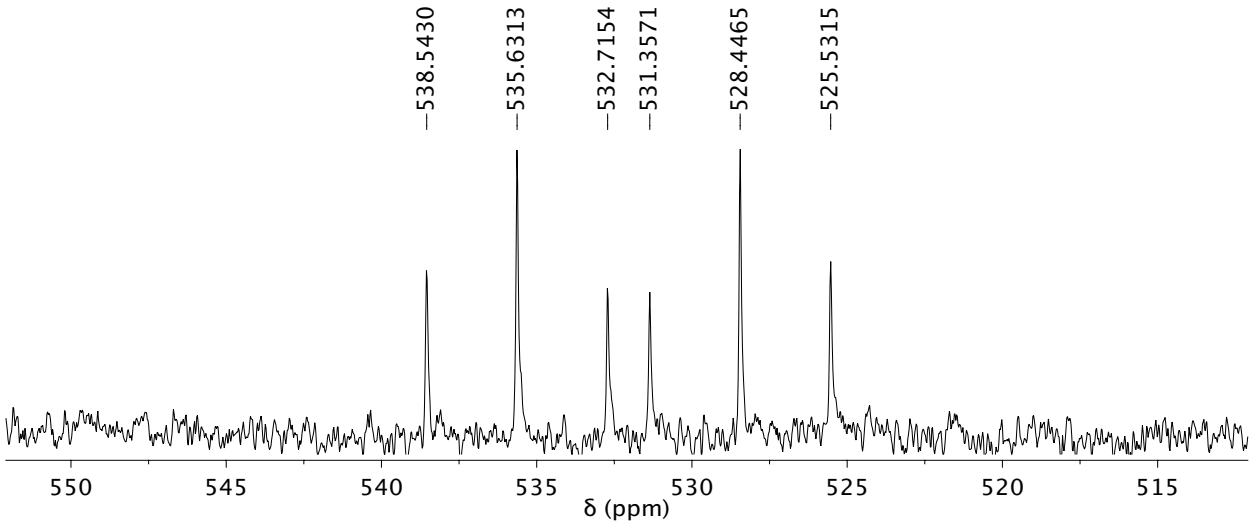

Figure 4.19. ^{109}Ag NMR (18.6 MHz, CD_2Cl_2) spectrum of $\{[(6Dipp)Ag]_2(\mu\text{-}H)\}^+[FHF]^-$ (**1c**[FHF]).

4.4.4 Kinetics of Dihydrogen Cleavage

For each experiment, the silver complex (0.050 mmol **5b**[OTf], 0.10 mmol **7b** or **7c)** and dimethoxybenzene (0.10 mmol, internal standard) were dissolved in CD_2Cl_2 (1.0 mmol) and a preliminary ^{1}H NMR spectrum was recorded. The solution was degassed by two freeze-pump-thaw cycles, then pressurized with hydrogen (H_2 or D_2, nominally 2.5 to 5.0 bar; *see safety note above on reactions run at elevated pressures*). The reaction was monitored at intervals through three half-lives by ^{1}H NMR spectroscopy. The concentration of hydrogen was determined by integration of the H_2 resonance with respect to internal standard; that of starting silver complex, by integration of an NHC resonance that remained distinct and baseline-resolved throughout the reaction (NC*H*$_2$ for (NHC)AgF; aryl *meta*-C*H* for $\{[(6Dipp)Ag]_2(O^tPent)\}^+$).

Kinetic linear regression models were constructed and rate constants were calculated using Microsoft Excel; standard errors of regression were calculated using AnalystSoft StatPlus.

4.4.4.1 Summary of Kinetics Data

Table 4.3. Summary of kinetics data

hydrogen-activating complex	experiment number	$p(H_2)$, bar[a]	$[H_2]$, mM[b]	k_{obs}, s^{-1} [c]	k, $M^{-1} \cdot s^{-1}$	calculated order in H_2
6DippAgF, **2b**	1	5.00 (± 0.14)	7.57 (± 0.13)	5.8 (± 0.3) × 10^{-5}	7.7 (± 0.4) × 10^{-3}	1.02 (± 0.05)
	2	4.00 (± 0.14)	6.6 (± 0.2)	4.8 (± 0.2) × 10^{-5}	7.3 (± 0.4) × 10^{-3}	
	3	2.5 (± 0.2)	3.66 (± 0.14)	2.72 (± 0.14) × 10^{-5}	7.4 (± 0.5) × 10^{-3}	
	average				**7.5 (± 0.3)** × 10^{-3}	
7DippAgF, **2c**	4	5.00 (± 0.14)	7.40 (± 0.16)	1.02 (± 0.04) × 10^{-4}	1.38 (± 0.06) × 10^{-2}	1.06 (± 0.07)
	5	3.00 (± 0.14)	4.30 (± 0.14)	5.75 (± 0.15) × 10^{-5}	1.34 (± 0.06) × 10^{-2}	
	average				**1.36 (± 0.04)** × 10^{-2}	
{[(6Dipp)Ag]$_2$ (μ-O^{t}Pent)}$^+$, **1b**	6	5.00 (± 0.14)	7.9 (± 0.3)	5.55 (± 0.15) × 10^{-5}	7.0 (± 0.3) × 10^{-3}	1.03 (± 0.05)
	7	3.50 (± 0.14)	5.21 (± 0.09)	3.62 (± 0.07) × 10^{-5}	6.96 (± 0.19) × 10^{-3}	
	average				**7.0 (± 0.2)** × 10^{-3}	

[a] Uncertainty in pressure represents manufacturer's precision rating of the pressure gauge (Grade B by standard of the American Society of Mechanical Engineers, +/-3-2-3% of 100 psi span). [b] $[H_2]$ represents the average as determined by integration of ^{1}H NMR signal relative to an internal standard (1,4-dimethoxybenzene) at intervals throughout each trial. Uncertainty in $[H_2]$ represents plus or minus two standard deviations. [c] k_{obs} is determined by a linear regression model of the pseudo-first-order kinetic plot for each trial. Uncertainty in k_{obs} represents plus or minus two times the standard error of regression.

Table 4.4. Summary of kinetic isotope effect data

hydrogen-activating complex	experiment number[a]	$p(D_2)$, bar[b]	k_{obs}, s^{-1} [c]	k_H/k_D
7DippAgF, **2c**	D1	5.00 (± 0.14)	6.49 (± 0.19) × 10^{-5}	1.58 (± 0.10)
	D2	3.00 (± 0.14)	3.68 (± 0.09) × 10^{-5}	1.56 (± 0.12)
	average			**1.57 (± 0.08)**

[a] Compare to experiments 4 and 5 in Table 4.3. [b] Uncertainty in pressure represents manufacturer's precision rating of the pressure gauge (Grade B by standard of the American Society of Mechanical Engineers, +/-3-2-3% of 100 psi span). [b] k_{obs} is determined by a linear regression model of the pseudo-first-order kinetic plot for each trial. Uncertainty in k_{obs} represents plus or minus two times the standard error of regression.

Table 4.5. Summary of HD heterolysis data

hydrogen-activating complex	experiment number	p(HD), bar[a]	time of measurement (h)	product distribution, 1c-*d*:1c
7DippAgF, **2c**	HD1	2	6	1.60
	HD1	2	12	1.58
	HD2	2	6	1.55
	HD2	2	12	1.57
	HD2	2	24	1.58
	average			**1.58 (± 0.04)**[b]

[a] HD pressure is estimated by assuming complete consumption of D_2O by excess $LiAlH_4$. [b] Uncertainty in product distribution represents plus or minus two standard deviations.

4.4.4.2 Kinetic Plots for $\{[(6Dipp)Ag]_2(\mu\text{-}O^tPent)\}^+$ (**5b**)

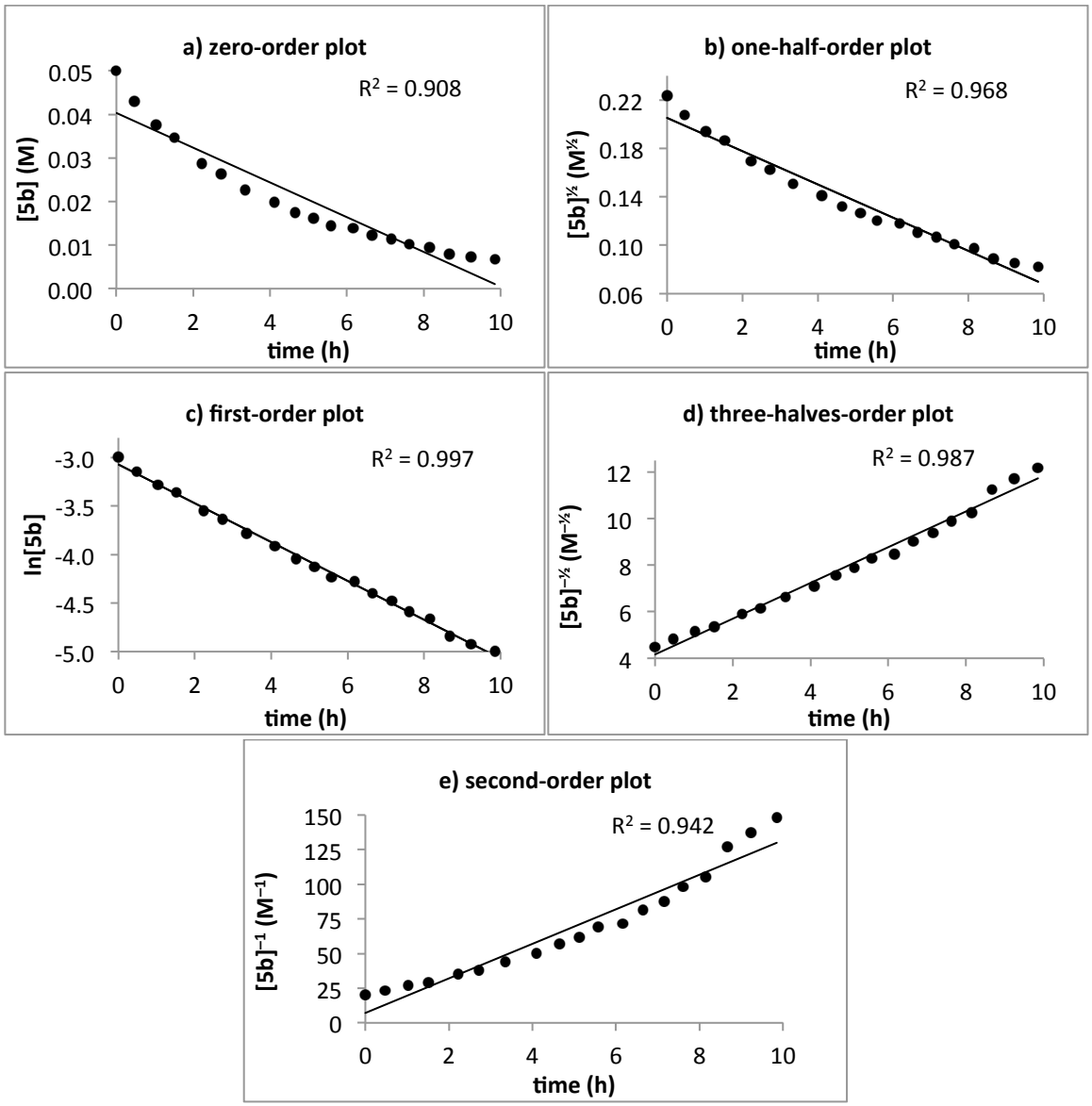

Figure 4.20. Kinetic plots for the hydrogenolysis of $\{[(6Dipp)Ag]_2(\mu\text{-}O^tPent)\}^+$ (**5b**), as its OTf^- salt, corresponding to **(a)** zero-order, **(b)** one-half-order, **(c)** first-order, **(d)** three-halves-order, and **(e)** second-order models with respect to silver.

4.4.4.3 Kinetic Plots for (6Dipp)AgF (**7b**)

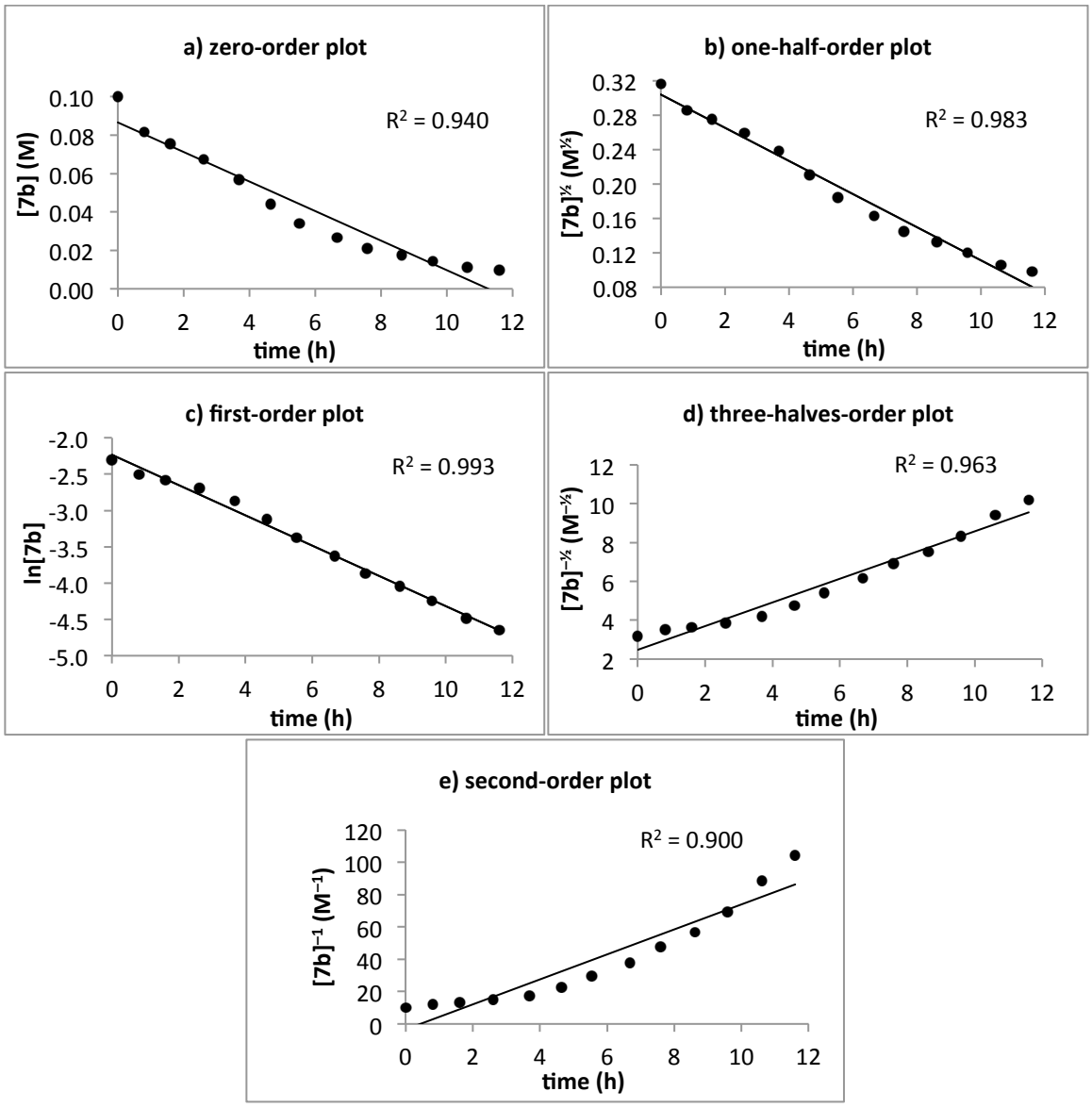

Figure 4.21. Kinetic plots for the hydrogenolysis of (6Dipp)AgF (**7b**) corresponding to **(a)** zero-order, **(b)** one-half-order, **(c)** first-order, **(d)** three-halves-order, and **(e)** second-order models with respect to silver.

4.4.4.4 Kinetic Plots for (7Dipp)AgF (**7c**)

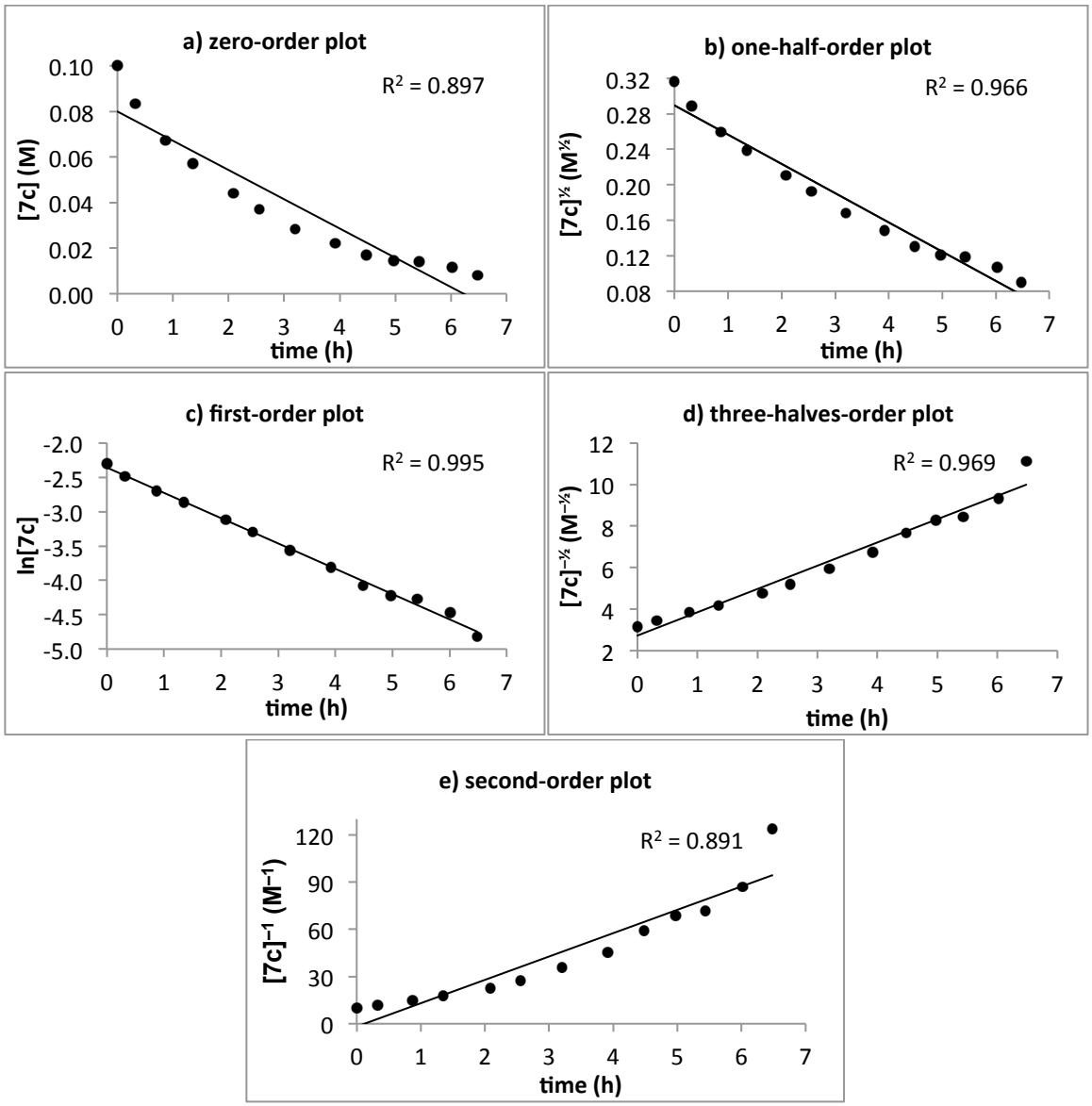

Figure 4.22. Kinetic plots for the hydrogenolysis of (7Dipp)AgF (**7c**), corresponding to **(a)** zero-order, **(b)** one-half-order, **(c)** first-order, **(d)** three-halves-order, and **(e)** second-order models with respect to silver.

4.4.4.5 Derivation of Rate Law for $\{[(6Dipp)Ag]_2(\mu\text{-}O^tPent)\}^+$ (**5b**)

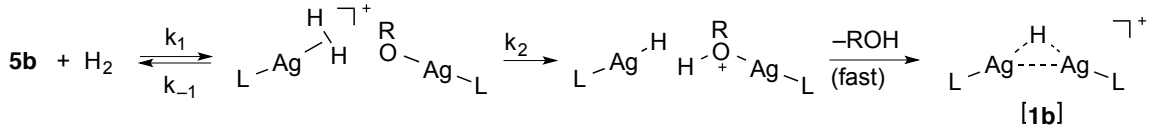

Assuming loss of alcohol to be fast,

$$\frac{d[\mathbf{1b}]}{dt} = k_2\,[LAg(\eta^2\text{-}H_2)^+][LAgOR]$$

Neither species is observed.

Assume rates of formation, consumption to be equal:

$$k_1\,[\mathbf{5b}][H_2] = k_{-1}\,[LAg(\eta^2\text{-}H_2)^+][LAgOR] + k_2\,[LAg(\eta^2\text{-}H_2)^+][LAgOR]$$

$$= (k_{-1} + k_2)[LAg(\eta^2\text{-}H_2)^+][LAgOR]$$

$$[LAg(\eta^2\text{-}H_2)^+][LAgOR] = \frac{k_1\,[\mathbf{5b}][H_2]}{(k_{-1} + k_2)}$$

$$\frac{d[\mathbf{1b}]}{dt} = k_2\,[LAg(\eta^2\text{-}H_2)^+][LAgOR] = \frac{k_2\,k_1\,[\mathbf{5b}][H_2]}{(k_{-1} + k_2)}$$

If $k_{-1} >> k_2$: $\frac{d[\mathbf{1b}]}{dt} \approx \frac{k_2\,k_1\,[\mathbf{5b}][H_2]}{k_{-1}} = k_2K_{eq}[\mathbf{5b}][H_2]$ $(K_{eq} = k_1/k_{-1})$

If $k_2 >> k_{-1}$: $\frac{d[\mathbf{1b}]}{dt} \approx \frac{k_2\,k_1\,[\mathbf{5b}][H_2]}{k_{-1}} = k_1[\mathbf{5b}][H_2]$

Scheme 4.8 Derivation of steady-state kinetics for the hydrogenolysis of $\{[(6Dipp)Ag]_2(\mu\text{-}O^tPent)\}^+[OTf]^-$ (**5b**[OTf]). The overall reaction rate should appear second-order regardless of the relative rates of deprotonation versus dihydrogen loss (k_2 versus k_{-1}).

4.4.4.6 Derivation of Rate Laws for (6Dipp)AgF (**7b**) and (7Dipp)AgF (**7c**)

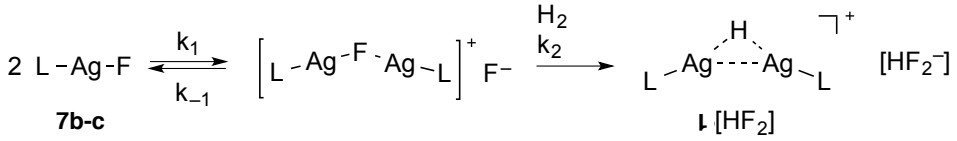

Overall:

$$\frac{d[\text{HF}_2]}{dt} = k_2\,[(\text{LAg})_2(\mu\text{-F})^+][\text{H}_2]$$

(μ-Fluoro)disilver intermediate is not observed.

Assume rates of formation, consumption to be equal:

$$k_1\,[\text{LAgF}]^2 = k_{-1}\,[(\text{LAg})_2(\mu\text{-F})^+][\text{F}^-] + k_2\,[(\text{LAg})_2(\mu\text{-F})^+][\text{H}_2]$$

$$k_1\,[\text{LAgF}]^2 = \{k_{-1}\,[\text{F}^-] + k_2\,[\text{H}_2]\}\,[(\text{LAg})_2(\mu\text{-F})^+]$$

$$[(\text{LAg})_2(\mu\text{-F})^+] = \frac{k_1\,[\text{LAgF}]^2}{k_{-1}\,[\text{F}^-] + k_2\,[\text{H}_2]}$$

$$\frac{d[\text{HF}_2]}{dt} = k_2\,[(\text{LAg})_2(\mu\text{-F})^+][\text{H}_2] = \frac{k_2\,k_1\,[\text{LAgF}]^2[\text{H}_2]}{k_{-1}\,[\text{F}^-] + k_2\,[\text{H}_2]}$$

If $k_{-1}[\text{F}^-] >> k_2\,[\text{H}_2]$: $\frac{d[\text{HF}_2]}{dt} \approx \frac{k_2\,k_1\,[\text{LAgF}]^2[\text{H}_2]}{k_{-1}\,[\text{F}^-]} = \frac{k_2 K_{eq}[\text{LAgF}]^2[\text{H}_2]}{[\text{F}^-]}$ $(K_{eq} = k_1/k_{-1})$

If $k_2\,[\text{H}_2] >> k_{-1}[\text{F}^-]$: $\frac{d[\text{HF}_2]}{dt} \approx \frac{k_2\,k_1\,[\text{LAgF}]^2[\text{H}_2]}{k_2\,[\text{H}_2]} = k_1\,[\text{LAgF}]^2$

Scheme 4.9. Derivation of steady-state kinetics for the hydrogenolysis of LAgF (**7b** or **7c**), in the case of a (μ-fluoro)disilver intermediate (see Scheme 4.6). In this scheme the second step, the hydrogenolysis of the (μ-fluoro)disilver intermediate once formed, should appear first-order in disilver complex and first-order in dihydrogen, whether it occurs as a single step or as a series of steps analogous to the (μ-alkoxy)disilver hydrogenolysis depicted in Scheme 4.8. The overall reaction rate should be second-order in silver fluoride for each of the limiting cases depicted here.

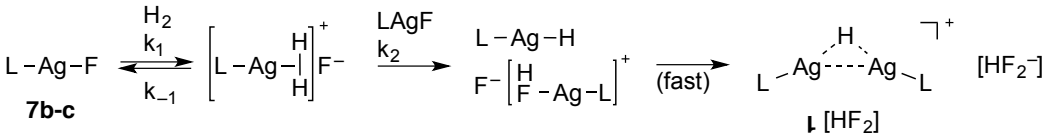

Overal, assuming that displacement of HF (or HF_2^-) by LAgH is rapid:

$$\frac{d[\downarrow HF_2]]}{dt} = k_2\,[LAg(\eta^2\text{-}H_2)^+][LAgF]$$

(η^2-H_2) complex is not observed.

Assume rates of formation, consumption to be equal:

$$k_1\,[LAgF][H_2] = k_{-1}\,[LAg(\eta^2\text{-}H_2)^+][F^-] + k_2\,[LAg(\eta^2\text{-}H_2)^+][LAgF]$$

$$k_1\,[LAgF][H_2] = \{k_{-1}\,[F^-] + k_2\,[LAgF]\}\,[LAg(\eta^2\text{-}H_2)^+]$$

$$[LAg(\eta^2\text{-}H_2)^+] = \frac{k_1\,[LAgF][H_2]}{k_{-1}\,[F^-] + k_2\,[LAgF]}$$

$$\frac{d[\downarrow HF_2]]}{dt} = k_2\,[LAg(\eta^2\text{-}H_2)^+][LAgF] = \frac{k_2\,k_1\,[LAgF]^2[H_2]}{k_{-1}\,[F^-] + k_2\,[LAgF]}$$

If $k_{-1}\,[F^-] >> k_2\,[LAgF]$: $\frac{d[\downarrow HF_2]]}{dt} \approx \frac{k_2\,k_1\,[LAgF]^2[H_2]}{k_{-1}\,[F^-]} = \frac{k_2 K_{eq}[LAgF]^2[H_2]}{[F^-]}$ $(K_{eq} = k_1/k_{-1})$

If $k_2\,[LAgF] >> k_{-1}\,[F^-]$: $\frac{d[\downarrow HF_2]]}{dt} \approx \frac{k_2\,k_1\,[LAgF]^2[H_2]}{k_2\,[LAgF]} = k_1\,[LAgF][H_2]$

Scheme 4.10. Derivation of steady-state kinetics for the hydrogenolysis of LAgF (**7b** or **7c**), in the case where a silver-bound fluoride deprotonates an (η^2-H_2) complex (see Scheme 4.6). In the case of preequilibrium kinetics, the reaction rate should be second-order in silver fluoride; only if deprotonation of coordinated H_2 is very fast relative to loss of coordinated H_2 will the kinetics appear first-order in silver.

4.4.5 Heterolysis of H–D

In an NMR tube equipped with a J. Young valve, (7Dipp)AgF (0.038 g, 0.70 mmol) was dissolved in CD_2Cl_2 (0.7 mL). The NMR tube was connected via braid-reinforced PVC tubing and a three-way-valve to a vacuum line, and to the sidearm of a septum-capped 50-mL Schlenk flask containing a stir bar and a suspension of lithium aluminum hydride (223 mg, 5.89 mmol) in diethyl ether (10 mL). The NMR tube and

Schlenk flask were each degassed by two freeze-pump-thaw cycles. Deuterium oxide (0.088 mL, 4.9 mmol) was added to the stirred suspension via syringe, in increments of 8 to 10 μL over 20 minutes at 0˚C. The resulting HD gas was allowed to expand into the PVC tubing and the NMR tube, reaching a calculated pressure of approximately 2 bar. The J. Young valve was sealed, and the ^{1}H NMR spectra were recorded at intervals over 24 h. The total amount of $\{[(7Dipp)Ag]_2(\mu\text{-}H)\}^+$ and $\{[(7Dipp)Ag]_2(\mu\text{-}D)\}^+$ was determined by integration of the 7Dipp NCH_2 signal, and $\{[(7Dipp)Ag]_2(\mu\text{-}H)\}^+$ was quantified by integration of the hydride signal. The ratio of deuteride to hydride complex was determined from five measurements taken at different times during two separate runs.

4.4.6 X-Ray Diffraction Studies

Crystals of $\{[(6Dipp)Ag]_2(\mu\text{-}H)]^+HF_2^-$ (**5b**[HF_2]) were grown by vapor diffusion of hexanes into a CH_2Cl_2 solution at –35˚C. A suitable crystal was selected and mounted on a loop with Paratone oil on a Bruker Apex-II CCD diffractometer. The crystal was kept cold during data collection. Using Olex2,[49] the structure was solved with the Superflip[50] structure solution program using Charge Flipping, and refined with the ShelXL[51] refinement package using Least Squares minimization. CCDC 1048819 contains the supplementary crystallographic data for this complex. These data can be obtained free of charge from the Cambridge Crystallographic Data Centre via www.ccdc.cam.ac.uk/data_request/cif.

4.4.7 Preliminary Hydrogenolysis Experiments

4.4.7.1 Reaction of $\{[(5Dipp)Ag]_2(\mu\text{-}O^tBu)\}^+$ (**5a**) with H_2

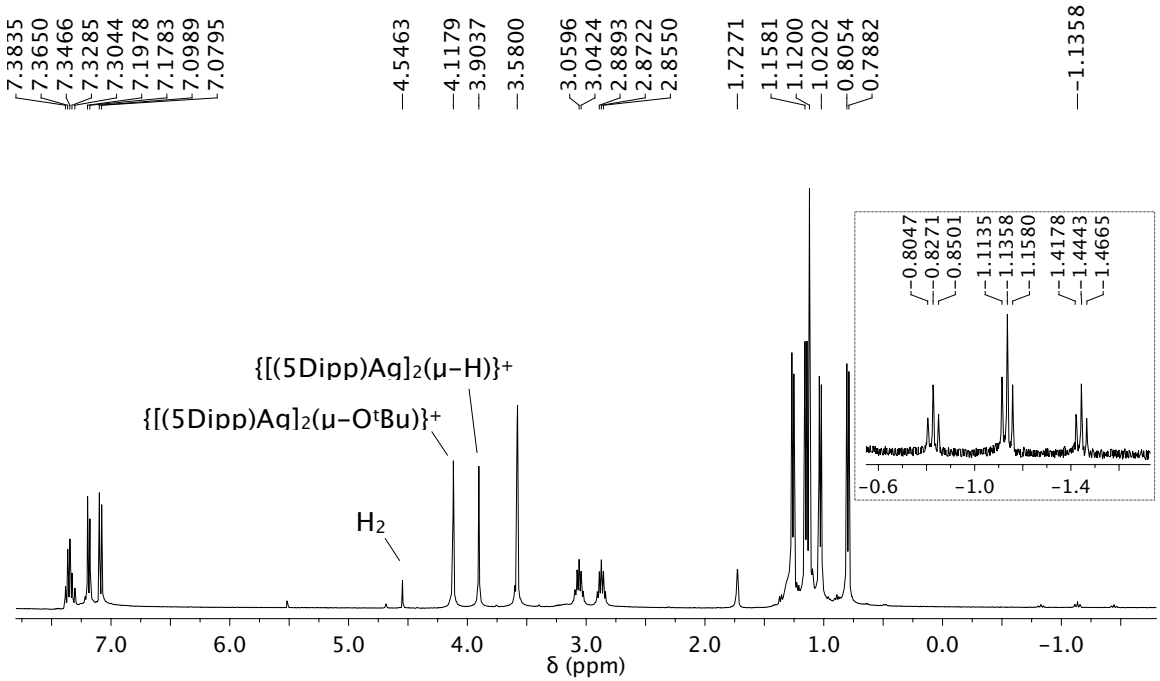

Figure 4.23. ^1H NMR (400 MHz, THF-d_8) spectrum showing the reaction of $\{[(5Dipp)Ag]_2(\mu\text{-}O^tBu)\}^+$ (**1a**), as its BF_4^- salt, with H_2 (3.0 bar) at 0˚C after 14 days. Resonances of dihydrogen and the imidazolylidene backbone (NC*H*$_2$) of each silver complex are labeled. Integration of these resonances indicates 55% conversion of $\{[(5Dipp)Ag]_2(\mu\text{-}O^tBu)\}^+$ to $\{[(5Dipp)Ag]_2(\mu\text{-}H)\}^+$. The signals of the *tert*-butoxy groups of $\{[(5Dipp)Ag]_2(\mu\text{-}O^tBu)\}^+$ and *tert*-butanol coalesce due to rapid exchange, appearing as a singlet at δ 1.12 ppm. **Inset:** Detail of hydride resonance.

4.4.7.2 Reaction of $\{[(5Dipp)Ag]_2(\mu\text{-}F)\}^+$ (**12**) with H_2

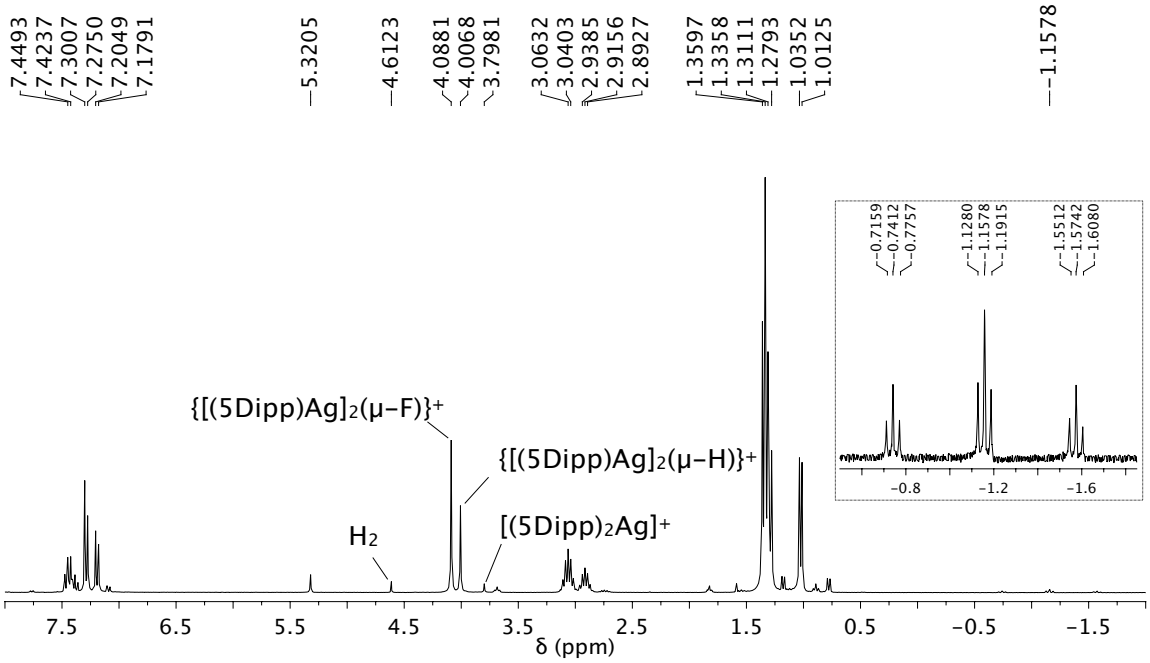

Figure 4.24. ^1H NMR (300 MHz, CD_2Cl_2) spectrum showing the reaction of $\{[(5Dipp)Ag]_2(\mu\text{-}F)\}^+$, as its OTf^- salt, with H_2 (3.0 bar) at room temperature after 22 hours. Resonances of dihydrogen and the imidazolylidene backbone (NCH_2) of each silver complex are labeled. Integration of these resonances indicates $\{[(5Dipp)Ag]_2(\mu\text{-}F)\}^+$ comprises 64%, $\{[(5Dipp)Ag]_2(\mu\text{-}H)\}^+$ 34%, and $[(5Dipp)_2Ag]^+$ 2% of the total. A faint deposition of elemental silver on the walls of the reaction tube was also observed, accounting for the apparent disappearance of silver from the spectrum. **Inset:** Detail of hydride resonance.

4.4.7.3 Reaction of (5Dipp)AgF (**7a**) with H_2

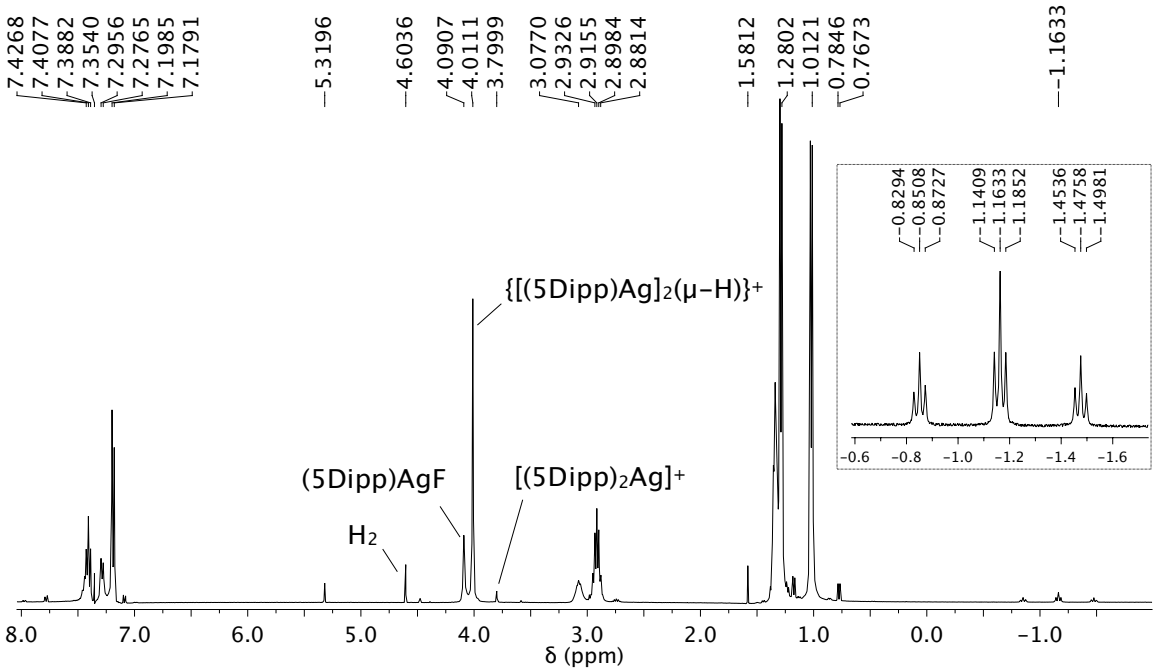

Figure 4.25. ^{1}H NMR (300 MHz, CD_2Cl_2) spectrum showing the reaction of (5Dipp)AgF (**7a**) with H_2 (3.0 bar) at 0˚C after 10 days. Resonances of dihydrogen and the imidazolylidene backbone (NC*H*$_2$) of each silver complex are labeled. Integration of these resonances indicates (5Dipp)AgF comprises 28%, $\{[(5Dipp)Ag]_2(\mu\text{-}H)\}^+$ 72%, and $[(5Dipp)_2Ag]^+$ 1% of the total. A faint deposition of elemental silver on the walls of the reaction tube was also observed, accounting for the apparent disappearance of silver from the spectrum. **Inset:** Detail of hydride resonance.

4.5 Acknowledgements

We thank the U.S. National Science Foundation for generous support of this research (CHE-1300659). Professors Seth R. Marder and Jake D. Soper kindly allowed us the use of their groups' FT-IR spectrometers. We are grateful to Prof. Gary B. Schuster for helpful discussions.

4.6 Notes and References

1 For selected overviews, see: (a) S. Werkmeister, K. Junge, M. Beller, *Org. Process Res. Dev.* **2014**, *18*, 289–302. (b) F. Zaera, *Phys. Chem. Chem. Phys.* **2013**, *15*, 11988–12003. (c) C. Sumner, Jr., W. Burchett, *Top. Catal.* **2012**, *55*, 480–485. (d) M. Crespo-Quesada, F. Cárdenas- Lizana, A.-L. Dessimoz, L. Kiwi-Minsker, *ACS Catal.* **2012**, *2*, 1773– 1786. (e) S. Gladiali, E. Alberico, I. Gridnev in *Innovative Catalysis in Organic Synthesis: Oxidation, Hydrogenation, and C–X Bond Forming Reactions* (Ed.: P. G. Andersson), Wiley-VCH, Weinheim, **2012**, pp. 103–129. (f) *Handbook of Homogeneous Hydrogenation* (Eds.: J. G. de Vries, C. J. Elsevier), Wiley-VCH, Weinheim, **2007**.

2 For a recent review, see: G. J. Kubas, *J. Organomet. Chem.* **2014**, *751*, 33–49.

3 For reviews, see: (a) D. W. Stephan, *Org. Biomol. Chem.* **2012**, *10*, 5740–5746. (b) G. Erker, *C. R. Chimie* **2011**, *14*, 831–841.

4 (a) C. Becker, I. Kieltsch, D. Broggini, A. Mezzetti, *Inorg. Chem.* **2003**, *42*, 8417–8429. (b) P. Barthazy, R. M. Stoop, M. Wörle, A. Togni, A. Mezzetti, *Organometallics* **2000**, *19*, 2844–2852. (c) P. Barthazy, L. Hintermann, R. M. Stoop, M. Wörle, A. Mezzetti, A. Togni, *Helv. Chim. Acta* **1999**, *82*, 2448–2453. (d) J. T. Poulton, M. P. Sigalas, O. Eisenstein, K. G. Caulton, *Inorg. Chem.* **1993**, *32*, 5490–5501.

5 G. R. Fulmer, A. N. Herndon, W. Kaminsky, R. A. Kemp, K. I. Goldberg, *J. Am. Chem. Soc.* **2011**, *133*, 17713–17729.

6 R. Noyori, *Angew. Chem. Int. Ed.* **2002**, *41*, 2008–2022.

7 Y . Blum, D. Czarkle, Y . Rahamim, Y . Shvo, *Organometallics* **1985**, *4*, 1459–1461.

8 O. Eisenstein, R. H. Crabtree, *New J. Chem.* **2013**, *37*, 21–27.

9 (a) J. Halpern, G. Czapski, J. Jortner, G. Stein, *Nature* **1960**, *186*, 629– 630. (b) A. J. Chalk, J. Halpern, A. C. Harkness, *J. Am. Chem. Soc.* **1959**, *81*, 5854–5857. (c) J. Halpern, *J. Phys. Chem.* **1959**, *63*, 398– 403. (d) A. H. Webster, J. Halpern, *J. Phys. Chem.* **1957**, *61*, 1245–1248. (e) A. H. Webster, J. Halpern, *J. Phys. Chem.* **1957**, *61*, 1239–1245. (f) A. H. Webster, J. Halpern, *Trans. Faraday Soc.* **1957**, *53*, 51–60. (g) A. H. Webster, J. Halpern, *J. Phys. Chem.* **1956**, *60*, 280–285.

10 (a) M. T. Beck, I. Gimesi, *Acta Chim. Acad. Sci. Hung.* **1964**, *42*, 343– 347. (b) M. T. Beck, I. Gimesi, J. Farkas, *Nature* **1963**, *197*, 73.

11 (a) G. V. Goeden, J. C. Huffman, K. G. Caulton, *Inorg. Chem.* **1986**, *25*, 2484–2485. (b) T. H. Lemmen, K. Folting, J. C. Huffman, K. G. Caulton, *J. Am. Chem. Soc.* **1985**, *107*, 7774–7775. (c) G. V. Goeden, K. G. Caulton, *J. Am. Chem. Soc.* **1981**, *103*, 7354–7355.

12 For selected refs., see: (a) S. Werkmeister, K. Junge, M. Beller, *Green Chem.* **2012**, *14*, 2371–2374. (b) H. Shimizu, N. Sayo, T. Saito, *Synlett* **2009**, 1295–1298. (c) H. Shimizu, D. Igarashi, W. Kuriyama, Y. Yusa, N. Sayo, T. Saito, *Org. Lett.* **2007**, *9*, 1655–1657. (d) J.-X. Chen, J. F. Daeuble, J. M. Stryker, *Tetrahedron* **2000**, *56*, 2789–2798. (e) J.-X. Chen, J. F. Daeuble, D. M. Brestensky, J. M. Stryker, *Tetrahedron* **2000**, *56*, 2153–2166.

13 R. S. Dhayal, J.-H. Liao, Y.-R. Lin, P.-K. Liao, S. Kahlal, J.-Y . Saillard, C. W. Liu, *J. Am. Chem. Soc.* **2013**, *135*, 4704–4707.

14 M. Girod, M. Krstić, R. Antoine, L. MacAleese, J. Lemoine, A. Zavras, G. N. Khairallah, V. Bonačić-Koutecký, P. Dugourd, R. A. J. O'Hair, *Chem. Eur. J.* **2014**, *20*, 16626–16633.

15 Selected recent overviews: (a) I. Schmidt, K. Müller, W. Arlt, *Energy Fuels* **2014**, *28*, 6540–6544. (b) S. Enthaler, B. Loges, *ChemCatChem* **2012**, *4*, 323–325. (c) A. Boddien, H. Junge, *Nature Nanotech.* **2011**, *6*, 265–266. (d) F. Joó, *ChemSusChem* **2008**, *1*, 805–808.

16 B. K. Tate, C. M. Wyss, J. Bacsa, K. Kluge, L. Gelbaum, J. P. Sadighi, *Chem. Sci.* **2013**, *4*, 3068–3074.

17 a) A. Zavras, G. N. Khairallah, T. U. Connell, J. M. White, A. J. Edwards, R. J. Mulder, P. S. Donnelly, R. A. J. O'Hair, *Inorg. Chem.* **2014**, *53*, 7429–7437. (b) A. Zavras, G. N. Khairallah, T. U. Connell, J. M. White, A. J. Edwards, P. S. Donnelly, R. A. J. O'Hair, *Angew Chem. Int. Ed.* **2013**, *52*, 8391–8394. (c) C. W. Liu, Y.-R. Lin, C.-S. Fang, C. Latouche, S. Kahlal, J.-Y. Saillard, *Inorg. Chem.* **2013**, *52*, 2070– 2077. (d) P.-K. Liao, K.-G. Liu, C.-S. Fang, C. W. Liu, J. P. Fackler, Jr., Y.-Y. Wu, *Inorg. Chem.* **2011**, *50*, 8410–8417. (e) C. W. Liu, P.-K. Liao, C.-S. Fang, J.-Y. Saillard, S. Kahlal, J.-C. Wang, *Chem. Commun.* **2011**, *47*, 5831–5833. (f) C. W. Liu, H.-W. Chang, C.-S. Fang, B. Sarkar, J.-C. Wang, *Chem. Commun.* **2010**, *46*, 4571–4573. (g) C. W. Liu, H.-W. Chang, B. Sarkar, J.-Y. Saillard, S. Kahlal, Y.-Y. Wu, *Inorg. Chem.* **2010**, *49*, 468–475. See also ref. 14.

18 Z. Jia, F. Zhou, M. Liu, X. Li, A. S. C. Chan, C.-J. Li, *Angew. Chem. Int. Ed.* **2013**, *52*, 11871–11874.

19 Y.-Y. Jiang, H.-Z. Yu, Y. Fu, *Organometallics* **2014**, *33*, 6577–6584.

20 A. J. Arduengo, III, R. Krafczyk, R. Schmutzler, H. A. Craig, J. R. Goerlich, W. J. Marshall, M. Unverzagt, *Tetrahedron* **1999**, *55*, 14523–14534.

21 This ligand is usually abbreviated as SIPr or SIDipp. We have chosen to keep notation consistent between NHCs of different ring sizes.

22 C. M. Wyss, B. K. Tate, J. Bacsa, M. Wieliczko, J. P. Sadighi, *Polyhedron* **2014**, *84*, 87–95.

23 R. G. Pearson, *J. Am. Chem. Soc.* **1963**, *85*, 3533–3539.

24 S. J. Blanksby, G. B. Ellison, *Acc. Chem. Res.* **2003**, *36*, 255–263.

25 C. Stein, R. Oswald, P. Sebald, P. Botschwina, H. Stoll, K. A. Peterson, *Mol. Phys.* **2013**, *111*, 2647–2652.

26 We cannot exclude the operation of such an equilibrium, but we have observed no evidence for the formation of the $[(LAg)_2(\mu\text{-}F)]^+$ cation in the absence of fluoride-abstracting reagents.

27 A. M. Magill, K. J. Cavell, B. F. Yates, *J. Am. Chem. Soc.* **2004**, *126*, 8717–8724.

28 (a) E. L. Kolychev, I. A. Portnyagin, V. V. Shuntikov, V. N. Khrustalev, M. S. Nechaev, *J. Organomet. Chem.* **2009**, *694*, 2454–2462. (b) W. A. Herrmann, S. K. Schneider, K. Öfele, M. Sakamoto, E. Herdtweck, *J. Organomet. Chem.* **2004**, *689*, 2441–2449.

29 (a) L. Schwartsburd, M. F. Mahon, R. C. Poulten, M. R. Warren, M. K. Whittlesey, *Organometallics*, **2014**, *33*, 6165–6170. (b) N. Bramananthan, M. Carmona, J. P. Lowe, M. F. Mahon, R. C. Poulten, M. K. Whittlesey, *Organometallics*, **2014**, *33*, 1986–1995. (c) C. Segarra, E. Mas-Marzá, J. P. Lowe, M. F. Mahon, R. C. Poulten, M. K. Whittlesey, *Organometallics* **2012**, *31*, 8584–8590.

30 N. Phillips, T. Dodson, R. Tirfoin, J. I. Bates, S. Aldridge, *Chem. Eur. J.* **2014**, *20*, 16721–16731.

31 M. Iglesias, D. J. Beetstra, J. C. Knight, L.-L. Ooi, A. Stasch, S. Coles, L. Male, M. B. Hursthouse, K. J. Cavell, A. Dervisi, I. A. Fallis, *Organometallics* **2008**, *27*, 3279–3289.

32 In dinuclear group 11 metal complexes bearing N,N'-diaryl-substituted NHCs, ^{1}H NMR resonances of the bridging anion typically occur significantly upfield of those bearing N,N'-dialkyl substituents. We attribute this phenomenon to anisotropic shielding of the bridging ligand by the N-aryl groups.

33 J. A. Ibers, *J. Chem. Phys.* **1964**, *40*, 402–404.

34 (a) B. J. Truscott, F. Nahra, A. M. Z. Slawin, D. B. Cordes, S. P. Nolan, *Chem. Commun.* **2015**, *51*, 62–65. (b) J. Vicente, J. Gil-Rubio, D. Bautista, A. Sironi, N.

Masciocchi, *Inorg. Chem.* **2004**, *43*, 5665–5675. (c) D. C. Roe, W. J. Marshall, F. Davidson, P. D. Soper, V. V. Grushin, *Organometallics* **2000**, *19*, 4575–4582. (d) T. Braun, S. P. Foxon, R. N. Perutz, P. H. Walton, *Angew. Chem. Int. Ed.* **1999**, *38*, 3326–3329. (e) V. J. Murphy, T. Hascall, J. Y. Chen, G. Parkin, *J. Am. Chem. Soc.* **1996**, *118*, 7428–7429. See also refs. 29b,c.

35 See, however: (a) T. Vergote, F. Nahra, A. Welle, M. Luhmer, J. Wouters, N. Mager, O. Riant, T. Leyssens, *Chem. Eur. J.* **2012**, *18*, 793–798. (b) N. A. Jasim, R. N. Perutz, S. P. Foxon, P. H. Walton, *J. Chem. Soc., Dalton Trans.* **2001**, 1676–1685. (c) M. S. Kirkham, M. F. Mahon, M. K. Whittlesey, *Chem. Commun.* **2001**, 813–814. (d) M. K. Whittlesey, R. N. Perutz, B. Greener, M. H. Moore, *Chem. Commun.* **1997**, 187–188.

36 G. J. Kubas, *Metal Dihydrogen and σ-Bond Complexes: Structure, Theory, and Reactivity,* Springer, New York, **2001**.

37 Transition metal η^2-(H_2) complexes can be remarkably acidic; see for example E. Rocchini, A. Mezzetti, H. Rüegger, U. Burckhardt, V. Gramlich, A. Del Zotto, P. Martinuzzi, P. Rigo, *Inorg. Chem.* **1997**, *36*, 711–720.

38 Concerted termolecular processes are invoked in the homolytic cleavage of H_2 by two metalloradicals. See for example: (a) B. B. Wayland, S. Ba, A. E. Sherry, *Inorg. Chem.* **1992**, *31*, 148–150. (b) J. Halpern, *Inorg. Chim. Acta* **1983**, *77*, L105–L106. (c) L. I. Simándi, E. Budó-Záhonyi, Z. Szeverényi, S. Németh, *J. Chem. Soc., Dalton Trans.* **1980**, 276–283. (d) T.-H. Chao, J. H. Espenson, *J. Am. Chem. Soc.* **1978**, *100*, 129–133. (e) J. Halpern, M. Pribanić, *Inorg. Chem.* **1970**, *9*, 2616–2618.

39 Attempts to observe neutral (NHC)AgH complexes, including those supported by 6Dipp and 7Dipp, result in the formation of silver metal, dihydrogen, free ligand and imidazoline decomposition products. The hydride may nonetheless be viable as a transient intermediate.

40 The comparison is inexact because the model complex bears an N,N'-dimethyl- rather than diaryl-substituted ligand. Stronger donation from the alkyl-substituted ligand could result in a greater *trans*-influence, and thus a lower barrier for H_2 dissociation from $[(6Me)Au(\eta^2\text{-}H_2)]^+$ than from $[(6Dipp)Au(\eta^2\text{-}H_2)]^+$. Still, we expect this difference to be less important than that between gold-ligand and silver-ligand binding energies.

41 (a) P. Mastrorilli, M. Latronico, V. Gallo, F. Polini, N. Re, A. Marrone, R. Gobetto, S. Ellena, *J. Am. Chem. Soc.* **2010**, *132*, 4752–4765. (b) R. D. Adams, B. Captain, M. D. Smith, C. Beddie, M. B. Hall, *J. Am. Chem. Soc.* **2007**, *129*, 5981–5991. (c) R. D. Adams, B. Captain, C. Beddie, M. B. Hall, *J. Am. Chem. Soc.* **2007**, *129*, 986–1000. (d) D. A. Wink, P. C. Ford, *J. Am. Chem. Soc.* **1987**, *109*, 436. (e) P. Zhou, A. A. Vitale, J. San Filippo, Jr., W. H. Saunders, Jr., *J. Am. Chem. Soc.* **1985**, *107*, 8049–8054. (f) L. M. Bavaro, P. Montangero, J. B.

Keister, *J. Am. Chem. Soc.* **1983**, *105*, 4977–4981. (g) P. B. Chock, J. Halpern, *J. Am. Chem. Soc.* **1966**, *88*, 3511–3514.

42 (a) M. Baya, O. Maresca, R. Poli, Y. Coppel, F. Maseras, A. Lledós, N. V. Belkova, P. A. Dub, L. M. Epstein, E. S. Shubina, *Inorg Chem.* **2006**, *45*, 10248–10262. (b) J. P. Collman, L. M. Slaughter, T. A. Eberspacher, T. Strassner, J. I. Brauman, *Inorg. Chem.* **2001**, *40*, 6272–6280.

43 J. P. Collman, W. R. Roper, *Adv. Organomet. Chem.* **1969**, *7*, 53–94.

44 F. Abu-Hasanayn, A. S. Goldman, K. Krogh-Jespersen, *J. Phys. Chem.* **1993**, *97*, 5890–5896. See also refs. 47a–c.

45 (a) D. M. Heinekey, *J. Label. Compd Radiopharm.* **2007**, *50*, 1063–1071. (b) K. Zhang, A. A. Gonzalez, C. D. Hoff, *J. Am. Chem. Soc.* **1989**, *111*, 3627–3632. (c) S. P. Church, F.-W. Grevels, H. Hermann, K. Schaffner, *J. Chem. Soc., Chem. Commun.* **1985**, 30–32.

46 B. R. Bender, G. J. Kubas, L. H. Jones, B. I. Swanson, J. Eckert, K. B. Capps, C. D. Hoff, *J. Am. Chem. Soc.* **1997**, *119*, 9179–9190.

47 (a) G. Parkin, *Acc. Chem. Res.* **2009**, *42*, 315–325. (b) T. Hascall, D. Rabinovich, V. J. Murphy, M. D. Beachy, R. A. Friesner, G. Parkin, *J. Am. Chem. Soc.* **1999**, *121*, 11402–11417. (c) D. Rabinovich, G. Parkin, *J. Am. Chem. Soc.* **1993**, *115*, 353–354. (d) M. J. Hostetler, R. G. Bergman, *J. Am. Chem. Soc.* **1992**, *114*, 7629–7636.

48 I. Wender, R. A. Friedel, M. Orchin, *J. Am. Chem. Soc.* **1949**, *71*, 1140.

49 O. V. Dolomanov, L. J. Bourhis, R. J. Gildea, J. A. K. Howard, H. Puschmann, *J. Appl. Cryst.* **2009**, *42*, 339–341.

50 (a) L. Palatinus, S. J. Prathapa, S. van Smaalen, *J. Appl. Cryst.* **2012**, *45*, 575–580. (b) L. Palatinus, A. van der Lee, *J. Appl. Cryst.* **2008**, *41*, 975–984. (c) L. Palatinus, G. Chapuis, *J. Appl. Cryst.* **2007**, *40*, 786–790.

51 G. M. Sheldrick, *Acta Cryst.* **2008**, *A64*, 112–122.

52 E. L. Kolychev, I. A. Portnyagin, V. V. Shuntikov, V. N. Khrustalev, M. S. Nechaev, *J. Organomet. Chem.* **2009**, *694*, 2454–2462.

53 M. Iglesias, D. J. Beetstra, J. C. Knight, Li-Ling Ooi, A. Stasch, S. Coles, L. Male, M. B. Hursthouse, K. J. Cavell, A. Dervisi, I. A. Fallis, *Organometallics* **2008,** *27,* 3279–3289.

CHAPTER 5

CLOSING A CYCLE: SILVER-CATALYZED HYDROGENATION OF CARBON DIOXIDE

5.1 Background

The activation of hydrogen and the transfer of hydride to carbon dioxide are key steps in the catalytic hydrogenation of CO_2. The ability to heterolyze H_2 (See Chapter 3) and reduce CO_2 (See Chapter 1) at the same metal center potentially opens the door for CO_2 hydrogenation catalysis, if those two steps can be incorportated into a thermodynamically favorable cycle of kinetically accessible steps. We have therefore investigated the application of NHC-supported silver scaffolds in the hydrogenation of CO_2.

The reduction of CO_2 by H_2 is appealing from several perspectives.[1] Hydrogen is a clean energy carrier, which can be renewably generated through the electrolysis or photolysis of water. In contrast to fossil fuels, the production and use of H_2 releases no greenhouse gases, acidic oxide gases (CO_x, NO_x, SO_x, etc.), particulate matter, volatile organic compounds, or heavy metals into the atmosphere. The energy density of H_2, however, is impractically low, requiring the development of technology for its efficient storage and transportation, or chemical conversion to a liquid fuel. Methods for the conversion of H_2 to carbon-based liquids are well established but conventionally rely on the reaction of H_2 with carbon monoxide. Mixtures of H_2 and CO, known as synthesis gas, are generally prepared through the gasification of coal or other nonrenewable processes which fail to circumvent the pollution associated with the mining and

combustion of fossil fuels and organic matter. A sustainable, carbon-neutral, environmentally benign alternative for the storage of hydrogen as a carbon-based liquid fuel would require the direct reaction of hydrogen with atmospheric carbon dioxide.

The conversion of CO_2 and H_2 to formic acid is thermodynamically unfavorable. However, in the presence of stoichiometric additives such as ammonia or methanol, the conversion of CO_2 and H_2 to formate derivatives is possible (Scheme 5.1).[1d] Still, these processes are kinetically demanding and require catalysts, typically based on transition metals or frustrated Lewis pairs.

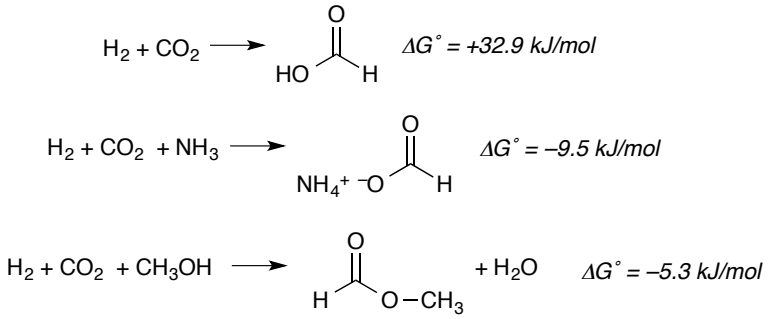

Scheme 5.1: Thermodynamic potentials of selected CO_2 hydrogenation processes.[1d]

A typical catalytic cycle for metal-catalyzed CO_2 hydrogenation involves oxidative addition of a H_2 to form a metal hydride, followed by insertion of CO_2 into the resulting metal-hydrogen bond (Scheme 5.2). Other transition metal catalysts involve the preliminary coordination of CO_2, or a derivative such as carbonate in basic media, to a metal center, followed by hydrogenation of the activated CO_2. Metal-free catalysts based on frustrated Lewis pairs activate hydrogen by heterolytic cleavage of the H–H bond. Pairs of Lewis acids and bases sufficiently strong to heterolyze H_2 are generally forced to coexist by steric constraints that prevent them from neutralizing one another. A similar strategy involving the cleavage of hydrogen by hard-soft mismatched acid-base pairs is

relatively rare but has been demonstrated for several systems in which the Lewis acid is a late transition metal with the potential to coordinate CO_2 and possibly reduce the activation barrier for C–H bond formation.

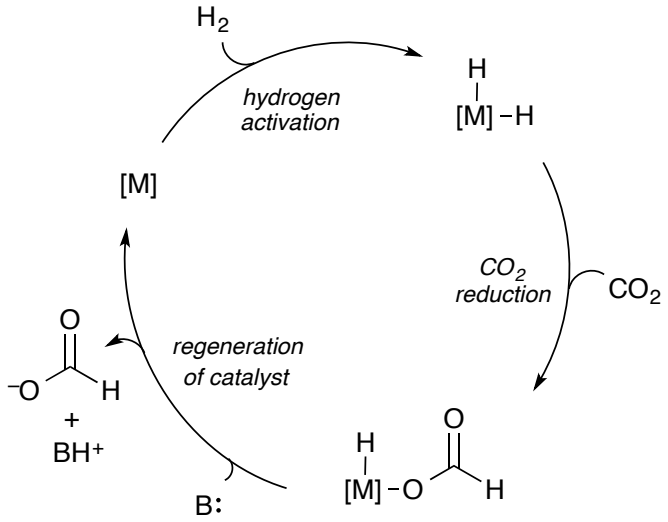

Scheme 5.2: A typical catalytic cycle for metal-catalyzed CO_2 hydrogenation.[1d]

As a late metal with low oxophilicity, silver(I) is a candidate for CO_2 hydrogenation catalysis. Silver(I) salts are known to activate H_2 in aqueous solution,[2] and we have previously demonstrated the heterolysis of H_2 by silver(I) complexes in a well-defined homogeneous system (see Chapter 4).[3] Furthermore, silver(I)-oxygen bonds are relatively weak such that catalytic turnover is feasible. This chapter describes our investigation of hard-soft mismatched silver complexes as catalysts for CO_2 hydrogenation to formate.

5.2 Results and Discussion

5.2.1 Effect of Expanded-Ring NHC on the Carboxylation of Ag_2H^+

Previously, we observed a very slow insertion of CO_2 into the Ag_2H^+ core of $\{[(5Dipp)Ag]_2(\mu\text{-}H)\}^+BF_4^-$ (**1a**), resulting in 5% conversion to a formate-bridged complex $\{[(5Dipp)Ag]_2(\mu\text{-}O_2CH)\}^+BF_4^-$ after four days.[4] In order to gauge the effect of expanded-ring NHC ligands as well as the potentially noninnocent HF_2^- anion resulting from the hydrogenolysis of fluorosilver complexes, we investigated the reaction of $\{[(6Dipp)Ag]_2(\mu\text{-}H)\}^+HF_2^-$ (**1b**[HF_2]) with CO_2 (1.7 bar) in CD_2Cl_2. We anticipated that the expanded NHC might enhance the hydricity of **1b** in analogy to the effect of expanded-ring NHCs on the ability of fluorides (6Dipp)AgF (**7b**) and (7Dipp)AgF (**7c**) to deprotonate H_2. ^{1}H NMR spectroscopy revealed the partial consumption of **1b** and the appearance of a new species, whose spectrum was consistent with the formate-bridged disilver complex $\{[(6Dipp)Ag]_2(\mu\text{-}O_2CH)\}^+$. Conversion of hydride to formate proceeded to 25% after 24 h, and to 60% after 96 h. No change was observed in the ^{19}F NMR spectrum except for the growth of a resonance corresponding to SiF_6^{2-} (δ –140 ppm), presumably resulting from the digestion of glass by HF_2^-. Clearly the reaction of **1b**[HF_2] with CO_2 was faster than that of **1a**[BF_4], suggesting a greater degree of hydricity for the expanded-ring NHC complex than for the conventional NHC complex.

5.2.2 Decomposition of Terminal Silver Hydrides

Based on our observation of CO_2 insertion into the dinuclear hydrides **1a** and **1b**, we anticipated that any catalytic hydrogenation of CO_2 by hard-soft mismatched silver complexes would likely involve the accumulation of intermediate formate. Excess formate would potentially coordinate to silver centers, breaking up the dinuclear system.

We therefore considered the feasibility of mononuclear silver catalysts. The heterolysis of H_2 by a terminal silver alkoxide would in theory lead to free alcohol plus a terminal silver hydride. Likewise, the reaction of a terminal fluoride in the presence of a noncoordinating base would in theory lead to a terminal silver hydride plus a fluoride salt.

Mononuclear gold(I) hydrides[5] and neutral copper(I) hydride dimers[6] supported by NHC ligands and cyclic(alkylamino)carbenes have been isolated and fully characterized. The thermal stability of these complexes varies, but thermal decomposition can occur at temperatures as low as –40˚C, in the case of $[(IDipp)CuH]_2$, resulting in the deposition of elemental copper.[6c]

Multiple attempts to prepare a terminal hydridosilver complex, using main-group hydrides or via hydrogen activation, have not resulted in an isolable product. Instead, elemental silver, dihydrogen, and various ligand decomposition products have resulted from these experiments (Scheme 5.3), suggesting that these terminal hydrides are thermally unstable and rapidly undergo a bimolecular reductive elimination of H_2 with concomitant deposition of silver metal. However, we suspect that terminal hydrides, though not isolable, may nonetheless serve as viable transient intermediates in the hydrogenation of CO_2. Our kinetic studies of the hydrogenolysis of silver alkoxides and fluorides further substantiate the hypothetical intermediacy of terminal silver hydrides (see Chapter 4).[3] Likewise, H_2 activation by simple aqueous silver salts, including silver formate, appears to proceed through short-lived mononuclear hydridosilver intermediates resulting from the heterolysis of H_2 by silver-ligand bonds.[4] Optimistically, the low

stability of terminal silver hydrides could translate to high activity under catalytic conditions.

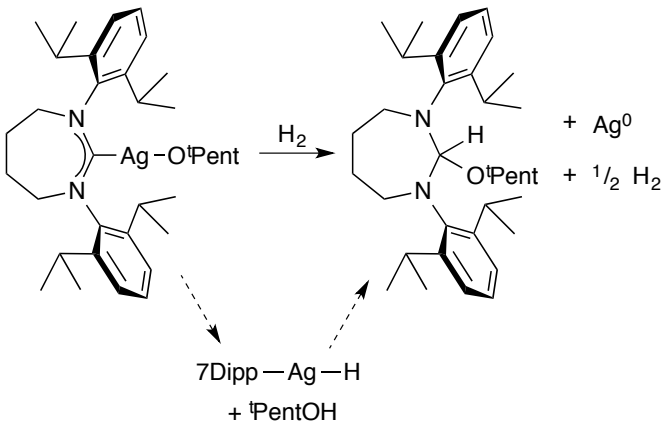

Scheme 5.3: The reaction of terminal alkoxide **3c** with H_2 (4.4 bar), including a hydridosilver intermediate, which was not directly observed.

5.2.3 Carboxylation of Transient Terminal Silver Hydrides

Attempts to generate the terminal hydride (6Dipp)AgH via hydrogenolysis of terminal alkoxide **2b** (2.0 bar H_2) in the presence of CO_2 (1.0 bar) leads to stoichiometric conversion to a formate complex and *tert*-pentanol (Scheme 5.4). Monitoring this reaction by ^{1}H NMR in a pressurized NMR tube reveals the presence of alkylcarbonate resulting from the insertion of CO_2 into the silver-alkoxide bond. It is unclear whether the alkylcarbonate is an intermediate to formate formation. Alternatively, if the insertion of CO_2 into the silver-alkoxide bond is reversible, formate production could proceed entirely through a hydridosilver intermediate. It is likely that any terminal hydride generated would quickly disproportionate if not consumed by CO_2 insertion, but no Ag^0 was observed in this experiment, suggesting that (6Dipp)AgH was indeed a competent intermediate in the formation of formate. Further experiments are needed to confirm this

hypothesis. Regardless of the mechanism, these results demonstrate the competence of silver in the conversion of H_2 and CO_2 to formate, with the sacrificial protonation of *tert*-butoxide.

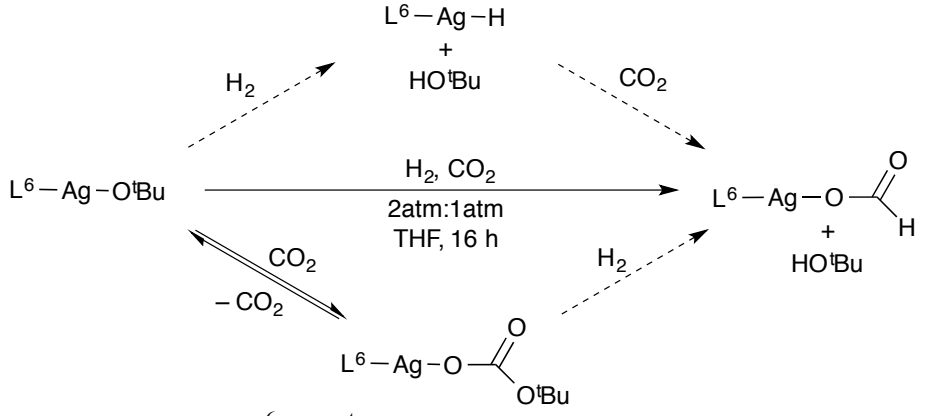

Scheme 5.4: Reaction of $L^6Ag(O^tBu)$, **2b**, with H_2 and CO_2, showing two potential intermediates.

The hydrogenolysis (4.4 bar H_2) of (6Dipp)AgF (**7b**) in the presence of CO_2 and DBU in CD_2Cl_2 likewise leads to the appearance of a formate resonance in the ^1H NMR spectrum of the reaction mixture. However, the rate of formate production is slower than that observed for **2b**, proceeding only to 14% conversion after 24 h.

5.2.4 Steps Towards Catalytic Turnover

We have investigated the use of several additives in the hydrogenation of CO_2 by silver alkoxide **3b**. Non-nucleophilic bases such as 1,8-diazabicyclo[5.4.0]undec-7-ene (DBU), 1,8-bis(dimethylamino)naphthalene (proton sponge), and diisopropylethylamine (Hünig's base) did not result in catalytic turnover; only one equivalent of formate was produced in the presence of these additives. Likewise, triethylamine was not a suitable additive. A separate experiment, in which acetate was used a proxy for formate,

demonstrated that triethylamine displaces acetate from (6Dipp)Ag(O_2CCH_3) in methanol-d_4 solution to form [(6Dipp)Ag(NEt_3)]$^+O_2CCH_3^-$, but no formate production was observed when the resulting solution of [(6Dipp)Ag(NEt_3)]$^+$ was pressurized with CO_2 (1.0 bar) and H_2 (2.0 bar).

Using sodium *tert*-pentoxide as a stoichiometric additive, we have formally demonstrated the completion of a catalytic cycle (Scheme 5.5) for the following overall process, catalyzed by (6Dipp)Ag(O^tPent), **3b**:

$$H_2 + CO_2 + NaO^tPent \rightarrow NaOOCH + HO^tPent$$

However, the incorporation of excess alkoxide into a true one-pot catalytic system has proven challenging because the alkoxide readily carboxylates, and the resulting alkylcarbonate is not sufficiently basic to displace formate from the silver center. Current efforts in our lab include the development of legitimately catalytic conditions and understanding the mechanism.

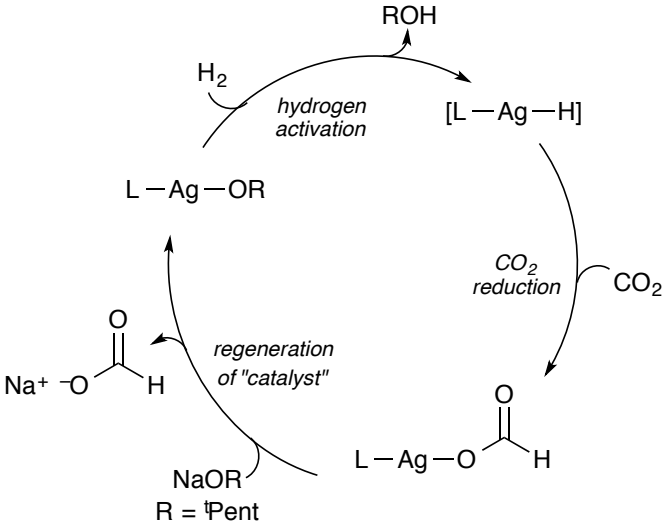

Scheme 5.5: Three steps, demonstrated separately, which if combined would constitute a cycle for silver-catalyzed CO_2 hydrogenation to formate with sacrificial alkoxide.

5.3 Recent Developments in Copper Catalysis

NHC-supported copper hydrides react readily with alcohols, releasing H_2. For this reason, we did not investigate the potential for NHC complexes of copper to facilitate CO_2 hydrogenation. However, Watari, Ikariya, and coworkers[7] recently demonstrated catalytic CO_2 hydrogenation in the presence of DBU, forming the $[DBU]H^+HCO_2^-$ salt, using any of several copper catalysts, including (IDipp)Cu(O^tBu). These results suggest that the hydrogenolysis of (IDipp)Cu(O^tBu), though unfavorable, affords a small equilibrium concentration of $[(IDipp)CuH]_2$, which is known to readily carboxylate. The addition of DBU provides a driving force for catalytic turnover. Appel and coworkers[8] have also reported a well-defined triphosphine-copper catalyst for the same reaction.

5.4 Conclusion

Although mononuclear silver hydrides are less thermally stable than their isolable dinuclear analogs, they may serve as intermediates in the silver(I)-catalyzed hydrogenation of CO_2 to formic acid derivatives. The three key steps required for such catalysis have been demonstrated: H_2 activation, CO_2 reduction, and regeneration of the catalyst. Further studies are needed to determine the optimal conditions for this process and to elucidate the mechanism.

5.5 Experimental

5.5.1 General Considerations

Unless otherwise indicated, manipulations were performed in an MBraun glovebox under an atmosphere of purified nitrogen, or in sealable glassware on a Schlenk

line under an atmosphere of argon. Glassware and magnetic stir bars were dried in a ventilated oven at 160˚C, and allowed to cool under vacuum.

^{1}H, and ^{19}F NMR spectra were obtained at the Georgia Institute of Technology NMR Center using a Varian Vx 400 MHz spectrometer or a Varian Vx 300 MHz spectrometer. ^{1}H NMR chemical shifts are referenced with respect to solvent signals[9] and are reported relative to $Si(CH_3)_4$. ^{19}F NMR chemical shifts were referenced to external neat C_6F_6 (Alfa-Aesar, δ −164.90 ppm) and are reported relative to $CFCl_3$.

5.5.2 Materials and Methods

1,8-Bis(dimethylamino)naphthalene (Sigma-Aldrich), DBU (Alfa-Aesar), diisopropylethylamine (Alfa-Aesar), triethylamine (Sigma-Aldrich), ethanolamine (Sigma-Aldrich), sodium *tert*-butoxide (TCI America), sodium 2,4,6-trimethylphenoxide (Acros), cesium fluoride (Alfa-Aesar), sodium bicarbonate (Alfa-Aesar), and hydrogen (Flynn Scientific) were used as received. Carbon dioxide (NexAir) was passed through a phosphorus pentoxide (Sigma-Aldrich) to ensure dryness.

Compounds **1b**[HF_2], **3b**, **3c**, **7b**, and **7c** were prepared as described previously.[3]

Dichloromethane-d_2 (Cambridge Isotope Labs) was dried by stirring overnight with calcium hydride (coarse powder, Alfa- Aesar), degassed by successive freeze-pump-thaw cycles, and vacuum- transferred into oven-dried resealable Schlenk flasks. Tetrahydrofuran-d_8 (Cambridge Isotope Labs) was dried over purple sodium benzophenone, degassed by successive freeze-pump-thaw cycles, and vacuum-transferred into oven-dried resealable Schlenk flasks. Deuterium oxide (Cambridge Isotope Labs) and methanol-d_4 (Cambridge Isotope Labs) were used as received.

5.5.2.1 Reaction of $\{[(6Dipp)Ag]_2(\mu\text{-}H)\}^+HF_2^-$ (**1b**$[HF_2]$) with CO_2

A solution of **1b**$[HF_2]$ (15 mg, mmol) in CD_2Cl_2 (1.0 mL) in an NMR tube equipped with a J. Young valve was degassed by two freeze-pump-thaw cycles and was pressurized with CO_2 (1.7 bar). The ^1H and ^{19}F NMR spectra were recorded at intervals over 4 days. New ^1H NMR resonances were attributed to $\{[(6Dipp)Ag]_2(\mu\text{-}O_2CH)\}^+HF_2^-$.

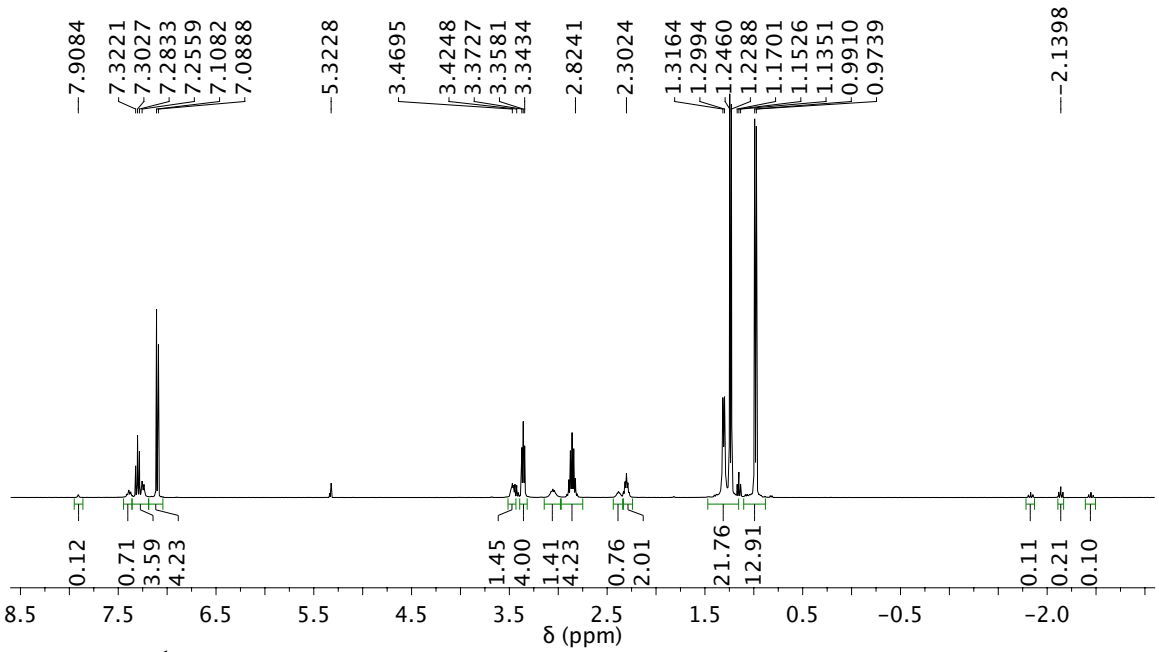

Figure 5.1: ^1H NMR (400 MHz, CD_2Cl_2) spectrum of the reaction of (**1b**$[HF_2]$) with CO_2 (1.7 bar) after 24 h.

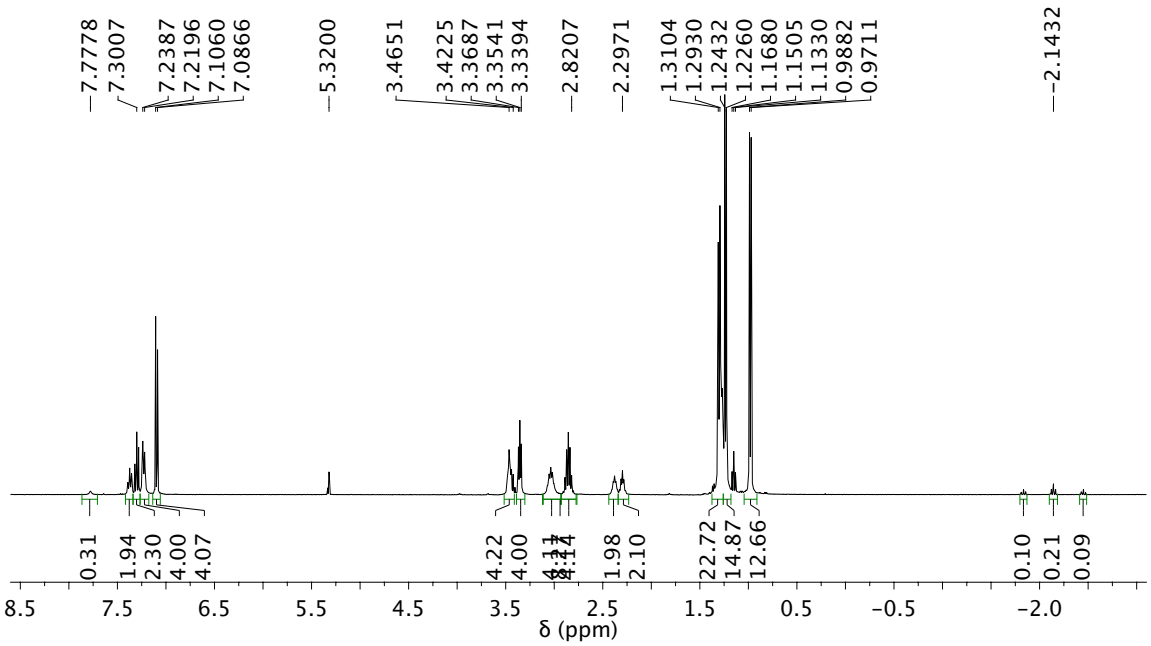

Figure 5.2: ^{1}H NMR (400 MHz, CD_2Cl_2) spectrum of the reaction of (**1b**[HF_2]) with CO_2 (1.7 bar) after 96 h.

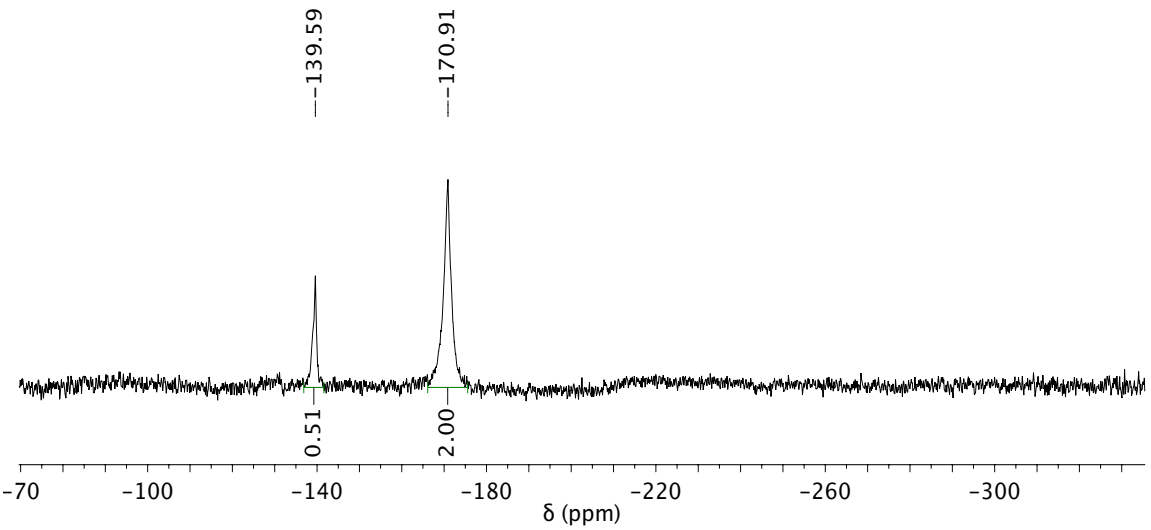

Figure 5.3: ^{19}F NMR (400 MHz, CD_2Cl_2) spectrum of the reaction of (**1b**[HF_2]) with CO_2 (1.7 bar) after 96 h.

5.5.2.2 Reaction of (7Dipp)Ag(O^{t}Pent) (**3c**) with H_2 and CO_2

A solution of **3c** (10 mg, mmol) in THF-d_8 (1.0 mL) in an NMR tube equipped with a J. Young valve was degassed by two freeze-pump-thaw cycles and was pressurized with CO_2 (1.0 bar) and H_2 (2.0 bar), resulting in a total pressure of 3.0 bar. The ^{1}H NMR spectrum was recorded at intervals over 24 hours. The consumption of **3c** was observed and new ^{1}H NMR resonances were attributed to (7Dipp)Ag(O_2CH) and *tert*-pentanol.

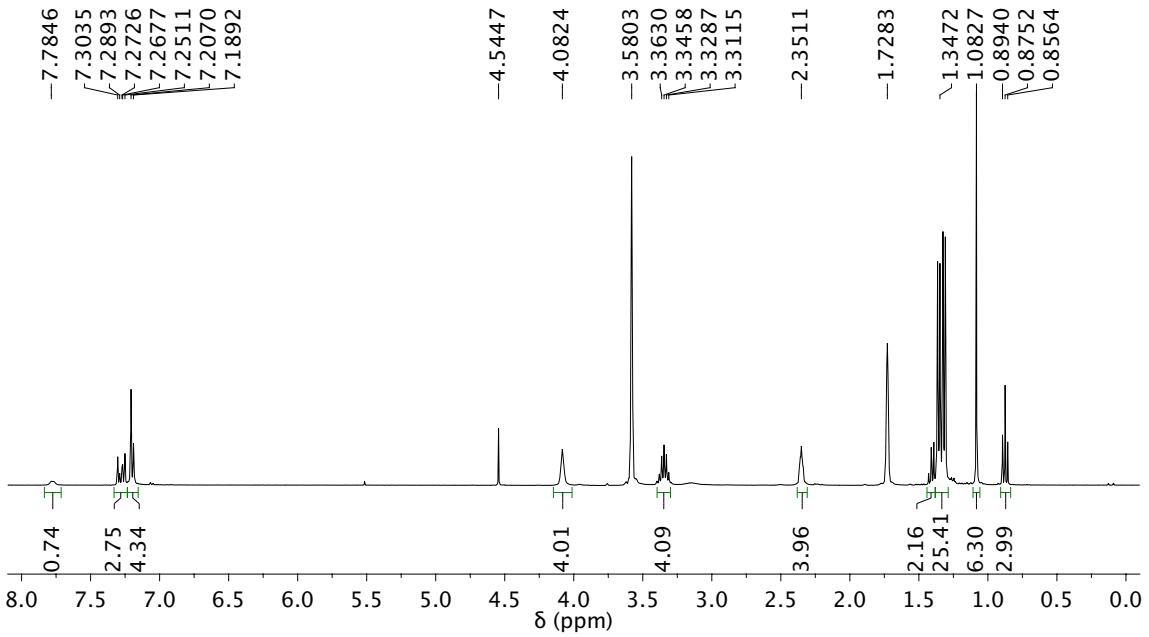

Figure 5.4: ^{1}H NMR (400 MHz, THF-d_8) spectrum of the reaction of **3c** with H_2 (2.0 bar, δ 4.54 ppm) and CO_2 (1.0 bar) after 24 h.

5.5.2.3 General Procedure for CO_2 Hydrogenation Experiments with Additives

A solution of **3b**, **3c**, **7b**, **7c** or (6Dipp)Ag(O_2CCH_3) (1 to 10 mg) and an excess (10–100-fold relative to silver) of additive (1,8-bis(dimethylamino)naphthalene, 1,8-diazabicyclo[5.4.0]undec-7-ene, diisopropylethylamine, triethylamine, ethanolamine,

sodium *tert*-butoxide, sodium 2,4,6-trimethylphenoxide, cesium fluoride, or sodium bicarbonate) in THF-d_8, CD_2Cl_2, methanol-d_4 or a mixture of THF-d_8 and D_2O in an NMR tube equipped with a J. Young valve was degassed by two freeze-pump-thaw cycles and was pressurized with CO_2 (1.0 bar) and H_2 (2.0 bar), resulting in a total pressure of 3.0 bar. The ^{1}H NMR spectrum was recorded at intervals until substantial decomposition was observed or until it became apparent that formate production was not catalytic.

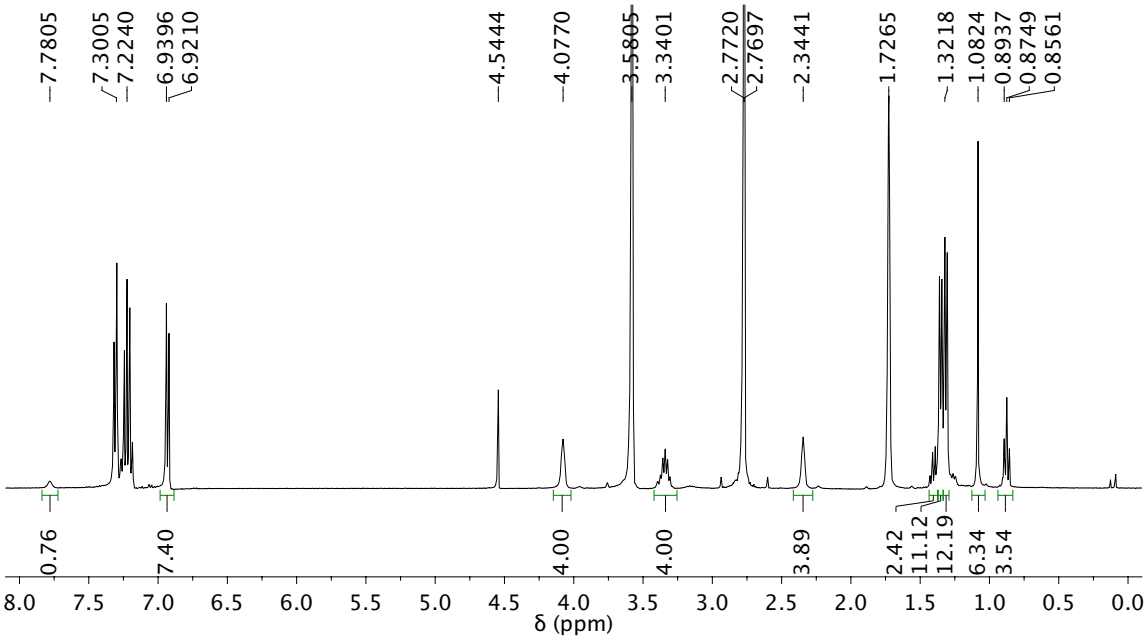

Figure 5.5: ^{1}H NMR (400 MHz, THF-d_8) spectrum of the reaction of **3c** with H_2 (2.0 bar, δ 4.54 ppm) and CO_2 (1.0 bar) in the presence of 1,8-bis(dimethylamino)naphthalene (δ 2.77 ppm) after 24 h.

5.6 Acknowledgements

We thank the U.S. National Science Foundation for generous support of this research (CHE-1300659).

5.7 References

1 (a) A. M. Appel, J. E. Bercaw, A. B. Bocarsly, H. Dobbek, D. L. DuBois, M. Dupuis, J. G. Ferry, E. Fujita, R. Hille, P. J. A. Kenis, C. A. Kerfeld, R. H. Morris, C. H. F. Peden, A. R. Portis, S. W. Ragsdale, T. B. Rauchfuss, J. N. H. Reek, L. C. Seefeldt, R. K. Thauer, G. L. Waldrop. *Chem. Rev.* **2013**, *113*, 6621−6658. (b) G. A. Olah, G. K. S. Prakash, A. Goeppert. *J. Am. Chem. Soc.* **2011**, *133*, 12881–12898. (c) P. G. Jessop, F. Joó, C.-C. Tai. *Coord. Chem. Rev.* **2004**, *248,* 2425–2442. (d) P. G. Jessop, T. Ikariya, R. Noyori. *Chem. Rev.* **1995**, *95*, 259–272.

2 (a) Y.-Y. Jiang, H.-Z. Yu, Y. Fu, *Organometallics* **2014**, *33*, 6577. (b) Z. Jia, F. Zhou, M. Liu, X. Li, A. S. C. Chan, C.-J. Li, *Angew. Chem. Int. Ed.* **2013**, *52*, 11871. (c) M. T. Beck, I. Gimesi, *Acta Chim. Acad. Sci. Hung.* **1964**, *42*, 343. (d) M. T. Beck, I. Gimesi, J. Farkas, *Nature* **1963**, *197*, 73. (e) J. Halpern, G. Czapski, J. Jortner, G. Stein, *Nature* **1960**, *186*, 629. (f) A. J. Chalk, J. Halpern, A. C. Harkness, *J. Am. Chem. Soc.* **1959**, *81*, 5854. (g) J. Halpern, *J. Phys. Chem.* **1959**, *63*, 398. (h) A. H. Webster, J. Halpern, *J. Phys. Chem.* **1957**, *61*, 1245. (i) A. H. Webster, J. Halpern, *J. Phys. Chem.* **1957**, *61*, 1239. (j) A. H. Webster, J. Halpern, *Trans. Faraday Soc.* **1957**, *53*, 51. (k) A. H. Webster, J. Halpern, *J. Phys. Chem.* **1956**, *60*, 280.

3 B. K. Tate, J. T. Nguyen, J. Bacsa, J. P. Sadighi, *Chem. Eur. J.* **2015**, *21*, 10160–10169.

4 B. K. Tate, C. M. Wyss, J. Bacsa, K. Kluge, L. Gelbaum, J. P. Sadighi, *Chem. Sci.,* **2013**, *4,* 3068–3074.

5 (a) E. Y. Tsui, P. Müller, J. P. Sadighi. *Angew. Chem. Int. Ed.* **2008**, *47*, 8937–8940. (b) N. Phillips, T. Dodson, R. Tirfoin, J. I. Bates, S. Aldridge, *Chem. Eur. J.* **2014**, *20*, 16721–16731. (c) H. B. Lv, J. H. Zhan, Y. B. Cai, Y. Yu, B. W. Wang, J. L. Zhang. *J. Am. Chem. Soc.* **2012**, *134*, 16216–16227.

6 (a) N. P. Mankad, D. S. Laitar, J. P. Sadighi, *Organometallics* **2004**, 23, 3369. (b) G. D. Frey, B. Donnadieu, M. Soleilhavoup, G. Bertrand, *Chem. Asian J.* **2011**, *6*, 402–405. (c) A. M. Suess, M. R. Uehling, W. Kaminsky, G. Lalic. *J. Am. Chem. Soc.* **2015**, *137*, 7747–7753.

7 R. Watari, Y. Kayaki, S. Hirano, N. Matsumoto, T. Ikariya. *Adv. Synth. Catal*. **2015**, *357*, 1369–1373.

8 C. M. Zall, J. C. Linehan, A. M. Appel. *ACS Catal.* **2015**, *5*, 5301−5305.

9 G. R. Fulmer, A. J. M. Miller, N. H. Sherden, H. E. Gottlieb, A. Nudelman, B. M. Stoltz, J. E. Bercaw, K. I. Goldberg, *Organometallics* **2010**, *29*, 2176–2179.

CHAPTER 6

THERMALLY STABLE ORGANOSILVER COMPOUNDS

6.1 Background

Although silver participates in a variety of interesting organic transformations, the organometallic chemistry of silver is underrepresented in comparison to that of most other transition metals, especially its congeners copper and gold. The study of organosilver compounds is often limited by their thermal instability and photosensitivity. For example, phosphine-supported alkylsilver complexes disproportionate quickly at room temperature, giving primarily the coupling products of organic radicals, elemental silver, and free phosphine.[1] Many organosilver compounds which are stable at room temperature, such as alkynylsilver compounds and phenylsilver, form coordination polymers, and low solubility limits their utility. Under the right conditions, however, organosilver compounds have been effectively utilized as sources of carbon-based radicals or carbanions,[2] and they are of interest as possible intermediates in silver-mediated C–C coupling processes.[3–5]

Silver complexes with sp-hybridized carbanions are among the oldest known organometallic species and have found relatively widespread synthetic applications.[6–9] The reaction of silver nitrate with acetylene in basic media, first described by Berthelot,[10] results in the precipitation of silver acetylide, which disporportionates violently upon thermal or physical shock, leading to its use as a primary explosive.[11] Substituted acetylides may be prepared under similar conditions and are generally stable at room

temperature in the dark.[12] Despite their typically low solubility in common solvents, alkynylsilver compounds have been utilized as mildly nucleophilic acetylide sources in the substitution of acyl halides[7] as well as activated carbonyls[8] and alkyl halides[9] for the syntheses of highly functionalized molecules. Alkynylsilver compounds are also likely intermediates in silver-catalyzed C–C and C–N coupling processes[13] as well as the silver-catalyzed carboxylation of terminal alkynes.[14]

Complexes of silver with sp^2 carbanions were also among the early known examples of organosilver but are generally more thermally sensitive than acetylides. Krause and Schmitz[15] prepared phenylsilver by transmetallation from tin, lead, or magnesium, isolated it as a complex with $AgNO_3$, and reported its violent decomposition upon evaporation of solvent. Later, alternative synthetic routes provided pure, isolable phenylsilver, which despite low solubility exhibits some reactivity towards acyl halides, producing biphenyl in addition to nucleophilic substitution products.[16] Mesitylsilver is stable at room temperature in the dark, is soluble in most organic solvents, and has been characterized crystallographically as a tetramer with symmetrically bridging aryl ligands.[17] The more sterically encumbered 2,4,6-(triphenyl)phenylsilver is also stable at room temperature but crystallizes as a monomer.[18] Diarylargentate ions, isolated as lithium salts, decompose slowly at room temperature.[19] Vinylsilver[1c–d,20] and allenylsilver[21] compounds have also been studied.

Early studies of alkylsilver complexes focused on the detection of thermal decomposition products. Semerano and Riccoboni[22] first inferred the intermediacy of alkylsilver compounds in the reaction of tetraalkyllead reagents with silver nitrate, which produces alkyl dimers and elemental silver.[23] Further studies followed, demonstrating

silver-mediated C–C coupling of organomagnesium and -lithium reagents.[3d–h] Whitesides and coworkers carried out mechanistic studies[1] of the reaction of Grignard reagents with phosphine-supported silver halides. The results suggested that the observed disproportionation to elemental silver and alkyl homocoupling products sometimes involves homolysis of Ag–C bonds, with release of free alkyl radicals, but in other cases proceeds through a concerted bimolecular process. These studies led to the development of methods for the silver-mediated synthesis of cycloalkanes,[3a] and to a variety of silver-catalyzed C–C coupling processes.[2,4] Alkylsilver complexes produced via the decarboxylation of silver carboxylates have also been studied in the gas phase.[24]

Complexes of electron-deficient carbanions with silver are relatively stable, and their reaction chemistry has been more widely investigated. The addition of silver(I) fluoride to perfluoroolefins, for example, gives rise to perfluoroalkylsilver compounds,[25] which can mediate the carboxylation of benzyl halides[26] and undergo reductive C–C homocoupling.[27] Perfluoroalkyl and pentafluorophenyl complexes of silver, which are generally stable at room temperature, can also be conveniently prepared by treatment of AgF with the corresponding trimethylsilyl reagent.[28] Synthetic applications of perfluoroorganosilver complexes include nucleophilic substitutions of acyl halides,[29–30] chlorosilanes,[30] benzyl bromide,[30] and alkyl and aryl iodides,[30] as well as oxidative transfer of the perfluoroorganic group to elemental copper or wide variety of elements of groups 12–16.[28b–i,30] Other halogens, alkoxy, amino, and trifluoromethyl substituents enhance the stability of arylsilver compounds, allowing further investigation of their structures and reactivity.[31] Silyl-substituted alkyl complexes of silver have also been structurally characterized.[32] Recently Shen and coworkers[33] have prepared NHC-

supported (difluoromethyl)silver complexes via metathesis of alkoxysilver precursors with (difluoromethyl)trimethylsilane, demonstrated silver-mediated difluoromethylation and difluorothiomethylation of a range of electrophiles, and developed a method for palladium/silver-catalyzed difluoromethylation of aryl halides.

The insertion of CO_2 into Ag–C bonds is inferred from several silver-catalyzed carboxylations[14,34] but is difficult to study in isolation due to the transient nature of intermediate silver-carbanion complexes. Alkyl, aryl, vinyl, and alkynyl complexes of copper and gold are generally more thermally stable than their silver analogs, and the insertion of CO_2 into Cu–C[35] and Au–C[36] bonds is therefore more thoroughly studied.

This chapter describes the preparation of a series of stable mononuclear and dinuclear complexes of silver with carbanion ligands featuring sp^3-, sp^2-, and sp-hybridization, supported by the NHC ligand 1,3-bis(2,6-diisopropylphenyl)imidazolin-2-ylidene (5Dipp). We have characterized these complexes using X-ray crystallography and ^{109}Ag NMR spectroscopy; the dinuclear complexes exhibit significant and varied intermetallic interactions. The mononuclear alkylsilver compounds react as carbon nucleophiles, adding CO_2 to form carboxylate complexes.

6.2 Results and Discussion

6.2.1 Terminal Organosilver Complexes

Various synthetic approaches were employed, including transmetalation from organozinc compounds, Grignard reagents, and a trimethylsilyl derivative, using known silver precursors (5Dipp)Ag(O^{t}Bu) (**3a**) and (5Dipp)AgCl (**2**) (Scheme 6.1). The C–H bond of phenylacetylene proved sufficiently acidic to permit direct deprotonation by the

silver *tert*-butoxide complex. Collectively, these approaches permit the synthesis of a range of carbanion precursors to broaden the scope of available organosilver reagents.

The preparation of (5Dipp)AgEt (**16**) via exchange of ligands between **3a** and one-half equivalent of diethylzinc proceeds rapidly and quantitatively in C_6D_6 or tetrahydrofuran-d_8 at ambient temperature (Scheme 6.1a), as judged by ^{1}H NMR spectroscopy. Complex **16** can be separated from the hydrocarbon-soluble bis(*tert*-butoxy)zinc byproduct by precipitation from THF with the addition of hexanes, allowing its isolation in 55% yield. The addition of excess diethylzinc does not impede the reaction or the separation of byproducts. The ethyl ligand exhibits ^{1}H NMR resonances with defined ^{1}H–^{107}Ag and ^{1}H–^{109}Ag nuclear dipole coupling for both the α and β protons, resulting in a superimposed pair of doublets of quartets at δ –0.25 ppm for the α protons (Figure 6.1a) and a pair of doublets of triplets at δ 0.89 ppm for the β protons (Figure 6.1b) in THF-d_8. Because the two-bond and three-bond ^{1}H–^{109}Ag coupling constants are similar ($^2J(^1\text{H}\text{-}^{109}\text{Ag})$ = 12.8 Hz, $^3J(^1\text{H}\text{-}^{109}\text{Ag})$ = 12.1 Hz), the ^{109}Ag NMR signal resolves as an apparent sextet (See Figure 6.9).

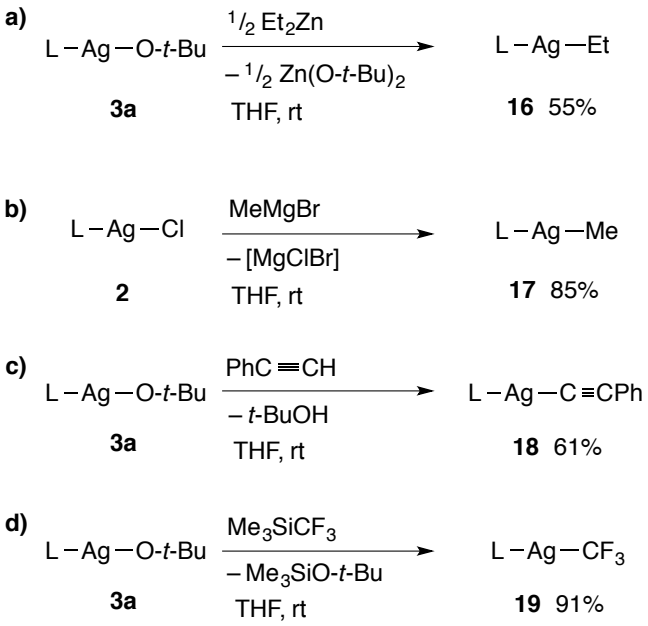

Scheme 6.1: Syntheses of monosilver-carbanion complexes **16–19**.

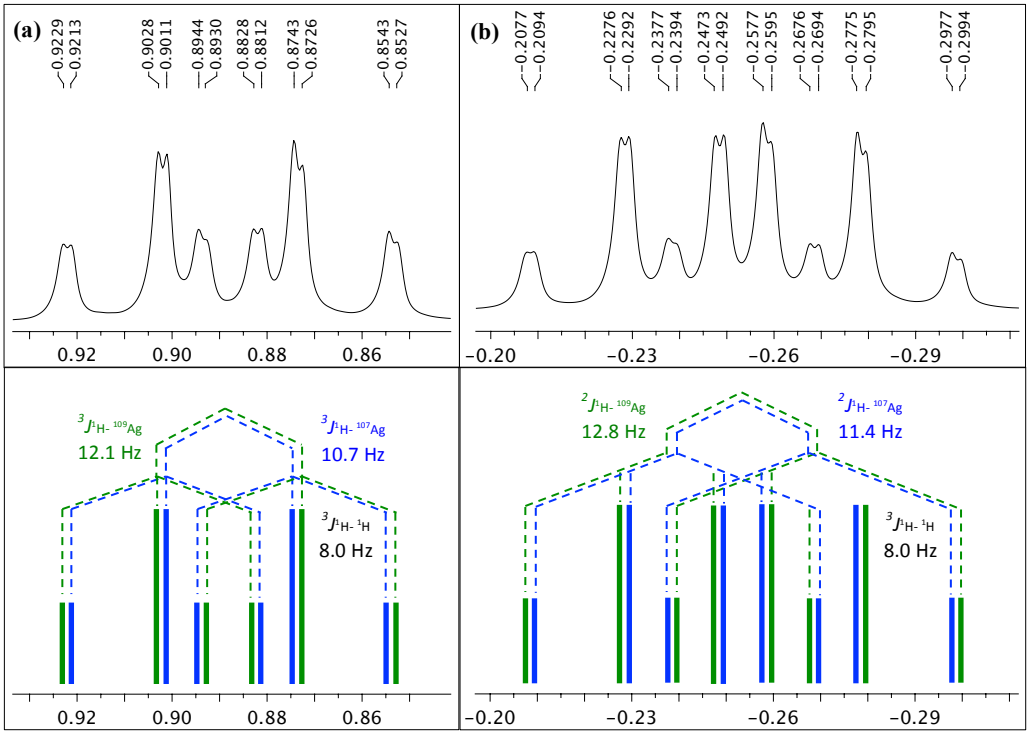

Figure 6.1: ^{1}H NMR (400 MHz, THF-d_8) resonances of the **(a)** CH_3 and **(b)** CH_2 protons of the ethyl ligand of (5Dipp)AgEt (**16**) and corresponding splitting diagrams.

Rather than using dimethylzinc, we chose to prepare (5Dipp)AgMe (**17**) using methylmagnesium bromide, a relatively inexpensive source of the methyl anion, and found that the reaction of MeMgBr with **2** proceeds quickly in C_6D_6 or THF (Scheme 6.1b). The magnesium halide byproducts were precipitated as dioxane adducts, allowing the isolation of **17** in 85% yield. The methyl ligand of **17** exhibits a ^{1}H NMR doublet at δ –1.38 ppm in CD_2Cl_2. Because coupling to the ^{107}Ag and ^{109}Ag nuclei is not resolved, the observed magnitude of 10 Hz is presumed an average of the ^{1}H coupling to the two silver isotopes. Indeed, a slightly greater coupling constant of 11 Hz is observed for the quartet resonance in the ^{109}Ag NMR spectrum of **17** as expected due to the 15% greater gyromagnetic ratio of ^{109}Ag relative to ^{107}Ag. Complex **17** crystallizes as a monomer with linear coordination about silver (C–Ag–C = 180.00˚) (Figure 6.2).

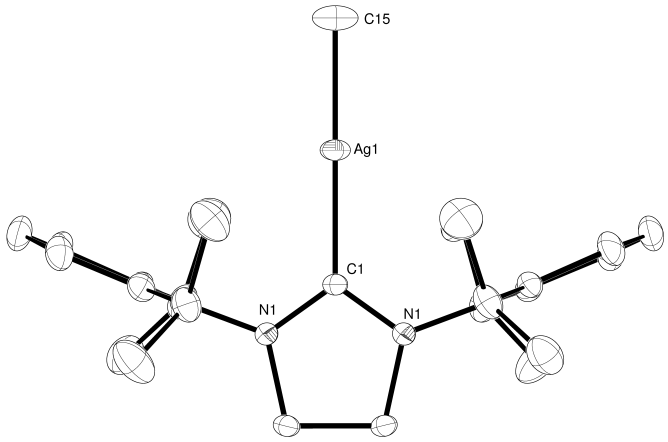

Figure 6.2: Solid state structure of **17**, shown as 50% probability ellipsoids. H atoms omitted for clarity.

Treatment of a suspension of (5Dipp)AgCl in C_6D_6 with vinylmagnesium bromide resulted in a clear solution within seconds, indicating rapid consumption of the

benzene-insoluble chlorosilver starting material. An ^{1}H NMR spectrum recorded 15 min after the addition of vinylmagnesium bromide exhibited broad ^{1}H NMR signals at δ 6.59, 5.78, and 5.74 ppm, presumably arising from a vinylsilver intermediate. Traces of 1,3-butadiene, the homocoupling product of the vinyl radical, were also detected. As disproportionation continued, the deposition of elemental silver became visibly apparent. After 24 hours, the integration of ^{1}H NMR signals against an internal standard suggested nearly complete conversion to free 5Dipp (>95%) and 1,3-butadiene (at least 80%[37]) (Scheme 6.2). Because of the thermal instability of the vinylsilver complex, an analytically pure sample was not isolated.

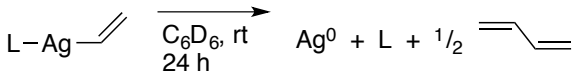

Scheme 6.2: Decomposition of inferred vinylsilver complex.

Deprotonation of phenylacetylene by **3a** affords (5Dipp)Ag(CCPh) (**18**) (Scheme 6.1c). This reaction proceeds rapidly and quantitatively in C_6D_6 or THF-d_8, as judged by ^{1}H NMR spectroscopy. Complex **18** can be separated from the *t*-butanol byproduct by precipitation from THF with the addition of hexanes, affording a 61% yield. Excess phenylacetylene may be used without adverse consequences and may be separated likewise.

(5Dipp)Ag(CF_3) (**19**) was prepared by treatment of **3a** with (trifluoromethyl)trimethylsilane in THF (Scheme 6.1d). Precipitation of the product by addition of hexanes allows its isolation in 91% yield. The ^{19}F NMR spectrum of **19**

exhibits distinct $^{19}F–^{107}Ag$ and $^{19}F–^{109}Ag$ nuclear dipole coupling, giving rise to a pair of doublets at δ –291.9 ppm with $J(^{19}F–^{107}Ag)$ = 92 Hz and $J(^{19}F–^{109}Ag)$ = 106 Hz. The ^{109}Ag NMR spectrum displays a quartet resonance, with the 106 Hz coupling constant observed in the ^{19}F NMR spectrum.

The silver-bound carbon nuclei of the terminal organosilver complexes exhibit ^{13}C NMR signals as pairs of coincident doublets due to well-resolved coupling to ^{107}Ag and ^{109}Ag, as shown in Table 6.1. The ^{13}C NMR signals of the donor carbons of **19** are further split into quartets due to coupling to ^{19}F ($J(^{13}C_{NHC}–^{19}F)$ = 5 Hz, $J(^{13}C_R-^{19}F)$ = 368 Hz).

Table 6.1. ^{13}C NMR data for donor carbons of monosilver complexes (5Dipp)AgR.

	R	δ($^{13}C_{NHC}$), ppm	$J(^{13}C_{NHC}–^{107/109}Ag)$, Hz	δ ($^{13}C_R$), ppm	$J(^{13}C_R–^{107/109}Ag)$, Hz
16	Et	214.6	100/115	1.4	129/149
17	Me	213.4	111/129	–15.7	120/138
18	CCPh	210.1	156/181	122.3	194/224
19	CF_3	209.6	152/175	154.0	272/314

6.2.2 Carbanion-Bridged Disilver Complexes

Disilver complexes were prepared either by treatment of the disilver precursor $\{[(5Dipp)Ag]_2(\mu\text{-}O^tBu)\}^+BF_4^-$ (**5a**) with a carbanion source or by the combination of a neutral organosilver species with equimolar (5Dipp)AgOTf (OTf = trifluoromethanesulfonate), which serves as a ready source of $[(5Dipp)Ag]^+$ (Scheme

6.3). Analogous dinuclear complexes of gold with carbanions are likely intermediates in several gold-catalyzed processes.[38]

These complexes feature three-center, two-electron bonding, characterized by short Ag–Ag distances, nonlinear geometry about each silver center, and ^{109}Ag–^{107}Ag nuclear dipolar coupling, as shown in Table 6.2. This structural motif was previously reported for the hydride-bridged disilver complex $\{[(5Dipp)Ag]_2(\mu\text{-}H)\}^+$ [39] and has been postulated in studies of hydrido-, alkyl-, and aryldisilver cations in the gas phase.[21f,h] Crystallographically characterized neutral organosilver oligomers also exhibit similar three-center, two-electron bonds.[11,13,25]

Table 6.2. Crystallographic Ag–Ag distances and ^{109}Ag NMR data for carbanion-bridged disilver complexes.

	R	Ag–Ag (Å)	δ (^{109}Ag), ppm[a]	J(^{109}Ag–^{107}Ag), Hz
8	Et	2.7091(8)	681.2	55
9	Ph	2.8168(4)	728.4	76
10	Me	2.706(1)	[b]	[b]
11	CCPh	3.3707(7), 3.2845(6)	673.9	18

[a]Chemical shift relative to 4.00 M $AgNO_3$ in D_2O. [b]No signal detected.

The ethyl-bridged $\{[(5Dipp)Ag]_2(\mu\text{-}Et)\}^+BF_4^-$ (**20**) was prepared by ligand exchange of **5a** and one-half equivalent of diethylzinc in THF (Scheme 6.3a). Precipitation of **20** by the addition of hexanes results in a 90% yield. The SIPrAg fragments of **20** are equivalent in solution on the NMR timescale. Although coupling to silver is observed for both the α and β protons of the bridging ethyl ligand, the two isotopes of silver do not give rise to well-resolved couplings in the ^{1}H NMR spectrum.

The two-bond and three-bond ^{1}H–^{109}Ag couplings in **20** are of approximately equal magnitude, and coincidentally roughly equal to the vicinal ^{1}H–^{1}H coupling ($^{2}J(^{1}H\text{-}^{107/109}Ag) \approx {}^{3}J(^{1}H\text{-}^{107/109}Ag) \approx {}^{3}J(^{1}H\text{-}^{1}H) \approx 7$ Hz), resulting in ^{1}H NMR signals resembling a sextet for the ethyl α protons at δ 0.64 ppm and a quintet for the β protons at δ 0.17 ppm. The ^{109}Ag NMR spectrum of **20** features an apparent triplet of sextets (Figure 6.3a) reflecting the roughly 7 Hz ^{1}H–Ag coupling observed in the ^{1}H NMR spectrum as well as substantial ^{109}Ag–^{107}Ag coupling ($J(^{109}Ag\text{–}^{107}Ag) = 56$ Hz). ^{1}H-decoupling reduces the ^{109}Ag NMR signal of **20** to an apparent triplet, as expected (Figure 6.3b). This signal is more properly described as a singlet arising from the homonuclear $^{109}Ag_2$ isotopologue, and a superimposed doublet arising from the heteronuclear $^{109}Ag^{107}Ag$ isotopologue. Complex **20** crystallizes with a triangular Ag–C–Ag structure featuring a Ag–Ag distance of 2.7091(8) Å, considerably shorter than twice the van der Waals radius of 1.72 Å (Figure 6.4).

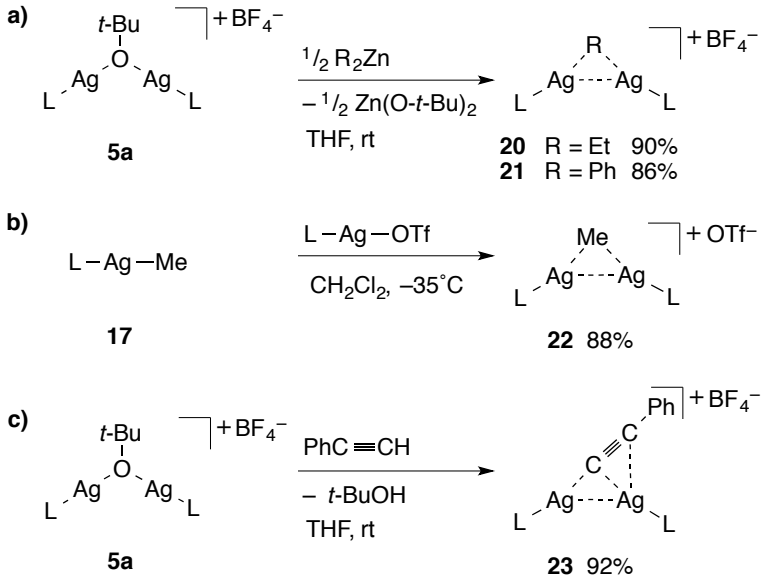

Scheme 6.3: Synthesis of disilver-carbanion complexes **20–23**.

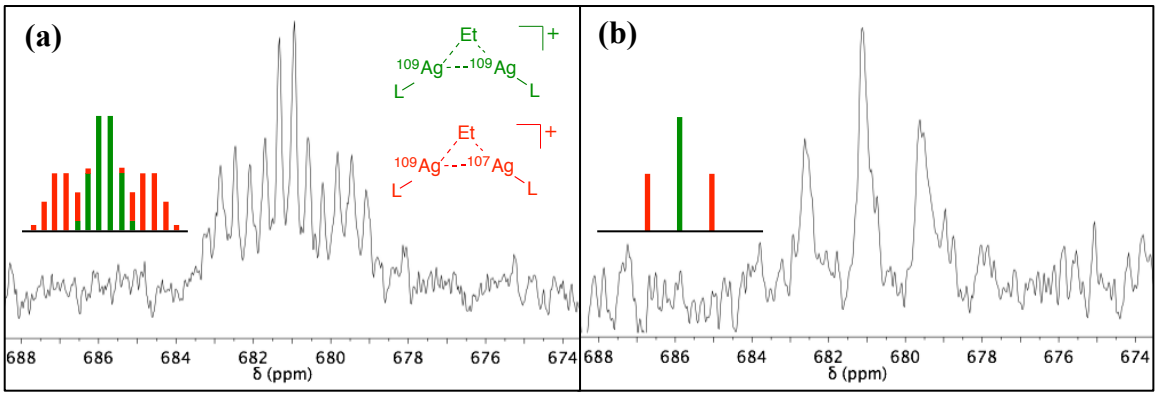

Figure 6.3. (a) ^{109}Ag and **(b)** ^{109}Ag{^{1}H} NMR spectra (18.6 MHz, CD_2Cl_2) of {[(5Dipp)Ag]$_2$(μ-Et)}$^+$ (**20**). $^2J(^{109}\text{Ag}–^1\text{H}) \approx {}^3J(^{109}\text{Ag}–^1\text{H}) \approx 7$ Hz; $J(^{109}\text{Ag}–^{107}\text{Ag}) = 57$ Hz. Insets show rationalization of the pattern as the coincident signals arising from the two ^{109}Ag-containing isotopologues.

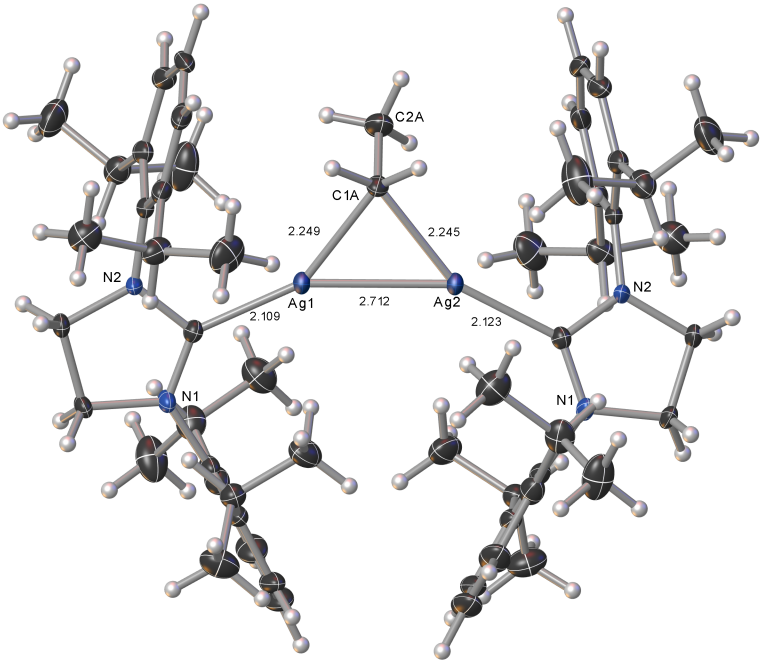

Figure 6.4. Solid state structure of {[(5Dipp)Ag]$_2$(μ-Et)}$^+$ (**20**), shown as 50% probability ellipsoids.

The phenyl-bridged disilver complex $\{[(5Dipp)Ag]_2(\mu\text{-}Ph)\}^+BF_4^-$ (**21**) was prepared by treatment of **5a** with diphenylzinc in THF (Scheme 6.3a) and precipitated with the addition of hexanes in 86% yield. As for **20**, the SIPrAg fragments of **21** are equivalent according to NMR spectroscopy, and its solid-state structure (Figure 6.5) likewise features a triangular Ag–C–Ag core. Interestingly the Ag–Ag distance of 2.8168(4) Å in **21** is somewhat longer than in **20**, implying a slightly weaker interaction, yet the ^{109}Ag–^{107}Ag coupling is greater in **21** ($J(^{109}Ag–^{107}Ag)$ = 76 Hz).

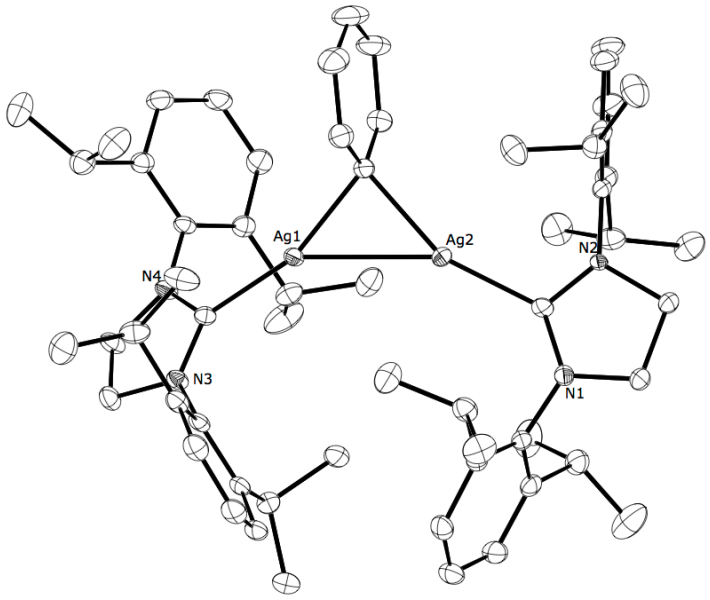

Figure 6.5. Solid state structure of $\{[(5Dipp)Ag]_2(\mu\text{-}Ph)\}^+$ (**21**), shown as 50% probability ellipsoids. H atoms omitted for clarity.

We synthesized the methyl-bridged complex $\{[(5Dipp)Ag]_2(\mu\text{-}Me)\}^+OTf^-$ (**22**) by treatment of the terminal analogue **17** with one molar equivalent of (5Dipp)AgOTf (**4**) in CH_2Cl_2 at –35˚C (Scheme 6.3b). Although cold reaction conditions are required to

prevent the formation of $[(5Dipp)_2Ag]^+$ and Ag^0, the dinuclear complex **22** is stable at room temperature. The methyl ligand exhibits a singlet in the ^1H NMR spectrum of **22**, lacking the ^1H–$^{107/109}Ag$ coupling observed for **17** as well as the ethyl-bridged analogue **20**. We were unable to detect a ^{109}Ag NMR signal for **22**. However, the triangular structural motif was confirmed by crystallography (Figure 6.6). The Ag–Ag distance of 2.706(1) Å is virtually equivalent to that of ethyl-bridged complex **20**.

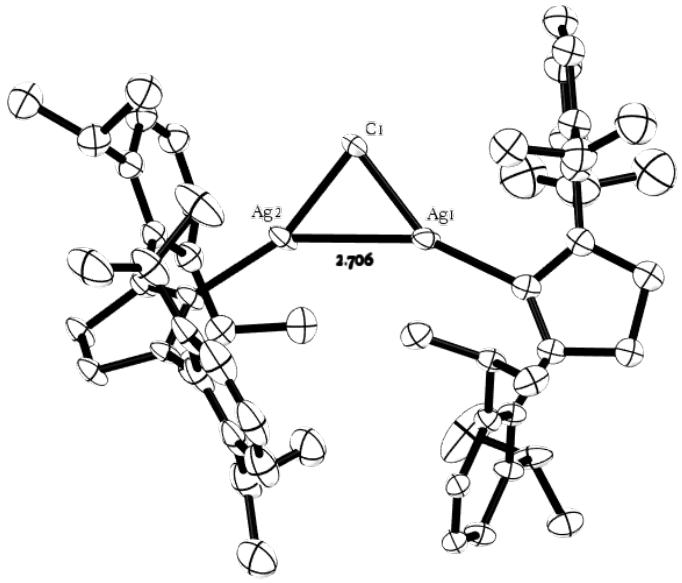

Figure 6.6. Solid state structure of $\{[(5Dipp)Ag]_2(\mu\text{-Me})\}^+$ (**22**), shown as 50% probability ellipsoids. H atoms omitted for clarity.

The disilver phenylethynyl complex $\{[(5Dipp)Ag]_2(\mu\text{-CCPh})\}^+BF_4^-$ (**23**) was synthesized via the deprotonation of phenylacetylene by **5a** in THF (Scheme 6.3c). The phenylethynyl ligand of **23** appears to bridge the metal centers symmetrically on the NMR timescale, but the complex crystallizes in an asymmetric σ,π binding mode, similar to that of the analogous gold complex reported by Brown and Widenhoefer.[38c,40]

Two crystallographically distinct molecules, one of which is shown in Figure 6.7, are present in the asymmetric unit of **11**. In contrast to the gold analogue, in which the Au–Au distance (3.6235(9) Å) is greater than twice the van der Waals radius of gold (1.66 Å), the Ag–Ag distance of **23** (3.3707(7) Å and 3.2845(6) Å) is shorter than twice the van der Waals radius of silver, consistent with some Ag–Ag interaction. In fact, the π-bound silver center is not equidistant from the two alkynyl carbon atoms but lies somewhat closer to the terminal carbon, resulting in a T-shaped binding mode.[41] We therefore believe an attractive intermetallic interaction influences the geometry of **23**. The complex exhibits an apparent triplet, actually a singlet and coincident doublet, in its ^{109}Ag NMR spectrum. At 18 Hz, the ^{109}Ag–^{107}Ag dipolar coupling of **23** is considerably less than that of **20** (55 Hz) and **21** (76 Hz).

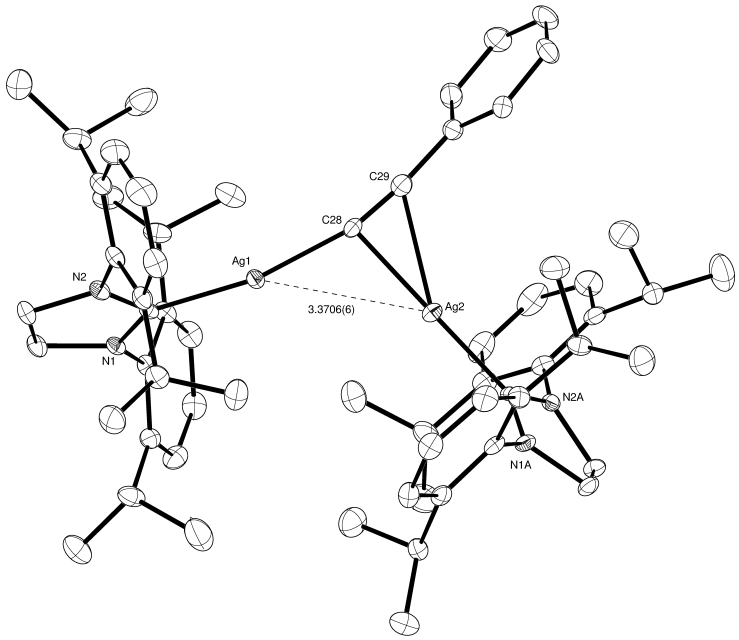

Figure 6.7. Solid state structure of $\{[(5Dipp)Ag]_2(\mu\text{-}CCPh)\}^+$ (**23**), shown as 50% probability ellipsoids. H atoms omitted for clarity.

6.2.3 Reactivity of Terminal Alkylsilver Complexes with CO_2

We anticipated that the silver-bound carbanions should exhibit nucleophilic behavior. We therefore investigated the reactivity of the NHC-supported organosilver compounds towards CO_2. Complex **16** reacts with CO_2 (1.0 bar) in CD_2Cl_2, fully converting to (5Dipp)Ag(O_2CEt) (**24**) in 16 h (Scheme 6.4). Evaporation of volatiles allows isolation of **12** in analytical purity. Complex **17** reacts relatively slowly with CO_2. After 92 h under CO_2 (1.0 bar) in THF-d_8, 79% conversion to (5Dipp)Ag(O_2CMe) is observed,[42] while 12% of **17** is unreacted and two unidentified new species comprise 9% of the products, as quantified by integration of ^{1}H NMR signals against an internal standard.

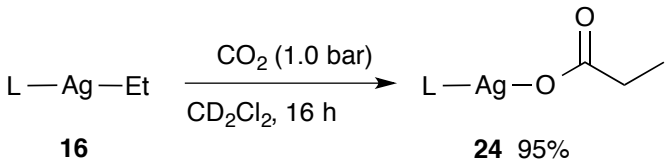

Scheme 6.4. Reaction of (5Dipp)AgEt (**16**) with CO_2.

6.3 Conclusion

Because NHC ligands, especially those featuring a saturated amidine heterocycle and 2,6-diisopropylphenyl *N*-substituents, e.g. 5Dipp and 6Dipp, have been utilized as ancillary ligands to support a number of otherwise thermally unstable complexes of silver,[33,39,42,43] we sought to use this class of ligand to prepare a series of mononuclear silver-carbanion complexes (Scheme 1), as well as a series of carbanion-bridged disilver complexes (Scheme 3), which are stable at room temperature. These series include donor

carbons ranging from sp^3 to sp^2 to sp hybridization, and we therefore suspect the stability imparted by the NHC ligands as well as the synthetic methods demonstrated here may be generalized to include a wide variety of carbanion ligands. Among these complexes are examples of simple alkylsilver complexes which are stable at room temperature. The dinuclear series includes several examples of three-center, two-electron systems featuring Ag–Ag interactions, as well as an alkynyl-bridged disilver complex with a T-shaped coordination mode. Clean insertion of CO_2 is observed for the terminal ethyl complex **16**, while the less nucleophilic methyl analog **17** reacts relatively slowly.

6.4 Experimental

6.4.1 General Considerations

Unless otherwise indicated, manipulations were performed in an MBraun glovebox under an inert atmosphere of purified nitrogen (NexAir), or in sealable glassware on a Schlenk line under an atmosphere of argon (NexAir). Glassware and magnetic stir bars were dried in a ventilated oven at 160°C and were allowed to cool under vacuum.

^{1}H, ^{13}C, ^{19}F, and ^{109}Ag NMR spectra were obtained at the Georgia Institute of Technology NMR Center using a Bruker DSX 400 MHz spectrometer or a Varian Vx 400 MHz spectrometer. ^{1}H and ^{13}C NMR chemical shifts were referenced with respect to solvent signals and are reported relative to tetramethylsilane. ^{109}Ag NMR chemical shifts were referenced with respect to an external solution of 4.00 M silver nitrate (Alfa-Aesar) in deuterium oxide (defined as δ 0 ppm). ^{19}F NMR chemical shifts were referenced to

external neat hexafluorobenzene (Alfa-Aesar, δ −164.90 ppm) and are reported with respect to trichlorofluoromethane.

Infrared spectra were collected using microcrystalline samples on a Bruker Alpha-P infrared spectrometer equipped with an attenuated total reflection (ATR) attachment. Samples were exposed to air as briefly as possible prior to data collection.

Elemental analyses were performed by Atlantic Microlab in Norcross, Georgia.

6.4.2 Methods and Materials

Dichloromethane (BDH), diethyl ether (EMD Millipore Omnisolv), hexanes (EMD Millipore Omnisolv), and THF (EMD Millipore Omnisolv) were sparged with argon for 30 minutes prior to first use and dried over 3 Å molecular sieves (1/16", Alfa-Aesar). Anhydrous benzene (EMD Millipore Drisolv) and anhydrous pentane (EMD Millipore Drisolv), were stored over 3Å molecular sieves. Dichloromethane-d_2 (Cambridge Isotope Labs) was dried over calcium hydride overnight, vacuum-transferred to an oven-dried sealable flask, and degassed by successive freeze-pump-thaw cycles. Tetrahydrofuran-d_8 (Cambridge Isotope Labs) and benzene-d_6 (Cambridge Isotope Labs) were dried over sodium benzophenone ketyl, vacuum-transferred to an oven-dried sealable flask, and degassed by successive freeze-pump-thaw cycles. Deuterium oxide (Cambridge Isotope Labs) was used as received.

Carbon dioxide (NexAir) was passed through phosphorus pentoxide (Sigma-Aldrich) to ensure dryness. Phenylacetylene (Sigma-Aldrich) and (trifluoromethyl)trimethylsilane (Sigma-Aldrich) were dried by passing through activated alumina. Diethylzinc (Acros, 1M in hexanes), 4,4′-dimethylbiphenyl (Sigma-Aldrich), diphenylzinc (Strem), methylmagnesium bromide (Strem, 3M in diethyl ether), and

vinylmagnesium bromide (Sigma-Aldrich, 0.70 M in THF) were used as received. Compounds **3a**,[39,44] **2**,[45] **5a**,[39] and **4**[39] were prepared according to published procedures.

6.4.2.1 (5Dipp)AgEt (**16**)

A solution of diethylzinc (1.0 M in hexanes, 0.21 mL, 0.21 mmol) was added dropwise to a solution of **3a** (200 mg, 0.350 mmol) in THF (2 mL). The solution was stirred for 10 minutes, and then hexanes (15 mL) was added, causing the product to slowly crystallize. The crystals were allowed to grow for 3 days at –35˚C. The precipitate was collected on a fritted glass filter by vacuum filtration, washed with hexanes (3 × 2 mL), and dried *in vacuo* for 30 minutes, affording **16** as a white powder (111 mg, 0.194 mmol, 55%). Compound **16** hydrolyzes readily in the presence of atmospheric moisture. ^{1}H NMR (400 MHz, THF-d_8): δ (ppm) 7.34 (mult, 2H, *para*-C*H*), 7.24 (mult, 4H, *meta*-C*H*), 3.99 (s, 4H, NCH_2), 3.19 (sept, J = 6.9 Hz, 4H, CH(CH_3)$_2$), 1.38 (d, J = 6.9 Hz, 12H, CH(CH_3)$_2$), 1.32 (d, J = 6.9 Hz, 12H, CH(CH_3)$_2$), 0.89 (app dtd, ^{3}J(^{1}H-^{109}Ag) = 12.1 Hz, ^{3}J(^{1}H-^{107}Ag) = 10.7 Hz, ^{3}J(^{1}H-^{1}H) = 8.0 Hz, 3H, CH$_2$CH_3), –0.25 (app dqd, ^{2}J(^{1}H-^{109}Ag) = 12.8 Hz, ^{2}J(^{1}H-^{107}Ag) = 11.4 Hz, ^{3}J(^{1}H-^{1}H) = 8.0 Hz, 2H, CH_2CH$_3$). ^{13}C{^{1}H} NMR (100 MHz, THF-d_8): δ (ppm) 214.6 (app dd, J(^{13}C-^{109}Ag) = 115 Hz, J(^{13}C-^{107}Ag) = 100 Hz, N*C*Ag), 147.5 (*ortho*-*C*), 136.5 (*ipso*-*C*), 129.7 (*para*-*C*), 124.6 (*meta*-*C*), 54.4 (d, J(^{13}C-$^{107/109}$Ag) = 4 Hz, N*C*H$_2$), 29.4 (*C*H(CH$_3$)$_2$), 25.4 (CH(*C*H$_3$)$_2$), 24.0 (CH(*C*H$_3$)$_2$), 16.9 (d, J(^{13}C-Ag) = 4 Hz, CH$_2$*C*H$_3$), 1.4 (app dd, J(^{13}C-^{109}Ag) = 149 Hz, J(^{13}C-^{107}Ag) = 129 Hz, *C*H$_2$CH$_3$). ^{109}Ag NMR (18.6 MHz, THF-d_8): δ (ppm) 790.3 (sextet, J (^{109}Ag-^{1}H) = 12.5 Hz). IR: ν (cm^{-1}) 2961, 2931, 2837, 1490, 1463, 1275, 1099, 1049 (s), 804, 758. Elemental analysis calculated for $C_{29}H_{43}N_2Ag$: C, 66.03; H, 8.05; N, 5.31. Found: C, 65.85; H, 8.21; N, 5.17.

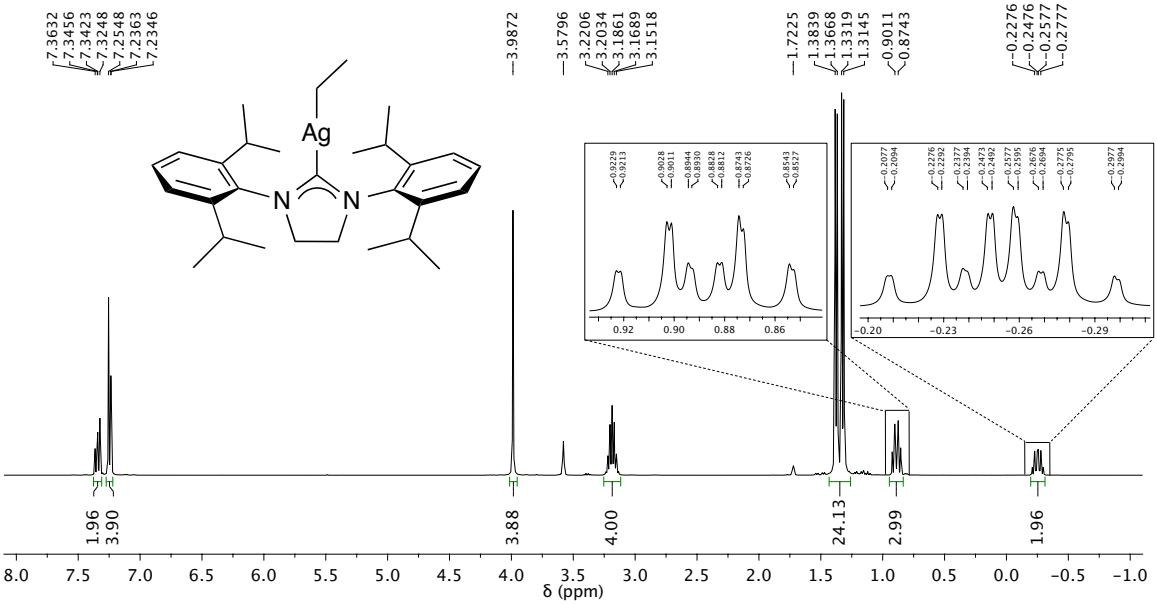

Figure 6.8. ^{1}H NMR (400 MHz, THF-d_8) spectrum of (5Dipp)AgEt (**16**).

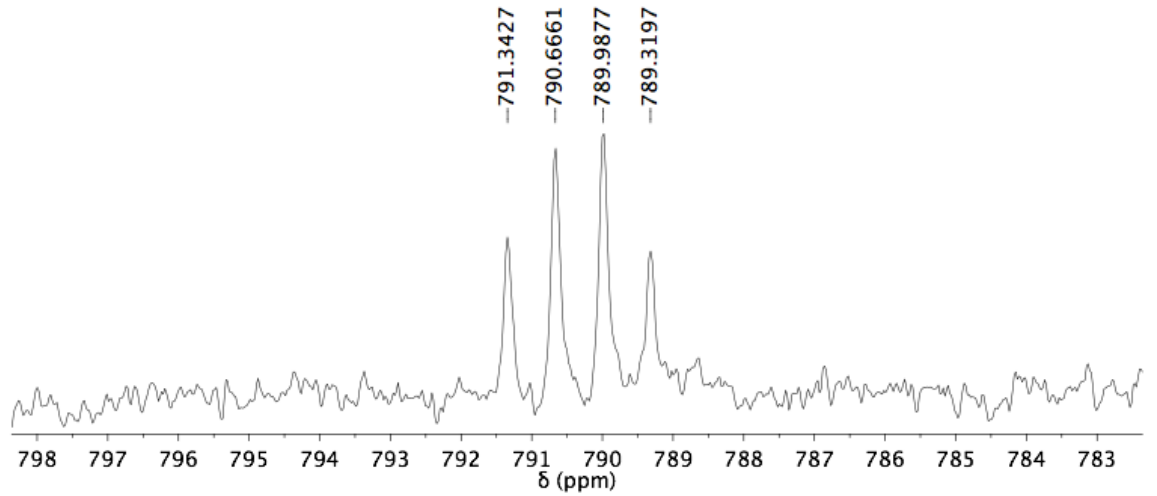

Figure 6.9. ^{109}Ag NMR (18.6 MHz, THF-d_8) signal of (5Dipp)AgEt (**16**). $^{2}J(^{109}\text{Ag}–^{1}\text{H}) \approx {}^{3}J(^{109}\text{Ag}–^{1}\text{H}) \approx 12.5$ Hz. The outermost peaks of the sextet are not resolved from noise, but the relative intensities of the four inner peaks are consistent with a sextet (1:5:10:10:5:1) rather than a quartet (1:3:3:1). Compare to the quartet ^{109}Ag NMR signal of **17** in Figure S5.

6.4.2.2 (5Dipp)Ag(CH_3) (**17**)

A solution of methylmagnesium bromide (3.0 M in THF, 0.30 mL, 0.90 mmol) was added to a suspension of **2** (400 mg, 0.75 mmol) in THF (2 mL). The mixture was stirred until it became clear, less than 5 minutes. Dioxane (18 mL) was added and the mixture was stirred for 16 h, inducing precipitation of a magnesium halides as a white powder, which was removed by filtration through Celite. Volatiles were removed from the filtrate *in vacuo*, and the product was extracted from the residue with CH_2Cl_2. The extract was filtered through Celite, the solvent was removed *in vacuo*, and the residue was dried *in vacuo* for 2 h, affording **17** as a white powder (341 mg, 0.66 mmol, 88%). Diffraction quality crystals were grown by diffusion of pentane vapor into a solution of **17** in CH_2Cl_2 at –35˚C over 3 days. Compound **17** hydrolyzes readily in the presence of atmospheric moisture. ^{1}H NMR (400 MHz, CD_2Cl_2): δ (ppm) 7.45 (t, J = 7.8 Hz, 2H, *para*-C*H*), 7.29 (d, J = 7.8 Hz, 4H, *meta*-C*H*), 3.99 (s, 4H, NCH_2), 3.13 (sept, J = 6.9 Hz, 4H, C*H*(CH_3)$_2$), 1.37 (d, J = 6.9 Hz, 12H, CH(CH_3)$_2$), 1.35 (d, J = 6.9 Hz, 12H, CH(CH_3)$_2$), –1.38 (d, J(^{1}H-Ag) = 10 Hz, 3H, AgCH_3). ^{13}C{^{1}H} NMR (100 MHz, CD_2Cl_2): δ (ppm) 213.4 (app dd, J(^{13}C-^{109}Ag) = 129 Hz, J(^{13}C-^{107}Ag) = 111 Hz, N*C*Ag), 147.4 (*ortho*-*C*), 135.7 (*ipso*-*C*), 129.6, (*para*-*C*), 124.6 (*meta*-*C*), 54.1 (d, J(^{13}C-$^{107/109}$Ag) = 5 Hz, N*C*H_2), 29.2 (*C*H(CH_3)$_2$), 25.3 (CH(*C*H_3)$_2$), 24.1 (CH(*C*H_3)$_2$), –15.7 (app dd, J(^{13}C-^{109}Ag) = 138 Hz, J(^{13}C-^{107}Ag) = 120 Hz, Ag*C*H_3). ^{109}Ag NMR (18.6 MHz, CD_2Cl_2): δ (ppm) 842.1 (q, J(^{109}Ag-^{1}H) = 11.2 Hz). IR: ν (cm^{-1}) 2962, 2926, 2870, 1481, 1467, 1457, 1328, 1265, 1258, 809, 763. Elemental analysis calculated for $C_{28}H_{41}N_2Ag$: C, 65.49; H, 8.05; N, 5.46. Found: C, 65.73; H, 7.89; N, 5.59.

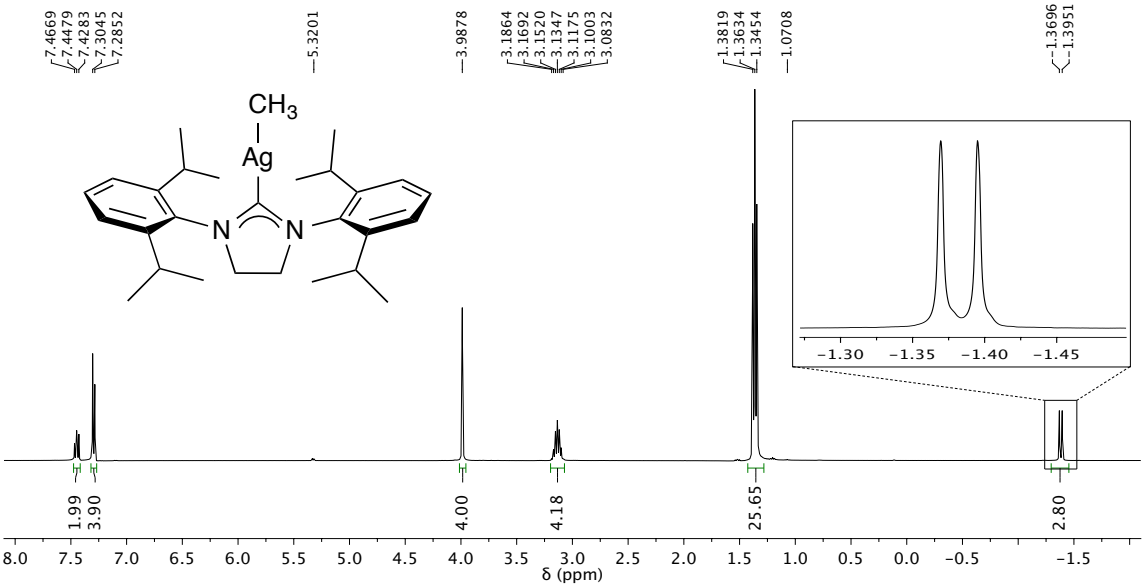

Figure 6.10. ^{1}H NMR (400 MHz, CD_2Cl_2) spectrum of (5Dipp)AgMe (**17**).

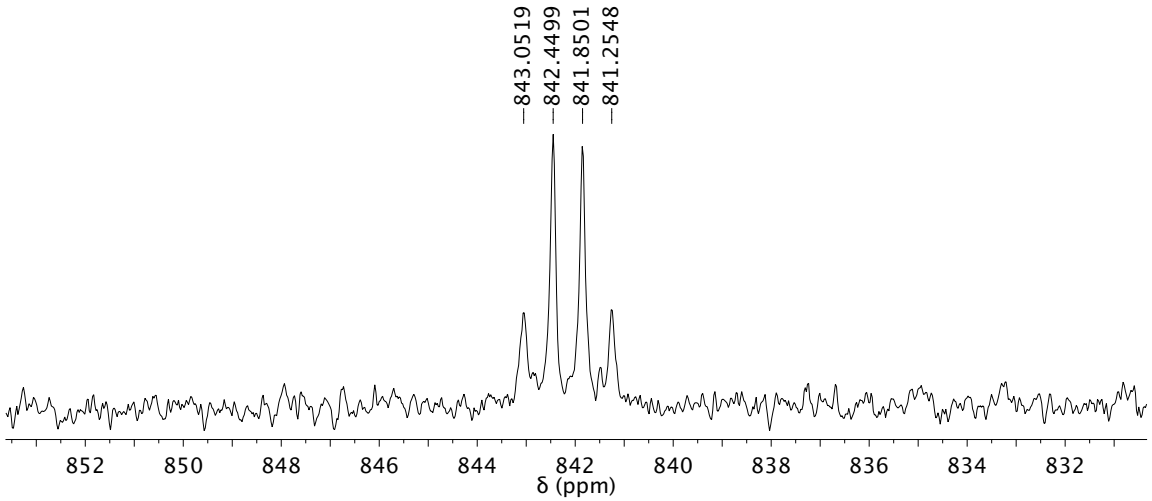

Figure 6.11. ^{109}Ag NMR (18.6 MHz, CD_2Cl_2) spectrum of (5Dipp)AgMe (**17**). $^{2}J(^{109}Ag–^{1}H)$ = 11.2 Hz. Note the relative peak intensities are consistent with a quartet (1:3:3:1) in contrast to the pseudo-sextet ^{109}Ag NMR signal of (5Dipp)Ag(CH_2CH_3) in Figure S3.

6.4.2.3 (5Dipp)Ag(CCPh) (**18**)

Phenylacetylene (0.047 mL, 0.42 mmol) was added to a solution of **3a** (200 mg, 0.350 mmol) in THF (2 mL). The solution was stirred for 10 minutes, and then hexanes (15 mL) was added, causing the product to slowly crystallize. The crystals were allowed

to grow for 3 days at –35˚C. The precipitate was collected on a fritted glass filter by vacuum filtration, washed with hexanes (3 × 2 mL), and dried *in vacuo* for 30 minutes, affording **18** as a white powder (128 g, 0.214 mmol, 61%). Compound **18** is air- and moisture-stable in the solid state and in solution. ^{1}H NMR (400 MHz, CD_2Cl_2): δ (ppm) 7.50 (t, *J* = 7.8 Hz, 2H, Dipp-*para*-C*H*), 7.33 (d, *J* = 7.8 Hz, 4H, Dipp-*meta*-C*H*), 7.19 (d, *J* = 7 Hz, 2H, CCPh-*ortho*-C*H*), 7.11 (t; *J* = 7 Hz; 2H; CCPh-*meta*-C*H*), 7.19 (t, *J* = 7 Hz, 1H, CCPh-*para*-C*H*), 4.05 (s, 4H, NCH_2), 3.11 (sept, *J* = 6.9 Hz, 4H, C*H*$(CH_3)_2$), 1.39 (d, *J* = 6.9 Hz, 12H, CH(CH_3)$_2$), 1.38 (d, *J* = 6.9 Hz, 12H, CH(CH_3)$_2$). ^{13}C{^{1}H} NMR (100 MHz, CD_2Cl_2): δ (ppm) 210.1 (app dd, *J*(^{13}C-^{109}Ag) = 181 Hz, *J*(^{13}C-^{107}Ag) = 156 Hz, N*C*Ag), 147.2 (Dipp-*ortho*-*C*), 135.2 (Dipp-*ipso*-*C*), 131.7 (CCPh-*ortho*-*C*), 130.1, (Dipp-*para*-*C*), 128.0 (CCPh-*meta*-*C*), 127.4 (CCPh-*para*-*C*), 125.7 (CCPh-ipso-*C*), 124.9 (Dipp-*meta*-*C*), 122.3 (app dd, *J*(^{13}C-^{109}Ag) = 224 Hz, *J*(^{13}C-^{107}Ag) = 194 Hz, *C*CPh) 106.5 (*J*(^{13}C-$^{107/109}$Ag) = 54 Hz, C*C*Ph), 54.3 (d, *J*(^{13}C-$^{107/109}$Ag) = 6 Hz, N*C*H_2), 29.2 (*C*H$(CH_3)_2$), 25.6 (CH(*C*H_3)$_2$), 24.1 (CH(*C*H_3)$_2$). IR: ν (cm^{-1}) 3076, 2963, 2929, 2871, 2093 (C≡C), 1597, 1486, 1464, 1270, 1059, 806, 758, 697, 622, 548, 528, 445. Elemental analysis calculated for $C_{35}H_{43}N_2Ag$: C, 70.11; H, 7.23; N, 4.67. Found: C, 69.88; H, 7.24; N, 4.70.

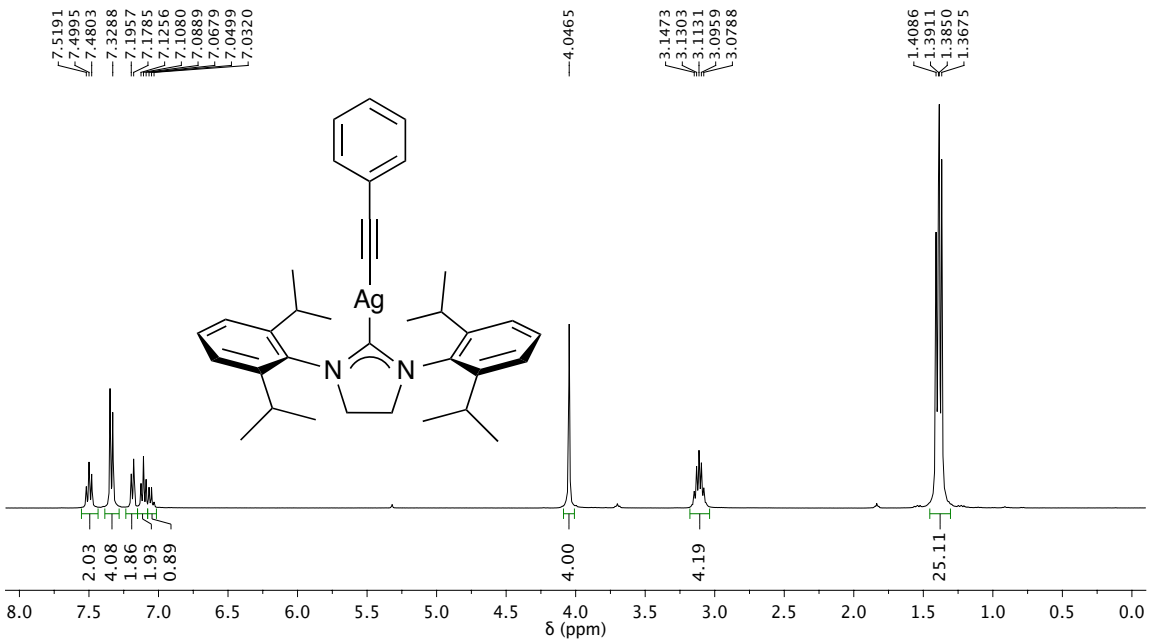

Figure 6.12. ^{1}H NMR (400 MHz, CD_2Cl_2) spectrum of (5Dipp)Ag(CCPh) (**18**).

6.4.2.4 (5Dipp)Ag(CF_3) (**19**)

(Trifluoromethyl)trimethylsilane (0.155 mL, 1.05 mmol) was added to a solution of **3a** (500 mg, 0.875 mmol) in THF (4 mL). The mixture was stirred for 30 min, and then hexanes (15 mL) was added, causing the product to precipitate. The precipitate was collected on a fritted glass filter by vacuum filtration, washed with hexanes (3 × 2 mL), and dried *in vacuo* for 30 minutes, affording **19** as a white powder (451 mg, 0.795 mmol, 91%). Compound **19** hydrolyzes readily in the presence of atmospheric moisture. ^{1}H NMR (400 MHz, CD_2Cl_2): δ (ppm) 7.46 (t, J = 7.8 Hz, 2H, *para*-C*H*), 7.30 (d, J = 7.8 Hz, 4H, *meta*-C*H*), 4.06 (s, 4H, NCH_2), 3.08 (sept, J = 6.9 Hz, 4H, C*H*(CH_3)$_2$), 1.35 (d, J = 6.9 Hz, 12H, CH(CH_3)$_2$), 1.33 (d, J = 6.9 Hz, 12H, CH(CH_3)$_2$. ^{13}C{^{1}H} NMR (100 MHz, CD_2Cl_2): δ (ppm) 209.6 (app ddq, J(^{13}C-^{109}Ag) = 175 Hz, J(^{13}C-^{107}Ag) = 152 Hz, J(^{13}C-^{19}F) = 5 Hz, N*C*Ag), 154.0 (app qdd, J(^{13}C-^{19}F) = 368 Hz, J(^{13}C-^{109}Ag) = 314 Hz, J(^{13}C-^{107}Ag) = 272 Hz, *C*F_3), 147.2 (Dipp-*ortho*-*C*), 134.9 (Dipp-*ipso*-*C*), 130.2, (Dipp-

para-*C*), 124.9 (Dipp-*meta*-*C*), 54.4 (d, $J(^{13}C\text{-}^{107/109}Ag)$ = 5 Hz, N*C*H_2), 29.2 (*C*H(CH_3)$_2$), 25.3 (CH(*C*H_3)$_2$), 24.1 (CH(*C*H_3)$_2$). ^{19}F NMR (376 MHz, CD_2Cl_2): δ (ppm) 251.3 (app dd, $J(^{107}Ag\text{-}^{19}F)$ = 92 Hz, $J(^{109}Ag\text{-}^{19}F)$ = 106 Hz). ^{109}Ag NMR (18.6 MHz, CD_2Cl_2): δ (ppm) 601.3 (q, $J(^{109}Ag\text{-}^{19}F)$ = 106 Hz). IR: ν (cm^{-1}) 2964, 2926, 2869, 1488, 1469, 1272, 1110, 938 (s), 807, 762, 446. Elemental analysis calculated for $C_{28}H_{38}N_2AgF_3$: C, 59.26; H, 6.75; N, 4.94. Found: C, 59.11; H, 6.78; N, 5.00.

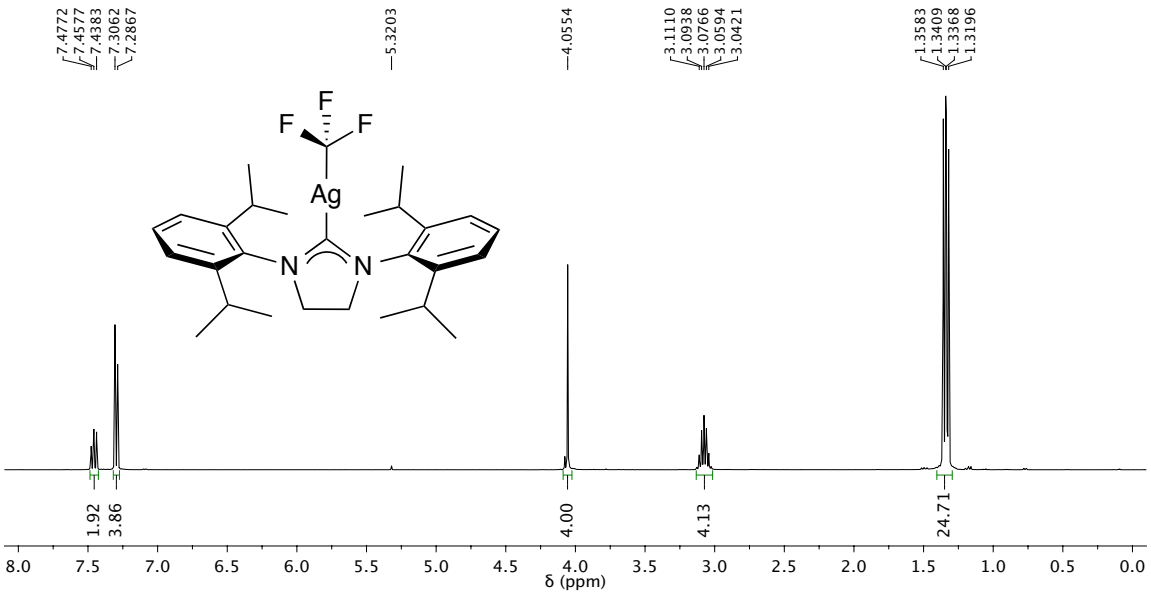

Figure 6.13. ^1H NMR (400 MHz, CD_2Cl_2) spectrum of (5Dipp)Ag(CF_3) (**19**).

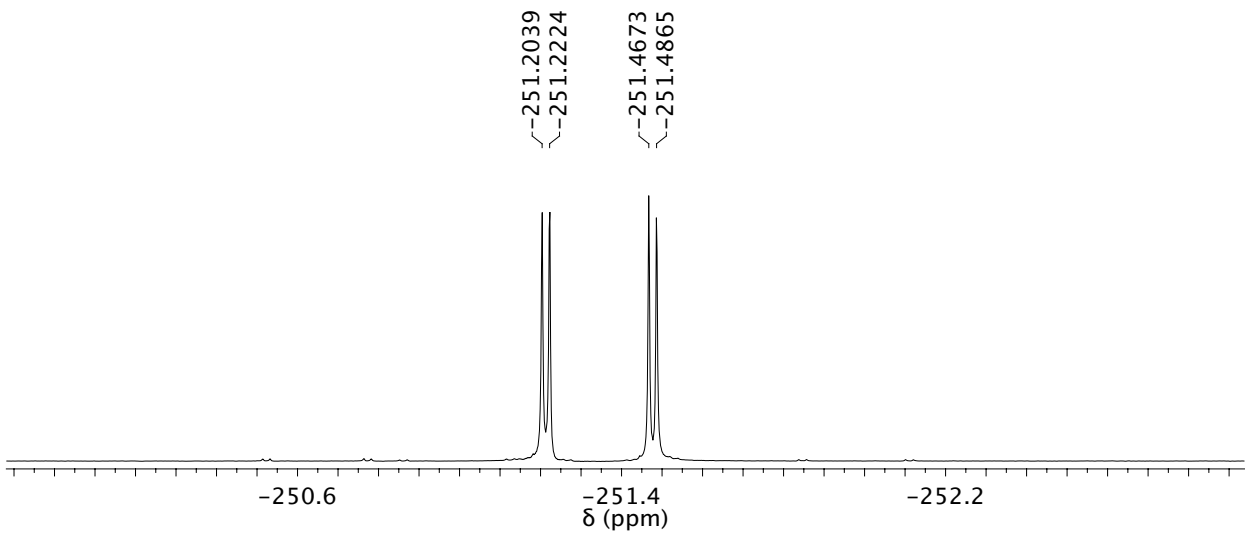

Figure 6.14. ^{19}F NMR (376 MHz, CD_2Cl_2) spectrum of (5Dipp)Ag(CF_3) (**19**). $J(^{107}Ag\text{-}^{19}F)$ = 92 Hz, $J(^{109}Ag\text{-}^{19}F)$ = 106 Hz.

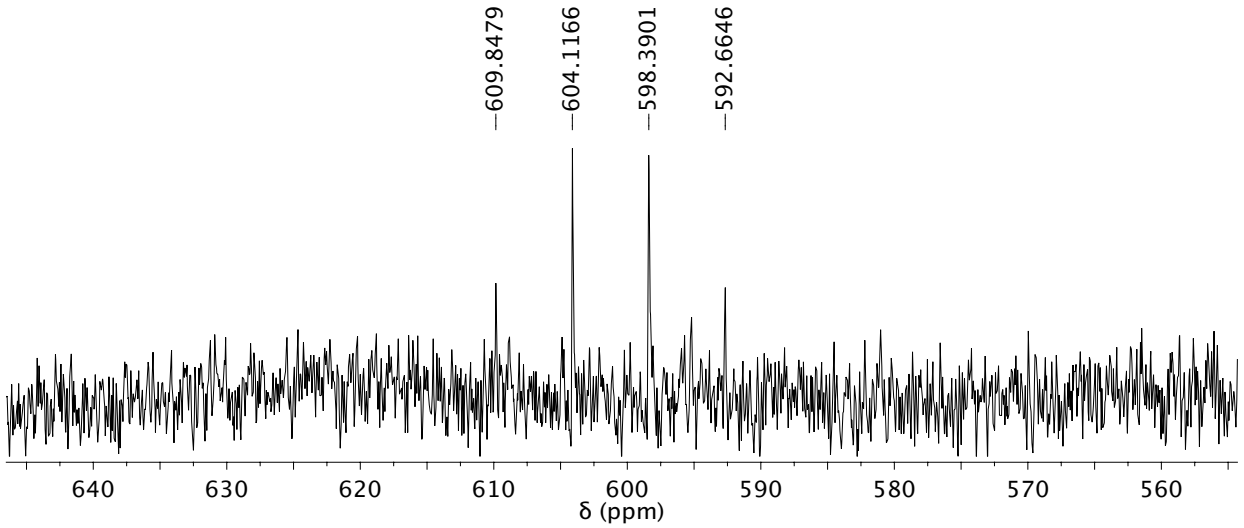

Figure 6.15. ^{109}Ag NMR (18.6 MHz, CD_2Cl_2) spectrum of (5Dipp)Ag(CF_3) (**19**). $J(^{109}Ag–^{19}F)$ = 107 Hz.

6.4.2.5 {[(5Dipp)Ag]$_2$(μ-Et)}$^+BF_4^-$ (**20**)

A solution of diethylzinc (1.0 M in hexanes, 0.10 mL, 0.10 mmol) was added dropwise to a solution of **5a** (200 mg, 0.173 mmol) in THF (2 mL). The solution was stirred for 10 minutes, and then hexanes (15 mL) was added with stirring, causing the

formation of a white precipitate. The precipitate was collected on a fritted glass filter by vacuum filtration, washed with hexanes (3 × 2 mL), and dried *in vacuo* for 30 minutes, affording **20** as a white powder (171 mg, 0.154 mmol, 90%). Diffraction-quality crystals were grown by diffusion of Et_2O vapor into a solution of **20** in CH_2Cl_2 at –35˚C for 48 hours. Compound **20** hydrolyzes readily in the presence of atmospheric moisture. ^{1}H NMR (400 MHz, CD_2Cl_2): δ (ppm) 7.40 (t, J = 7.8 Hz, 4H, *para*-C*H*), 7.18 (d, J = 7.8 Hz, 8H, *meta*-C*H*), 4.02 (s, 8H, NCH_2), 2.92 (sept, J = 6.9 Hz, 8H, CH(CH_3)$_2$), 1.28 (d, J = 6.9 Hz, 24H, CH(CH_3)$_2$), 1.01 (d, J = 6.9 Hz, 24H, CH(CH_3)$_2$), 0.64 (app sext, ^2J(^{1}H-^{109}Ag) ≈ ^2J(^{1}H-^{107}Ag) ≈ ^3J(^{1}H-^{1}H) ≈ 7 Hz, 2H, CH_2CH$_3$), 0.17 (app quin, ^3J(^{1}H-^{109}Ag) ≈ ^3J(^{1}H-^{107}Ag) ≈ ^3J(^{1}H-^{1}H) ≈ 7 Hz, 3H, CH$_2$CH_3). ^{13}C{^{1}H} NMR (100 MHz, CD_2Cl_2): δ (ppm) 208.8 (mult, N*C*Ag), 146.9 (*ortho*-*C*), 135.0 (*ipso*-*C*), 130.0 (*para*-*C*), 124.8 (*meta*-*C*), 54.4 (app 1:1:1 t, J(^{13}C-$^{107/109}$Ag) = 6 Hz, N*C*H$_2$), 28.9 (*C*H(CH_3)$_2$), 25.3 (CH(*C*H$_3$)$_2$), 23.9 (CH(*C*H$_3$)$_2$), 13.4 (t, J(^{13}C-Ag) = 2 Hz, CH$_2$*C*H$_3$), –1.9 (app tt, J(^{13}C-^{109}Ag) = 74 Hz, J(^{13}C-^{107}Ag) = 64 Hz, *C*H$_2$CH$_3$). ^{109}Ag NMR (18.6 MHz, CD_2Cl_2): δ (ppm) 681.2 (app t of sext, ^3J(^{1}H-^{109}Ag) ≈ ^2J(^{1}H-^{109}Ag) ≈ 7 Hz, J(^{109}Ag-^{107}Ag = 55 Hz). ^{109}Ag{^{1}H} NMR (18.6 MHz, CD_2Cl_2): δ (ppm) 681.2 (app t, J(^{109}Ag-^{107}Ag = 55 Hz). IR: ν (cm^{-1}) 2957, 2929, 2871, 1490, 1462, 1275, 1099, 1056 (s), 803, 756. Elemental analysis calculated for $C_{56}H_{81}N_4Ag_2BF_4$: C, 60.44; H, 7.34; N, 5.03. Found: C, 60.47; H, 7.33; N, 4.91.

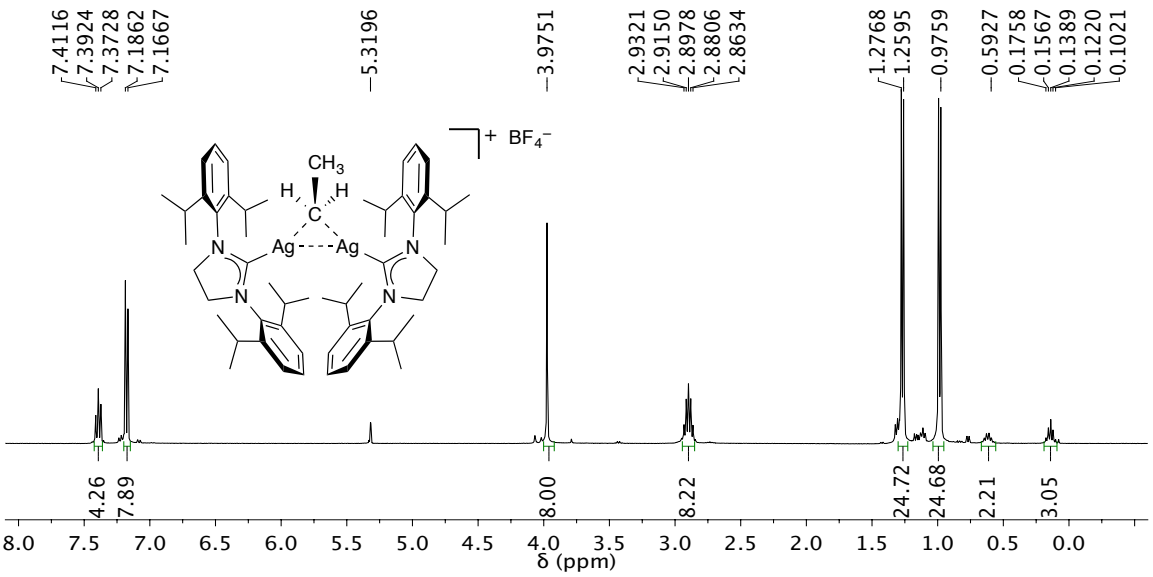

Figure 6.16. ^{1}H NMR (400 MHz, CD_2Cl_2) spectrum of $\{[(5Dipp)Ag]_2(\mu\text{-}Et)\}^+$ (**20**).

6.4.2.6 $\{[(5Dipp)Ag]_2(\mu\text{-}Ph)\}^+BF_4^-$ (**21**)

Diphenylzinc (23 mg, 0.10 mmol) was added to a solution of **5a** (200 mg, 0.173 mmol) in THF (2 mL). The solution was stirred for 10 minutes, and then hexanes (15 mL) was added with stirring, causing the formation of a white precipitate. The precipitate was collected on a fritted glass filter by vacuum filtration, washed with hexanes (3 × 2 mL), and dried *in vacuo* for 30 minutes, affording **21** as a white powder (173 mg, 0.149 mmol, 86%). Diffraction-quality crystals were grown by diffusion of pentane vapor into a solution of **21** in THF at –35˚C for 48 hours. Compound **21** hydrolyzes readily in the presence of atmospheric moisture. ^{1}H NMR (400 MHz, CD_2Cl_2): δ (ppm) 7.38 (t, J = 7.8 Hz, 4H, Dipp-*para*-C*H*), 7.12 (d, J = 7.8 Hz, 8H, Dipp-*meta*-C*H*), 6.99 (t, J = 7.5 Hz, 1H, μ-Ph-*para*-C*H*), 6.69 (t, J = 7.5 Hz, 2H, μ-Ph-*meta*-C*H*), 6.14 (mult, 2H, μ-Ph-*ortho*-C*H*), 3.96 (s, 8H, NCH_2), 2.82 (sept, J = 6.9 Hz, 8H, CH(CH_3)$_2$), 1.22 (d, J = 6.9 Hz, 24H, CH(CH_3)$_2$), 0.84 (d, J = 6.9 Hz, 24H, CH(CH_3)$_2$). ^{13}C{^{1}H} NMR (100 MHz,

CD_2Cl_2): δ (ppm) 208.9 (mult, N*C*Ag), 146.9 (Dipp-*ortho*-*C*), 144.74 (t, $J(^{13}C\text{-Ag})$ = 3 Hz, μ-Ph-*C*) 136.0 (app tt, $J(^{13}C\text{-}^{109}Ag)$ = 94 Hz, $J(^{13}C\text{-}^{107}Ag)$ = 81 Hz, μ-Ph-*ipso*-*C*), 134.7 (Dipp-*ipso*-*C*), 131.5 (μ-Ph-*para*-*C*), 130.0, (Dipp-*para*-*C*), 127.7 (t, $J(^{13}C\text{-Ag})$ = 3 Hz, μ-Ph-*C*), 124.8 (Dipp-*meta*-*C*), 54.3 (app 1:1:1 t, $J(^{13}C\text{-}^{107/109}Ag)$ = 3 Hz, N*C*H_2), 28.9 (*C*H$(CH_3)_2$), 25.1 (CH(*C*$H_3)_2$), 24.0 (CH(*C*$H_3)_2$). ^{109}Ag NMR (18.6 MHz, CD_2Cl_2): δ (ppm) 728.4 (app t, $J(^{109}Ag\text{-}^{107}Ag)$ = 76 Hz). IR: ν (cm^{-1}) 2956, 2929, 2872, 1490, 1460, 1273, 1098, 1051 (s), 804, 769, 758. Elemental analysis calculated for $C_{31}H_{47}N_2AgO$: C, 62.08; H, 7.03; N, 4.83. Found: C, 62.03; H, 6.91; N, 4.81.

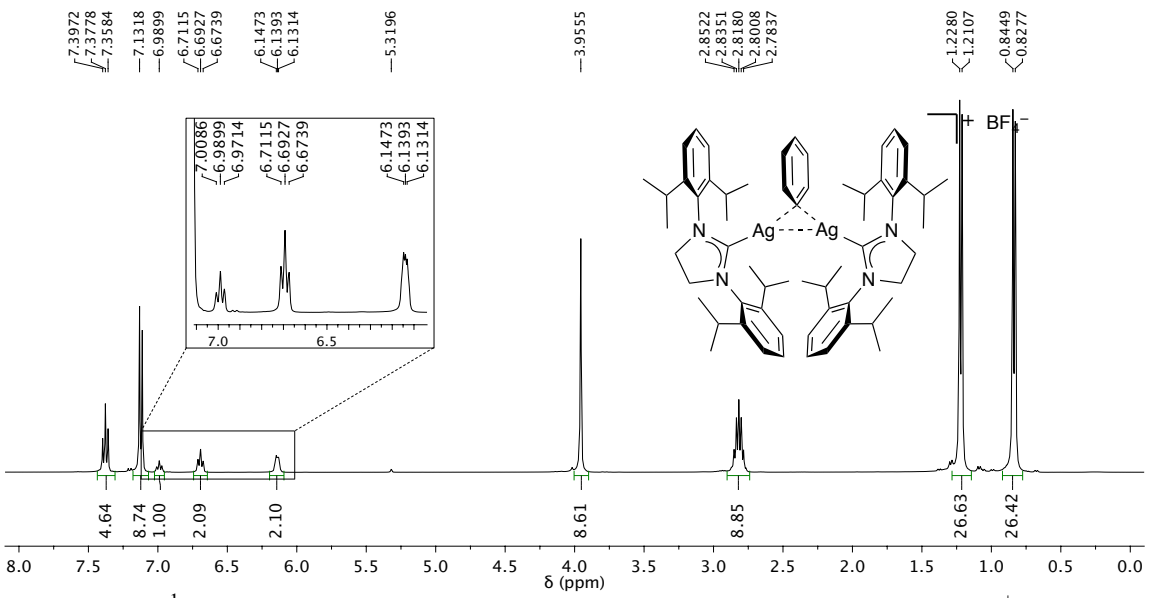

Figure 6.17. ^{1}H NMR (400 MHz, CD_2Cl_2) spectrum of $\{[(5Dipp)Ag]_2(\mu\text{-Ph})\}^+$ (**21**).

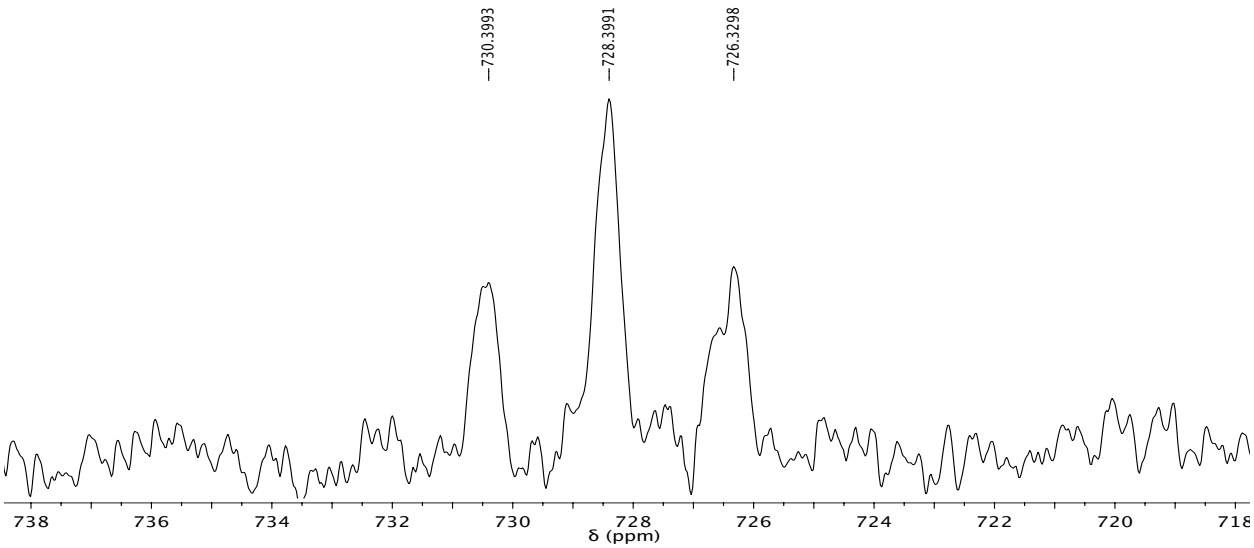

Figure 6.18. ^{109}Ag NMR (18.6 MHz, THF-d_8) signal of $\{[(5Dipp)Ag]_2(\mu\text{-Ph})\}^+$ (**21**). $J(^{109}Ag–^{107}Ag)$ = 76 Hz. ^{109}Ag–^{1}H coupling is not observed.

6.4.2.7 $\{[(5Dipp)Ag]_2(\mu\text{-}CH_3)\}^+OTf^-$ (**22**)

A solution of **17** (50 mg, 0.097 mmol) in THF (2 mL) and a solution of **4** (63 mg, 0.097 mmol) in THF (2 mL) were chilled to –35˚C. The (5Dipp)Ag(OTf) solution was added to the solution of **12** dropwise with stirring. The mixture was allowed to warm to room temperature. After 15 min, the mixture was filtered to remove traces of a barely perceptible gray precipitate. Diethyl ether (15 mL) was added to the filtrate, causing the formation of a white precipitate, which was collected on a fritted glass filter by vacuum filtration, washed with diethyl ether (3 × 2 mL), and dried *in vacuo* for 2 h, affording the product as a white powder (94 mg, 0.081 mmol, 84%). Diffraction-quality crystals were grown by the diffusion of a layer of Et_2O into a CH_2Cl_2 solution of **22** at –35˚C over 3 days. Compound **22** hydrolyzes readily in the presence of atmospheric moisture. ^{1}H NMR (400 MHz, CD_2Cl_2): δ (ppm) 7.40 (t, J = 7.8 Hz, 4H, *para*-C*H*), 7.18 (d, J = 7.8 Hz, 8H, *meta*-C*H*), 3.98 (s, 8H, NCH_2), 2.89 (sept, J = 6.9 Hz, 8H, C$H(CH_3)_2$), 1.27 (d, J = 6.9

Hz, 24H, CH(CH_3)$_2$), 0.98 (d, J = 6.9 Hz, 24H, CH(CH_3)$_2$), –0.87 (s, 3H, AgCH_3). ^{13}C{^{1}H} NMR (100 MHz, CD_2Cl_2): δ (ppm) 208.4 (app dd, J(^{13}C-^{109}Ag) = 216 Hz, J(^{13}C-^{107}Ag) = 186 Hz, N*C*Ag), 146.9 (*ortho*-*C*), 134.8 (*ipso*-*C*), 130.1, (*para*-*C*), 124.9 (*meta*-*C*), 121.4 (q, J(^{13}C-^{19}F) = 319 Hz, O_3SCF_3), 54.4 (NCH_2), 28.9 (*C*H(CH$_3$)$_2$), 25.4 (CH(*C*H$_3$)$_2$), 23.9 (CH(*C*H$_3$)$_2$), –15.7 (dd, J(^{13}C-^{109}Ag) = 138 Hz, J(^{13}C-^{107}Ag) = 120 Hz, Ag*C*H$_3$), Ag_2CH_3 not detected. ^{109}Ag NMR (18.6 MHz, CD_2Cl_2): no signal observed. IR: ν (cm^{-1}) 2961, 2927, 2872, 1488, 1457, 1267 (s), 1149, 1031, 804, 759, 637 (s). Elemental analysis calculated for $C_{56}H_{79}N_4Ag_2F_3O_3S$: C, 57.93; H, 6.86; N, 4.83. Found: C, 58.14; H, 6.80; N, 4.89.

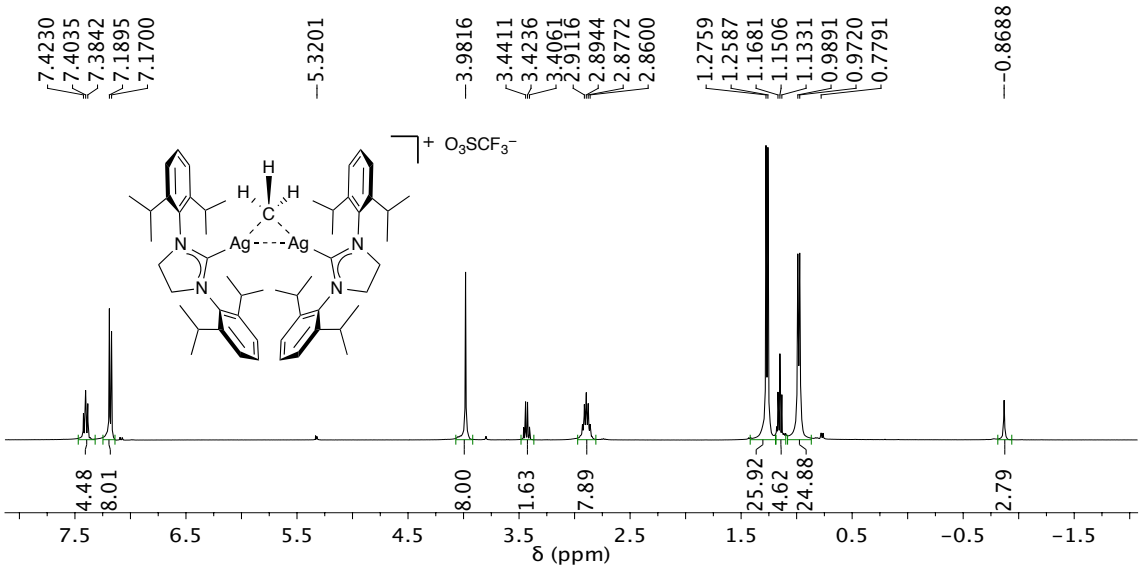

Figure 6.19. ^{1}H NMR (400 MHz, CD_2Cl_2) spectrum of {[(5Dipp)Ag]$_2$(μ-Me)}$^+$ (**22**). Diethyl ether (q, δ 3.41 ppm; t, δ 0.99 ppm) is present.

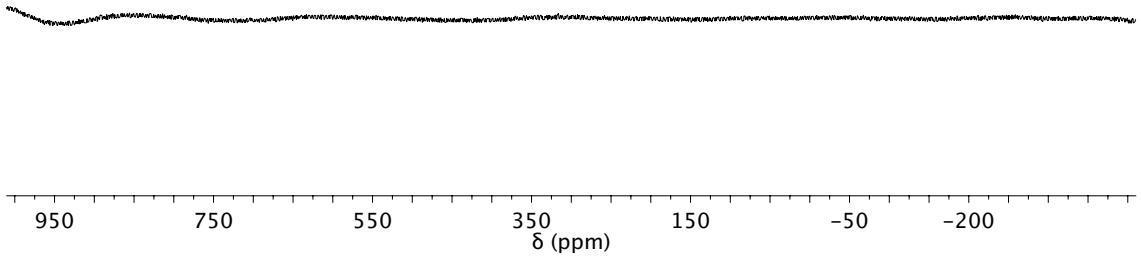

Figure 6.20. No signal is apparent in the ^{109}Ag NMR (18.6 MHz, THF-d_8) spectrum of $\{[(5Dipp)Ag]_2(\mu\text{-}Me)\}^+$ (**22**).

6.4.2.8 $\{[(5Dipp)Ag]_2(\mu\text{-}CCPh)\}^+BF_4^-$ (**23**)

Phenylacetylene (0.023 mL, 0.21 mmol) was added to a solution of **5a** (200 mg, 0.173 mmol) in THF (2 mL). The solution was stirred for 10 minutes, and then hexanes (15 mL) was added with stirring, causing the formation of a white precipitate. The precipitate was collected on a fritted glass filter by vacuum filtration, washed with hexanes (3 × 2 mL), and dried *in vacuo* for 30 minutes, affording the product as a white powder (188 mg, 0.159 mmol, 92%). Diffraction-quality crystals were grown by diffusion of pentane vapor into a solution of **23** in THF at –35˚C for 48 hours. Compound **23** is air- and moisture-stable in the solid state and in solution. ^{1}H NMR (400 MHz, CD_2Cl_2): δ (ppm) 7.40 (t, J = 7.8 Hz, 4H, Dipp-*para*-C*H*), 7.25 (t, J = 8 Hz, 1H, CCPh-*para*-C*H*), 7.19 (d, J = 8 Hz, 8H, Dipp-*meta*-C*H*), 7.12 (t; J = 7.2 Hz, 8 Hz; 2H; CCPh-*meta*-C*H*), 6.65 (d, J = 6.9 Hz, 2H, CCPh-*ortho*-C*H*), 4.03 (s, 8H, NCH_2), 2.96 (sept, J = 6.9 Hz, 8H, C*H*(CH_3)$_2$), 1.29 (d, J = 6.9 Hz, 24H, CH(CH_3)$_2$), 1.05 (d, J = 6.9 Hz, 24H, CH(CH_3)$_2$). ^{13}C{^{1}H} NMR (100 MHz, CD_2Cl_2): δ (ppm) 207.3 (app dd, J(^{13}C-^{109}Ag) =

233 Hz, $J(^{13}C\text{-}^{107}Ag)$ = 201 Hz, N*C*Ag), 147.0 (Dipp-*ortho*-*C*), 134.7 (Dipp-*ipso*-*C*), 132.9 (CCPh-*ortho*-*C*), 130.2, (Dipp-*para*-*C*), 129.3 (CCPh-*para*-*C*), 128.4 (CCPh-*meta*-*C*), 125.0 (CCPh-*ipso*-*C*) 124.8 (Dipp-*meta*-*C*), 121.3 (mult, *C*CPh), 98.5 (mult, *C*CPh) 54.4 (app 1:1:1 t, $J(^{13}C\text{-}^{107/109}Ag)$ = 4 Hz, N*C*H_2), 29.0 (*C*H$(CH_3)_2$), 25.5 (CH(*C*$H_3)_2$), 24.0 (CH(*C*$H_3)_2$). ^{109}Ag NMR (18.6 MHz, CD_2Cl_2): δ (ppm) 673.9 (app t, $J(^{109}Ag\text{-}^{107}Ag)$ = 18 Hz). IR: ν (cm^{-1}) 2961, 2930, 2871, 1487, 1459, 1272, 1048 (s), 804, 756, 443. Elemental analysis calculated for $C_{62}H_{81}N_4Ag_2BF_4$: C, 62.85; H, 6.89; N, 4.75. Found: C, 62.85; H, 6.96; N, 5.76.

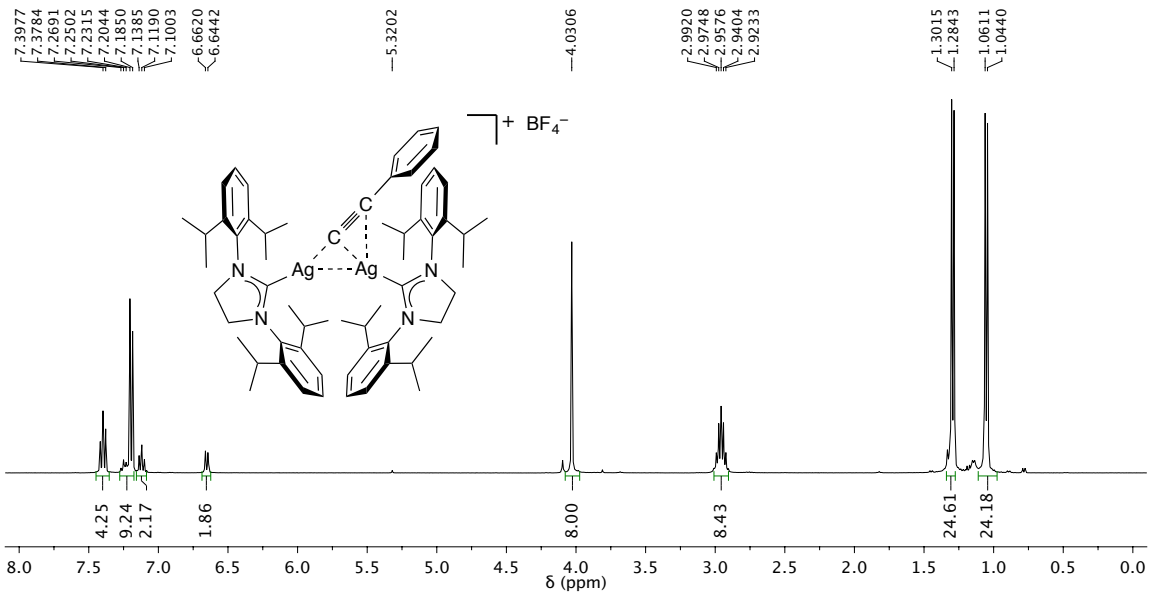

Figure 6.21. ^{1}H NMR (400 MHz, CD_2Cl_2) spectrum of $\{[(5Dipp)Ag]_2(\mu\text{-}CCPh)\}^+$ (**23**).

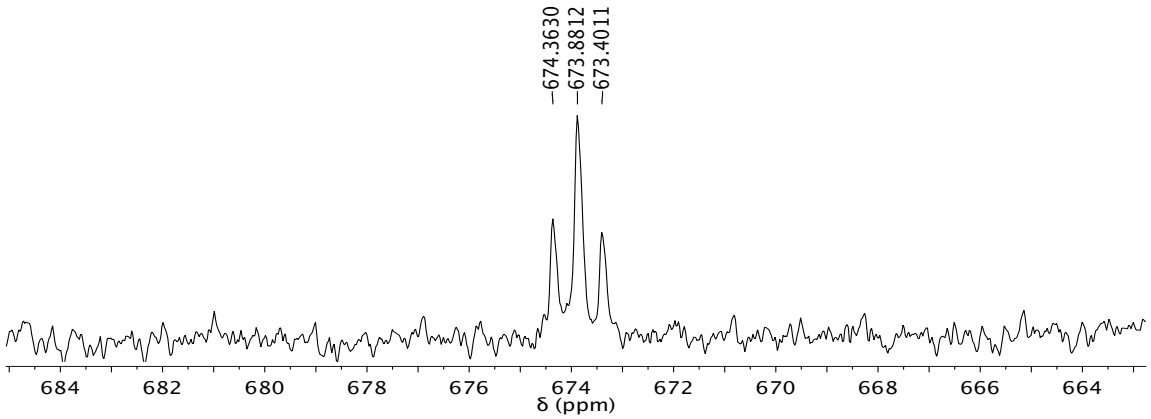

Figure 6.22. ^{109}Ag NMR (18.6 MHz, THF-d_8) signal of $\{[(5Dipp)Ag]_2(\mu\text{-}CCPh)\}^+$ (**23**). $J(^{109}Ag–^{107}Ag)$ = 18 Hz.

6.4.2.9 (5Dipp)Ag(O_2CEt) (**24**)

A solution of (5Dipp)AgEt (120 mg, 0.227 mmol) in CD_2Cl_2 (1.0 mL) in a J. Young NMR tube was degassed by two freeze-pump-thaw cycles, and the tube was backfilled with carbon dioxide (1.0 bar). After 16 h, the ^{1}H and ^{13}C NMR spectra of the product were recorded. The tube was opened to air and no more effort was made to maintain an inert atmosphere. The solution was transferred to a vial and the volatiles were removed *in vacuo*. The residue was dried for 4 h at 40˚C, affording **24** as a white powder (123 mg, 0.216 mmol, 95%). Compound **24** is air- and moisture-stable in the solid state and in solution. ^{1}H NMR (400 MHz, CD_2Cl_2): δ (ppm) 7.46 (t, J = 7.8 Hz, 2H, *para*-C*H*), 7.30 (d, J = 7.8 Hz, 4H, *meta*-C*H*), 4.08 (s, 4H, NCH_2), 3.09 (sept, J = 6.9 Hz, 4H, C*H*(CH_3)$_2$), 1.95 (q, J = 7.6 Hz, 2H, C$H_2$$CH_3$), 1.36 (d, J = 6.9 Hz, 12H, CH(CH_3)$_2$), 1.35 (d, J = 6.9 Hz, 12H, CH(CH_3)$_2$), 0.87 (t, J = 7.6 Hz, 3H, CH_2CH_3). ^{13}C{^{1}H} NMR (100 MHz, CD_2Cl_2): δ (ppm) 207.8 (app dd, $J(^{13}C\text{-}^{109}Ag)$ = 247 Hz, $J(^{13}C\text{-}^{107}Ag)$ = 205 Hz, N*C*Ag), 180.6 (O_2C) 147.2 (Dipp-*ortho*-*C*), 135.2 (Dipp-*ipso*-*C*), 130.1, (Dipp-*para*-*C*), 124.9 (Dipp-*meta*-*C*), 54.5 (d, $J(^{13}C\text{-}^{107/109}Ag)$ = 9 Hz, N*C*H_2), 29.4 (*C*$H_2$$CH_3$), 29.2

(*C*H(CH$_3$)$_2$), 25.4 (CH(*C*H$_3$)$_2$), 24.1 (CH(*C*H$_3$)$_2$) 11.1 (CH$_2$*C*H$_3$). IR: ν (cm^{-1}) 2965, 2920, 2868, 2850, 1727 (C=O), 1588, 1488, 1461, 1385, 1275, 1058, 805, 760. Elemental analysis calculated for $C_{30}H_{43}N_2AgO_2$: C, 63.04; H, 7.58; N, 4.90. Found: C, 62.77; H, 7.64; N, 4.86.

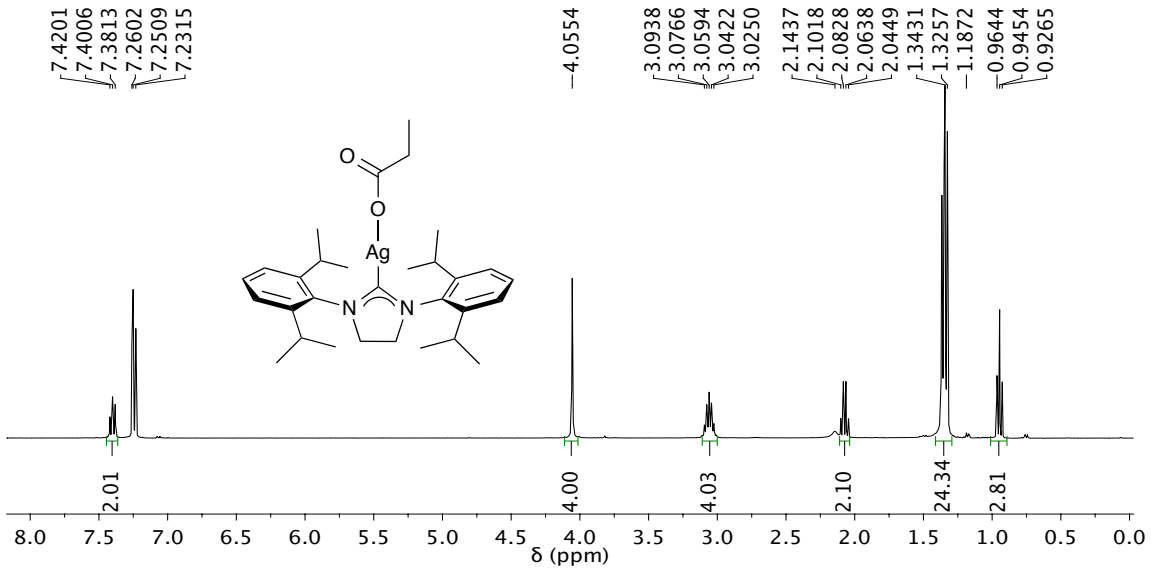

Figure 6.23. ^{1}H NMR (400 MHz, $CDCl_3$) spectrum of (5Dipp)Ag(O_2CEt) (**24**).

6.4.2.10 Reaction of Vinylmagnesium Bromide with (5Dipp)AgCl (**2**)

A solution of vinylmagnesium bromide (0.70 M in THF) was added to a suspension of **2** (30 mg, 0.056 mmol) in C_6D_6, resulting instantly in transiently clear solution from which elemental silver gradually precipitated. The ^{1}H NMR spectrum was recorded after 15 min (see Figure 6.24). The reaction was repeated with the addition of an internal standard of 4,4′-dimethylbiphenyl (10 mg, 0.056 mmol) in a sealed NMR tube, and the ^{1}H NMR spectrum was recorded after 24 h.

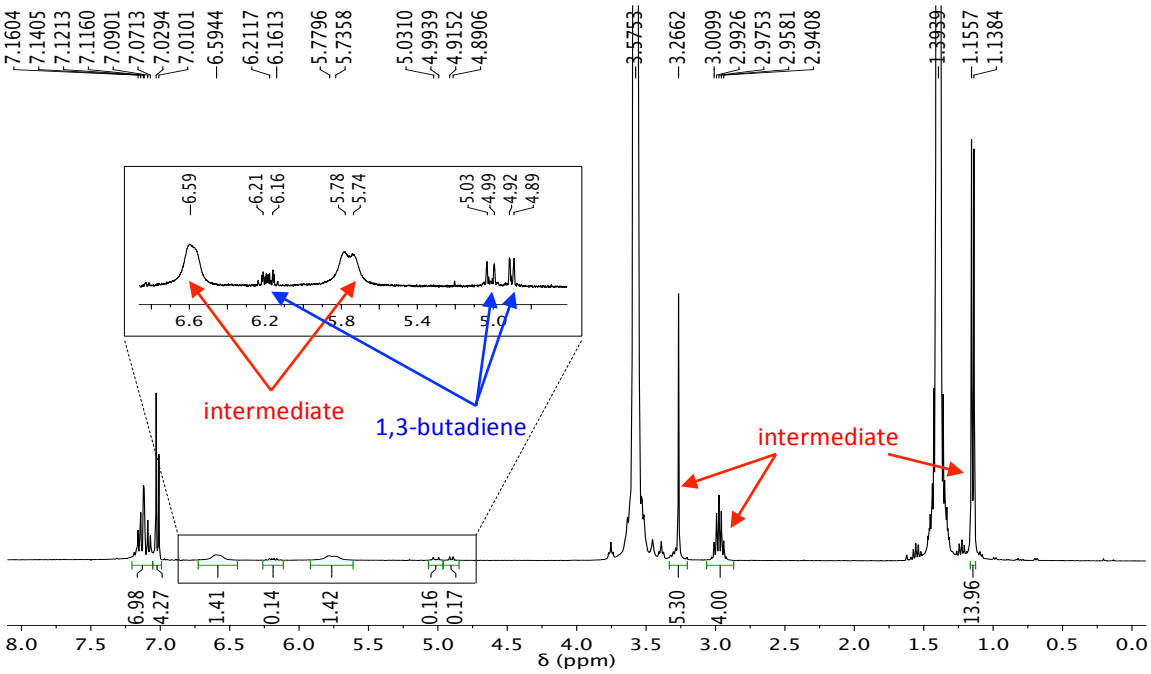

Figure 6.24. ^{1}H NMR (400 MHz, C_6D_6) spectrum recorded 15 min after the addition of vinylmagnesium bromide (0.70 M solution in THF) to a suspension of (5Dipp)AgCl (**2**) in C_6D_6. An intermediate benzene-soluble species gives way to 1,3-butadiene, free 5Dipp, and elemental silver.

6.4.2.11 Reaction of (5Dipp)Ag(CH_3) (**17**) with CO_2

Several crystals of 4,4′-dimethylbiphenyl (internal standard) were added to a solution of **17** (40 mg, 0.076 mmol) in THF-d_8 (1.0 mL) in a J. Young NMR tube. A preliminary ^{1}H NMR spectrum was recorded to quantify the amount of internal standard relative to **17**. The solution was degassed by two freeze-pump-thaw cycles, and the tube was backfilled with carbon dioxide (1.0 bar). After 92 h, the ^{1}H NMR spectrum was again recorded (see Figure 6.25), and the products quantified by integration of NMR signals.

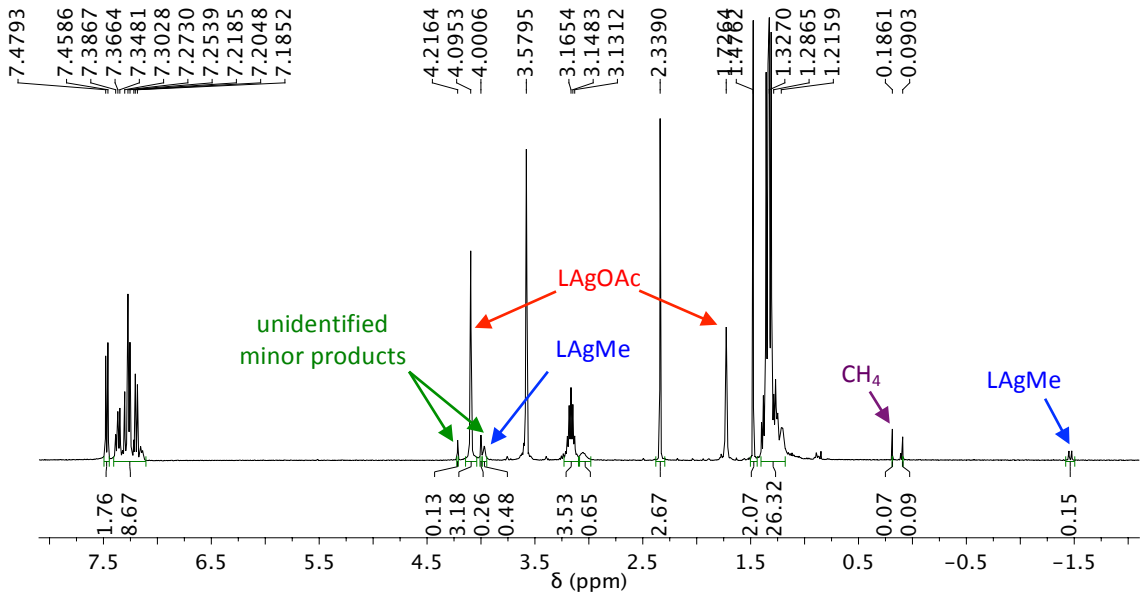

Figure 6.25. ^{1}H NMR (400 MHz, THF-d_8) spectrum recorded 92 h after the addition of CO_2 (1.0 bar) to a sample of (5Dipp)Ag(CH_3) (**17**).

6.5 Acknowledgements

We thank the U.S. National Science Foundation for generous support of this research (CHE-1300659). We thank Professor Jake D. Soper and Mr. Chandler Harris for the use of their IR spectrometer. We thank Dr. Leslie Gelbaum for assistance with configuring NMR experiments.

6.6 Notes and References

1 (a) G. M. Whitesides, D. E. Bergbreiter, P. E. Kendall, *J. Am. Chem. Soc.* **1974**, *96*, 2806–2813. (b) G. M. Whitesides, E. J. Panek, E. R. Stedronsky, *J. Am. Chem. Soc.* **1972**, *94*, 232–239. (c) G. M. Whitesides, C. P. Casey, J. K. Krieger, *J. Am. Chem. Soc.,* **1971**, *93*, 1379–1389. (d) G. M. Whitesides, C. P. Casey, *J. Am. Chem. Soc.* **1966**, 88, 4541–4543.

2 (a) *Silver in Organic Chemistry*; M. Harmata, Ed.; John Wiley & Sons Inc., **2010**. ISBN 978-0470466117. (b) J.-M. Weibel, A. Blanc, P. Pale, *Chem. Rev.* **2008**, *108*, 3149–3173.

3 Stoichiometric processes: (a) G. M. Whitesides, F. D. Gutowski, *J. Org. Chem.*, **1976**, *41*, 2882–2885. (b) R. Murphy, R. H. Prager, *Aust. J. Chem.* **1976**, *29*, 617–626. (c) R. Murphy, R. H. Prager, *Tetrahedron Lett.* **1976**, 463–464. (d) H. C. Brown, C. Verbrugge, C. H. Snyder, *J. Am. Chem. Soc.* **1961**, *83*, 1001. (e) H. C. Brown, C. H. Snyder, *J. Am. Chem. Soc.* **1961**, *83*, 1002–1003. (f) H. C. Brown, N. C. Hebert, C. H. Snyder, *J. Am. Chem. Soc.* **1961**, *83*, 1001–1002. (g) L. Joseph, J. H. Gardner, *J. Org. Chem.* **1940**, *5*, 61–67. (h) J. H. Gardner, L. Joseph, F. Gollub, *J. Am. Chem. Soc.* **1937**, *59*, 2583–2584. (i) J. H. Gardner, P. Borgstrom, *J. Am. Chem. Soc.* **1929**, *51*, 3375–3377.

4 Catalytic processes: (a) H. Someya, H. Yorimitsu, K. Oshima, *Tetrahedron Lett.* **2009**, *50*, 3270–3272. (b) H. Someya, H. Ohmiya, H. Yorimitsu, K. Oshima, *Org. Lett.* **2008**, *10*, 969–971. (c) J. K. Kochi, *J. Organomet. Chem.* **2002**, *653*, 11. (d) M. Tamura, J. M. Kochi, *Bull. Chem. Soc. Jpn.* **1972**, *45*, 1120. (e) M. Tamura, J. K. Kochi, *Synthesis* **1971**, 303.

5 Gas-phase studies: G. N. Khairallah, R. A. J. O'Hair, *Angew. Chem. Int. Ed.* **2005**, *44*, 728–731.

6 For a review, see: U. Halbes-Letinois, J.-M. Weibel, P. Pale, *Chem. Soc. Rev.* **2007**, *36*, 759–769.

7 R. B. Davis, D. H. Scheiber, *J. Am. Chem. Soc.* **1956**, *78*, 1675–1678.

8 (a) T. Naka, K. Koide, *Tetrahedron Lett*. **2003**, *44*, 443–445. (b) Y. Fukue, S. Oi, Y. Inoue, *J. Chem. Soc. Chem. Commun.* **1994**, 2091. (c) L. V. Yerino, M. E. Osborn, P. S. Mariano, *Tetrahedron* **1982**, *38*, 1579–1591. (d) J. Inanga, T. Katsuki, S. Takimoto, S. Ouchida, K. Inoue, A. Nakano, N. Okukado, M. Yamaguchi, *Chem. Lett.* **1979**, 8, 1021–1024. (e) T. Tsuda, K. Udea, T. Saegusa, *J. Chem. Soc. Chem. Commun.* **1974**, 380–381.

9 (a) R. H. Pouwer, J. B. Harper, K. Vyakaranam, J. Michl, C. M. Williams, C. H. Jessen, P. V. Bernhardt, *Eur. J. Org. Chem.* **2007**, 241–248. (b) F. G. De la Heras, S. Y. K. Tam, R. S. Klein, J. J. Fox, *J. Org. Chem.* **1976**, *41*, 84–90. (c) H. P.

Albrecht, D. B. Repke, J. G. Moffatt, *J. Org. Chem.* **1974**, *39*, 2176–2182. (d) M. E. Isabelle, L. C. Leitch, *Can. J. Chem.* **1958**, 36, 440–448.

10 (a) M. Berthelot, *B. Soc. Chim. Fr.* **1866**, 176–191. Other silver complexes of acetylide dianion: (b) T. C. W. Mak, X.-L. Zhao, Q.-M. Wang, G.-C. Guo, *Coord. Chem. Rev.* **2007**, *251*, 2311–2333, and refs. cited therein.

11 (a) R. Matyáš, J. Šelešovský, T. Musil, *J. Hazard. Mater.* **2012**, *213–214*, 236–241. (b) A. Stettbacher, *Zeitschrift für das gesamte Schieß- und Sprengstoffwessen* **1916**, *11*, 1–4.

12 (a) R. Nast, H. Schindel, *Z. anorg. allg. Chem.* **1963**, *326*, 201–208. (b) E. C. Royer, M. C. Barral, V. Moreno, A. Santos, *J. Inorg. Nucl. Chem.* **1981**, *43*, 705–709. (c) C. Glaser, *Liebigs Ann. Chem.* **1870**, *154*, 137–171. (d) C. Liebermann, *Liebigs Ann. Chem.* **1865**, *135*, 266–290. Alkynylsilver compounds may also be prepared using Grignard reagents: (e) J. P. Danehy, J. A. Nieuwland, *J. Am Chem. Soc.* **1936**, *58*, 1609–1610.

13 (a) M. Trose, M. Dell'Acqua, T. Pedrazzini, V. Pirovano, E. Gallo, E. Rossi, A. Caselli, G. Abbiati, *J. Org. Chem.,* **2014**, *79*, 7311–7320. (b) M. Gao, C. He, H. Chen, R. Bai, B. Cheng, A. Lei, A. *Angew. Chem.* **2013**, *125*, 7096–7099. (c) M.-T. Chen, B. Landers, O. Navarro, *Org. Biomol. Chem.*, **2012**, *10*, 2206–2208. (d) X. Yao, C.-J. Li, *Org. Lett.,* **2005**, *7*, 4395–4398. (e) Z. Li, C. Wei, L. Chen, R. S. Varmaband, C.-J. Li, *Tetrahedron Lett.* **2004**, *45*, 2443–2446. (f) C. Wei, Z. Li, C.-Z. Li, *Org. Lett.*, **2003**, *5*, 4473–4475.

14 (a) J. Jover, F. Maseras, *J. Org. Chem.* **2014**, *79*, 11981−11987. (b) S. Kikuchi, T. Yamada, *Chem. Rec.* **2014**, *14*, 62–69. (c) M. Arndt, E. Risto, T. Krause, L. J. Gooßen. *ChemCatChem* **2012**, *4*, 484–487. (d) X. Zhang, W.-Z. Zhang, X. Ren, L.-L. Zhang, X.-B. Lu, *Org. Lett.*, **2011**, *13*, 2402–2405.

15 (a) E. Krause, M. Schmitz, *Ber. dtsch. Chem. Ges. A/B*, **1919**, 52, 2150–2164. Reich also reports an explosive product from the reaction of AgBr with PhMgBr: (b) R. Reich, *C. R. Acad. Sci.* **1923**, 177, 322.

16 (a) J. Boersma, F. J. A. des Tombe, F. Weijers, G. J. M. van der Kerk, *J. Organometal. Chem.* **1977**, *124*, 229–233. (b) C. D. M. Beverwijk, G. J. M. van der Kerk, *J. Organometal. Chem.* **1972**, 43, C11–C12. (c) H. Hashimoto, T. Nakano, *J. Org. Chem.* **1966**, *31*, 891–894. (d) H. Gilman, J. M. Straley, *Recl. Trav. Chim. Pays-Bas* **1936**, *55*, 821.

17 (a) S. Gambarotta, C. Floriani, A. Chiesi-Villa, C. Guastini, *J. Chem. Soc., Chem. Commun.* **1983**, 1087–1089. See also the related compound 2,4,6-triethylphenylsilver: (b) M. Håkanssona, H. Erikssonb, S. Jagnerb, *Inorg. Chim. Acta* **2006**, *359*, 2519–2524.

18 R. Lingnau, J. Strähle, *Angew. Chem. Int. Ed. Engl.* **1988** *27*, 436.

19 J. Blenkers, H. K. Hofstee, J. Boersma, G. J. M. van der Kerk, *J. Organometal. Chem.* **1979**, *168*, 251–258.

20 (a) G. Köbrich, H. Fröhlich, W. Drischel. *J. Organmetal. Chem.* **1966**, *6*, 194. (b) F. Glockling, *J. Chem. Soc.* **1956**, 3640–3642. (c) F. Glockling, *J. Chem. Soc.* **1955**, 716–720.

21 (a) K. Ruitenberg, H. Kleijn, J. Meijer, E. A. Oostveen, P. Vermeer, *J. Organometal. Chem.* **1982**, *224*, 399. (b) J. Meijer, K. Ruitenberg, H. Westmijze, P. Vermeer, *Synthesis* **1981**, *7*, 551–554. (c) H. Westmijze, H. Kleijn, H. J. T. Bos, P. Vermeer, *J. Organometal. Chem.* **1980***, 199*, 293–297 (d) H. Westmijze, K. Ruitenberg, J. Meijer, P. Vermeer, *Tetrahedron Lett.* **1980**, *21*, 1771-1772.

22 (a) G. Semerano, L. Riccoboni, *Ber. dtsch. Chem. Ges. A/B* **1941**, *74*, 1089–1099.

23 (a) H. Westmijze, H. Kleijn, P. Vermeer, *J. Organomet. Chem.* **1979**, *172*, 377–383. (b) H. Gilman, L. A. Woods, *J. Am. Chem. Soc.*, **1943**, *65*, 435–437. (c) F. Glockling, D. Kingston, *J. Chem Soc.*, **1959**, 3001–3004.

24 (a) K. Vikse, G. N. Khairallah, J. S. McIndoe, R. A. J. O'Hair, *Dalton Trans.* **2013**, *42*, 6440–6449. (b) C. Brunet, R. Antoine, M. Broyer, P. Dugourd, A. Kulesza, J. Petersen, M. I. S. Röhr, R. Mitrić, V. Bonačić-Koutecký, R. A. J. O'Hair, *J. Phys. Chem. A*, **2011**, *115*, 9120–9127. (c) N. J. Rijs, R. A. J. O'Hair, *Organometallics*, **2010**, *29*, 2282–2291. (d) R. A. J. O'Hair, *Chem. Commun.*, **2002**, 20–21. (e) P. F. James, R. A. J. O'Hair, *Org. Lett.* **2004**, *6*, 2761–2764. (f) R. A. Flurer, K. L. Busch, *J. Am. Chem. Soc.* **1991**, *113*, 3656–3663. (g) R. L. DeKock, R. D. van Zee, T. Ziegler, *Inorg. Chem.* **1987**, *26*, 563–567. (h) K. L. Busch, R. G. Cooks, R. A. Walton, K. V. Wood, *Inorg. Chem.* **1984**, *23*, 4093–4097.

25 W. T. Miller, R. J. Burnard, *J. Am. Chem. Soc.* **1968**, *90*, 7367–7368.

26 G. Dubot, D. Mansuy, S. Lecolier, J. F. Normant, *J. Organomet. Chem.* **1972**, 42.

27 B. Gao, Y. Zhao, C. Ni, J. Hu, *Org. Lett.* **2014**, *16*, 102–105.

28 (a) M. F. Ibad, A. Schulz, A. Villinger, *Organometallics* **2015**, *34*, 3893−3901. (b) M. M. Kremlev, A. I. Mushta, W. Tyrra, Y. L. Yagupolskii, D. Naumann, A. Möller, *J. Fluorine Chem.* **2012**, *133*, 67–71. (c) W. Tyrra, S. Aboulkacem, B. Hoge, W. Wiebe, I. Pantenburg, I. *J. Fluorine Chem.* **2006**, *127*, 213–217. (d) W. Tyrra, D. Naumann, *J. Fluorine Chem.* **2004**, *125*, 823–830. (e) W. Tyrra, *Heteroatom Chem.* **2002**, *13*, 561–566. (f) W. Tyrra, M. S. Wickleder, *Z. Anorg. Allg. Chem.* **2002**, *628*, 1841–1847. (g) W. Tyrra, *J. Fluorine Chem.* **2001**, *112*, 149–152. (h) D. Naumann, W. Wessel, J. Hahn, W. Tyrra, *J. Fluorine Chem.* **1997**, *547*, 79–88. (i) A. Laguna, E. J. Fernández, A. Mendía, M. E. Ruiz-Romero, P. G. Jones, *J. Organometal. Chem.* **1989**, *365*, 201–206.

29 M. M. Kremlev, W. Tyrra, D. Naumann, Y. L. Yagupolskii, *J. Fluorine Chem.* **2005**, *126*, 1327–1331.

30 W. T. Miller, Jr., K. K. Sun, *J. Am. Chem. Soc.* **1970**, *92*, 6985–6987.

31 (a) H. Voelker, D. Labahn, F. M. Bohnen, R. Herbst-Irmer, H. W. Roesky, D. Stalke, F. T. Edelmann, *New J. Chem.* **1999**, *23*, 905–909. (a) D. A. Edwards, R. M. Harker, M. F. Mahon, K. C. Molloy, *J. Chem. Soc. Dalton Trans.* **1997**, 3509–3513. (c) E. J. Fernández, A. Laguna, A. Mendìa, *Inorg. Chim. Acta* **1994**, *223*, 161–164. (d) E. M. Meyer, A. Gambarotta, C. Floriani, A. Chiesi-Villa, C. Guastini, *Organometallics*, **1989**, *8,* 1067–1079. (e) R. Usón, A. Laguna, E. J. Fernández, A. Mendia, P. G. Jones, *J. Organomet. Chem.* **1988**, *350*, 129–138. (f) A. J. Leusink, G. van Koten, G.; Noltes, J. G. *J. Organometal. Chem.* **1973**, *56*, 379–390. (g) Wennerström, O. *Acta Chem. Scand.* **1971**, *25*, 2341–2349.

32 (a) Eaborn, C.; Hitchcock, P. B.; Smith, J. D.; Sullivan, A. C. *J. Chem. Soc., Chem. Commun.*, **1984**, 870-871. (b) Papasergio, R. I.; Raston, C. L.; White, A. H. *J. Chem. Soc., Chem. Commun*. **1984**, 612-613. (c) Yamamoto, K.; Nakanishi, K. Kumada, M. *J. Organometal. Chem.* **1967**, *7*, 197.

33 (a) Gu, Y.; Chang, D.; Leng, X.; Gu, Y.; Shen, Q. *Organometallics*, **2015**, *34*, 3065–3071. (b) Wu, J.; Gu, Y.; Leng, X.; Shen, Q. *Angew. Chem. Int Ed.* **2015**, *54*, 7648–7652. (c) Gu, Y.; Leng, X.; Shen, Q. *Nature Commun.* **2014**, *5*, 5405.

34 Zhang, X.; Zhang, W.-Z.; Shi, L.-L.; Guo, C.-X.; Zhang, L.-L.; Lu, X.-B. *Chem. Commun.*, **2012**, *48*, 6292–6294.

35 (a) Boogaerts, I. I. F.; Fortman, G. C.; Furst, M. R. L.; Cazin, C. S. J.; Nolan, S. P. *Angew. Chem. Int. Ed.* **2010**, *49*, 8674–8677. (b) Ohmiya, H.; Tanabe, M.; Sawamura, M.; *Org. Lett.* **2011***, 13*, 1086–1088. (c) Ohishi, T.; Zhang, L.; Nishiura, M.; Hou, Z. *Angew. Chem. Int. Ed.* **2011**, *50*, 8114–8117. (d) Goossen, L. J.; Rodriguez, N.; Manjolinho, F.; Lange, P. P. *Adv. Synth. Catal.* **2010**, *352*, 2913–2917. (e) Zhang, L.; Cheng, J.; Ohishi, T.; Hou, Z. *Angew. Chem. Int. Ed.* **2010**, *49*, 8670–8673. (f) Takaya, J.; Tadami, S.; Ukai, K.; Iwasawa, N. *Org. Lett.* **2008**, *10*, 2697–2700. (g) Ohishi, T.; Nishiura, M.; Hou, Z. *Angew. Chem. Int. Ed.* **2008**, *47*, 5792–5795. (h) Mankad, N. P.; Gray, T. G.; Laitar, D. S.; Sadighi, J. P. *Organometallics*, **2004**, *23*, 1191–1193.

36 (a) Zhanga, X., Genga, Z., Wanga, Y.; Houa, X.; Wanga, D. *J. Mol. Catal. A: Chem.* **2012**, 31–40. (b) Johnson, M. T.; van Rensburg, J. M. J.; Axelsson, M.; Ahlquist, M. S. G.; Wendt, O. F. *Chem. Sci.*, **2011**, *2*, 2373-2377. (c) Boogaerts, I. I. F.; Nolan, S. P. *J. Am. Chem. Soc.* **2010**, *132*, 8858–8859.

37 Due to its volatility, quantification of 1,3-butadiene by integration of NMR signals results in a low estimate of conversion; presumably a fraction of the product occupies the headspace of the NMR sample.

38 Bucher, J.; Wurm, T.; Nalivela, K. S.; Rudolph, M.; Rominger, F.; Hashmi, A. S. K. *Angew. Chem. Int. Ed.,* **2014**, *53*: 3854–3858. Graf, K.; Hindenberg, P. D.; Tokimizu, Y.; Naoe, S.; Rudolph, M.; Rominger, F.; Ohno, H.; Hashmi, A. S. K.

ChemCatChem, **2014**, *6*, 199–204. Brown, T. J.; Widenhoefer, R. A. *Organometallics* **2011**, *30*, 6003−6009. P. H. Cheong, P. H.; Morganelli, P.; Luzung, M. R.; Houk, K. N.; Toste, F.D. *J. Am. Chem. Soc.* **2008**, *130*, 4517–4526.

39 Tate, B. K.; Wyss, C. M.; Bacsa, J.; Kluge, K.; Gelbaum, L.; Sadighi, J. P. *Chem. Sci.* **2013**, *4*, 3068–3074.

40 This digold analog is supported by the ligand IDipp (1,3-bis(2,6-diisopropylphenyl)imidazol-2-ylidene); see ref. 37c.

41 The π interaction of silver cations with silver acetylides has been observed: (a) Corfield, P. W. R.; Shearer, H. M. M. Acta Cryst. **1966**, 20, 502–508. And with gold acetylides: (b) Jašíková, L.; Roithová, J. Organometallics, **2013**, 32, 7025–7033. And with acetylides of other metals: (c) Land, H.; Köhler, K.; Blau, S. Coord. Chem. Rev. **1995**, 143, 113–168. (d) Lang, H.; Mansilla, N.; Claus, R.; Rüffer, T. Rheinwald, G; Inorg. Chim. Acta **2011**, 373, 93–99. And with alkynes: (e) Létinois-Halbes, U. Pale, P.; Berger, S. J. Org. Chem. **2005**, 70, 9185–9190. (f) Janssen, M. D.; Köhler, K.; Herres, M.; Dedieu, A.; Smeets, W. J. J.; Spek, A. L.; Grove, D. M.; Lang, H.; G. van Koten, *J. Am. Chem. Soc.* **1996**, 118, 4817–4829.

42 (5Dipp)Ag(O_2CMe) is known and fully characterized: D. V. Partyka, T. J. Robilotto, J. B. Updegraff III, M. Zeller, A. D. Hunter, T. G. Gray, *Organometallics* **2009**, *28*, 795–801.

43 (a) B. K. Tate, J. T. Nguyen, J. Bacsa, J. P. Sadighi, *Chem. Eur. J.* **2015**, *21*, 10160–10169. (b) C. M. Wyss, B. K. Tate, J. Bacsa, M. Wieliczko, J. P. Sadighi, *Polyhedron* **2014**, *84*, 87–95.

44 D. S. Laitar, "Synthetic and catalytic studies of Group 11 N-heterocyclic carbene complexes," Ph.D. Thesis, Massachusetts Institute of Technology (Cambridge), **2006**; http://dspace.mit.edu/ handle/1721.1/36268

45 D. S. Laitar, P. Müller, T. G. Gray, J. P. Sadighi, *Organometallics* **2005**, *24*, 4503–4505.

CHAPTER 7

CONCLUSIONS

This thesis describes the synthesis and characterization of a variety of mononuclear and dinuclear coordination complexes of silver supported by bulky, electron-rich NHC ligands. Also described are reactions that demonstrate potential applications of these complexes in small-molecule activation and catalysis relevant to renewable fuels and sustainability. The isolation and characterization of NHC-stabilized versions of otherwise unstable organometallic complexes and the demonstration of fundamental steps such as H–H bond heterolysis and C–H bond formation in a well-defined homogeneous system can provide valuable information, including mechanistic insight into key chemical transformations and structures of potential catalytic intermediates.

For instance, the activation of hydrogen via oxidative addition to a metal center or via heterolysis by a frustrated Lewis acid-base pair has been studied extensively.[1] These methods of hydrogen activation have been applied effectively in efficient catalytic processes and have been incorporated into promising strategies for the production of synthetic fuels and hydrocarbons. In contrast, examples of the heterolysis of hydrogen by mismatched metal–ligand bonds are relatively uncommon.[2] Phosphine-supported copper hydrides prepared by the reaction of hydrogen with copper alkoxides have proven highly useful as a mild, selective reducing agent in organic synthesis, representing the most extensively studied example of hydrogen activation by metal-ligand bonds.[3] However,

the rational design of ligands to improve or modify the selectivity of this important class of copper compounds is limited by a lack of mechanistic understanding.[4] Unfortunately these systems are difficult to study mechanistically due to the complex, fluxional aggregation of copper alkoxides and copper hydrides in solution. Though NHC-supported copper alkoxides have more well-defined nuclearity and are competent hydrogenation catalysts,[5] the equilibrium for hydrogenolysis of these compounds apparently favors the alkoxide heavily over the hydride (Chapter 5). The transient nature of the hydrides in these systems prevents the study of either the hydrogen activation, or the reduction of the substrate, in isolation.[6]

The hydrogenolysis of mononuclear and dinuclear silver complexes supported by NHC ligands (Chapter 4) provides an avenue to study this class of hydrogen activation in a context in which hydrogen activation and subsequent hydride transfer can be studied as isolated steps. The study of these complexes in solution is aided by the nuclear properties of ^{107}Ag and ^{109}Ag. The observation of coupling to these silver nuclei by NMR spectroscopy lends insight into the structure and nuclearity of silver complexes in solution, and ^{109}Ag–^{107}Ag coupling allows the identification of metal-metal interactions (Chapters 2 and 4). We have learned, for instance, that mechanisms for hydrogen activation likely proceed through nonclassical η^2-dihydrogen complexes (Chapter 4), which are otherwise unknown for the group 11 metals. Furthermore, we can conclude that the cooperation of two mononuclear fluoride complexes in dihydrogen cleavage likely does not involve the interaction of two fluoride complexes before the coordination of H_2 (Chapter 4). This mechanistic insight might aid the further development of silver-

mediated hydrogenation chemistry or may translate to similar systems based on copper, gold, or other soft transition metals paired with hard bases.

In addition to the insight this work may lend to related copper-mediated processes, it demonstrates the generalization of hydrogen activation by mismatched metal-ligand bonds not only to silver alkoxides but also to silver complexes of the substantially weaker base fluoride. By taking advantage of hard-soft mismatches, this underexplored method of hydrogen activation has the potential to incorporate hard yet relatively weak bases, such as fluoride or carboxylates, when paired with soft late transition metals. This could open the door to reactivity distinct from that found in conventional metal-free frustrated Lewis pairs, potentially taking advantage of the coordination of hydrogenation substrates to the metal center. The borrowing of ideas between the various methods of hydrogen activation could also lead to advancements in the field. For instance, acid-base pairs featuring both steric frustration and hard-soft mismatch might exhibit unique reactivity.

Further consequences of the hard-soft mismatch in group 11 fluorides are reported in this thesis. The exchange of halogens between a fluoride-bridged digold complex and dichloromethane (Chapter 3), for instance, represents a fundamental transformation and demonstrates the potential utility of NHC-supported group 11 fluorides as aprotic, organic-soluble alternatives to HF as a source of fluoride in nucleophilic substitutions. The deprotonation of mildly acidic C–H bonds such as those of terminal alkynes by alkoxysilver complexes (Chapter 6) extend the applications of mismatched silver-ligand bonds to C–H activation.

The potential for silver ions or complexes to mediate C–H activation and other transformations of organic substrates underscores the significance of silver complexes of carbanions. The stabilizing effect of NHC ligands allows the spectroscopic and crystallographic characterization of a wide variety of mononuclear and dinuclear complexes of carbanions with silver, revealing interesting structural features such as three-center, two-electron bonds with silver-silver interactions in the dinuclear complexes (Chapter 6). This study also demonstrates silver-mediated C–C bond formation in the form of the homocoupling of vinyl radicals as well as the insertion of CO_2 in to Ag–C bonds.

In addition to the demonstration of several fundamental silver-mediated chemical transformations and thorough spectroscopic and structural analyses of a diverse library of NHC-supported silver complexes, this body of work highlights the importance of carefully choosing an NHC and clearly demonstrates that both steric and electronic considerations are critical. The interplay of steric and electronic properties is perhaps best demonstrated by the reaction of NHC-supported monosilver fluorides with hydrogen (Chapter 4). In this case, the replacement of the conventional five-membered NHC 5Dipp with the expanded-ring NHCs 6Dipp or 7Dipp slowed or eliminated an undesired decomposition pathway, while increasing the rate of the desired reactivity, namely the activation of hydrogen. Based on steric considerations alone, one would expect both types of reactivity to be impaired, but clearly the increased basicity of the expanded NHCs outweighed their steric effects in this case. However, decomposition was not inhibited by less bulky expanded NHCs. The diisopropylphenyl substituents of 6Dipp and 7Dipp were necessary to prevent the formation of undesired bis(NHC) complexes,

suggesting that electronic considerations alone were not sufficient to achieve a system suitable for hydrogen activation.

7.1 Notes and References

1 (a) N. M. West, A. J. M. Miller, J. A. Labinger, J. E. Bercaw, *Coord. Chem. Rev.* **2011**, *255*, 881–898. (b) P. G. Jessop, F. Joó, C.-C. Tai. *Coord. Chem. Rev.* **2004**, *248,* 2425–2442. (c) P. G. Jessop, T. Ikariya, R. Noyori. *Chem. Rev.* **1995**, *95*, 259–272.

2 (a) C. Becker, I. Kieltsch, D. Broggini, A. Mezzetti, *Inorg. Chem.* **2003**, *42*, 8417–8429. (b) L. Maron, O. Eisenstein, *J. Am. Chem. Soc.* **2001**, *123*, 1036–1039. (c) P. Barthazy, R. M. Stoop, M. Wörle, A. Togni, A. Mezzetti, *Organometallics* **2000**, *19*, 2844–2852. (d) P. Barthazy, L. Hintermann, R. M. Stoop, M. Wörle, A. Mezzetti, A. Togni, *Helv. Chim. Acta* **1999**, *82*, 2448–2453. (e) J. C. Lee Jr., E. Peris, A. L. Rheingold, R. J. Crabtree, *J. Am. Chem. Soc.* **1994**, *116*, 11014–11019. (f) J. T. Poulton, M. P. Sigalas, O. Eisenstein, K. G. Caulton, *Inorg. Chem.* **1993**, *32*, 5490–5501. (g) A. M. Joshi, B. R. James, *Organometallics* **1990**, *9*, 199–205. (h) P. L. Watson, G. W. Parshall, *Acc. Chem. Res.* **1985**, 18, 51–56.

3 (a) G. V. Goeden, J. C. Huffman, K. G. Caulton, *Inorg. Chem.* **1986**, *25*, 2484–2485. (b) T. H. Lemmen, K. Folting, J. C. Huffman, K. G. Caulton, *J. Am. Chem. Soc.* **1985**, *107*, 7774–7775. (c) G. V. Goeden, K. G. Caulton, *J. Am. Chem. Soc.* **1981**, *103*, 7354–7355. (d) S. Werkmeister, K. Junge, M. Beller, *Green Chem.* **2012**, *14*, 2371–2374. (e) H. Shimizu, N. Sayo, T. Saito, *Synlett* **2009**, 1295–1298. (f) H. Shimizu, D. Igarashi, W. Kuriyama, Y. Yusa, N. Sayo, T. Saito, *Org. Lett.* **2007**, *9*, 1655–1657. (g) J.-X. Chen, J. F. Daeuble, J. M. Stryker, *Tetrahedron* **2000**, *56*, 2789–2798; (h) J.-X. Chen, J. F. Daeuble, D. M. Brestensky, J. M. Stryker, *Tetrahedron* **2000**, *56*, 2153–2166.

4 (a) M. S. Eberhart, J. R. Norton, A. Zuzek, W. Sattler, S. Ruccolo *J. Am. Chem. Soc.* **2013**, *135*, 17262−17265. (b) B. H. Lipshutz, K. Noson, W. Chrisman, A. Lower, *J. Am. Chem. Soc.* **2003**, 125, 8779–8789; and refs. cited therein.

5 R. Watari, Y. Kayaki, S. Hirano, N. Matsumoto, T. Ikariya. *Adv. Synth. Catal.* **2015**, *357*, 1369–1373.

6 NHC-supported copper hydrides prepared from stronger hydride donors such as boranes and silanes are known and fully characterized: (a) C. M. Wyss, B. K. Tate, J. Bacsa, T. G. Gray, J. P. Sadighi. *Angew. Chem. Int. Ed.* **2013**, *52*, 12920–12923. (b) G. D. Frey, B. Donnadieu, M. Soleilhavoup, G. Bertrand, *Chem.–Asian J.* **2011**, *6*, 402–405. (c) N. P. Mankad, D. S. Laitar, J. P. Sadighi, *Organometallics* **2004**, *23*, 3369–3371.

APPENDIX A

COLLABORATOR CONTRIBUTIONS

Chapter 2: An NHC-Supported Disilver Hydride

Synthesis, NMR characterization, and reactivity studies were performed by Brandon K. Tate. Chelsea M. Wyss contributed significantly to the development of synthetic methods. John Bacsa and Kelly Kluge of the Emory University X-ray Crystallography Center collected and solved X-ray diffraction data. Leslie Gelbaum assisted in the acquisition and analysis of ^{109}Ag NMR data. The principal investigator was Joseph P. Sadighi.

Chapter 3: Fluoride-Bridged Complexes of the Group 11 Metals

Synthesis, NMR characterization, and reactivity studies of silver compounds were performed by Brandon K. Tate. Synthesis, NMR characterization, and reactivity studies of copper and gold compounds were performed by Chelsea M. Wyss. John Bacsa and Marika Wieliczko of the Emory University X-ray Crystallography Center collected and solved X-ray diffraction data. The principal investigator was Joseph P. Sadighi. Much of experimental section of this chapter also appears in the Ph.D. dissertation of Chelsea M. Wyss and was originally written as a collaborative publication (C. M. Wyss, B. K. Tate, J. Bacsa, M. Wieliczko, J. P. Sadighi. *Polyhedron* **2014**, *84*, 87–95) to which all authors made significant contirbutions.

Chapter 4: Hydrogen Activation By Hard-Soft Mismatched Silver Complexes

Synthesis and NMR characterization of 6Dipp compounds were performed by Brandon K. Tate. Synthesis and NMR characterization of 7Dipp compounds were

performed by Jenna T. Nguyen under the mentorship of Brandon K. Tate. Kinetics experiments were performed by Brandon K. Tate. John Bacsa of the Emory University X-ray Crystallography Center collected and solved X-ray diffraction data. The principal investigator was Joseph P. Sadighi.

Chapter 5: Closing a Cycle: Silver-Catalyzed Hydrogenation of Carbon Dioxide

All experimental work was performed by Brandon K. Tate under the advisement of Joseph P. Sadighi.

Chapter 6: Thermally Stable Organosilver Compounds

Synthesis and NMR characterization were performed by Brandon K. Tate. John Bacsa of the Emory University X-Ray Crystallography Center collected and solved X-ray diffraction data. The principal investigator was Joseph P. Sadighi.

APPENDIX B

PERMISSIONS TO REPRODUCE PUBLISHED MATERIAL

Chapter 2: An NHC-Supported Disilver Hydride

This chapter is largely reproduced from the following article with permission from the publisher and copyright holder, the Royal Society of Chemistry:

> Tate, B. K.; Wyss, C. M.; Bacsa, J.; Kluge, K.; Gelbaum, L.; Sadighi, J. P. *Chem. Sci.* **2013**, *4*, 3068–3074.

Chapter 3: Fluoride-Bridged Complexes of the Group 11 Metals

This chapter is adapted from the following article with permission from the publisher and copyright holder, Elsevier:

> C. M. Wyss, B. K. Tate, J. Bacsa, M. Wieliczko, J. P. Sadighi. *Polyhedron* **2014**, *84*, 87–95.

Chapter 4: Hydrogen Activation By Hard-Soft Mismatched Silver Complexes

This chapter is largely reproduced from the following article with permission from the publisher and copyright holder, John Wiley & Sons:

> Tate, B. K.; Nguyen, J. T.; Bacsa, J.; Sadighi, J. P. *Chem. Eur. J.* **2015**, *21*, 10160–10169.

Chapter 6: Thermally Stable Organosilver Compounds

This chapter is largely reproduced from the following article with permission from the publisher and copyright holder, the American Chemical Society:

> Tate, B. K.; Bacsa, J.; Sadighi, J. P. Submitted to *Organometallics*.

VITA

Brandon K. Tate

Brandon was born in Columbus, Georgia, in 1987, and grew up in Phenix City, Alabama. He attended elementary and middle school at Grace Christian School in Columbus and high school at Glenwood School in Phenix City, graduating in 2005. He attended Auburn University in Auburn, Alabama, where he participated in undergraduate research in the lab of Professor Anne E. V. Gorden, and received a B.S. in chemistry and a B.A. in German language and literature in 2010. He attended graduate school at the Georgia Institute of Technology in Atlanta, Georgia, where he conducted graduate research under the advisement of Professor Joseph P. Sadighi, and obtained his Ph.D. in inorganic chemistry in 2015.